RADIOLOGY AND ONCOLOGY

vol.46 no.2
june 2012

SKRAJŠAN POVZETEK GLAVNIH ZNAČILNOSTI ZDRAVILA

Ime zdravila ALIMTA 100 mg prašek za koncentrat za raztopino za infundiranje in ALIMTA 500 mg prašek za koncentrat za raztopino za infundiranje **Kakovostna in količinska sestava** ALIMTA 100 mg: vsaka viala vsebuje 100 mg pemetrekseda (v obliki dinatrijevega pemetrekseda). Po pripravi vsebuje vsaka viala 25 mg/ml pemetrekseda. Pomožne snovi: Vsaka viala vsebuje približno 11 mg natrija, manitol, klorovodikova kislina, natrijev hidroksid. ALIMTA 500 mg: vsaka viala vsebuje 500 mg pemetrekseda (v obliki dinatrijevega pemetrekseda). Po pripravi vsebuje vsaka viala 25 mg/ml pemetrekseda. Pomožne snovi: Vsaka viala vsebuje približno 54 mg natrija, manitol, klorovodikova kislina, natrijev hidroksid. **Terapevtske indikacije:** ALIMTA je v kombinaciji s cisplatinom indicirana za zdravljenje bolnikov z neresektabilnim malignim plevralnim mezoteliomom, ki jih še nismo zdravili s kemoterapijo. ALIMTA je v kombinaciji s cisplatinom indicirana kot zdravljenje prvega izbora za bolnike z lokalno napredovalim ali metastatskim nedrobnoceličnim karcinomom pljuč, ki nima pretežno ploščatocelične histologije. ALIMTA je indicirana kot monoterapija za zdravljenje lokalno napredovalega ali metastatskega nedrobnoceličnega pljučnega karcinoma, ki nima pretežno ploščatocelične histologije pri bolnikih, pri katerih bolezen ni napredovala neposredno po kemoterapiji na osnovi platine. ALIMTA je indicirana kot monoterapija za zdravljenje drugega izbora bolnikov z lokalno napredovalim ali metastatskim nedrobnoceličnim pljučnim karcinomom, ki nima pretežno ploščatocelične histologije. **Odmerjanje in način uporabe:** *Odmerjanje:* ALIMTO smemo dajati le pod nadzorom zdravnika, usposobljenega za uporabo kemoterapije za zdravljenje raka. ALIMTA v kombinaciji s cisplatinom Priporočeni odmerek ALIMTE je 500 mg/m2 telesne površine (TP), dan kot intravenska infuzija v 10 minutah prvi dan vsakega 21-dnevnega ciklusa. Priporočeni odmerek cisplatina je 75 mg/m2 TP, infundiran v dveh urah približno 30 minut po zaključku infuzije pemetrekseda prvi dan vsakega 21 dnevnega ciklusa. Bolniki morajo prejeti zadostno antiemetično zdravljenje, pred in/ali po prejemanju cisplatina jih moramo tudi ustrezno hidrirati. *ALIMTA kot samostojno zdravilo* Priporočeni odmerek ALIMTE je 500 mg/m2 TP, dan kot intravenska infuzija v 10 minutah prvi dan vsakega 21 dnevnega ciklusa. *Režim premedikacije* Da zmanjšamo incidenco in resnost kožnih reakcij, dajemo kortikosteroid dan pred dajanjem pemetrekseda, na dan dajanja pemetrekseda in naslednji dan. Kortikosteroid naj ustreza 4 mg deksametazona, danega peroralno dvakrat dnevno. Za zmanjšanje toksičnosti morajo bolniki dnevno jemati tudi peroralno folno kislino ali multivitaminski pripravek, ki jo vsebuje (350 do 1000 mikrogramov). V sedmih dneh pred prvim odmerkom pemetrekseda morajo vzeti vsaj pet odmerkov folne kisline, odmerjanje pa morajo nadaljevati ves čas zdravljenja in še 21 dni po zadnjem odmerku pemetrekseda. Bolniki morajo prejeti tudi intramuskularno injekcijo vitamina B12 (1000 mikrogramov) v tednu pred prvim odmerkom pemetrekseda in enkrat vsake tri cikluse zatem. Kasnejše injekcije vitamina B12 lahko dajemo isti dan kot pemetreksed. **Kontraindikacije:** Preobčutljivost za zdravilno učinkovino ali katerokoli pomožno snov. Dojenje. Sočasno cepljenje proti rumeni mrzlici. **Posebna opozorila in previdnostni ukrepi:** Pemetreksed lahko zavre delovanje kostnega mozga, kar se kaže kot nevtropenija, trombocitopenija in anemija (ali pancitopenija). Mielosupresija običajno predstavlja toksičnost za omejitev odmerka. Pri bolnikih, ki pred zdravljenjem niso prejemali kortikosteroidov, so poročali o kožnih reakcijah. Uporabe pemetrekseda pri bolnikih z očistkom kreatinina < 45 ml/min ne priporočamo. Bolniki z blagim do zmernim popuščanjem delovanja ledvic naj se izogibajo jemanju nesteroidnih protivnetnih zdravil (NSAID), denimo, ibuprofena in acetilsalicilne kisline 2 dni pred dajanjem pemetrekseda, na dan dajanja in še 2 dni po dajanju pemetrekseda. Vsi bolniki, ki jih lahko zdravimo s pemetreksedom, naj se izogibajo jemanju NSAID-ov z dolgimi razpolovnimi časi izločanja vsaj 5 dni pred dajanjem pemetrekseda, na dan dajanja in še vsaj 2 dni po dajanju pemetrekseda. Poročali so o resnih ledvičnih primerih, vključno z akutno ledvično odpovedjo, s pemetreksedom samim ali v povezavi z drugimi kemoterapevtiki. Pri bolnikih s klinično pomembno tekočino tretjega prostora moramo razmisliti o drenaži izliva pred dajanjem pemetrekseda. Kot posledico toksičnosti pemetrekseda v kombinaciji s cisplatinom za prebavila so opažali hudo dehidracijo, zato moramo bolnike pred prejemanjem terapije in/ali po njej ustrezno hidrirati, prejeti morajo zadostno antiemetično zdravljenje. Občasno so v kliničnih študijah pemetrekseda, običajno ob sočasnem dajanju z drugo citotoksično učinkovino, poročali o resnih srčnožilnih dogodkih, vključno z miokardnim infarktom in možganskožilnimi dogodki. Odsvetujemo uporabo živih oslabljenih cepiv. Spolno zrelim moškim odsvetujemo zaploditev otroka v času zdravljenja in še 6 mesecev zatem. Priporočamo ukrepe proti zanositvi ali vzdržnost. Zaradi možnosti, da zdravljenje s pemetreksedom povzroči trajno neplodnost, naj se moški pred začetkom zdravljenja posvetujejo o shranjevanju semena. Ženske v rodni dobi morajo v času zdravljenja s pemetreksedom uporabljati učinkovito kontracepcijo. Poročali so o primerih radiacijske pljučnice pri bolnikih, ki so jih zdravili z radiacijo pred, med ali po zdravljenju s pemetreksedom. Poročali so o radiacijskem izpuščaju pri bolnikih, ki so se zdravili z radioterapijo pred tedni ali leti. **Medsebojno delovanje z drugimi zdravili in druge oblike interakcij:** Sočasno dajanje nefrotoksičnih zdravil (denimo, aminoglikozidov, diuretikov zanke, spojin platine, ciklosporina) lahko potencialno povzroči zakasnjeni očistek pemetrekseda. Sočasno dajanje snovi, ki se tudi izločajo s tubulno sekrecijo (denimo, probenecid, penicilin), lahko potencialno povzroči zakasnjeni očistek pemetrekseda. Pri bolnikih z normalnim delovanjem ledvic lahko visoki odmerki nesteroidnih protivnetnih zdravil (NSAID-i, denimo, ibuprofen) in acetilsalicilna kislina v visokih odmerkih zmanjšajo eliminacijo pemetrekseda in tako lahko povečajo pojavnost neželenih učinkov pemetrekseda. Pri bolnikih z blagim do zmernim popuščanjem delovanja ledvic se moramo izogibati sočasnemu dajanju pemetrekseda z NSAID-i (denimo, ibuprofenom) ali acetilsalicilne kisline v visokih odmerkih 2 dni pred dajanjem pemetrekseda, na dan dajanja in še 2 dni po dajanju pemetrekseda. Sočasnemu dajanju NSAID-ov z daljšimi razpolovnimi časi s pemetreksedom se moramo izogibati vsaj 5 dni pred dajanjem pemetrekseda, na dan dajanja in še vsaj 2 dni po dajanju pemetrekseda.Velika različnost med posamezniki v koagulacijskem statusu v času bolezni ter možnost medsebojnega delovanja med peroralnimi antikoagulacijskimi učinkovinami ter kemoterapijo proti raku zahtevata povečano pogostnost spremljanja INR. **Kontraindicirana sočasna uporaba:** Cepivo proti rumeni mrzlici: tveganje za smrtno generalizirano bolezen po cepljenju. **Odsvetovana sočasna uporaba:** Živa oslabljena cepiva (razen proti rumeni mrzlici): tveganje za sistemsko, potencialno smrtno bolezen. **Neželeni učinki** Klinične študije malignega plevralnega mezotelioma *Zelo pogosto:* znižani nevtrofilci/granulociti, znižani levkociti, znižan hemoglobin, znižani trombociti, nevropatija-senzorna, diareja, bruhanje, stomatitis/faringitis, slabost, anoreksija, zaprtje, izpuščaj, alopecija, povišan kreatinin, znižan očistek kreatinina, utrujenost. *Pogosti:* dehidracija, motnje okusa, konjuktivitis, dispepsija. Klinične študije nedrobnoceličnega pljučnega karcinoma - ALIMTA monoterapija, zdravljenje 2. izbora: *Zelo pogosti:* znižan nevtrofilci/granulociti, znižani levkocitit, znižan hemoglobin, diareja, bruhanje, stomatitis/faringitis, slabost, anoreksija, izpuščaj/luščenje, utrujenost. *Pogosti:* znižani trombociti, zaprtje, povišanje SGPT (ALT), povišanje SGOT (AST), srbenje, alopecija, povišana telesna temperatura. Klinične študije nedrobnoceličnega pljučnega karcinoma - ALIMTA v kombinaciji s cisplatinom, zdravljenje 1. izbora: *Zelo pogosti:* znižan hemoglobin, znižani nevtrofilci/granulociti, znižani levkocitit, znižani trombociti, slabost, bruhanje, anoreksija, zaprtje, stomatitis/faringitis, diareja brez kolostomije, alopecija, izpuščaj/luščenje, povišan kreatinin, utrujenost. *Pogosti:* nevropatija-senzorična, motnje okusa, dispepsija/zgaga. Klinične študije nedrobnoceličnega pljučnega karcinoma - ALIMTA monoterapija, vzdrževalno in nadaljevalno zdravljenje: *Zelo pogosti:* znižan hemoglobin, slabost, anoreksija, utrujenost. *Pogosti:* znižani levkociti, znižani nevtrofilci, nevropatija-senzorična, bruhanje, mukozitis/stomatitis, povišanje ALT (SGPT), povišanje AST (SGOT), izpuščaj/luščenje, bolečina. Občasno so v kliničnih študijah pemetrekseda poročali o primerih resnih srčnožilnih in možganskožilnih dogodkov, vključno z miokardnim infarktom, angino pektoris, cerebrovaskularnim insultom in prehodnimi ishemičnimi atakami; primerih kolitisa ter o primerih intersticijske pljučnice z respiratorno insuficience, primerih edema, o ezofagitisu/radiacijskem ezofagitisu in o primerih sepse. Redkeje pa o primerih potencialno resnega hepatitisa in pancitopenije. Po uvedbi zdravila na trg so poročali o primerih akutne odpovedi ledvic s pemetreksedom samim ali v povezavi z drugimi kemoterapevtiki, primerih radiacijske pljučnice pri bolnikih, ki so jih zdravili z radiacijo pred, med ali po njihovem zdravljenju s pemetreksedom, primerih radiacijskega izpuščaja pri bolnikih, ki so se v preteklosti zdravili z radioterapijo, o primerih periferne ishemije, ki je včasih vodila v nekrozo okončin, redkih primerih buloznih stanj, kot sta Stevens-Johnsonov sindrom in toksična epidermalna nekroliza, ki so bila v nekaterih primerih usodna in o redkih primerih hemolitične anemije. **Imetnik dovoljenja za promet** Eli Lilly Nederland B.V., Grootslag 1 5, NL 3991 RA, Houten, Nizozemska. Datum zadnje revizije besedila 24.10.2011. **Način izdaje zdravila:** H. SAMO ZA STROKOVNO JAVNOST.

Podrobnejše informacije o zdravilu Alimta, so dostopne na spletni strani Evropske agencije za zdravila EMA http://www.ema.europa.eu in na lokalnem predstavništvu.

SIALM00025

Eli Lilly Farmacevtska družba, d.o.o.
Brnčičeva 41G, 1231 Ljubljana - Črnuče, Slovenija
Telefon: +386 (0)1 5800 010
Faks: +386 (0)1 5691 705

RADIOLOGY AND ONCOLOGY

March 2012
Vol. 46 No. 2
Pages 89-178
ISSN 1318-2099
UDC 616-006
CODEN: RONCEM

Publisher
Association of Radiology and Oncology

Affiliated with
Slovenian Medical Association – Slovenian Association of Radiology, Nuclear Medicine Society,
Slovenian Society for Radiotherapy and Oncology, and Slovenian Cancer Society
Croatian Medical Association – Croatian Society of Radiology
Societas Radiologorum Hungarorum
Friuli-Venezia Giulia regional groups of S.I.R.M.
Italian Society of Medical Radiology

Aims and scope
Radiology and Oncology is a journal devoted to publication of original contributions in diagnostic and interventional radiology, computerized tomography, ultrasound, magnetic resonance, nuclear medicine, radiotherapy, clinical and experimental oncology, radiobiology, radiophysics and radiation protection.

Editorial office

Radiology and Oncology
Zaloška cesta 2
P. O. Box 2217
SI-1000 Ljubljana
Slovenia
Phone: +386 1 5879 369
Phone/Fax: +386 1 5879 434
E-mail: gsersa@onko-i.si

Reader for English

Vida Kološa

Secretary

Mira Klemenčič

Zvezdana Vukmirović

Design

Monika Fink-Serša, Samo Rovan, Ivana Ljubanović

Layout

Matjaž Lužar

Printed by

Tiskarna Ozimek, Slovenia

Published quarterly in 600 copies

Beneficiary name: DRUŠTVO RADIOLOGIJE IN ONKOLOGIJE
Zaloška cesta 2
1000 Ljubljana
Slovenia

Beneficiary bank account number: SI56 02010-0090006751
IBAN: SI56 0201 0009 0006 751
Our bank name: Nova Ljubljanska banka, d.d.,
Ljubljana, Trg republike 2,
1520 Ljubljana; Slovenia

SWIFT: LJBASI2X

Subscription fee for institutions EUR 100, individuals EUR 50

The publication of this journal is subsidized by the Slovenian Book Agency.

Indexed and abstracted by:

Science Citation Index Expanded (SciSearch®)
Journal Citation Reports/Science Edition
Scopus
EMBASE/Excerpta Medica
DOAJ
Open J-gate
Chemical Abstracts
Biomedicina Slovenica
Summon by Serial Solutions (ProQuest)

This journal is printed on acid- free paper

On the web: ISSN 1581-3207

http://versitaopen.com/ro

http://www.radioloncol.com

http://versita.com/science/medicine/ro/

http://www.onko-i.si/radioloncol/

contents

radiophysics

I *slovenian abstracts*

Radiology and Oncology is covered in Science Citation Index Expanded (SciSearch®),Journal Citation Reports/Science Edition, Scopus, DOAJ, EMBASE/Excerpta Medica, Open J-gate, Chemical Abstracts, Biomedicina Slovenica, Summon by Serial Solutions (ProQuest)

research article

Double BioDisk: a new bioprosthetic device for transcatheter closure of atrial septal defects - a feasibility study in adult sheep

Dusan Pavcnik[1], Kurt Tekulve[2], Barry T. Uchida[1], Zhong-Huo Luo[1], Miran Jeromel[1,4], William G. Van Alstine[3], Frederick S. Keller[1], Josef Rösch[1]

[1] Dotter Interventional Institute, Oregon Health Sciences University, Portland, Oregon, USA
[2] Cook Medical Incorporated, Bloomington, Indiana, USA
[3] School of Veterinary Medicine, Purdue University, West Lafayette, Indiana, USA
[4] Institut of Radiology, University Clinical Center, Ljubljana, Slovenia

Radiol Oncol 2012; 46(2):89-96.

Received 15 April 2012
Accepted 2 May 2012

Correspondence to: Prof. Dusan Pavcnik, M.D., Ph.D., Dotter Interventional Institute, Oregon Health Sciences University, L342, 3181 SW Sam Jackson Park Road, Portland, Oregon, 97201, USA. Phone: (503) 494-3669; Fax: (503) 494-4258; E-mail: pavcnikd@ohsu.edu

Conflict of interest: D.P. reports receiving research grants from Cook Medical. K.T. is Cook Medical employee. W.G.V.A. reports receiving consulting fees from Cook Medical.

Background. To evaluate the long-term effectiveness and safety of a new Double BioDisk (DBD) device for closure of atrial septal defect (ASD).

Materials and methods. ASD was created with transeptal needle (TS) followed by balloon dilatation in 12 sheep weighing 40.1 to 64 kg (mean 55.2 ± 7.1). The ASD diameters were measured after creation and two weeks later before DBD implantation. The DBDs consists of two nitinol rings 18 to 28 mm in diameter connected with small cannulas and covered with a porcine small intestinal submucosa (SIS). They were implanted via a 10 Fr sheath. DBD effectiveness was evaluated by angiocardiography and by intra-cardiac echogram (ICE) with Doppler studies. Two animals were acute, two were followed for 6 weeks, three for 3 months, three for 6 months and two for 12 months.

Results. TS punctures were successful in 10 sheep. In two sheep ASD was created by existing PFO dilation. The ASD size ranged from 13-15 mm (mean 14.1± 0.73 mm) after initial balloon dilation and from 9-13 mm (mean 10.06 ± 1.37 mm) after two weeks. In all animals none of the successfully implanted DBDs spontaneously embolized on release or on follow up. ICE demonstrated no shunting around the DBDs during follows ups. Macroscopic and histologic evaluation of the 6, 12, 24 and 52 weeks animals showed that DBDs were well incorporated in the atrial septum with complete shunt closure. The SIS showed progressive remodeling with the host cells, including endothelization of the DBD devices.

Conclusions. ASD closure with the Double BioDisk is safe and effective in adult sheep.

Key words: atrial septal defect; transcatheter closure; small intestinal submucosa; biomaterial; embolism; heart septal defects

Introduction

Since King and Mills reported percutaneous treatment of an atrial septal defect (ASD) in the 1970s, many transcatheter ASD closure devices have been developed.[1-5] These ASD closure devices have been also used for patent foramen ovale (PFO) closure. We developed and tested a single disk device covered with porcine small intestinal submucosa (SIS) – BioDisk (BD) - for the closure of PFO in a piglet model.[6] For closure of ASD in large animals we developed a Double BioDisk (DBD) covered with SIS. We report on the feasibility, long-term effectiveness and safety of DBD application in adult sheep with percutaneously created ASD. Sheep were used for testing, since the DBD biological cover is of a porcine origin.

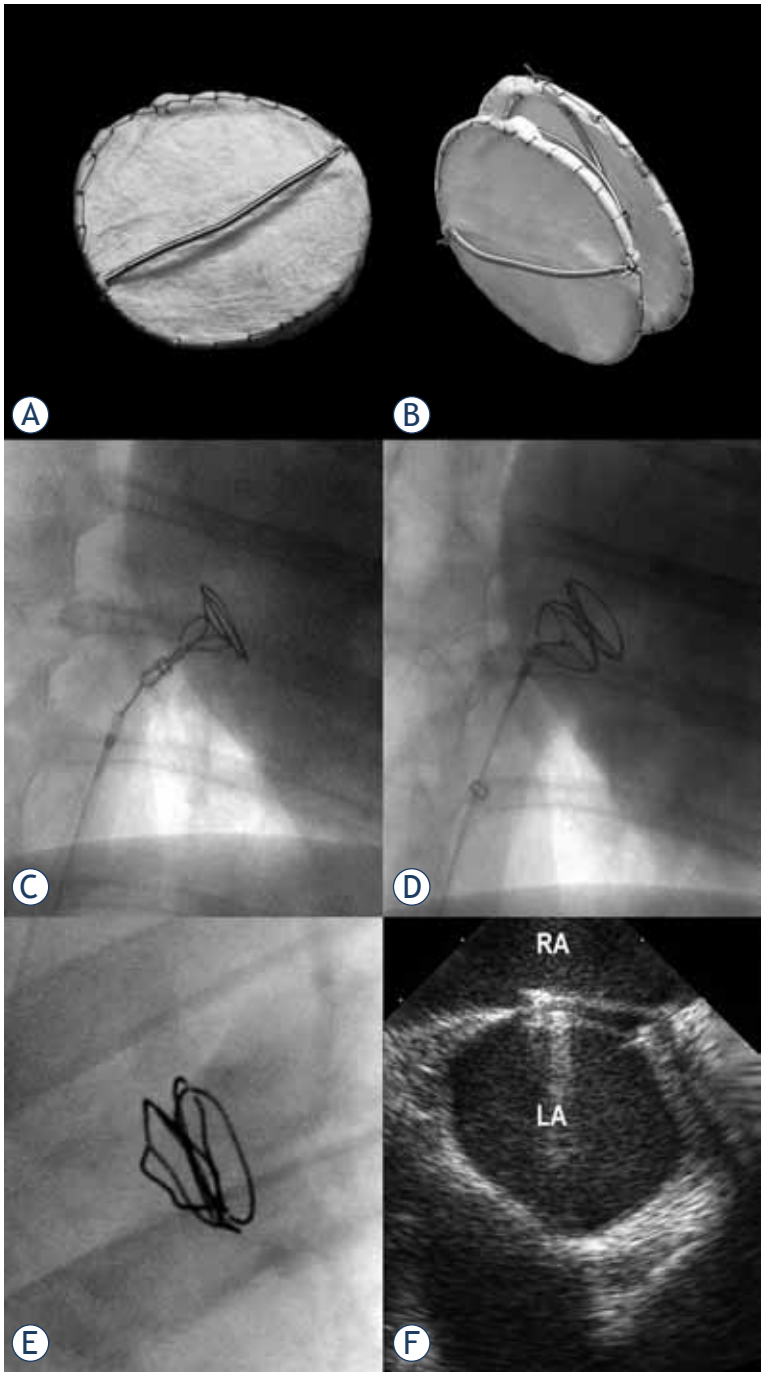

FIGURE 1. The double BioDisk (DBD) ASD occlusive device 18 mm in diameter.
A. Right atrial side with delivery bar.
B. Oblique projection.
C. Deployment of the left atrial DBD disk.
D. Deployment of DBD across ASD with delivery bar still attached to the delivery wire.
E. X-ray of DBD at 3 months.
F. Intracardiac echocardiogram 6 months after DBD deployment shows device with thickened discs. No shunting was seen.

Material and methods

The study protocol was approved by the institutional Animal Care and Use Committee. Twelve adult weighing 40.1 to 64 kg (mean 55.2 ± 7.1 kg) were used for testing the DBD device. A cardiac mobile system (GE/OEC 9800; GE Medical Systems, OEC, Salt Lake City, UT) with digital imaging was used for fluoroscopy and angiocardiography. Angiocardiography was performed with an injector (Medrad Mark Plus, Medrad, Inc. Warrendale, PA). For intracardiac echocardiographic (ICE) studies, the AcuNav System (Acuson, Siemens Inc., Mountain View, California) was used.

Percutaneous transcatheter creation of ASD

Preparation of animals and their anesthesia were described in previous paper.[7] Electro cardiogram (EKG), heart rate, oxygen saturation and end tidal CO_2 were monitored during the procedure. After induction of general endotracheal anesthesia, the sheep were secured with their back on the radiographic table with their hind limbs in moderate abduction. The neck and the right groin were shaved and prepped. 6 F vascular sheath was percutaneously placed into the right jugular vein and a short 14 F sheath into the right femoral vein. The jugular vein sheath was used for physiologic monitoring, the femoral vein sheath for procedure performance.

The ASDs were created percutaneously with modified transeptal needles (TS) followed by 14 mm balloon dilatation (Cook Medical, Bloomington, IN) as previously described.[8] The stretched ASD diameter was then measured with a Coda balloon catheter (Cook Medical). The animals were then recovered and returned to the Department of Comparative Medicine (DMC) for monitoring by veterinarians. Fourteen days after ASDs creation, the sheep were restudied by angiocardiography, ICE study and Coda balloon measurement of the shunts. DBDs were then implanted.

Double BioDisk (DBD) device

The DBD were constructed as a joint effort between Cook Medical and the Dotter Institute specifications. The DBD consisted of two nitinol rings covered with platinum coil. Both flexible rings were connected with small cannulas and covered with SIS. The cross bar of the right atrial disk was the delivery bar. SIS was sutured with Prolene 6.0 to the radio-opaque rings (Figure 1AB). The DBD was lyophilized and

then preloaded by the manufacturer into a 10 Fr cartridge. The delivery system was similar to the system used in the jugular Tulip filter delivery system (Cook Medical). The DBD is self-expanding and self-centering device. The DBD sizes for this study were 18 mm, 23 mm and 28 mm in diameter. Device to defect ratio of 1.8 or larger was used.

DBD closures of ASD

Preparation of animals, their anesthesia and sheaths placements were similar as for ASD creation. The animals received heparin in dose of 100 IU/kg of body weight. Intravenous saline was administered as needed and respiration rate, expired carbon dioxide, oxygen saturation and EKG were monitored during the procedure. A 5 Fr multipurpose catheter (Cook Medical) was introduced through the femoral vein sheath into the right atrium to catheterize the ASD. A 0.035" Road Runner guide wire (Cook Medical) was used to advance the catheter under fluoroscopy into the left atrium. The Road Runner was then replaced with a long, 0.035" stiff Amplatz wire (Cook Medical). To measure diameter of the ASD, a Coda balloon (Cook Medical) was used. An hourglass appearance of the Coda balloon was indicative of ASD size. No attempts were made to dilate the ASD. After the Coda balloon was removed, a10F Flexor sheath (Cook Medical) was advanced across the ASD into the left atrium.

The preloaded DBD was first rehydrated with injection of 10-20 ml of heparinized saline into the cartridge. The delivery bar of the right atrial disk of the DBD was then connected to a hook of a stiff introducing wire. The DBD was introduced into the Flexor delivery sheath and advanced through the ASD into the left atrium. The left atrial disk was then delivered by holding the DBD and by withdrawing the delivery sheath (Figure 1CD). Since the disk is self expanding, it assumed its original rounded shape in the left atrium after exiting the sheath. The DBD was then pulled back against the septum while the other disk connected to the delivery bar was still inside the Flexor sheath in the right atrium. Before releasing the device, the sheath was pulled back to expose the right atrial disk with delivery bar still connected to the hook. Prior to deployment, the DBD position was assessed by contrast injection into the right atrium in the RAO view. When no reflux into the left atrium was found, delivery bar of the DBD was released from the holding catheter. The DBD sizes used for ASD closure were 18 mm in 5 sheep, 23 mm in 4 sheep and 28 mm in one sheep.

After DBD deployments angiocardiograms in left anterior oblique and lateral views followed to document the position of the DBD and its effectiveness in occluding the ASD. The delivery catheter and 10 Fr sheath were then removed and replaced with an ICE catheter to evaluate DBD effectiveness with Doppler studies. Two animals were acute; two were followed for six weeks, three for 3 months, three for 6 months and two for 12 months.

Acute studies

In two acute animals, DBD repositioning and removal were tested prior to delivery catheter removal. First the DBD was expanded and then retracted into the delivery sheath. Then the entire DBD was deployed, but not released. Afterwards it was pulled back into the sheath and redeployed into the ASD. To test its retrievability, the DBD was removed from its ASD position and intentionally embolized into the right atrium. Both the Amplatz gooseneck snare and vascular forceps were used for the retrieval of the embolized DBDs. After retrieval a new DBD was deployed and after 3 hours observation, the acute animals were euthanized. The harvested hearts were cut longitudinally and photographs of the atrial septums were made.

Follow-up studies

Ten chronic animals were recovered after the procedure and returned to the DMC where veterinarians checked them on a daily basis.

Follow-up angiocardiograms of the right atrium and ICE with Doppler studies were done at 6 weeks (n=2), 3 months (n=3), 6 months (n=3) and 12 months (n=2) after DBD placement under the same procedure protocol as in initial studies. After satisfactory views of the DBD effectiveness for ASD closure were obtained, the animals were euthanized and their hearts harvested. After photographs of the atrial septa, the hearts was preserved in buffered formalin and were sent for detailed histological evaluation. Each DBD specimen was embedded in methylmethacrylate blocks. Four cross sections of each device were processed using plastic embedding. All slides were stained with hematoxylin and eosin (H and E) stain using routine methods.

Results

The ASDs were created safely in all 12 sheep and did not lead to any complications. In 10 sheep ASD

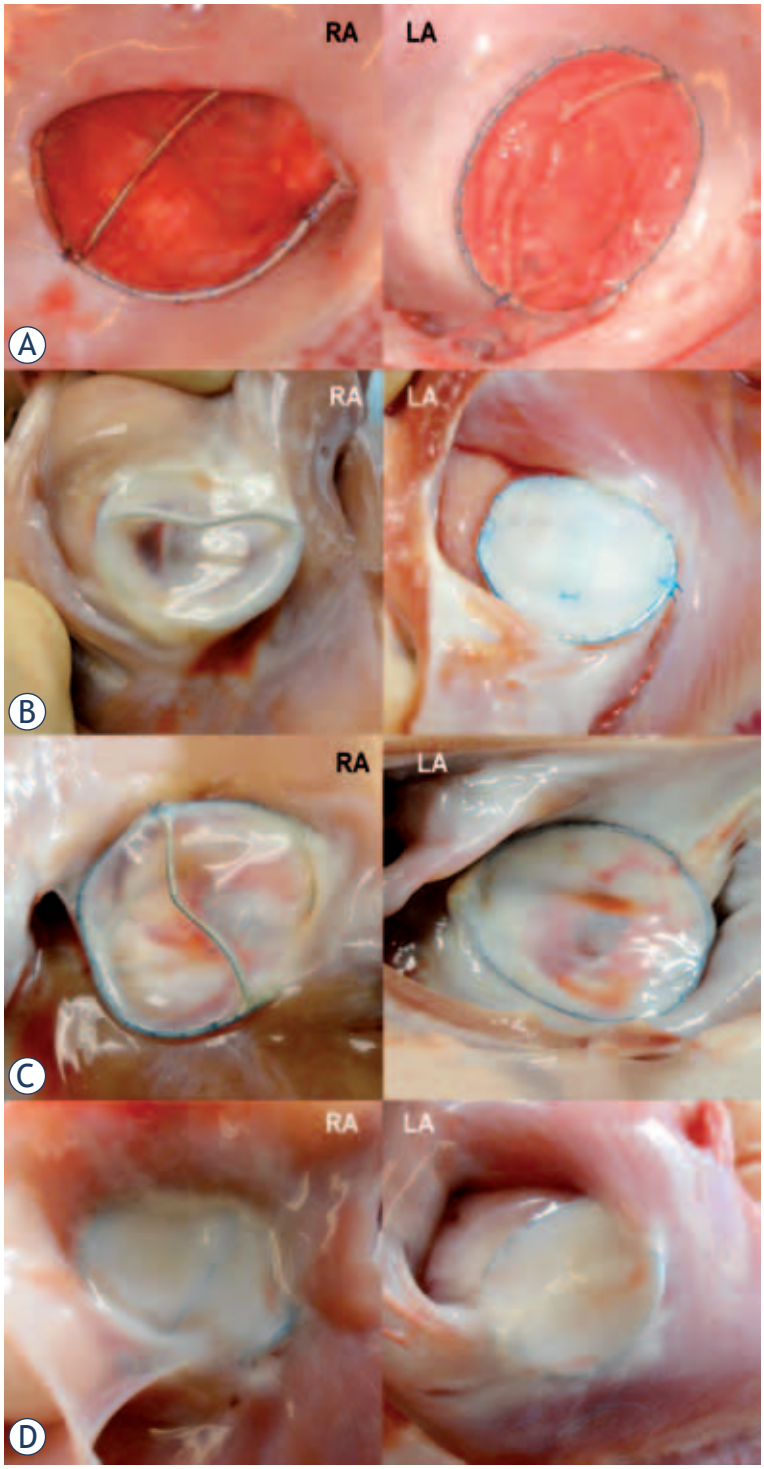

FIGURE 2. Gross specimens of the deployed double Biodisks into the adult sheep ASDs.

A. Three hours after deployment, thin layers of early thrombus cover right and left atrium disk of the 28 mm device.
B. At 3 months, the 18 mm DBD is almost completely incorporated into myocardium. Glistening disk surfaces indicate complete endothelization.
C. At 6 months, the DBD is almost completely incorporated into myocardium of the right and left atrium.
D. At 12 months, the DBD is completely incorporated into myocardium of the right and left atrium.

were created by puncture and balloon dilation at the fossa ovalis, in the other 2 sheep by balloon dilation of the existing PFO. The stretched ASD size immediately after balloon dilation ranged from 13 to 15 mm (mean 14.1 ± 0.73 mm). At 2 weeks prior to DBD placement the ASD size ranged from 9 -13 mm with a mean 10.06 ± 1.37 mm (Table1).

All DBDs were successfully implanted and none spontaneously embolized on release or on follow up. In the first two acute animals, the DBDs were easily retracted into the delivery sheath after their partial or full deployment and redeployed into the ASD. The two intentionally embolized DBDs into the right atrium were safely retrieved and new DBDs were placed into the ASD. Angiocardiograms after DBD deployment showed good placement and absence of shunting. ICE evaluation with Doppler studies did not reveal any shunting around the DBDs. EKGs did not demonstrate any arrhythmias. In the chronic studies, the DBDs were highly visible on x-ray (Figure 1E). There were no fractures of the device frame. Follow up angiocardiograms and ICE Doppler studies documented complete closures of the ASDs and no shunting in all 8 sheep (Figure 1F).

Gross examination

The implanted DBDs in all animals, acute and chronic, were well self-centered and attached to the ASDs with good apposition to the interatrial septum and adjacent myocardium (Figure 2). Both discs were flattened against the intra-atrial septum and held in place by the connection between the DBD. The DBDs did not obstruct blood flow in to coronary sinus or pulmonary veins nor did it compromise mitral or tricuspid valves. In two acute animals euthanized 3 hours after DBD placement both discs were covered by thin red layer of early thrombus (Figure 2A). In two animals euthanized at 6 weeks, the SIS surfaces on both disks were shiny, transparent and without thrombus. Disks were partially incorporated into the myocardium. In three animals sacrificed at 12 weeks, DBD rings were almost completely incorporated into the myocardium wall. The SIS of the left and right atrium disks were well apposed to the myocardium excluding the ASD opening. The SIS was glistering and shiny indicating endothelization (Figure 2B). The SIS was less transparent than that at 6 weeks. At 24 weeks and 52 weeks DBDs were free from adjacent important cardiac structures in all of the specimens. The SIS membranes of the DBDs were positioned with a good apposition across the ASD

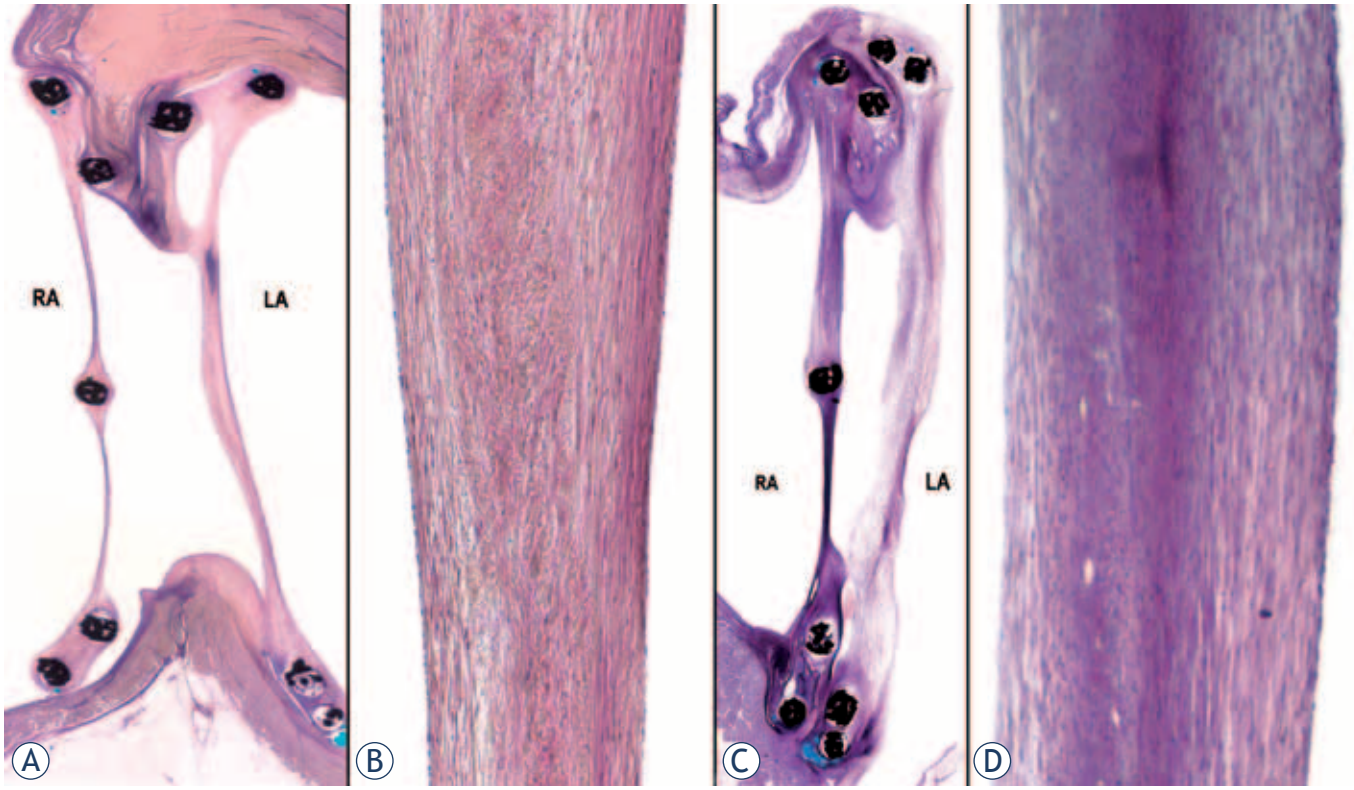

FIGURE 3. Histologic cross sections of the deployed double BioDisks into the adult sheep ASDs.

A. At 3 months, the right atrial disk of the 18 mm device is apposed and the left atrial disk is incorporated into myocardium. The crossbar is incorporated into the right disk. The disk thickness ranges between 0.1 to 0.25 mm at the right atrial disk and between 1 to 2 mm at the left atrial disk. (Low magnification Hand E)

B. At 3 months the center of the left disc is partially remodeled into neointima/connective tissue and contains no inflammatory cells. Remnant SIS is visible in the core of the leaflet. (H and E stain, 40x)

C. At 6 months, the 18 mm disks are completely imbedded into myocardium and the distance between them ranges from 2 to 3 mm. The crossbar is incorporated into the right disk. Right atrial disk thickness ranges from 0.4 to 0.8 mm and left atrial disk thickness from 1.5 to 3 mm. (Low magnification Hand E)

D. At 6 months the center of the right atrial disk is remodeled into mature neointima/connective tissue and contains no inflammatory cells. Remnant SIS is not visible. All luminal surfaces are lined by endothelium (H and E stain, 40x).

TABLE 1. Results of percutaneous atrial septal defect closure

Animal No	Weight kg	Stretched ASD diameter mm		DBD size mm	Placement successful Yes or No	Follow Up Weeks	ICE Follow Up
		day 1	day 14				
1	49.8	15	acute	28	Y	acute	no shunt
2	57.6	13	acute	23	Y	acute	no shunt
3	60.7	14	11	23	Y	6	no shunt
4	61.6	14	10	23	Y	6	no shunt
5	44.3	15	9	18	Y	12	no shunt
6	47.4	14	9.5	18	Y	12	no shunt
7	53.2	14	9	18	Y	12	no shunt
8	46.3	13	10	18	Y	24	no shunt
9	64.0	15	13	23	Y	24	no shunt
10	46.2	14	9	18	Y	24	no shunt
11	40.1	14	9.2	18	Y	52	no shunt
12	52.2	15	9	18	Y	52	no shunt

ASD=atrial septal defect, DBD=Double BioDisk, Y=yes, ICE= Intra-cardiac Echogram

and fused together with myocardium (Figure 2C). At 12 months, the disks apposition and incorporation into adjacent myocardium was complete, in the right and in the left atrium (Figure 2D). Glistening SIS surfaces were seen in all specimens. The delivery crossbars of the DBDs were covered with shiny tissue and partially fused with device.

Histological evaluation

Histological sections through the center of the DBDs exhibited well covered ASDs by the device disks. At follow up, there was progressive device apposition and incorporation of disks with adjacent myocardium, progressive SIS remodeling into neointima-connective tissue and progressive SIS endothelization. At six weeks follow up, almost 85% of the rings on the right and 50% on the left atrial side were incorporated into the myocardium and surrounded by fibrous tissue less than 200 microns thick. The residual ring parts not embedded in the myocardium were surrounded by fibrous connective tissue and lined by endothelium. The SIS thickness ranged from 0.1 mm in the center to 2.5 mm near the rings and was covered by spindle shaped cells forming a neointima. Flat endothelium covered most of the SIS. The crossbars were surrounded by fibrous tissue. Only minimal inflammatory changes with a few lymphocytes were seen. At 3 months, approximately 95% of the rings on the right side and 60% on the left side were embedded into adjacent myocardium and surrounded by fibrous tissue less than 0.1 mm thick. The SIS showed progressive remodeling into fibrous connective tissue. The SIS disks were 0.1-0.5 mm thick at their centers and 1.5- 3 mm at their periphery. The right disk was thinner than the left disk (Figure 3AB). All discs surfaces were covered by mature endothelium. Crossbars were surrounded by neointima and incorporated into disks. At 6 months, the disks apposition and incorporation into adjacent myocardium was almost complete, 96% in the right atrium and 85% in the left atrium (Figure 3C). The ring wires not embedded into the myocardium were surrounded by neointima lined by endothelium. The SIS discs were composed of mature neointima consisting of fibrous connective tissue. SIS collagen fibers were not observed indicating complete remodeling (Figure 3D). The disks were 0.4-0.9 mm thick at the center and 1.5-3mm at the periphery. The crossbars were incorporated into the disk (Figure 3C). All lumen surfaces of the discs and crossbars were covered by flat mature endothelium.

Discussion

Adult sheep were used to test the DBD for several reasons. We reported several minimally invasive studies in sheep and we are familiar with this model.[9,10] The size of their heart size approximates the size of the human heart and allows large closure devices to be tested. Adult sheep have a stable body size and when compared to swine that continue to grow and put on weight.[6,11] They allow for long-term follow-up. In addition, the sheep coagulation and fibrinolytic systems are closer to that of humans compared to those in canine or swine.[12] Since the DBD cover is composed of swine origin, SIS is a xenogenic biomaterial to sheep.[13] The cardiac anatomy of sheep with a more anteriorly positioned heart has a significantly steeper interatrial septum compared to humans that can be challenging for TS puncture. A long TS needle was developed corresponding to the length of sheep body with a curved needle tip allowing TS punctures to be easily and safely accomplished in all of our animals.[8] We always punctured and established the ASDs in the area of the fossa ovalis because it allows for a mature stable ASD size. Two weeks after its creation, the ASD size in our animals decreased slightly from a mean 14.1 ± 0.73 mm to a mean 10.06 ± 1.37 mm. The ASD creation was not attempted in the septum secundum because in sheep this structure is significantly thicker than it is in humans. Previous experience showed us that punctures followed by dilations at the septum secundum do not lead to stable ASDs. They heal in two weeks.[8]

This is our third generation device for cardiac septal closure. The first one, the Monodisk, was developed in the early nineties.[4] It consisted of a stainless steel ring covered with two layers of nylon mesh that was positioned on the left atrial ASD side. Three coiled stainless steel wires on the back side of the Monodisk served for its delivery and anchoring at the right atrial ASD side. A 9F introducing sheath was used for its delivery. Six months follow-up studies in canines showed it was effective for closure of ASD 8-10 mm in size. However problems with the Monodisk were its rigid frame, complex delivery, difficult post delivery retrieval and our inability to find a FDA approved nylon mesh alternative.

The second generation of the disk closure device – the Biodisk – was developed about 15 years later after we gained experience with nitinol and SIS. The nitinol that was used as a pliable material for the disk frame and the biomaterial SIS was used for the covering. The Biodisk was intended for closure

of PFO. It consisted of one disk inserted into the left atrial ASD side. Nitinol wires of the disk were covered by platinum coil and a crossbar attached to the disk was used for delivery and for anchoring on the right atrial ASD side. An 8F sheath was used for Biodisk delivery. Initial testing in piglets showed its easy delivery, good retrievability and long-term effectiveness for closure of PFO measured with the 10-14 mm balloons.[6]

The DBD with two disks was developed for closure of ASD. The Biodisk with only one disk would not be sufficient for the occasional complex anatomy and large size of ASDs. The DBD feasibility study demonstrated that this new bioprosthetic device has excellent potential for ASD closures. The DBD was easy to deploy, it self-centered during deployment and covered the entire ASD without encroachment on structures in both atria. When needed, the DBD could be repositioned or retrieved if released inappropriately or lost as shown after its intentional embolization. The DBD showed excellent effectiveness for ASD closures and no residual shunting was seen at ICE examinations with color Doppler studies. The gross studies showed good apposition of the disks to the septum and myocardium without compromise of valves and other cardiac structures. At 3 hours after DBD placement, a thin layer of early thrombus covered the SIS disks as initial the phase of neointimal formation. Otherwise, no thrombus was found on the follow-up studies as the DBDs rapidly endotheliolized. The histologic follow-up studies then revealed progressive apposition leading to full incorporation of the DBD disks with adjacent myocardium, progressive SIS remodeling into connective tissue and complete DBD endothelization. These healing processes were well demonstrated on the histologic DBD cross sections. The space between the disks, originally separated by thick septum secundum and residual septum primum progressively decreased by neointimal formation and some atrophy of residual septum. The neointimal formation started at the disks periphery, extended to the center of the disks. It was more pronounced on the left atrial SIS disks. The 6 and 12 months follow-up showed complete SIS remodeling into the heart connective tissue.

The DBD feasibility study did not compare the biomaterial SIS with septal occluders covered with synthetic fabrics. This was done in detail by Jux *et al.* in 2006.[14] They compared the first septal occluder device with biodegradable matrix, the Biostar covered with the purified intestinal collagen layer (ICL) with the Starflex covered with a knitted polyester fabric. The ICL, similar to SIS, originated from porcine small intestinal mucosa and both had similar thickness between 150-200 microns. A 10F sheath was used for deployment of both the Biostar and DBD. The study by Jux *et al.* in young sheep that from 7 days to 2 years showed distinct advantages of the biomaterial matrix. Biostar had decreased thrombogenicity, particularly when the device was heparin coated. It showed accelerated healing with early endothelization and low immune response with fast ICL remodeling into connective cardiac tissue. Because of these positive results, the Biostar has already been applied successfully in treatment of ASD in children and adults.[15,16,17]

Conclusions

Long term both right and left atrial SIS disks were remodeled into the heart connective tissue, so that only a minimal amount of metal spring material has been left behind. ASD closure with the Double BioDisk is safe and effective in adult sheep.

Acknowledgments

This study was sponsored by Cook Medical, Bloomington, Indiana. The authors thank William E. Schoenlein and the team from Purdue University, West Lafayette, Indiana and Garry Pressler and the team from MED Institute, Inc., West Lafayette, Indiana for their assistance with the animal experiments and the histology. The authors thank Sheri Imai-Swiggart for her assistance.

References

1. King TD, Mills NL. Nonoperative closure of atrial septal defect. *Surgery* 1976; **75:** 383-8.
2. Rao PS. History of atrial septal occlusion devices. In Rao PS and Kern MJ: *Catheter based devices: for the treatment of non-coronary cardiovascular disease in adults and children.* Philadelphia: Lippincott Williams&Wikins; 2003. p. 3-9.
3. Majunke N, Sievert H. ASD/PFO Devices: What Is in the Pipeline? *J Intervent Cardiol* 2007; **20:** 517-23.
4. Pavcnik D, Wright KC, Wallace S. Monodisk: device for percutaneous transcatheter closure of cardiac septal defects. *Cardiovasc Intervent Radiol* 1993; **16:** 308-12.
5. Kim MS, Klein AJ, Carroll JD. Transcatheter closure of intracardiac defects in adults. *J Interv Cardiol* 2007; **20:** 524-45.
6. Pavcnik D, Tekulve K, Uchida B, Pavcnik Arnol M, Van Alstine WG, Keller FS, et al. Biodisk: a new device for closure of patent foramen ovale. *Catheter Cardiovasc Interv* 2010; **75:** 861-7.

7. Ni RF, Kranokpiraksa P, Pavcnik D, Kakizawa H, Uchida BT, Keller FS, et al. Testing percutaneous arterial closure devices: An animal model. *Cardiovasc Intervent Radiol* 2009; **32:** 313-6.

8. Uchida BT, Pavcnik D, Shimohira M, Choi YH, Jeromel M, Keller FS, et al. New coaxial transseptal needle for creation of atrial septal defects in adult sheep. *Cardiovasc Intervent Radiol* 2011; **34:** 620-5.

9. Kranokpiraksa P, Pavcnik D, Kakizawa H, Uchida BT, Jeromel M, Keller FS, et al. Hemostatic efficacy of chitosan-based bandage for closure of percutaneous arterial access sites: An experimental study in heparinized sheep model. *Radiol Oncol* 2010; **44:** 86-91.

10. Wei Lu, Pavcnik D, Uchida B, Park WK, Liu L, Timmermans HA, et al. The ovine jugular vein as a model for interventional radiology procedures. *Radiol Oncol* 2008; **42:** 59-65.

11. Jeromel P, Pavcnik D. Infrahepatic caudal/inferior vena cava interruption with azygos/hemiazygos continuation. Vascular anomaly in swine. *Radiol Oncol* 2010; **44:** 149-52.

12. Narayanawamy M, Wright KC, Kandarpa K. Animal models for atherosclerosis, restenosis, and endovascular graft research. *J Vasc Interv Radiol* 2000; **11:** 5-17.

13. Badylak SF. The extracellular matrix as a biologic scaffold material. *Biomaterials* 2007; **28:** 3587-93.

14. Jux C, Bertram H, Wohlsein P, Bruegmann M, Paul T. Interventional atrial septal defect closure using a totally bioresorbable occluder matrix: development and preclinical evaluation of the BioSTAR device. *J Am Coll Cardiol* 2006; **48:** 161-9.

15. Hoehn R, Hesse C, Ince H, Peuster M. First experience with the biostar-device for various applications in pediatric patients with congenital heart disease. *Catheter Cardiovasc Interv* 2010; **75:** 72-7.

16. Morgan G, Lee KJ, Charturvedi R, Benson L. A biodegradable device (Biostar) for atrial septal defect in children *Catheter Cardiovasc Interv* 2010; **76:** 241-5.

17. Mullen MJ, Hildick-Smith D, De Giovanni JV, Duke C. BioSTAR evaluation study (BEST): a prospective, multicenter, phase I clinical trial to evaluate the feasibility, efficacy, and safety of the BioSTAR bioabsorbable septal repair implant for the closure of atrial-levels shunts. *Circulation* 2006; **114:**1962-7.

research article

Outcome of MRI-guided vacuum-assisted breast biopsy – initial experience at Institute of Oncology Ljubljana, Slovenia

Marta Zebic-Sinkovec[1], Kristijana Hertl[1], Maksimiljan Kadivec[1], Mihael Cavlek[1], Gasper Podobnik[1], Marko Snoj[2]

[1] Department of Radiology, Institute of Oncology Ljubljana, Ljubljana, Slovenia
[2] Department of Surgery, Institute of Oncology Ljubljana, Ljubljana, Slovenia

Radiol Oncol 2012; 46(2): 97-105.

Received 13 October 2011
Accepted 28 November 2011

Correspondence to: Marta Zebič-Šinkovec, MD, Department of Radiology, Institute of Oncology Ljubljana, Zaloška 2, 1000 Ljubljana, Slovenia. Phone: +386 1 5879 940; Fax: +386 1 5879 407; E-mail: mzebic@onko-i.si

Disclosure: No potential conflicts of interest were disclosed.

Background. Like all breast imaging modalities MRI has limited specificity and the positive predictive value for lesions detected by MRI alone ranges between 15 and 50%. MRI guided procedures (needle biopsy, presurgical localisation) are mandatory for suspicious findings visible only at MRI, with potential influence on therapeutic decision. The aim of this retrospective study was to evaluate our initial clinical experience with MRI-guided vacuum-assisted breast biopsy as an alternative to surgical excision and to investigate the outcome of MRI-guided breast biopsy as a function of the MRI features of the lesions.

Patients and methods. In 14 women (median age 51 years) with 14 MRI-detected lesions, MRI-guided vacuum-assisted breast biopsy was performed. We evaluated the MRI findings that led to biopsy and we investigated the core and postoperative histology results and follow-up data.

Results. The biopsy was technically successful in 14 (93%) of 15 women. Of 14 biopsies in 14 women, core histology revealed 6 malignant (6/14, 43%), 6 benign (6/14, 43%) and 2 high-risk (2/14, 14%) lesions. Among the 6 cancer 3 were invasive and 3 were ductal carcinoma in situ (DCIS). The probability of malignancy in our experience was higher for non-mass lesion type and for washout and plateau kinetics.

Conclusions. Our initial experience confirms that MRI-guided vacuum-assisted biopsy is fast, safe and accurate alternative to surgical biopsy for breast lesions detected at MRI only.

Key words: breast cancer; MRI; MRI guided vacuum assisted biopsy

Introduction

Magnetic resonance imaging (MRI) is a method for the detection of many cancers.[1,2] Contrast-enhanced magnetic resonance imaging (CE-MRI) is currently the most sensitive additional imaging method for the detection of invasive breast carcinoma and seems to be able to detect ductal carcinoma in situ (DCIS), especially high grade DCIS without necrosis.[3] Compared with studies of MRI performance published in the 1990s, the specificity of breast MRI has gradually improved, mostly because of improved technology and increased reader experience.[4]

Suspicious MRI detected lesions are not always detectable by mammography and ultrasound. Positive predictive value for lesions detected by MRI alone ranges between 15% and 50% and it depends upon patient selection and MR interpretation algorythm.[5-8] MRI guided procedures (needle biopsy, presurgical localisation) are mandatory for lesions visible at MRI only, when they look suspicious and have potential influence on therapeutic decision.[9] MRI-guided vacuum assisted biopsy

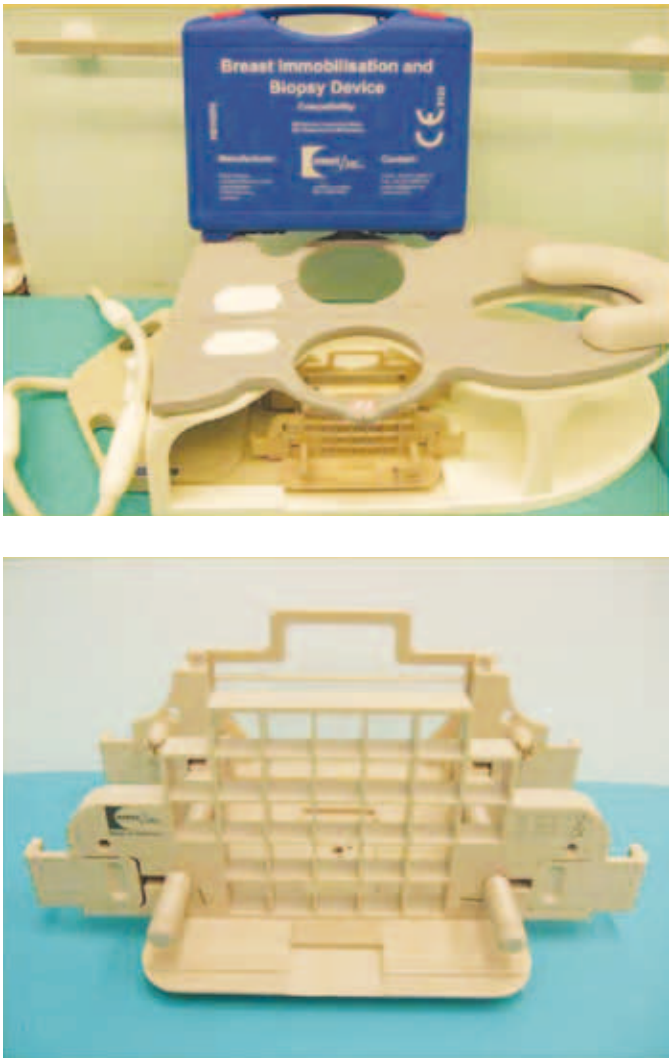

FIGURE 1 A,B. Biopsy coil device. Photographs show a four-channel breast biopsy coil with positioning device (A) and a grid-positioning device (B).

(MR-VAB) was pioneered by Sylvia H. Heywang-Köbrunner and first described in 1999.[10]

Since then, the technique has been optimized and its reproducibility proven in an European multicenter study.[11] Some other authors have published their experience with this method and also with other vacuum devices.[12,13] In 2006 there was an interdisciplinary consensus conference in Nordestedt, Germany.[14] The purpose of this meeting was to determine technique and optimize quality assurance protocols. MR-VAB was first time performed at our institution in 2008 and since then it has become routinely used in our practice.

The aim of the present retrospective study was to evaluate the initial clinical experience with MRI-guided vacuum-assisted breast biopsy as an alternative to surgical excision and to investigate the outcome of MRI-guided breast biopsy as a function of the MRI features of the lesions.

Patients and methods

Patients and lesions

The selection criteria for the MR-guided biopsy were the presence of Breast Imaging Reporting and Data System (BI-RADS) 5, BI-RADS 4 and BI-RADS 3 lesions that were visible by CE-MRI only. Initially, fifteen patients with 15 lesions had been referred for MR-VAB. In 1 patient the lesion could not be reproduced on the preinterventional planning MRI because of the technical problem. The median age of patients was 51 years (range, 35-71 years). In 6 patients mammography performed before biopsy showed dense breast or benign changes, in 2 patients asymmetry was described, in three cases there was architectural distortion only in one projection, in two cases mammographic and MRI findings were discordant and one patient was too young to perform mammography. In 7 patients sonography performed before biopsy failed to reveal a sonographic correlate and in 4 others sonography and MRI findings were discordant. In 3 patients sonography was not performed at the discretion of the radiologist because the possibility of identifying a sonographic lesion was presumed to be very low.

MRI findings before biopsy

Except the MRI examinations of 2 women who underwent MRI at another institution, breast MRI was performed using a 1.5-T magnet (Magnetom Avanto, Siemens Medical Solution, Erlangen, Germany) with a dedicated bilateral breast surface coil with a prone position. The imaging protocol and parameters were as follows: axial T1-weighted image (TR/TE, 593/13) and short time inversion recovery (STIR) (TR/TE/TI, 12390/76/130) of both breasts were obtained with 3 mm slice thickness. Next, T1-weighted images were acquired using a 3D fast low-angle shot pulse sequence (FLASH) through both breasts (TR/TE 7, 8/4, 72, flip angle 25°). Precontrast images were obtained over a 313 × 448 matrix in the axial plane with a slice thickness of 1.0 mm with distance factor 20% before administration of the contrast agent. Then, contrast-enhanced dynamic imaging was performed with an injection of 0.1 mmol per kilogram of body weight of gadopentetate dimeglumine (Magnevist, Schering, Berlin, Germany); five se-

quential contrast-enhanced images were acquired at every 1 min 23 s. The precontrast images were then subtracted from the corresponding postcontrast images on a pixel-by-pixel bias with the use of the standard software subtraction function available on our console. Two radiologists reviewed all imaging studies in consensus. The BI-RADS MRI lexicon was used.

MRI-guided biopsy

MRI-guided vacuum-assisted breast biopsy was performed using a 1.5-T magnet (Magnetom Avanto, Siemens, Erlangen, Germany) with MRI-supported Breast Immobilization and Biopsy System with the 4-channel breast coil (Noras MRI products GmbH, Höchberg, Germany) in prone position. Marker Block filled with diluted gadolinium contrast agent was used for reference point. The positioning device has medial and lateral compression plates for moderate compression.

An axial T1- weighted images were acquired using a 3D FLASH through both breasts (TR/TE 7, 6/4, 72, flip angle 25°). Precontrast images were obtained over a 256 × 320 matrix in the axial plane with a slice thickness of 1.0 mm with distance factor 20% before administration of the contrast agent. Twenty seconds after contrast agent had been in-

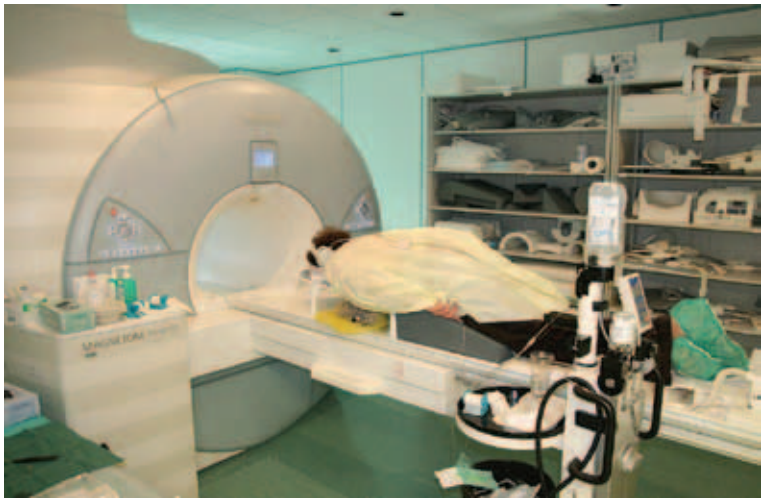

FIGURE 2. 1.5 T Magnetom Avanto (Siemens, Erlangen, Germany). Patient lie face down on the exam table. Breast is moderately compressed in the mediolateral direction.

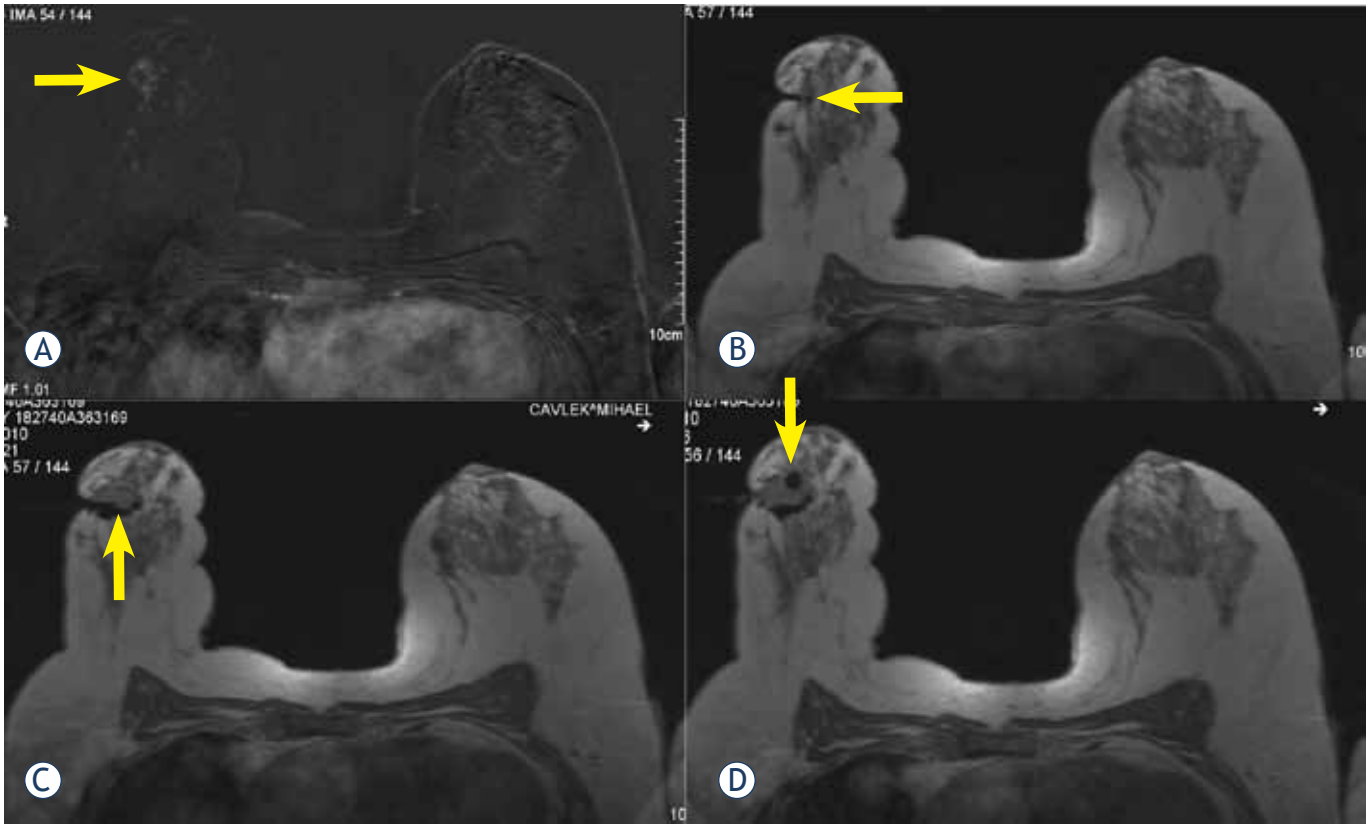

FIGURE 3A-D. MRI-guided biopsy using axial, contrast-enhanced FLASH 3D T1W images. The pre-biopsy fat-suppressed image (A) shows an enhancing lesion in the right breast. The biopsy needle (B) is seen after localization, along with the lesion. Following the biopsy (D) the small magnetic susceptibility artefact due to the clip in situ is seen.

A

B

FIGURE 4. MRI-guided biopsy device (a) is inserted into breast to acquire tissue specimens (b)

jected; another axial T1-3D FLASH sequence was performed. 0.1 mmol per kilogram of body weight of gadopentetate dimeglumine (Magnevist, Schering, Berlin, Germany) was injected with a rate of 2 ml/s using an automated injector (CT/MRI injector Mississippi, Ulrich medical, Ulm, Germany). The volume of interest was selected to include the compression device and a Marker Block.

Biopsies were performed with a 9-gauge MRI compatible vacuum-assisted biopsy device (ATEC, Suros Surgical Systems, Indianapolis, USA). CAD stream diagnostic and interventional guidance tool, Version 4.1 (Confirma, Washington, USA) was used to target coordinates for biopsy. An axial T1-3D FLASH sequence was performed to control the needle placement.

The biopsy device was then placed into the breast through the coaxial needle. Multiple samples were obtained by turning the needle clockwise and around its axis. The biopsy site was marked with a titanium clip (ATEC TRI mark TD 13 – MR Biopsy Site Marker). "Postclip" axial 3D FLASH was performed to assess clip deployment. After biopsy, the breast is compressed with ice, sterile strips are applied, and a sterile gauze bandage is applied.

MRI-guided wire localization

The procedure for wire placement was the same as that for breast biopsy. After localizing the lesion, a cannula with a wire loaded into it was inserted to the required depth. After confirming the position on axial images, the wire was placed into the lesion and the position was verified with a repeat axial scan. The wire gives a thin linear magnetic susceptibility artefact, and the lesion can be seen near the tip of the wire. It was then fixed with a lock at the skin surface to prevent dislodgement. The same positioning device for lesion localization with an MRI-compatible needle with a hooked wire, made of a special alloy for easy and safe penetration of the solid tumour tissue (TULOC, Somatex, Germany) were used. It has a diameter of 0.95 mm and it is 90 mm long. The wire was fixed into the lesion with the hooks at the end of the wire and onto the skin with a lock which prevents any dislodgement of the wire.

Indication for MRI and MRI-VAB

The indications for MRI were classified into a screening setting and a diagnostic setting.

The indications for (MR-VAB) were:

MRI only seen lesions - targeted » second look« ultrasound and/or mammography showed normal or benign findings or findings that were not concordant with MRI findings.

Ultrasound was not performed at the discretion of radiologist, because the probability that lesion would be seen by ultrasound was very low.

Management, follow-up, data collection, analysis

The MR-VAB was presumed to be adequate if imaging performed immediately after biopsy showed

TABLE 1. MRI findings of 14 targeted lesions and the probability of malignancy

Features	No. of Lesions/ Total No. of Lesions (%)	No. of Malignant Lesions/ No. of Lesions (%)
Lesion type		
Focus	0	0
Mass	5/14 (36)	1/5 (20)
Nonmass	9/14 (64)	5/9 (55)
Total	14/14 (100)	6/14 (43)
Morphology		
Margin of mass		
Smooth	2/14 (14)	0/2 (0)
Nonsmooth	3/14 (21)	1/3 (33)
Distribution of Nonmass		
Regional	1/14 (7)	1/1 (100)
Segmental	1/14 (7)	1/1 (100)
Ductal	6/14 (43)	2/6 (33)
Focal areas	1/14 (7)	1/1 (100)
Total	9/14 (64)	5/9 (55)
Kinetic feature		
Persistent	1/14 (7)	0/1 (0)
Plateau	6/14 (43)	2/6 (33)
Washout	7/14 (50)	4/7 (57)
Total	14/14 (100)	6/14 (43)
Signal intensity T2-weigted images		
High	4/14 (23)	2/4 (50)
Intermediate	8/14 (57)	3/8 (37)
Low	2/14 (14)	1/2 (50)
Total	14/14 (100)	6/14 (43)

a cavity that unequivocally included the area of highest suspicion. Two view mammograms were also performed after biopsy to confirm clip localization. Surgical follow–up was recommended for all malignant lesions, for one high-risk lesion, and in one case, when the benign lesion was judged to have pathology result that was discordant with imaging findings. 6 of the 6 malignant lesions and 1 of the 2 high-risk lesions were operated upon at our institution and confirmed by operative histology. In 4 cases breast ablation and in 3 cases sentinel node and occult lesion localization (SNOLL) under X-ray guidance and surgical excision was performed. The reference standards were core biopsy results and postoperative histology. Medical records were reviewed for patient age, personal history of breast cancer, indication for MR mammography, radiologic results, histopathologic results and follow-up results. Histopathologic results were examined on the basis of pathologic report of MR-VAB and postoperative histology. The probability of malignancy for an MRI abnormality was calculated as the ratio between the number of lesions with pathologically proven malignancy and the number of biopsied lesions. We investigated the probability of malignancy for MRI abnormalities according to the MRI features of the lesions.

The retrospective study was carried out according to the Helsinki Declaration.

Results

The biopsy was technically successful in 14 (93%) of 15 women. Median age was 51 years (range, 35-71 years). In 1 woman the biopsy was deferred because of a technical problem.

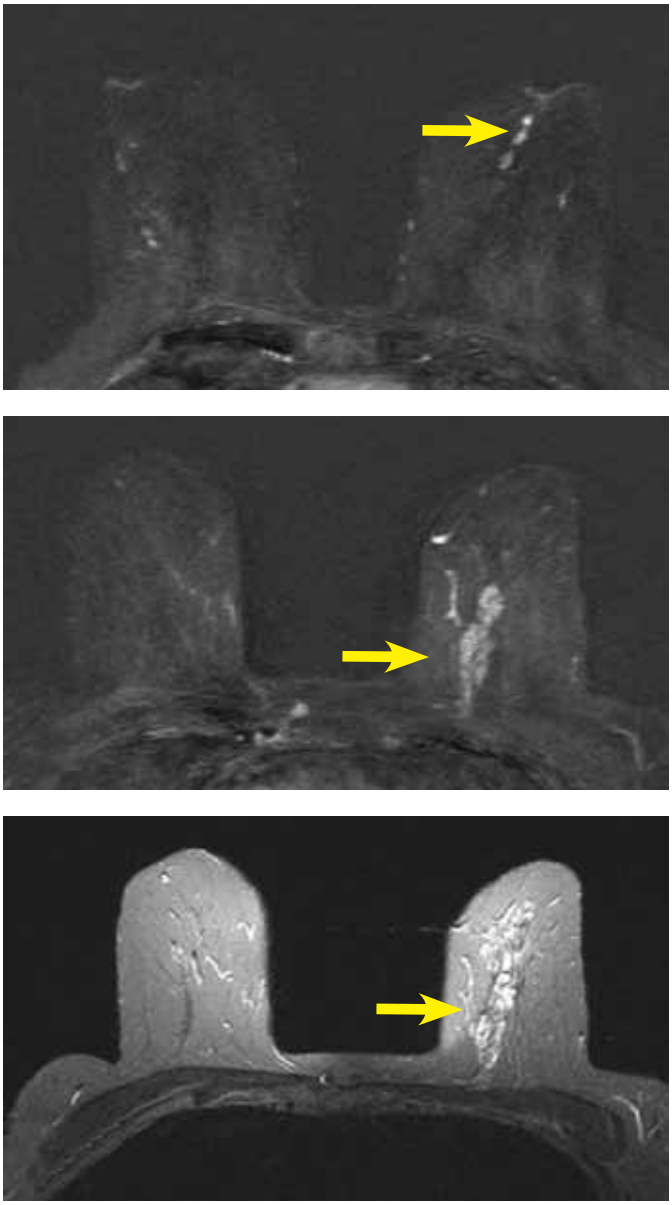

FIGURE 5A-C. 65 year old woman with a history of nipple-discharge in her left breast. Mammographic asimmetry. Ultrasound images showed dilated empty ducts, ductography was suspicious for papilloma. Axial T1-weighted subtracted image after Gadolinium injection(2nd minute) .(a) small round sharply circumscribed masses within a duct sistem–papillomas.(b) segmental, clumped, asymmetric enhancement, fast initial increase and postinitial wash out. (c) high signal intensity on T2 –weighted image - BI-RADS 5. Pathologic diagnosis through MRI-guided vacuum-assisted biopsy was massive DCIS with foci of microinvasion.

TABLE 2. The characteristics of the malignant lesions

Site of the lesion	Right	2
	Left	4
Type of the lesion	MLE	1
	NMLE	5
T2-weighted images Signal intensity	High	2
	Intermediate	3
	Low	1
Kinetics	Rapid-plateau	2
	Wash-out	4
Size	2.6cm (range; 0.8 – 6)	
Histologic type Of cancer	Invazive lobular	2
	Invazive tubular	1
	DCIS	3

MLE = masslike enhancemnt; NMLE = nonmasslike enhancement; DCIS = ductal carcinoma in situ

Fourteen lesions underwent biopsy, among them 4 lesions were categorized as BI-RADS 5, 8 lesions as BI-RADS 4 and 2 as BI-RADS 3. The median size of these 14 lesions was 2 cm (range, 0.8-6 cm). Among those 14 lesions, 4 were located between lower quadrants, 2 in lower outer quadrant, one between outer quadrants, 3 in upper outer quadrant, 3 between upper quadrants and one in upper inner quadrant. For 13 of the14 lesions a single skin incision was made; for one lesion, a second incision was required for repositioning the stylet before biopsy. The median number of specimens obtained per lesion was 8 (range, 4-17). In 11 lesions, only a single round of tissue acquisition was necessary, in 3 lesions the MRI after the first round of tissue acquisition did not ensure lesion sampling, and a second round of tissue acquisition was performed. Clip placement was attempted in 14 lesions and was successful in 13 (93%). The median time to perform MRI-guided vacuum-assisted biopsy, from the original axial localizing images to the final images obtained after clip deployment was 39 min (range, 28-60 min). A complication was encountered in 1 of 14 patients (7%). The complication was a clinical haematoma.

Cancer was found in 6 of 14 lesions and in 6 of 14 women, based on the review of vacuum-assisted biopsy and surgical histology. Six were benign lesions and 2 were high-risk lesions. In two cases MR-VAB was considered uncertain according to the correlation of imaging and histopathology, therefore surgical biopsy and re-biopsy were performed.

Among these 6 cancers (Figures 1-6) 3 were invasive cancers (2 invasive lobular carcinoma and 1 invasive tubular carcinoma) and other 3 were DCIS (1 massive DCIS with foci of well differentiated invasive carcinoma). Three of 6 cancers were found in women with personal history of breast carcinoma. The median size of the MRI lesions in

these 6 cancers was 2.6 cm (range 0.8-6.0 cm). MRI-guided vacuum-assisted biopsy revealed 2 high-risk lesions, in one case there was atypical ductal hyperplasia and in other papilloma. Papilloma was operated on and was proved to be benign.

MRI review suggested that the MRI target might have been excised at vacuum-assisted biopsy in one of these cancers and was sampled in five. Surgery was performed in our institution on 6 of the 6 malignant lesions on 1 of the 2 high-risk lesions and on 1 lesion with discordant result. Finally, 6 of the 14 biopsy lesions were malignant the overall probability of malignancy for an MRI abnormality was 43% (6/14).

The MRI features of the lesions and the probabilities of malignancy according to lesion features are summarized in Table 1. The characteristics of malignant lesions are summarized in Table 2.

Discussion

MRI-guided-vacuum assisted biopsy has many advantages compared with other biopsy methods for the diagnosis of MRI-detected lesions. In our initial experience with this method, the technical success rate was 93%. In 57% of women MR-VAB yielded benign results and spared most women with MRI-detected lesions the need for the surgical excision. With MR-VAB a continuous suction and acquisition of larger tissue volume is possible. Only MR-VAB allows good visualisation of the cavity and/or direct visualisation of the size reduction of the enhancing lesion. It retrieves larger volume of tissue, so we have fewer inadequate specimens. If a lesion is deemed to be not accessible to MR-VAB, MR-guided needle localization followed by surgery can be performed. Our results are in agreement with previous findings in literature.[15-19]

MR-VAB can be performed quickly.[20] Average time to perform biopsy of a single lesion was 39 min in our study. Lesion visibility decreases rapidly over time during the biopsy, due to wash out of contrast in the lesion. The lesion must be identified immediately after the contrast injection. Sampling is dependent on identification and immobilizing the lesion. Lesions that underwent MR-VAB were rated by 2 experienced radiologists in consensus. The BI-RADS MRI lexicon was used. The publication of BI-RADS MRI lexicon in 2003 was an important step toward a standardized approach on the lesion description, but should be regarded as work in progress. Since then some studies have been published about the value of the BI-RADS lexicon

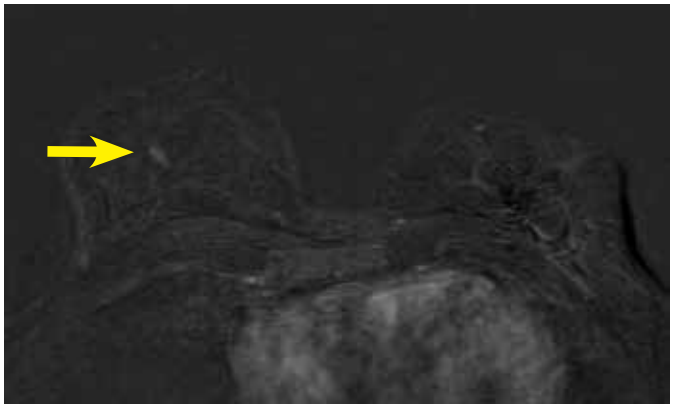

A

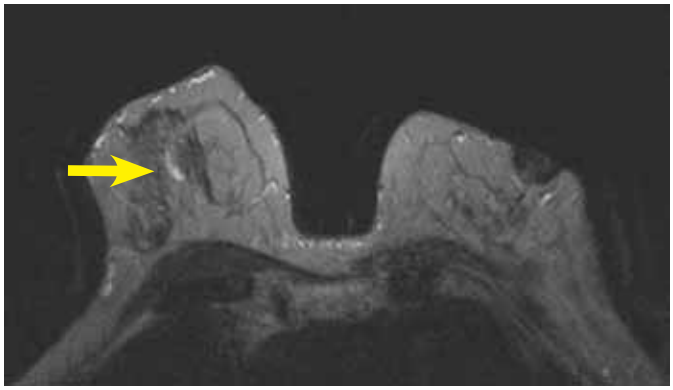

B

FIGURE 6AB. 47 year old woman with history of invasive breast carcinoma 10 years ago in her left breast. Retraction of mammila on the right, mammograpic dense breast and benign calcifications. First look and second look ultrasound images showed a cyst. Axial T1-weighted subtracted image after Gadolinium injection (2nd minute).(A) 8x3 mm ductal - linear homogenous, asymmetric enhancement, fast initial increase with postinitial plateau (B) high signal intensity on T2-weighted images, categoriaztion BI-RADS 4. MRI-guided vacuum-assisted biopsy revealed high-grade DCIS withouth microcalcification.

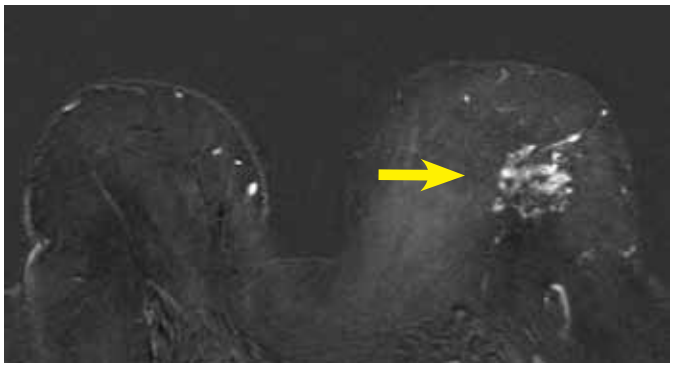

FIGURE 7. 64-year old woman with history of invasive breast carcinoma in her right breast 10 years ago. Mammography and ultrasound images showed discrete architectural distortion in the left breast. US-guided core biopsy was inconclusive. Axial T1-weighted subtracted image after Gadolinium injection (2nd minute) shows regional, heterogeneous, asymmetric, non-mass like enhancement, fast initial increase, post initial wash-out, intermediate signal intensity on T2-weighted images - BI-RADS 5. Pathologic diagnosis through MRI-guided vacuum-assisted biopsy was DCIS.

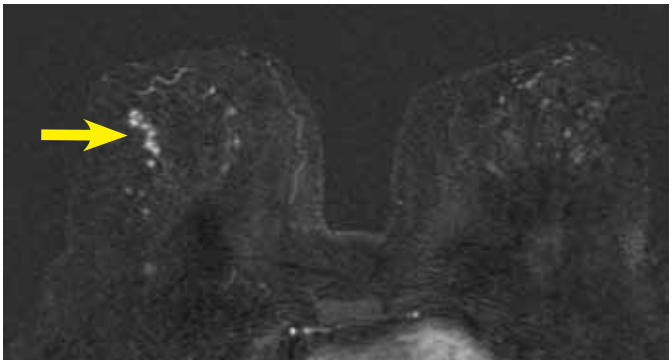

FIGURE 8. 57-year old woman, US-guided fine needle biopsy performed at another institution was suspicious for pappilary carcinoma. Mammographically dense breast, first and second look ultrasound images at institute of oncology showed simple cyst. Axial T1-weighted subtracted image after. Gadolinium injection (2nd minute) shows ductal, reticular- dendritic, asymmetric, non-mass like enhancement, fast initial enhancement with post initial plateau. Intermediate signal intensity on T2-weighted images. BI-RADS 4. MRI-guided vacuum-assisted biopsy revealed invasive tubular carcinoma.

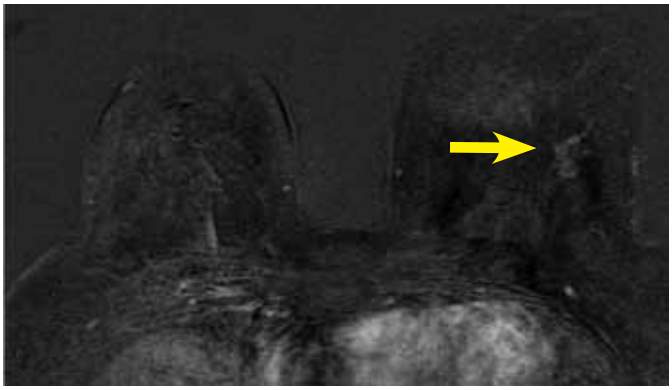

FIGURE 9. 63-year old woman with history of invasive ductal carcinoma in her right breast 8 years ago. Clinical exam revealed enlarged lymph node in the left axilla. Fine needle aspiration biopsy showed metastatic lymph node. Mammographically discrete architectural distortion only in one projection in the left and postoperative changes in the right breast. Ultrasound was not performed at the discretion of the radiologist. Axial T1-weighted subtracted image after Gadolinium injection (2nd minute) shows focal, heterogeneous, asymmetric, non–mass like enhancement in the left breast, the kinetic curve shows fast initial enhancement with post-initial wash out, low signal intensity on T2-weighted images – BI-RADS 4. MRI –guided vacuum-assisted biopsy revealed invasive lobular carcinoma.

and some new predictors for the differentiation of benign from malignant non-mass lesions have been suggested.[21-24] Most of the patients in our series underwent mammography and sonography before MRI-VAB. Only in 3 patients sonography was not performed at the discretion of radiologist. This criteria increased the relative number of non-mass lesions in our study (9/14, 64%) and the number of lesions that are 1cm or smaller in size (6/14, 43%). These lesions are by their nature not well shown by sonography or mammography. Among the cancers, the lesions had non-mass like enhancement characteristics in 5 of 6 cases (83%) and 2 of 6 cancers were smaller than 1cm. Among 5 patients with non-mass like enhancement pattern and proved malignancy, 3 had personal history of breast carcinoma – should be MRI screening a part of an annual follow-up for patients diagnosed with breast cancer.[25]

On T2-weighted images one cancer showed low signal intensity, three intermediate and 2 high signal intensities. Among 5 non-mass like enhancing lesions there was one lesion with low signal intensity on T2 weighted image, 2 lesions with intermediate and 2 lesions with high signal on T2 weighted images. Both lesions with high-signal were DCIS, one with ductal, homogenous enhancement smaller than 1 cm and the other one with segmental clumped enhancement 6 cm in size. As published in literature, the permeability of the basement membrane of DCIS-containing ducts, is increased, allowing gadolinium chelates to penetrate the membrane and accumulate within the DCIS-filed milk ducts. That is proposed to be the explanation for enhancement of purely DCIS on breast MR Images.[26-31]

In some cases, after MRI-VAB, benign histology offers no explanation for a contrast-enhancing lesion. The radiologic/pathologic mismatch is more problematic for MRI-VAB than for mammographically-guided interventions because no specimen radiography can be used to verify appropriate core biopsy. If any doubt persists, early post-biopsy breast MRI is performed in our practice but not earlier than after 6 months.[32] There were 2 cases, where after 6-months follow up the lesions were

FIGURE 10. 71-year old woman, MR mammography performed in the other institution. Axial T1-weighted subtracted image after Gadolinium injection (2nd minute) shows 3 round masses in her left breast, with spiculated margins, rim like enhancement, intermediate signal intensity on T2-weighted images. Kinetic curve shows fast initial enhancement with post-initial wash out. Lesions were categorized as BI-RADS 5. Pathologic diagnosis through MRI- guided vacuum-assisted biopsy was invasive lobular carcinoma.

unchanged in size and morphology. In one case the surgical excision revealed radial scar. In the other one re-biopsy was done and the lesion proved to be benign.

Our study has some limitations. Our series is small and represents our initial experience. Because this study is retrospective, the lesion descriptions in a few cases did not use terms from the BI-RADS MRI lexicon, thus, we modified them as much as possible. Two patients underwent MRI before biopsy at other institution and we could not analyze morphologic and kinetics, only the reports were available. In one case, where discordant findings were4 showed, we had incomplete follow-up data.

In conclusion, MRI-guided vacuum- assisted breast biopsy in our initial experience proved to be a fast, save and accurate method. The cancer rate of women who underwent MR-VAB was 43% in our cohort. The morphologic pattern of non-mass like enhancement and washout or plateau kinetics showed a higher cancer rate than mass like enhancement and persistent kinetics.

References

1. Podobnik J, Kocijancic I, Kovac V, Sersa I. 3T MRI in evaluation of asbestos-related thoracic diseases - preliminary results. *Radiol Oncol* 2010**; 44:** 92-6.
2. Stanic K, Kovac V. Prophylactic cranial irradiation in patients with small-cell lung cancer: the experience at the Institute of Oncology Ljubljana. *Radiol Oncol* 2010; **44:** 180-6.
3. Kuhl CK, Schrading S, Bieling HB, Wardelmann E, Leutner CC, Koenig R, et al. MRI for diagnosis of pure ductal carcinoma in situ: a prospective observational study. *Lancet* 2007; **370:** 485-92.
4. Lehman CD, Deperi ER, Peacock S, McDonough MD, Demartini WB, Shook J. Clinical experience with MRI-guided vacuum-assisted breast biopsy. *AJR Am J Roentgenol* 2005; **184:** 1782-7.
5. Lehman CD, DeMartini W, Anderson BO, Edge SB. Indications for breast MRI in the patient with newly diagnosed breast cancer. Indications for breast MRI in the patient with newly diagnosed breast cancer. *J Natl Compr Canc Netw* 2009; **7:** 193-201.
6. Sardanelli F, Podo F, D'Agnolo G, Verdecchia A, Santaquilani M, Musumeci R, et al. Multicenter comparative multimodality surveillance of women at genetic-familial high risk for breast cancer (HIBCRIT study): interim results. *Radiology* 2007; **242:** 698-715.
7. Liberman L, Mason G, Morris EA, Dershaw DD. Does size matter? Positive predictive value of MRI-detected breast lesions as a function of lesion size. *AJR Am J Roentgenol* 2006; **186:** 426-30.
8. Warner E, Plewes DB, Hill KA, Causer PA, Zubovits JT, Jong RA, et al. Surveillance of BRCA1 and BRCA2 mutation carriers with magnetic resonance imaging, ultrasound, mammography, and clinical breast examination. *JAMA* 2004; **292:** 1317-25.
9. Sardanelli F, Boetes C, Borisch B, Decker T, Federico M, Gilbert FJ, et al. Magnetic resonance imaging of the breast: recommendations from the EUSOMA working group. *Eur J Cancer* 2010; **46:** 1296-316.
10. Heywang-Köbrunner SH, Heinig A, Schaumlöffel U, Viehweg P, Buchmann J, Lampe D, et al. MR-guided percutaneous excisional and incisional biopsy of breast lesions. *Eur Radiol* 1999; **9:** 1656-65.
11. Prat X, Sittek H, Grosse A, Baath L, Perlet C, Alberich T, et al. European quadricentric evaluation of a breast MR biopsy and localization device: technical improvements based on phase I evaluation. *Eur Radiol* 2002; **12:** 1720-7.
12. Tozaki M, Yamashiro N, Fukuma E. MR-guided vacuum-assisted breast biopsy using a non-titanium needle. *Magn Reson Med Sci* 2007; **6:** 259-64.
13. Perlet C, Heywang-Kobrunner SH, Heinig A, Sittek H, Casselman J, Anderson I, et al. Magnetic resonance-guided, vacuum-assisted breast biopsy: results from a European multicenter study of 538 lesions. *Cancer* 2006; **106:** 982-90.
14. Heywang-Köbrunner SH, Sinnatamby R, Lebeau A, Lebrecht A, Britton PD, Schreer I. Consensus Group Interdisciplinary consensus on the uses and technique of MR-guided vacuum-assisted breast biopsy (VAB): results of a European consensus meeting. *Eur J Radiol* 2009; **72:** 289-94.
15. Heywang- Köbrunner SH, Schaumlöffel-Schulze U, Heinig A, Beck RM, Lampe D, Buchmann J. MR-guided percutaneous vacuum biopsy of breast lesions: experiences with 100 lesions. [Abstract]. *Radiology* 1999; **213(P):** 289.
16. Liberman L, Bracero N, Morris E, Thornton C, Dershaw DD. MRI-guided 9-gauge vacuum-Assisted breast biopsy: initial clinical Experience. *AJR Am J Roentgenol* 2005; **185:** 183-93.
17. Orel SG, Rosen M, Mies C, Schnall MD. MR imaging-guided-9-gauge vasuum-assisted core-needle breast biopsy: initial experience. *Radiology* 2006; **238:** 54-61.
18. Perlet C, Heywang-Kobrunner SH, Heinig A, Sittek H, Casselman J, Anderson I, et al. Magnetic resonance-guided, vacuum-assisted breast biopsy: results from a European multicenter study of 538 lesions. *Cancer* 2006; **106:** 982-90.
19. Tozaki M, Yamashiro N, Sakamoto M, Sakamoto N, Mizuuchi N, Fukuma E. Magnetic resonance-guided vacuum-assisted breast biopsy: results in 100 Japanese women. *Jpn J Radiol* 2010; **28:** 527-33.
20. Noroozian M, Gombos EC, Chikarmane S, Georgian-Smith D, Raza S, Denison CM, et al. Factors that impact the duration of MRI-guided core needle biopsy. *AJR Am J Roentgenol* 2010; **194:** 150-7.
21. American College of Radiology. *ACR BI-RADS MRI. ACR Breast Imaging Reporting and Data System, breast imaging atlas.* Reston, VA: American College of Radiology; 2003.
22. Kuhl CK, Shild HH, Morakkabati N. Dynamic bilateral contrast-enhanced MR imaging of the breast: trade-off between spatial and temporal resolution. *Radiology* 2005; **236:** 789-800.
23. Goto M , Ito H , Akazawa K, Kubota T, Kizu O, Yamada K, et al. Diagnosis of breast tumors by contrast-enhanced MR imaging: comparison between the diagnostic performance of dynamic enhancement patterns and morphologic features. *J Magn Reson Imaging* 2007; **25:** 104-12.
24. Sohns C, Scherrer M, Staab W, Obenauer S. Value of the BI-RADS Classification in MR-mammography for diagnosis of benign and malignant breast tumors. *European Radiology* 2011; **21:** 2475-83.
25. Zebic-Sinkovec M, Kadivec M, Podobnik G, Skof E, Snoj M. Mammographycally occult high grade ductal carcinoma in situ (DCIS) as second primary breast cancer, detected with MRI, a case report. *Radiol Oncol* 2010; **44:** 228-31.
26. Baltzer PA, Dietzel M, Kaiser WA. Nonmass lesions in magnetic resonance imaging of the breast: additionhal T2-weigted images improve diagnostic accuracy. *J Comput Assist Tomogr* 2011; **35:** 361-6.
27. Jansen SA, Paunesku T, Fan X, Woloschak GE, Vogt S, Conzen SD, et al.. Ductal carcinoma in situ: x-ray fluorescence microscopy and dynamic contrast-enhanced MR imaging reveals gadolinium uptake within neoplastic mammary ducts in a murine model. *Radiology* 2009; **253:** 399–406.
28. CK Kuhl: Why do purely intraductal cancers enhance on breast MR Images? *Radiology* 2009; **253:** 281-3.
29. Mossa-Basha M, Fundaro GM, Shah BA, Ali S, Pantelic MV.Ductal carcinoma in situ of the breast: MR imaging findings with histopathologic correlation. *Radiographics* 2010; **30:** 1673-87.
30. Newstead GM. MR Imaging of ductal carcinoma in situ. *Magn Reson Imaging Clin N Am* 2010; **18:** 225-40.
31. Miklavcic D, Towhidi L. Numerical study of the electroporation pulse shape effect on molecular uptake of biological cells. *Radiol Oncol* 2010; **44:** 34-41.
32. Li J, Dershaw DD, Lee CH, Kaplan J, Morris EA. MRI follow-up after concordant, histologically benign diagnosis of breast lesions sampled by MRI-guided biopsy. *AJR Am J Roentgenol* 2009; **193:** 850-5.

research article

Differentiation of malignant and benign lung lesions with diffusion-weighted MR imaging

Sevtap Gümüştaş[1], Nagihan Inan[1], Gür Akansel[1], Ercüment Çiftçi[1], Ali Demirci[1], Sevgiye Kaçar Özkara[2]

[1] Department of Radiology, [2] Department of Pathology, School of Medicine, University of Kocaeli, Turkey

Radiol Oncol 2012; 46(2): 106-113.

Received: 1 August 2011
Accepted: 8 January 2012

Correspondence to: Sevtap Gümüştaş, Kocaeli Uni. Tip Fak Radyoloji AD, 41380 Umuttepe Kocaeli, Turkey. Phone: +90 262 3037126; Fax: +90 262 303 80 03; E-mail: svtgumustas@hotmail.com

Disclosure: No potential conflicts of interest were disclosed.

Background. The aim of the study was to evaluate the role of diffusion-weighted magnetic resonance imaging in the differential diagnosis of lung lesions.

Patients and methods. Sixty-seven patients with lung lesions (48 malignant, 19 benign) were included in this prospective study. Signal intensities (SIs) were measured in diffusion-weighted MR images that were obtained with b=0, 500 and 1000 s/mm² values. Apparent diffusion coefficient (ADC) maps were calculated by using images with b=0 and 1000 s/mm² values. The statistical significance was determined using the Student-t test.

Results. The SIs of malignant lesions were significantly higher than those of benign lesions ($p<0.004$ for b=0 s/mm² and $p<0.000$ for the other b values). Using b=500 s/mm², SI≥391 indicated a malignant lesion with a sensitivity of 95%, specificity of 73% and positive predictive value of 87%. Using b=1000 s/mm², SI≥277 indicated a malignant lesion with a sensitivity of 93%, specificity of 69% and positive predictive value of 85%. There was no significant difference between malignant and benign lesions regarding ADC values ($p=0.675$). There was no significant difference in SIs or ADC values between small cell carcinoma and non-small cell carcinoma. When comparing undifferentiated with well- partially differentiated cancers, SIs were higher with all b values, but the difference was statistically significant only with b=1000 s/mm² ($p<0.04$).

Conclusions. Diffusion-weighteted MR trace image SI is useful for the differentiation of malignant versus benign lung lesions.

Key words: pulmonary lesions; diffusion-weighted imaging; apparent diffusion coefficient; magnetic resonance imaging

Introduction

Lung cancer is one of the leading causes of death.[1] It usually arises as a solid nodule or mass on chest radiography or computed tomography (CT). Although many well known characteristics have been described for nodule differentiation on CT, it remains a challenge for radiologists to differentiate lesions as malignant or benign.[2-5] In recent years, fluorine-18 fluorodeoxyglucose positron emission tomography (PET) has been used for this purpose. Both CT and PET deliver high doses of radiation. In addition PET has been known to give false-positive results in inflammatory masses.[6-9] For these reasons, an accurate and safe alternative method is still desirable for the determination of malignant versus benign pulmonary lesions.

Recent advances in fast imaging techniques like echo-planar imaging, makes magnetic resonance imaging (MRI) more suitable for chest applications.[10-12] There are reports using dynamic contrast MRI of lung masses.[13,14] Diffusion-weighted magnetic resonance imaging (DWI), initially used in the central nervous system, has been increasingly applied in other body areas, such as the mediastinum[15], pancreas[16], and liver.[17,18]

The aim of our study was to determine whether quantitative analysis of DWI could be helpful in the differentiation of malignant and benign pulmonary lesions.

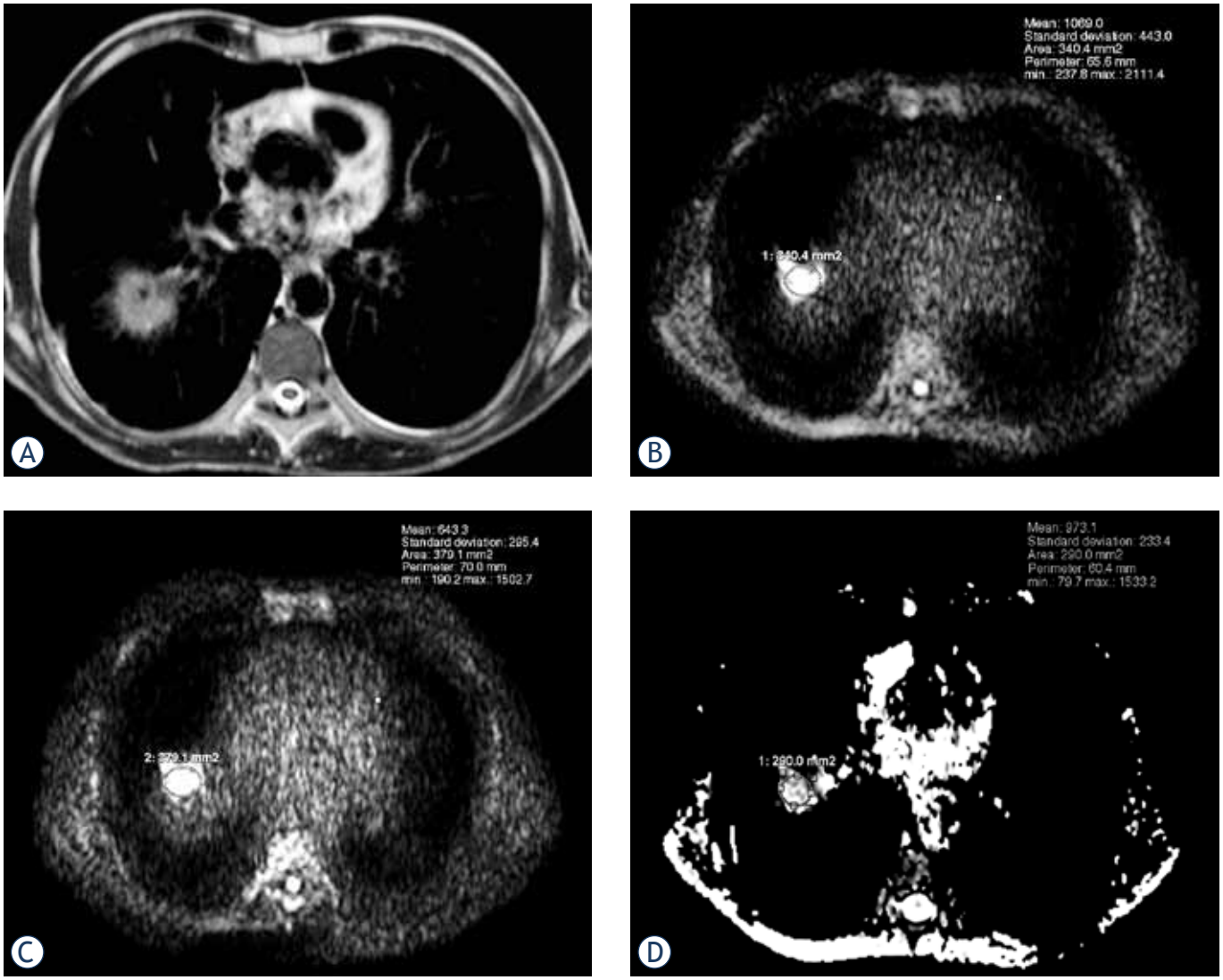

FIGURE 1. A 56-year-old man with poorly-differentiated non-small cell carcinoma. (A) Axial T2-weighted MR image shows mass in the right lung. (B) diffusion-weighted magnetic resonance image with b value of 500 sec/mm² shows hyperintense mass (SI = 1069). (C) diffusion-weighted magnetic resonance image with b value of 1000 sec/mm² shows hyperintensity of the mass is still remarkable (SI = 643). (D) ADC map shows ADC value is (0.97x10-3) sec/mm².

Patients and methods

Patients

The study was approved by our institutional review board and protocol review committee. Because the tests used were a part of the routine clinical workup of these patients, the informed consent was not required by the review board. We obtained a blanket consent from all patients for the use of their findings for research and educational purposes, with patient privacy secured.

From March 2009 to July 2010, 66 consecutive patients (49 males, 17 females) with 67 lung lesions found on CT were included in this prospective study according to our entry criteria. The entry criteria were: (a) presence of a solid pulmonary lesion. In the case of ground glass opacity (GGO) with the solid part on CT images, the GGO part was avoided to the extent possible and the solid part was measured on DWI with the reference of CT images, since air itself in GGO might reduce the true apparent diffusion coefficient (ADC) value of the lesion.[18] Lesions containing large amounts of necrosis and calcification were also excluded; (b) lesion size >10 mm in diameter in view of the limited planar resolution of DWI; (c) presence of a specific proven diagnosis of the lesion either histopathologically or by using clinical, radiologi-

cal and laboratory data or based on at least 1-year radiological follow-up; (d) no current administration of chemotherapeutic or radiotherapeutic treatment; (e) absence of any contraindications for MRI; and (f) ability of patients to lie still and hold their breath approximately 26 seconds in the MRI unit.

Biopsies of lung lesions were carried out by the radiologist (EÇ) in the interventional radiology department of the same hospital. MRI was performed on these patients on the same day but before the percutaneous biopsy in order to avoid hemorrhage-related distortions.

The study was carried out according to the Helsinki Declaration.

TABLE 1. Histopathological and clinical diagnosis of lesions

	Diagnosis
Benign lesions (n=19)	Chronic inflammatory changes (n=9) Sarcoidosis (n=3) Acute bacteriel pneumonia (n=2) Tuberculosis pneumonia (n=2) Romatoid nodule (n=1) Granuloma (n=1) Hamartoma (n=1)
Malignant lesions (n= 48)	SCLC (n=6) NSCLC (n=42) NSCLC subgroup; Adenocarcinoma (n=13) Squamous cell carcinoma (n=5) Large cell carcinoma (n=2) Nonidentified NSCLC (n=22)

SCLC = small cell lung cancer, NSCLC = non-small cell lung cancer

MR Imaging

All patients were examined with a 1.5 Tesla MR unit (Gyroscan Intera; Philips Medical Systems, Eindhoven, The Netherlands) using a four-element phased-array body coil. This system had a maximal gradient strength of 30 mT/m and a slew rate of 150 mT/m/msec. All patients were examined initially with the routine MRI protocol for the thorax that included: precontrast axial T1-weighted (W) breath-hold spoiled gradient echo (fast field echo: FFE) (TR/TE/FA/NEX:169/4.6/80/1) and coronal and axial T2-W single-shot turbo spin-echo (TR/TE/NEX/TSE factor: 700/80/1/72). Subsequently, three series of axial single-shot spin-echo echo-planar (SS-SE-EPI) DWI (1,000/81; echo-planar imaging (EPI) factor, 77; sensitizing gradients in *x*, *y*, and *z* directions) were acquired using b = 0, 500 and 1000 s/mm² values. ADC maps were reconstructed from the b = 0 and b = 1000 s/mm² images. MRI, including DWI, consisted of a multisection acquisition with a slice thickness of 6 mm, an intersection gap of 1 mm, and an acquisition matrix of 128 × 256. All sequences were acquired using a partially parallel imaging acquisition and SENSE (sensitivity encoding) reconstruction with a reduction factor (*R*) of 2. The scanning time of the acquisition of each DWI series during a single breath-hold was 26 seconds.

Quantitative analysis

Quantitative measurements were made using a dedicated Workstation (Dell Workstation Precision 650, with the View Forum software platform provided by Philips Healthcare). All images were assessed by two radiologists (SG, NI) who were blinded to the clinical history of the patients. First, CT images were evaluated in order to assess the calcification, necrosis and GGO components. CT scans were also evaluated for contour characteristics of the lesions (irregular or smooth) and concomitant interstitial findings were recorded. Those findings were compared with the DWI findings. The range of interval between the CT and MRI examinations was 0-10 days (mean, 5. 6 days). Then, the lesion was visualized once more on the conventional T1-W and T2-W MRI in terms of location, size and content of cystic-necrotic parts to detect interval changes since the time of the CT scan. These conventional images were only used for the lesion identification and not for the analysis. Afterwards, signal intensity (SI) of the lesion was measured for each b value (0, 500 and 1000 s/mm²) on DWI using a round or elliptical region of interest (ROI). The ROI was placed centrally, and the size of the ROI was kept as large as possible, covering at least two-thirds of the lesion, yet avoiding the interference from the surrounding lung tissue, necrotic parts and major blood vessels. ADCs were then calculated from the ADC maps that were reconstructed from b = 0 and b = 1000 s/mm² values.

Statistical analysis

SIs and ADCs were compared between the groups. The fitness of numeric data set to normal distribution was determined using the Kolmogorov-Smirnov test**.** The data were normally distributed, so the differences in SIs and ADCs were analyzed using the Student-t test. A *p* value of less than 0.05 was considered statistically significant. To evaluate the diagnostic performance of the quantitative tests for differentiating malignant and benign lesions and to describe the sensitivity and specifi-

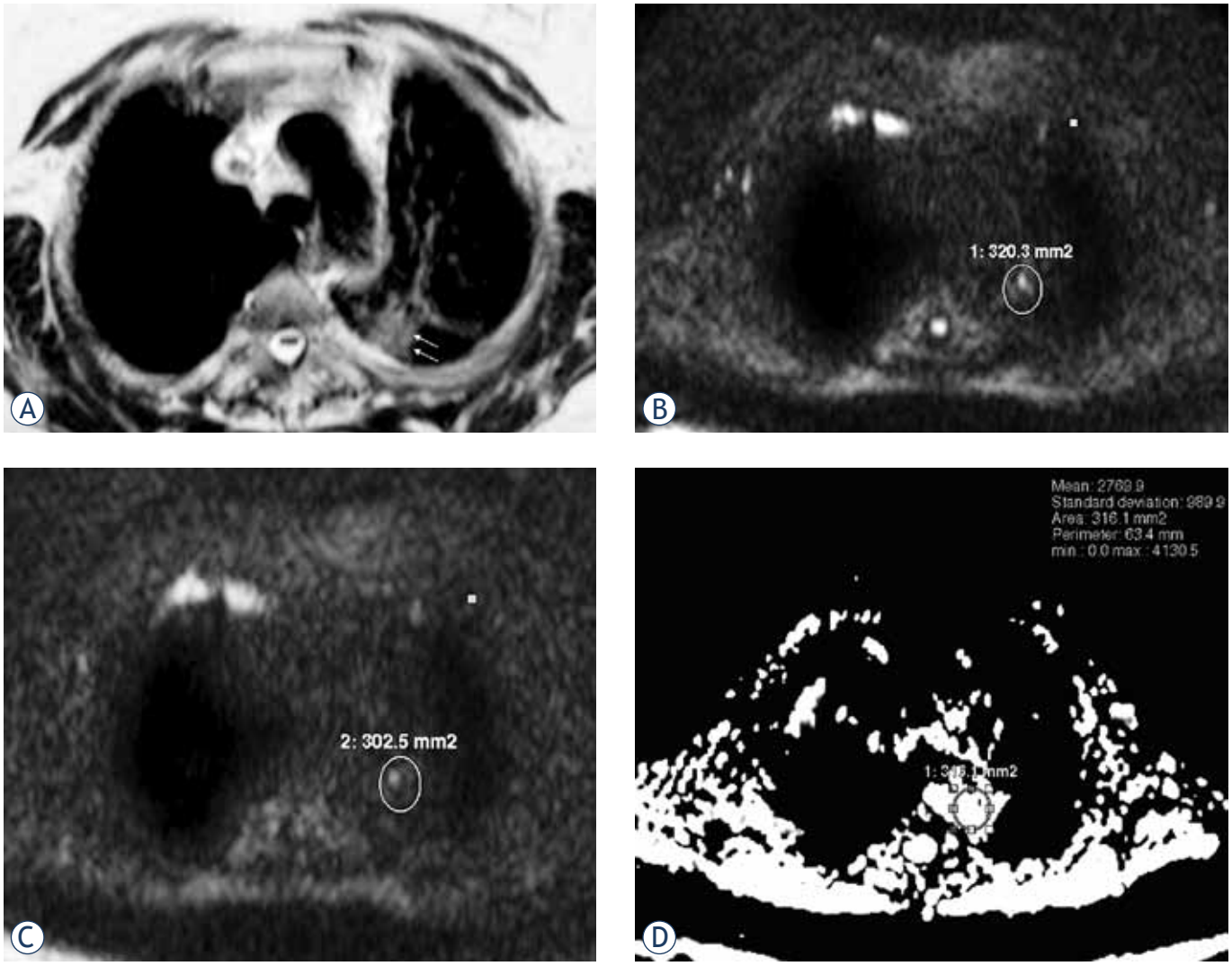

FIGURE 2. A 32-year-old woman with bacterial pneumonia. (A) Axial T2-weighted MR image shows ill-defined peripheral mass in the superior segment of the lower lobe of the left lung (arrows). (B) diffusion-weighted magnetic resonance image with b value of 500 sec/mm² shows minimal hyperintense mass (SI = 203). (C) diffusion-weighted magnetic resonance image with b value of 1000 sec/mm² shows hyperintensity of the mass is less remarkable (SI = 162). (D) ADC map shows ADC value is (2.76x10-3) sec/mm².

city of the tests, receiver operating characteristic (ROC) analysis was performed. The optimum cut-off value was determined as the value that best discriminates between the two groups in terms of maximum sensitivity and minimum number of false-positive results. All statistical analyses were performed using the statistical software SPSS.[15]

Results

The mean age of all patients was 64 ± 21 years (range: 41-83 years). The mean age of the patients in the benign group was 61 ± 19 years (range: 41-72 years) and in the malignant group was 66 ± 21 years (range: 44-83 years). The difference in age between groups was not statistically significant ($p = 0.5$).

The mean diameter of masses for the entire group was 33 ± 18 mm. The mean diameter of malignant lesions was 37 ± 19 mm (range: 20-130 mm) and of benign lesions was 25 ± 15 mm (range: 15-60 mm), respectively. The difference in diameter between groups was statistically significant ($p = 0.005$). Except for one patient who had two nodules (the primary tumor and its pulmonary metastasis), one lesion was measured in the remaining patients.

Of the 67 lesions, 48 were malignant and 19 were benign (Table 1). The malignant lesions consisted of 42 non-small cell lung cancers (NSCLCs) and 6 small cell lung cancers (SCLCs). NSCLC subgroups

TABLE 2. Quantitative analysis of diffusion-weighted magnetic resonance imaging (mean ± SD) of malignant and benign lesions (b=0, 500, 1000 sec/mm² and ADC values)

b and ADC values	malignant lesions (n=48)	benign lesions (n=19)	P
b 0 (sec/ mm²)	1500.40 ± 820	960.31 ± 550	*0.004*
b 500 (sec/ mm²)	611.32 ± 343	247.10 ± 124	*0.000*
b 1.000 (sec/ mm²)	371.00 ± 194	175.68 ± 94	*0.000*
ADC (x10⁻³) mm²/sec	1.65 ± 0.90	1.75± 0.70	0.675

TABLE 3. Quantitative analysis of diffusion-weighted magnetic resonance imaging (mean ± SD) of poorly-differentiated and medium- well differentiated malignant lessions (b=0, 500, 1000 sec/mm² and ADC values)

b and ADC values	poorly-differentiated (n=11)	medium-well differentiated (n=31)	P
b 0 (sec/ mm²)	1646 ± 787	1453.3 ± 837	0.497
b 500 (sec/ mm²)	751.4 ± 440	568.87 ± 304	0.245
b 1.000 (sec/ mm²)	517.27 ± 273	323.67 ± 135	*0.044*
ADC (x10⁻³) mm²/sec	1.5 ± 0.5	1.8 ± 0.8	0.240

TABLE 4. Quantitative analysis of diffusion-weighted magnetic resonance imaging (mean ± SD) of non-small cell lung cancer (NSCLC) and small cell lung cancer (SCLC) (b=0, 500, 1000 sec/mm² and ADC values)

b and ADC values	NSCLCs (n=42)	SCLCs (n=6)	P
b 0 (sec/ mm²)	1110.8 ± 209	1705 ± 873	*0.001*
b 500 (sec/ mm²)	468.6 ± 238	646.9 ± 350	0.186
b 1.000 (sec/ mm²)	366 ± 177	379.1 ± 197	0.881
ADC (x10⁻³) mm²/sec	1.9 ± 0.8	1.5 ± 1.0	0.464

included 13 adenocarcinomas, 5 squamous-cell carcinomas, 2 large-cell carcinomas, and 22 unidentified NSCLCs that could not be subgrouped in any of these. Eleven of the malignant lesions were poorly-differentiated, the others were medium- or well- differentiated. The benign lesions consisted of 9 chronic inflammatory changes, 3 sarcoidosis, 2 acute bacterial pneumonias, 2 tuberculosis pneumonias, 1 rheumatoid nodule, 1 granuloma, and 1 hamartoma.

In 51 patients, the final diagnosis was made by histopathological confirmation on the basis of percutaneous biopsy, and included 48 primary lung cancers, 2 nonspecific inflammatory changes and 1 hamartoma. The diagnosis was confirmed with laboratory, radiological and clinical parameters in 3 sarcoidosis, 2 bacterial pneumonias, and 2 tuberculosis pneumonias. In sarcoidosis patients, the lesions regressed with a specific treatment. Two tuberculosis (Mycobacterium tuberculosis) and 2 bacterial pneumonia cases were diagnosed bacteriologically. In 9 patients (1 granuloma, 1 rheumatoid nodule and 7 chronic inflammatory changes) lesions remained stable on follow-up CT for 12 months or more.

We could obtain DWI SI and an ADC value for all lesions. The results of the quantitative analysis of SIs and ADC values are reviewed in Table 2. The mean SI of malignant lesions was higher than that of benign lesions (Figure 1, 2). The difference between malignant and benign lesions was significant for all b values ($p < 0.004$ for b = 0 s/mm² and $p < 0.000$ for the other b values) (Figure 3). The area under the ROC curve was 0.933 ± 0.031 for the SI on images with b = 500 s/mm². Using b = 500 s/mm², a SI ≥391 indicated a malignant lesion with a sensitivity of 95%, specificity of 73% and positive predictive value of 87%. Six among 48 malignant lesions (4 NSCLCs and 2 SCLCs) revealed SIs <391, which could be confused as benign.

For the SI on images with b = 1000 s/mm², the area under the ROC curve was 0.831 ± 0.055. A SI ≥227 with b = 1000 s/mm² indicated a malignant lesion with a sensitivity of 93%, specificity of 69% and positive predictive value of 85%. Seven among 48 malignant lesions (6 NSCLCs and 1 SCLCs) re-

vealed SIs <227 which could be confused as benign. Among the benign lesions, 1 sarcoidosis and 1 acute bacterial pneumonia had SI higher than the cut-off value on DWI with both b = 500 and b = 1000 s/mm². A patient with a chronic inflammatory lesion had a SI higher than the cut-off value only for b = 1000 s/mm². Although the mean ADC of the malignant lesions (1.5 $x10^{-3}$ mm^2/sec) was lower than of the benign group (1.9 $x10^{-3}$ mm^2/sec), the difference was not statistically significant ($p < 0.675$).

The results of the subgroup quantitative analysis are reviewed in Table 3. When we analyzed the malignant lesions in accordance with the histologic differentiation, the SI of poorly-differentiated cancers was higher for all b values, but statistically a significant difference was observed only with b = 1000 s/mm² ($p < 0.04$). Although the ADC of poorly-differentiated lesions was lower than of the medium-well differentiated lesions, the difference was not statistically significant ($p < 0.240$). A comparison of the NSCLCs and the SCLCs demonstrated that the SIs of SCLCs were higher than those of NSCLCs. Although the ADC value of the SCLCs was lower than the ADC value of the NSCLCs, the difference was not statistically significant ($p < 0.464$) (Table 4).

When we compare CT images with the DWI, all of the malignant lesions had irregular contours on CT images. Of the benign lesions 16 had also irregular contours but 3 (1 rheumatoid nodule, 1 granuloma, and 1 hamartoma) had smooth contours. The difference was not statistically significant (p = 0.3). Lymphangitic tumoral spread as irregular septal thickening was detected as a concomitant interstitial finding in 6 of the malignant masses on CT images.

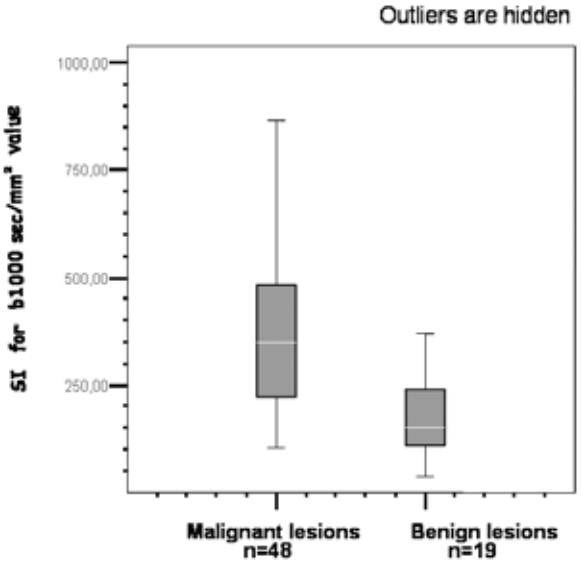

FIGURE 3. Comparison of SI with b value of 1000 s/mm² in malignant and benign lesions. The SIs of malignant lesions were significantly higher than those of benign lesions.

Discussion

The aim of DWI is to evaluate the diffusion process *in vivo*. ADC values are quantitative expressions of the diffusion characteristics of tissues. These characteristics are related to several factors such as tissue cellularity, cell density and extracellular-intracellular components.[16] DWI has been an important diagnostic tool for neuroradiology, especially for ischemic events of the brain.[19] Although DWI has been used to differentiate malignant and benign lesions in several other locations, there are few studies about the intrathoracic lesion characterization.[20,21-27]

In our study, we found SIs of malignant masses on diffusion trace imaging were significantly higher than of benign masses with low (b = 500 s/mm²) and high (b = 1000 s/mm²) b values. In the study of Uto *et al.* the SI ratio of malignant lesions to the spinal cord was found higher than that of benign lesions.[21] Satoh *et al.* also found a higher qualitative score in SI of malignant versus benign masses but they did not measure quantitatively.[22] In our study, the patient population was larger than in these two studies.

Although malignant lesions showed lower ADC values than benign masses in our study, the difference was not significant. One reason may be the use of fixed TRs, due to which the DW series were acquired in different phases of the cardiac cycle. Therefore, DW images of different patients may have been affected differently by the pulsatile motion. Another reason may be the distortion artifacts, which limited the reliability of the ADC measurements for small and low-lateral segmental lesions. In the literature, some studies did not evaluate ADC values probably because of susceptibility artifacts.[22,25] Uto *et al.* found no significant difference between malignant and benign lesions by means of ADC.[21] Mori *et al.* found a significant difference between malignant and benign lesions by using an ADC cut-off value of $1.1x10^{-3}$ mm^2/sec.[23] The large number of patients may be the explanation for this result. Liu *et al.* reported that ADC values in malignant lesions were significantly lower than in benign lesions.[24] In the same study, there was no significant difference between malignant and benign lesions in DWI SIs.

Histopathologically, tumoral cellularity of SCLC is high, and these tumoral cells have very large nuclei and almost no cytoplasm.[28] All these features were expected to restrict the tissue diffusion and reduce ADC values. In our study, the SI of SCLC lesions was higher than of the NSCLC subgroup but the difference was significant only with b = 0 s/mm². Thus, hyperintensity of lesions may be related to the T2 shine-through effect. Although ADCs were lower in the SCLC subgroup, the difference was not statistically significant. This may be because of the limited number of patients (n=6). In their study of tissue characterization in lung cancers, Abdel Razek *et al.* found significantly lower ADC values for SCLC when comparing with NSCLC groups in a similar patient population.[26] Liu *et al.* also found lower ADC values for the SCLC than the NSCLC group.[24] However, Koyama *et al.* found no significant differences between subtypes of lung cancers.[27]

In our study, SI of poorly- differentiated malignant masses was higher than of medium-well differentiated masses on all trace images and the difference with b value of 1,000 s/mm² was statistically significant. ADC values were lower in the poorly-differentiated subgroup although the difference was not statistically significant. Histologically, tumor cellularity is higher in the poorly-differentiated cancers which could explain the low ADC values.[29] Similar results of significantly lower ADCs in poorly-differentiated adenocarcinomas compared medium-well- differentiated cancer types are reported in the literature and are in accordance with our findings.[20,26,30,31]

When compared with CT images, contour characteristics of the lesions cannot be assessed with DWI but it does not seem to be a significant disability because contour characteristics are not reliable in differentiating malignant and benign lesions. On CT images lymphangitic tumoral spread was detected as a concomitant interstitial finding in some of the malignant masses. This finding is very helpful to estimate the malignant character of the lesion. The sensitivity and specificity achieved by DWI suggest it could be used for malignant versus benign differentiation. However, the inability of MRI to properly assess the interstitium and lymphangitic tumoral spread is a limitation for predicting malignancy. In addition, although just primary lung cancers are involved into our study, it must be kept in mind that calcified metastases such as those from osteosarcoma may be difficult to detect because of relatively lower proton density resulting in low signal intensity.

Our study had some technical limitations. The use of DWI in the thorax was hindered by certain limitations such as physiologic motion artifacts (respiration and cardiac motion), low signal-to-noise ratio (SNR) of the low lung proton density and the susceptibility artifacts caused by air-tissue interfaces.[18] We used the EPI sequence with high b values, which had a lower SNR, thus resulting in greater image distortion. In addition, we obtained DW images using a breath-hold echo-planar sequence with SENSE and this made the measurements vulnerable to susceptibility effects. We did not use pulse-triggered DWI, known to reduce the accuracy of ADC measurements.[18] Finally, the patient population, especially the benign subgroup, was relatively small, which might compromise the accuracy of the results.

In conclusion, DWI may be used to differentiate malignant and benign lung lesions in addition to other radiologic imaging techniques even with high b values such as b = 1000 s/mm². DW trace image SI, together with ADC measurements is useful for the differentiation of malignant versus benign lung lesions.

References

1. Jemal A, Siegel R, Ward E, Murray T, Xu J, Smigal C, et al. Cancer statistics. *CA Cancer J Clin* 2006; **56:**106-30.
2. Erasmus JJ, Connolly JE, McAdams HP, Roggli VL. Solitary pulmonary nodules. Part 1. Morphologic evaluation for differentiation of benign and malignant lesions. *RadioGraphics* 2000; **20:** 43-58.
3. Swensen SJ, Viggiano RW, Midthun DE, Müller NL, Scherrick A, Yamashita K, et al. Lung nodule enhancement at CT: multicenter study. *Radiology* 2000; **214:** 73-80.
4. Henschke CI, Yankelevitz DF, Naidich DP, McCauley ID, McGuinness G, Libby MD, et al. CT screening for lung cancer: suspiciousness of nodules according to size on baseline scans. *Radiology* 2004; **231:** 164-8.
5. Jeong YJ, Lee KS, Jeong SY, Chung MJ, Shim SS, Kim H, et al. Solitary pulmonary nodule: characterization with combined wash-in and washout features at dynamic multidetector row CT. *Radiology* 2005; **237:** 675-83.
6. Gould MK, MacLean CC, Kuschner WG, Rydzak CE, Owens DK. Accuracy of positron emission tomography for diagnosis of pulmonary nodules and mass lesions. *JAMA* 2001; **285:** 914-24.
7. Yi CA, Lee KS, Kim B, Choi JY, Kwon JO, Kim H, et al. Tissue characterization of solitary pulmonary nodule: comparative study between helical dynamic CT and integrated PET/CT. *J Nucl Med* 2006; **47:** 443-50.
8. Cheran SK, Nielsen ND, Patz EF Jr. False-negative findings for primary lung tumors on FDG positron emission tomography: staging and prognostic implications. *AJR* 2004; **182:** 1129-32.
9. Nomori H, Watanabe K, Ohtsuka T, Naruke T, Suemasu K, Uno K. Evaluation of F-18 fluorodeoxyglucose (FDG) PET scanning for pulmonary nodules less than 3cm in diameter, with special reference to CT images. *Lung Cancer* 2004; **45:** 19-27.
10. Tanaka R, Horikoshi H, Nakazato Y, Seki E, Minato K, Iijima M, et al. Magnetic resonance imaging in peripheral lung adenocarcinoma; correlation with histopathologic features. *J Thorac Imaging* 2009; **24:** 4-9.
11. Ohno Y, Sugimura K, Hatabu H. MR imaging of lung cancer. *EJR* 2002; **44:** 172-81.

12. Podobnik J, Kocijancic I, Kovac V, Sersa I. 3T MRI in evaluation of asbestos-related thoracic diseases – preliminary results. *Radiol Oncol* 2010; **44:** 92-6.

13. Schaefer JF, Vollmar J, Schick F, Vonthein R, Seemann MD, Aebert H, et al. Solitary pulmonary nodules: dynamic contrast-enhanced MR imaging-perfusion differences in malignant and benign lesions. *Radiology* 2004; **232:** 544-53.

14. Ohno Y, Hatabu H, Takenaka D, Adachi S, Kono M, Sugimura K, et al. Solitary pulmonary nodules: Potential role of dynamic MR imaging in management: initial experience. *Radiology* 2002; **224:** 503-11.

15. Abdel Razek A, Elmorsy A, Elshafey M, Elhadedy T, Hamza O. Assessment of mediastinal tumors with diffusion-weighted single-shot echo-planar MRI. *J Magn Reson Imaging* 2009; **30:** 535-40.

16. Ichikawa T, Erturk SM, Motosugi U, Sou H, Iino H, Araki T, et al. High-b value diffusion-weighted MRI for detecting pancreatic adenocarcinoma: Preliminary results. *AJR* 2007; **188:** 409-14.

17. Inan N, Kilinc F, Sarisoy T, Gumustas S, Akansel G, Demirci A. Diffusion weighted MR imaging in the differential diagnosis of haemangiomas and metastases of the liver. *Radiol Oncol* 2010; **44:** 24-9.

18. Murtz P, Flacke S, Traber F, van den Brink JS, Gieseke J, Schild HH. Abdomen: diffusion weighted MR imaging with pulse-triggered singleshot sequences. *Radiology* 2002; **224:** 258-64.

19. Ozsunar Y, Sorensen AG. Diffusion- and perfusion- weighted magnetic resonance imaging in human acute ischemic stroke: technical considerations. *Top Magn Reson Imaging* 2000; **11:** 259-72.

20. Matoba M, Tonami H, Kondou T, Yokota H, Higashi K, Toga H, et al. Lung carcinoma: diffusion weighted MR imaging—Preliminary evaluation with apparent diffusion coefficient. *Radiology* 2007; **243:** 570-7.

21. Uto T, Takehara Y, Nakamura Y, Naito T, Hashimoto D, Inui N, et al. Higher sensitivity and specificity for diffusion- weighted imaging of malignant lung lesions without apparent diffusion coefficient quantification. *Radiology* 2009; **252:** 247-54.

22. Satoh S, Kitazume Y, Ohdama S, Kimula Y, Taura S, Endo Y. Can malignant and benign pulmonary nodules be differentiated with diffusion-weighted MRI? *AJR* 2008; **191:** 464-70.

23. Mori T, Nomori H, Ikeda K, Kawanaka K, Shiraishi S, Katahira K, et al. Diffusion-weighted magnetic resonance imaging for diagnosing malignant pulmonary nodules/masses. Comparison with positron emission tomography. *J Thorac Oncol* 2008; **3:** 358-64.

24. Liu H, Liu Y, Yu T, Ye N. Usefulness of diffusion-weighted MR imaging in the evaluation of pulmonary lesions. *Eur Radiol* 2010; **20:** 807-15.

25. Qi LP, Zhang XP, Tang T, Li J, Sun YS, Zhu GY. Using diffusion-weighted MR imaging for tumor detection in the collapsed lung: a preliminary study. *Eur Radiol* 2009; **19:** 333-41.

26. Abdel Razek A, Fathy A, Abdel Gawad T. Correlation of apparent diffusion coefficient value with prognostic parameters of lung cancer. *JCAT* 2011; **35:** 248-52.

27. Koyama H, Ohno Y, Aoyama N, Onishi Y, Matsumoto K, Nagomi M, et al. Comparison of STIR turbo SE imaging and diffusion-weighted imaging of the lung: capability for detection and subtype classification of pulmonary adenocarcinomas. *Eur Radiol* 2010; **20:** 790-800.

28. Cotran RS, Kumar V, Robbins SL: Robbins Pathologic Basis of Disease, 5th edition. Philadelphia, W.B. Saunders, 1994, pp. 720-25.

29. Clayton F. Bronchioloalveolar carcinoma: Cell types, patterns of growth, and prognostic correlates. *Cancer* 1986; **57:** 1555-64.

30. Kanauchi N, Oizumi H, Honma T, Kato H, Endo M, Suzuki J, et al. Role of diffusion-weighted magnetic resonance imaging for predicting of tumor invasiveness for clinical stage IA non-small cell lung cancer. *Eur J Cardiothorac Surg* 2009; **35:** 706-11.

31. Henzler T, Schmid-Bindert G, Schoenberg SO, Fink C. Diffusion and perfusion MRI of the lung and mediastinum. *Eur J Radiol* 2010; **76:** 329-36.

research article

Evaluation of penile erection rigidity in healthy men using virtual touch tissue quantification

Xiaozhi Zheng, Ping Ji, Hongwei Mao, Jing Wu

Department of Ultrasound, The Fourth Affiliated Hospital of Nantong University (The First People's Hospital of Yancheng), 14 Yuehe Road, Yancheng 224006, Jiangsu Province, P.R. China.

Radiol Oncol 2012; 46(2): 114-118.

Received 1 August 2011
Accepted 19 December 2011

Correspondence to: Jing Wu, Department of Ultrasound, The Fourth Affiliated Hospital of Nantong University (The First People's Hospital of Yancheng), 14 Yuehe Road, Yancheng 224006, Jiangsu Province, P.R. China; Phone: +86 0515 88508717; Fax: +86 0515 88500299; E-mail: wujingzxz@163.com

Disclosure: No potential conflicts of interest were disclosed.

Background. The aim of the study was to describe the shear wave velocity (SWV) values of the penis by virtual touch tissue quantification (VTTQ) and to examine the clinical usefulness of this procedure in evaluation of the rigidity changes in penile erection.

Patients and methods. VTTQ was performed in 37 healthy volunteers. In the course of erection, SWV values of glans penis, corpus penis and radix penis were quantified and grades of erection were documented. The SWV values at different grades of erection were compared.

Results. The axial and radial SWV values of glans penis, corpus penis and radix penis all significantly decreased from Grade 0 to Grade 4 of erection. At Grade 4, they were less than one-third of that at Grade 0 (axial direction: 0.79 ± 0.13 vs. 2.79 ± 0.32 for glans penis, $P<0.001$; 0.77 ± 0.19 vs. 2.84 ± 0.30 for corpus penis, $P<0.001$ and 0.76 ± 0.15 vs. 2.81 ± 0.34 for radix penis, $P<0.001$; radial direction: 0.82 ± 0.15 vs. 2.83 ± 0.31 for glans penis, $P<0.001$; 0.79 ± 0.18 vs. 2.81 ± 0.27 for corpus penis, $P<0.001$ and 0.81 ± 0.16 vs. 2.82 ± 0.33 for radix penis, $P<0.001$).

Conclusions. VTTQ can provide numerical measurements of penile rigidity and can effectively and sensitively indicate the axial and radial rigidity changes in penile erection, which provide a new approach to assessing the erectile function.

Key words: virtual touch tissue quantification; axial and radial rigidity; erection; shear wave velocity.

Introduction

Penile erection rigidity is one of the key factors for successful sexual intercourse, as well as an important index in the diagnosis and treatment of erectile dysfunction (ED). Ideally, the evaluation of ED should include the measurement of axial rigidity and radial rigidity. This requires special devices, such as RigiScan, Digital Inflexion Rigidometer. However, each device has its pros and cons, related to availability, convenience, validity and costs. For example, RigiScan is the most widely utilized device for measuring penile radial rigidity[1-5], but this device does not directly determine axial rigidity.[3,6,7] On the contrast, Digital Inflexion Rigidometer is a useful device for measuring penile axial rigidity[3,8,9], but it does not directly determine radial rigidity. Complete erection rigidity assessment needs a combinatorial use of RigiScan and Digital Inflexion Rigidometer, which increased the cost and inconvenience. Alternative methods for penile erection rigidity assessment are needed.

Ultrasound is widely used for clinical imaging[10,11], and virtual touch tissue quantification (VTTQ) is a new, promising implementation of the ultrasound acoustic radiation force impulse (ARFI) imaging, which can effectively and objectively detect the tissue rigidity by measuring the shear wave velocity (SWV) values.[12-14] Due to the non-invasive and easily accessible nature of VTTQ, this tech-

nology makes it possible to conduct a thoroughly evaluation of erectile rigidity at any portion and any direction in the penis without any discomfort and special preparation. Recently, VTTQ has been used to quantify the rigidity of the liver, kidneys, pancreas, spleen, prostate and breast.[12-19]

In our recent study, in order to provide a supplementary approach to assess the penile erection rigidity, we described the normal axial and radial SWV values of the penis by VTTQ and examined the clinical usefulness of this procedure in evaluation of the rigidity changes in penile erection.

Patients and methods

Study Population

Our study was approved by the local human research ethics committee and free informed consent was obtained from all the subjects. 37 healthy men with a mean age of 34.6 years (range: from 18 to 63 years) were recruited. All the subjects were evaluated by means of clinical and physical assessment, detailed sexual history, laboratory data (glucose, cholesterol, and triglycerides serum levels), and endocrine assays (testosterone, prolactin, follicular stimulation hormone, and luteinizing hormone), electrocardiogram, radiology, ultrasonographic (US) examinations and computer tomography. The inclusion criteria were: absence of any history of focal or diffuse disease at any of the examined organs. The subjects with risk factors for ED, such as diabetes mellitus, hypertension, ischemic heart disease, neurogenic injury to the spinal cord, and with psychogenic factors were excluded from the study.

Examination protocol

Two urologists with 10 years of experience in diagnosing and treating ED performed clinical assessments. Erectile response was induced by masturbation one hour after 100 mg sildenafil citrate (Pfizer, New York, NJ, USA) administration, and it was evaluated and judged by the urologist and subject at the same time. Penile erection was categorized into four grades using the following criteria.[20,21] Grade 0 (G0), flaccid; Grade 1(G1), mild tumescence; Grade 2(G2), moderate tumescence but inadequate rigidity for vaginal penetration; Grade 3(G3), full tumescence with moderate rigidity allowing vaginal penetration with some difficulty; and Grade 4(G4), full tumescence and full rigidity allowing vaginal penetration without difficulty.

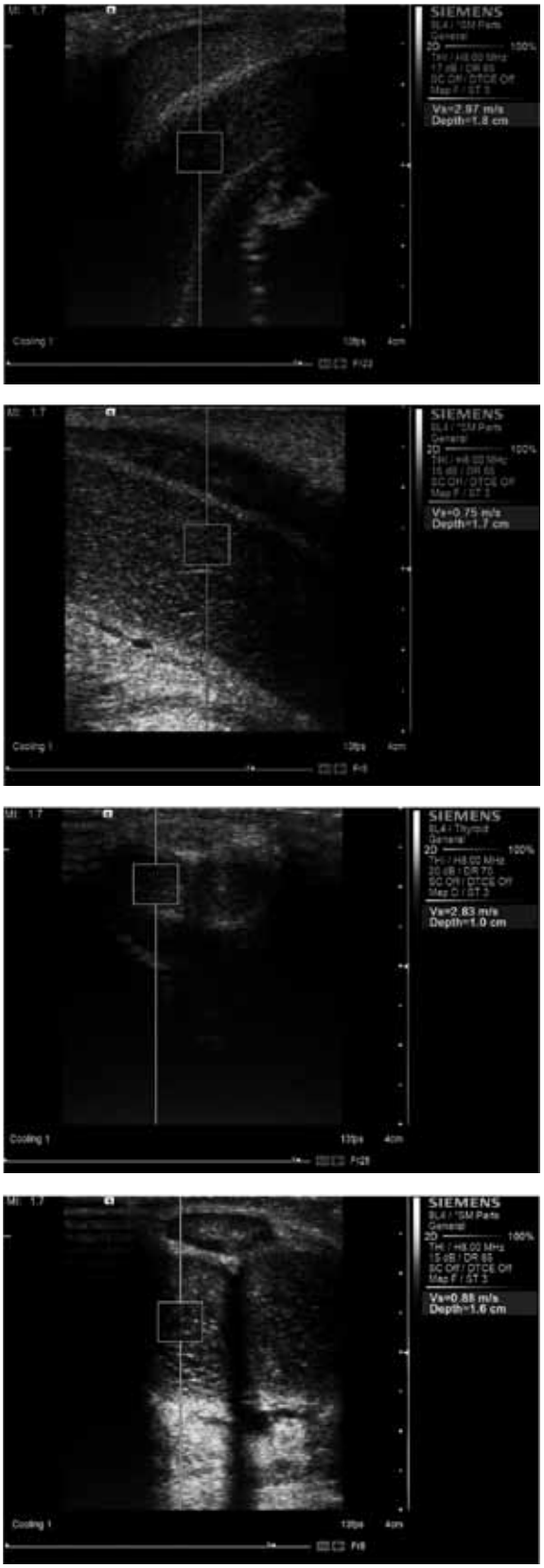

FIGURE 1. Shear wave velocity measurement in the penis with virtual touch tissue quantification during the erection (A and C: Grade 0; B and D: Grade 4) from the axial direction(A and B) and radial direction (C and D), respectively.

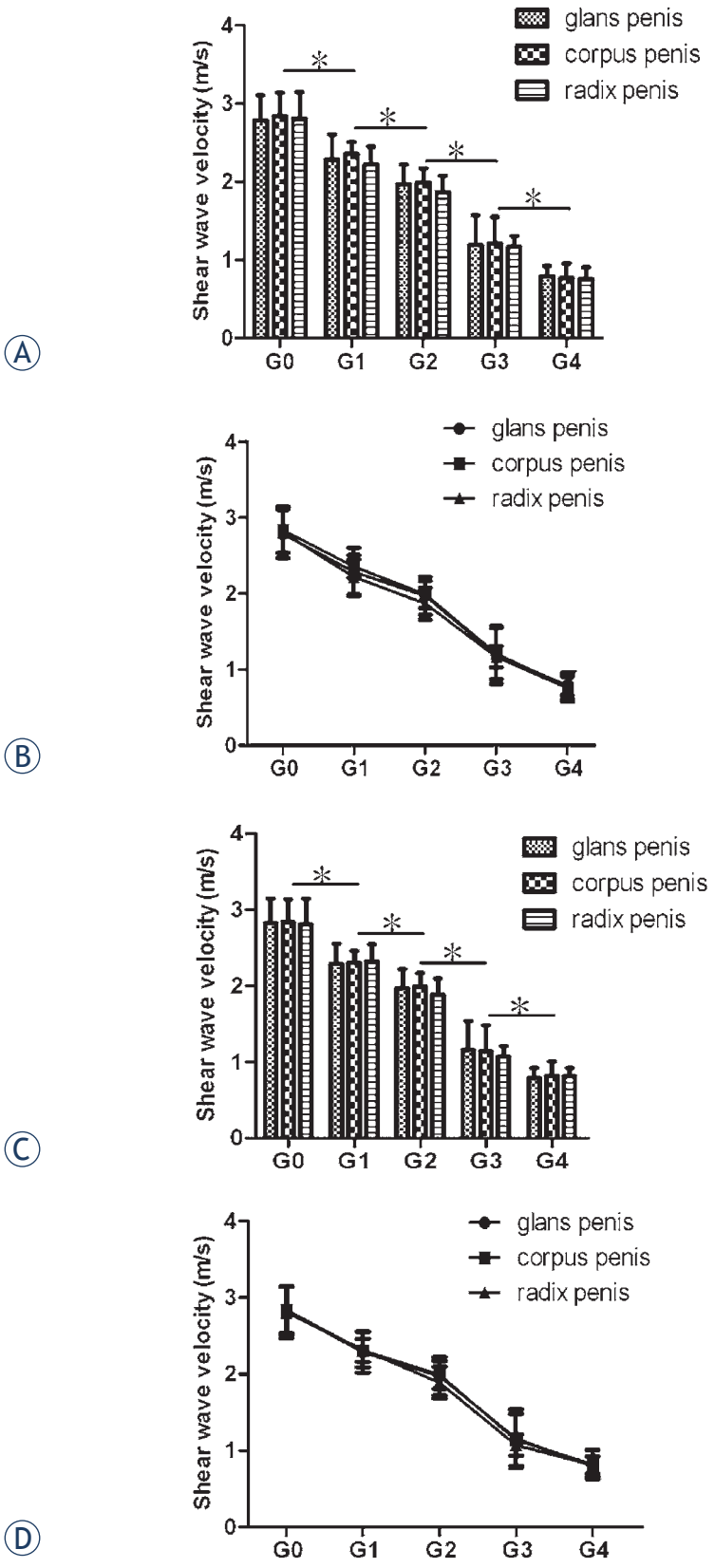

FIGURE 2. Comparison of penile shear wave velocities among different grades of penile erection. A and B: axial direction; C and D: radial direction. Error bars indicate SD, and asterisks indicate significant differences (*P < 0.05).

All US examinations were performed by two radiologists with 15 years of experience in US examinations. A Siemens ACUSON S200 0 US system (Siemens, Germany) equipped with a linear array transducer (9L4) was used in this study. A mechanical index of 1.0 and tissue harmonic imaging of 8 MHz were chosen. VTTQ was performed with the preliminary identification of a target region of interest (ROI) (box with fixed dimension of 6×5mm) on a conventional US image. Then, an acoustic push pulse was transmitted immediately on the right side of the ROI where the SWVs were calculated and expressed with a numerical value (metre/second, m/s) as a result of multiple measurements made for the same spatial location.

For the penis study, an optional cavernous body was chosen. Firstly, the long axis view was obtained. Three SWV measurements (anterior, center and posterior, *i.e.*, axial direction) at glans penis, corpus penis and radix penis in the course of erection were performed, respectively. Secondly, the short axis view was obtained. Three SWV measurements (left, center and right, *i.e.*, radial direction) at glans penis, corpus penis and radix penis in the course of erection were performed, respectively (Figure 1). Finally, the average SWV values of each portion were obtained.

Reproducibility

Intraobserver variability was assessed in 15 subjects by repeating the measurements on two occasions (7 days apart) under the same basal conditions. To test the interobserver variability, the measurements were performed on the same subject by a second observer who was blinded to the first observer's results. Variability was calculated as the mean percentage error, derived as the difference between the two sets of measurements, divided by the mean observations.

Statistical analysis and ethical consideration

Data were expressed as the mean ± SD. Differences between the mean values of the two groups were analyzed by unpaired t tests. Differences were considered significant at $p<0.05$. SPSS version 13.0 (SPSS, Chicago, IL, USA) was used for all statistical analysis.

The study was carried out according to the Declaration of Helsinki.

TABLE 1. Intraobserver and interobserver variability for shear wave velocity measurements.

Sites	Intraobserver variability(%)	Interobserver variability(%)
Axial direction		
Glans penis	2.2±1.3	2.6±1.5
Corpus penis	1.9±1.4	1.9±1.7
Radix penis	2.4±1.5	2.3±1.6
Radial direction		
Glans penis	2. 3±1. 1	2.5±1.4
Corpus penis	1.9±1.6	1.9±1.5
Radix penis	2.4±1.6	2.6±1.7

Results

As shown in Figure 2, the axial and radial SWV values did not differ at the same portion, neither did they among the glans penis, corpus penis and radix penis at the same grades of erection. They all significantly decreased from Grade 0 to Grade 4 grades of erection. At Grade 4, they were less than one-third of that at Grade 0 (axial direction: 0.79 ± 0.13 vs. 2.79 ± 0.32 for glans penis, $P<0.001$; 0.77 ± 0.19 vs. 2.84 ± 0.30 for corpus penis, $P<0.001$ and 0.76 ± 0.15 vs. 2.81 ± 0.34 for radix penis, $P<0.001$; radial direction: 0.82 ± 0.15 vs. 2.83 ± 0.31 for glans penis, $P<0.001$; 0.79 ± 0.18 vs. 2.81 ± 0.27 for corpus penis, $P<0.001$ and 0.81 ± 0.16 vs. 2.82 ± 0.33 for radix penis, $P<0.001$).

Intraobserver and interobserver variability for shear wave velocity measurements are shown in Table 1. They were all smaller than 5%.

Discussion

The results presented here indicate that VTTQ can provide numerical measurements of penile rigidity and can effectively and sensitively indicate the rigidity changes in penile erection, which provide a new approach to assessing the erectile function.

ARFI imaging is a new ultrasound imaging modality to evaluate the stiffness of tissues by short-duration acoustic radiation forces that produce localized displacements in a 'pushed' ROI,[13,22,23] where shear waves (transverses wave propagating perpendicular to the direction of tissue displacement) are generated without the need for external compression.[24] The induced displacements are indicative of local tissue mechanical properties[14], and the velocities of shear waves are proportional to tissue rigidity. Fundamentally, SWV is positively correlated with the major mechanical properties indicating material rigidity assuming the material is a linear, isotropic, elastic body.[25] The stiffer the tissue, the faster the shear wave will be propagated. However, our study showed that the greater the grades of erection, the smaller the SWV values were measured, *i.e.*, the stiffer the penis, the slower the shear wave would be propagated. In our study, SWV was negatively correlated with penile rigidity. This finding can be explained by the fact that cavernous body of penis is not a linear, isotropic, elastic body and the penile erection is a multiple neurovascular event as follow[26]: 1) nerve impulses cause the release of neurotransmitters and relaxing factors; 2) relaxation of smooth muscle in the arteries and arterioles supplies the erectile tissue; 3) several times increase in the blood flow to the penis; 4) relaxation of the trabecular smooth muscle increases the compliance of the sinusoids, facilitating rapid filling and expansion of the sinusoidal system; 5) venular subtunical plexes are compressed between the trabeculae and the tunica albuginea, resulting in almost total occlusion of venous outflow. In the process of penile tumescence, erectile tissue within the ROI gradually decreased and the blood flow within the ROI gradually increased. So the penile SWV values accordingly decreased from Grade 0 to Grade 4 of erection, because a low SWV value, even a "XXXX/0" value is always obtained from the fluids such as blood, water.[13]

In our study, axial rigidity and radial rigidity was separately assessed at the long axis view and the short axis view of the corpora cavernosa by measuring the SWV values. They did not differ at the same portion, neither did they among the glans penis, corpus penis and radix penis at the same grades of erection, because they share a common dependency upon intracavernosal pressure. As a surrogate measure of erection, both axial rigidity and radial rigidity assessed by the SWV values are the most accurate one.

Although VTTQ can potentially be an important quantitative tool for erectile function, there are some limits in the present study. For example, the specimens of subjects are limited. Not all subjects have a satisfactory erectile response to the induction of masturbation after sildenafil citrate administration. Semiquantitative clinical grading of an erection is not very accurate. In the further study, a comparison of VTTQ and RigiScan or Digital Inflexion Rigidometer for the evaluation of penile erection rigidity should be done. There are also some problems with the use of VTTQ for the penile erection rigidity assessment. The fixed box dimension (6×5mm) of the target ROI and the sensitivity to movement artifacts may become obstacles to the extensive application of this new technology.

Conclusion

This is the first study on the evaluation of penile erection rigidity using VTTQ. Our study indicates that VTTQ can simultaneously provide numerical measurements of penile axial rigidity and radial rigidity at a precise image-based anatomical location, and can effectively and sensitively indicate the rigidity changes in penile erection. Although several limitations mentioned above, this method still holds considerable clinical promise for the assessment of erectile function

Acknowledgements

The authors gratefully acknowledge the technical assistance and helpful discussion of Zhou J Zhang YJ at the department of Urology, and Fan GX, Chen J at the department of ultrasound, The First People's Hospital of Yancheng, Jiangsu Province, P.R.China.

References

1. Eardley I, Ellis P, Boolell M, Wulff M. Onset and duration of action of sildenafil citrate for the treatment of erectile dysfunction. *Br J Clin Pharmacol* 2002; **53:** 61S-65S.
2. Yaman O, Tokatli Z, Akand M, Elhan AH, Anafarta K. Characteristics of sildenafil erections in healthy young men. *Asian J Androl* 2005; **7:** 395-8.
3. Mizuno I, Komiya A, Watanabe A, Fuse H.Importance of axial penile rigidity in objective evaluation of erection quality in patients with erectile dysfunction--comparison with radial rigidity. *Urol Int* 2010; **84:** 194-7.
4. Yuan YM, Zhou S, Zhang K. Methods for evaluation of penile erection hardness. *Zhonghua Nan Ke Xue* 2010; **16:** 642-5.
5. Elhanbly S, Elkholy A, Elbayomy Y, Elsaid M, Abdel-gaber S. Nocturnal penile erections: the diagnostic value of tumescence and rigidity activity units Nocturnal penile erections. *Int J Impot Res* 2009; **21:** 376-81.
6. Ku JH, Song YS, Kim ME, Lee NK, Park YH. Is there a role of radial rigidity in the evaluation of erectile dysfunction? *Int J Impot Res* 2001; **13:** 200-4.
7. Allen RP, Smolev JK, Engel RM, Brendler CB. Comparison of Rigiscan and formal nocturnal penile tumescence testing in the evaluation of erectile rigidity. *J Urol* 1993; **149:** 1265-8.
8. Rosselló Barbará M. Digital inflection rigidometry in the study of erectile dysfunction. A new technique. *Arch Esp Urol* 1996; **49**: 221-7.
9. El-Sakka AI. Association between International Index of Erectile Function and axial penile rigidity in patients with erectile dysfunction. *Int J Impot Res* 2003; **15:** 426-9.
10. Kutlu R, Soylu A. Deep dorsal vein embolization with N-butyl-2-cyanoacrylate and lipiodol mixture in venogenic erectile dysfunction: early and late results. *Radiol Oncol* 2009; **43:** 17-25.
11. Rados M, Sunjara V, Sjekavica I, Padovan RS. Post-traumatic high-flow priapism treated by endovascular embolization using N-butyl-cyanoacrylate. *Radiol Oncol* 2010; **44:** 103-6.
12. Zheng XZ, Ji P, Mao HW, Zhang XY, Xia EH, Gu X, et al. A novel approach to assessing the changes in prostatic stiffness with age using virtual touch tissue quantification. *J Ultrasound Med* 2011; **30:** 387-90.
13. Gallotti A, D'Onofrio M, Pozzi Mucelli R. Acoustic radiation force impulse (ARFI) technique in ultrasound with virtual touch tissue quantification of the upper abdomen. *Radiol Med* 2010; **115:** 889-97.
14. Osaki A, Kubota T, Suda T, Igarashi M, Nagasaki K, Tsuchiya A, et al. Shear wave velocity is a useful marker for managing nonalcoholic steatohepatitis. *World J Gastroenterol* 2010; **16:** 2918-25.
15. D'Onofrio M, Gallotti A, Mucelli RP. Tissue quantification with acoustic radiation force impulse imaging: Measurement repeatability and normal values in the healthy liver. *Am J Roentgenol* 2010; **195:**132-6.
16. D'Onofrio M, Gallotti A, Salvia R, Capelli P, Mucelli RP. Acoustic radiation force impulse (ARFI) ultrasound imaging of pancreatic cystic lesions. *Eur J Radiol* 2011; **80:** 241-4.
17. Clevert DA, Stock K, Klein B, Slotta-Huspenina J, Prantl L, Heemann U, et al. Evaluation of Acoustic Radiation Force Impulse (ARFI) imaging and contrast-enhanced ultrasound in renal tumors of unknown etiology in comparison to histological findings. *Clin Hemorheol Microcirc* 2009; **43:** 95-107.
18. Meng W, Zhang G, Wu C, Wu G, Song Y, Lu Z.Preliminary Results of Acoustic Radiation Force Impulse (ARFI) Ultrasound Imaging of Breast Lesions. *Ultrasound Med Bio*. 2011; 37**:** 1436-43.
19. Zheng XZ, Ji P, Mao HW, Hu JQ. A comparison of virtual touch tissue quantification and digital rectal examination for discrimination between prostate cancer and benign prostatic hyperplasia. *Radiol Oncol* 2012; **46:** 69-74.
20. Huang ST, Hsieh ML. Different hemodynamic responses by color Doppler ultrasonography studies between sildenafil non-responders and responders. *Asian J Androl* 2007; **9:** 129-33.
21. Gontero P, Sriprasad S, Wilkins CJ, Donaldson N, Muir GH, Sidhu PS. Phentolamine re-dosing during penile dynamic colour Doppler ultrasound: a practical method to abolish a false diagnosis of venous leakage in patients with erectile dysfunction. *Br J Radiol* 2004; **77:** 922-6.
22. Nightingale K, Soo MS, Nightingale R, Trahey G. Acoustic radiation force impulse imaging: in vivo demonstration of clinical feasibility. *Ultrasound Med Biol* 2002; **28:** 227-35.
23. D'Onofrio M, Gallotti A, Martone E, Pozzi Mucelli R. Solid appearance of pancreatic serous cystadenoma diagnosed as cystic at ultrasound acoustic radiation force impulse imaging. *JOP* 2009; **10:** 543-6.
24. Nightingale K, Bentley R, Trahey G. Observations of tissue response to acoustic radiation force: opportunities for imaging. *Ultrason Imaging* 2002; **24:** 129-38.
25. Palmeri ML, Sharma AC, Bouchard RR, Nightingale RW, Nightingale KR. A finite-element method model of soft tissue response to impulsive acoustic radiation force. *IEEE Trans Ultrason Ferroelectr Freq Control* 2005; **52:** 1699-712.
26. Martínez-Salamanca JI, Martínez-Ballesteros C, Portillo L, Gabancho S, Moncada I, Carballido J. Physiology of erection. *Arch Esp Urol* 2010; **63:** 581-8.

research article

Lucifer Yellow uptake by CHO cells exposed to magnetic and electric pulses

Leila Towhidi[1,3], Seyed Mohammad P Firoozabadi[1], Hossein Mozdarani[2], Damijan Miklavcic[3]

[1] Tarbiat Modares University, Department of Medical Physics, Tehran, Iran
[2] Tarbiat Modares University, Department of Medical Genetics, Tehran, Iran
[3] University of Ljubljana, Faculty of Electrical Engineering, Ljubljana, Slovenia

Radiol Oncol 2012; 46(2): 119-125.

Received 2 August 2011
Accepted 15 December 2011

Correspondence to: Prof. Seyed Mohammad P Firoozabadi, Tarbiat Modares University, Jalal Ale Ahmad Highway, PO Box 14395-587 Tehran Iran. Phone: +98(21) 88011001, ext 3821; Fax: +98(21) 88006544; E-mail: pourmir@modares.ac.ir

Disclosure: No potential conflicts of interest were disclosed.

Background. The cell membrane acts as a barrier that hinders free entrance of most hydrophilic molecules into the cell. Due to numerous applications in medicine, biology and biotechnology, the introduction of impermeant molecules into biological cells has drawn considerable attention in the past years. One of the most famous methods in this field is electroporation, in which electric pulses with high intensity and short duration are applied to the cells. The aim of our study was to investigate the effect of time-varying magnetic field with different parameters on transmembrane molecular transport.

Materials and methods. 'Moreover, a comparison was made between the uptake results due to magnetic pulse exposure and electroporation mediated uptake.' at the end of Background part. The Chinese hamster ovary (CHO) cells were exposed to magnetic pulses of 2.2 T peak strength and 250 μs duration delivered by Magstim stimulator and double 70 mm coil. Three different frequencies of 0.25, 1 and 10 Hz pulses with 112, 56 and 28 number of pulses were applied (altogether nine experimental groups) and Lucifer Yellow uptake was measured in each group. Moreover, maximum uptake of Lucifer Yellow obtained by magnetic pulses was compared to the measured uptake due to electroporation with typical parameters of 8 pulses of 100 μs, repetition frequency of 1 Hz and electric field intensities of 200 to 600 V/cm.

Results and conclusions. Our results show that time-varying magnetic field exposure increases transmembrane molecular transport and this uptake is greater for lower frequencies and larger number of pulses. Besides, the comparison shows that electroporation is more effective than pulsed magnetic field, but the observed uptake enhancement due to magnetic exposure is still considerable.

Key words: electroporation; electro-endocytosis; time-varying magnetic field; transmembrane molecular transport.

Introduction

The cell membrane acts as a barrier that hinders free entrance of most hydrophilic molecules into the cell. Effects of electromagnetic fields on biological systems have been intensively investigated for possible damaging, diagnostic and therapeutic effects[1-3] considering the cell membrane as the primary site of interaction.[4] One of the interesting aspects of electromagnetic exposures is the incorporation of impermeant molecules such as macromolecules, drugs and proteins into biological cells without affecting cell physiological functioning and viability which can have numerous applications in medicine and biology. This has been mainly achieved, both *in vitro* and *in vi*vo by electroporation[5-8], a process in which cells are exposed to a short duration (μs -ms) high intensity electric pulses (hundreds of V/cm).[8-10] Electroporation is nowadays widely used in biotechnology[11,12] and in the medical applications such as electrochemotherapy[13-16] and gene electrotransfer.[5,17-21] The suggested mechanism for this phenomenon is a structural change in plasma membrane resulting in pores formation.[6,22]

However, train of pulsed low electric field with a field strength value as low as 2.5-20 V/cm, frequency of a few hundred Hz and total exposure time of 1-10 min has been shown to be effective in enhancing uptake of large molecules into the cells. In this technique the pulse amplitude is not high enough to create pores and, assumingly, there are different pathways of molecular transport (*i.e.* electro-endocytosis).[23-25] Furthermore, it was previously shown that the 900 MHz continuous sine wave and Global System for Mobile Communications (GSM) electromagnetic field increased *in vitro* molecular uptake by cells.[26] The considered GSM were square pulses with a low frequency envelope of 217 Hz and high frequency carrier sine wave of 900 MHz. In that study it was also demonstrated that pulsed electric field of low intensity (2.6 V/cm), duration of 580 μs and with the frequency of the applied GSM (217 Hz) produced the same effect on LY uptake.[26] In another study, the activation of K^+ and Na^+ pumping by an oscillating electric field (20 V/cm, 1 KHz) has been reported.[27]

Despite intensive studies on uptake increase due to different exposures, the possible effect of magnetic pulses on cell membrane permeability has not yet been tested. We hypothesize that pulsed magnetic field exposure, which induces electric field, will increase the molecular uptake of biological cells. In this paper, we present results of an experimental study of the effect of magnetic pulses on the cellular uptake. We determined the uptake of fluorescent dye Lucifer Yellow into adherent Chinese Hamster Ovary (CHO) cells due to time-varying magnetic field exposure. The uptake of fluorescent dye was determined for different frequencies and number of pulses. In addition, a comparison between the molecular uptake due to magnetic pulse exposure and the "conventional" electroporation was performed.

Materials and methods

Cells

Chinese hamster ovary cells (CHO-K1) (Pasteur Institute, Iran) were grown in HAM-F12 (Dulbecco's modification of the Eagle's Minimum Essential Medium – EMEM) containing 8% foetal calf serum, 160 μg/ml L-glutamine (all from Invitrogen-GIBCO BRL, Grand Island, NY, USA), 100 units/ml penicillin and 16 μg/mg gentamicin and incubated in 5% CO_2 at 37°C. The cells were plated in 35 mm Petri dishes at 10^6 cells per dish and incubated in HAM-F12 the day before the experiments. At the time of the experiments, the cells cover the surface of Petri dish completely in the form of monolayer. Just before applying the pulses, the culture medium in Petri dishes was replaced with 2 ml (2 mm media height in the dish) pulsing buffer (consisting of 250 mM sucrose, 10 mM KH_2PO_4/K_2HPO_4 and 1 mM $MgCl_2$) containing 500 μM Lucifer Yellow (Invitrogen-Molecular Probes, Eugene, OR, USA).

Magnetic pulse exposure

The magnetic pulse generator used in this study was Magstim (Magstim Rapid, Magstim Company, Withland, UK) which is usually used for non-invasive transcranial magnetic stimulation of human tissue.[28-30] Such devices consist of a stimulating coil connected to a high-voltage discharge system which produces a very strong and short discharge current resulting in induced time varying magnetic fields. Based on Maxwell-Faraday equation, this strong pulsed magnetic field induces an electric field of the order of tens of volts per centimetre in the space around the coil.[31,32]

It has been demonstrated that figure-of-eight coils allow for a more focused and greater peak electric field than simple round coils.[31,33] Moreover, the smaller coils induce higher magnetic field intensities than larger coils but the field falls off much more rapidly with distance.[31,33] The optimum coil for our experiments in order to deliver the most intense fields with larger decay time constant was a 70 mm figure-of-eight coil with 100% energy transfer (Figure 1A). The magnetic field strength decreases rapidly with the distance from the stimulating coil so that the field strength is peaked close to the coil surface.[31,34] Therefore, the Petri dishes containing the cells were placed under the coil where two windings meet and attached to the coil in order to expose cells to the strongest possible magnetic field. The geometry of the coils, the Petri dish in the experiments and direction of current flow through each winding of the coil are shown in Figure 1B.

During the exposures, the cells were attached at the bottom of the Petri dishes with radius of 17.5 mm and height of 10 mm. In previous studies, the distribution of magnetic and induced electric fields for different coils including the chosen coil in our experiments (70 mm figure-of-eight)[31,35] are obtained. Considering results of these studies and the dimensions of the Petri dishes, the spatial distribution of field delivered to cells was approximately uniform at the Petri dish location. The strength

and duration of pulses in all experiments were the same and investigated parameters were pulse repetition frequencies (0.25, 1 and 10 Hz) and number of pulses in each train of pulses (112, 56 and 28 pulses). The main frequency considered in this study was 0.25 Hz in order to have several minutes exposure time before warming up the device and the coil. In this frequency, the maximum possible number of delivered pulses was about 112. Then, to demonstrate the effect of number of pulses, half and a quarter of 112 (*i.e.* 56 and 28 pulses) for each pulse repetition frequency were also studied.

Electric pulse exposure

A pair of parallel Pt/Ir wire electrodes with 0.8 mm diameter and 25 mm length spaced 5 mm from each other was positioned at the bottom of Petri dishes. Electric pulses were generated by a Cliniporator device (IGEA s.r.l., Carpi, Modena, Italy). The electroporation results depend on pulse parameters such as pulse shape, frequency, duration and number of pulses.[8,10,35] We have chosen some typical electroporation parameters of 8 pulses of 100 μs and repetition frequency of 1 Hz. Based on previous electroporation studies on suspension and attached biological cells[10,36,37], the voltages delivered to the electrodes were selected to be between 100 and 300 V (*i.e.* voltage-to-distance ratios of 200 to 600 V/cm) with increment of 50 V (*i.e.* voltage-to-distance ratio incrementing by 100 V/cm).

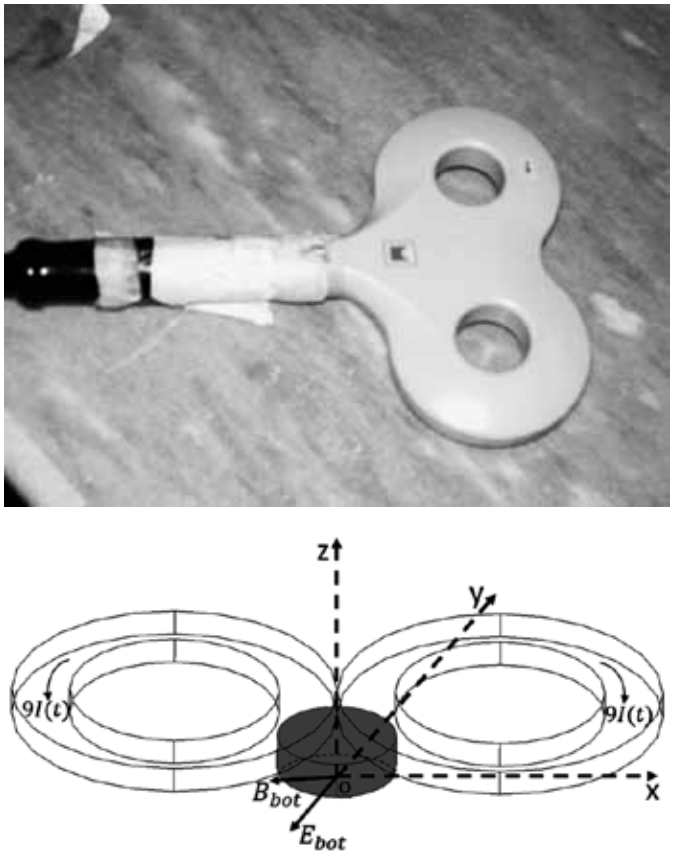

FIGURE 1. (A) Photograph of a 70 mm figure-of-eight coil used in the magnetic pulse exposure experiments. (B) Schematic of Petri dish location under figure-of-eight coil during magnetic field exposure. The direction of current passing through each winding is shown. The direction of resulted electric and magnetic field at the bottom of the Petri dish are displayed.

Determination of Lucifer Yellow uptake

Lucifer yellow (LY) is an impermeant florescent dye[38] which in case of penetrating through the membrane, stays inside the cell and does not affect the cell viability due to its non-toxicity.[39] Thus using a standard protocol[40], the quantity of Lucifer Yellow taken up by the cells can be measured at given time after the exposure of cells to magnetic or electric pulses. In our experiments, after the exposure of cells to the magnetic or electric pulses, the cells were incubated at room temperature for 40 minutes to allow resealing of the plasma membrane.[8,41] The cells were then washed four times with phosphate buffer saline (PBS, Life Technologies, Paisley, UK) to remove Lucifer Yellow from extracellular medium. Cells were then broken down by adding diluted HCl for 12 hours and then the total fluorescence taken up by the cells was measured in arbitrary units on a spectrofluorometer (Shimadzu RF-5000, Japan). The excitation and emission wavelengths were set at 418 and 525 nm, respectively.

As the electroporation electric pulses were applied to the cells via two electrodes separated 5 mm and positioned at the bottom of the Petri dishes, only the cells located between these two electrodes are exposed to the electric field (25×5 mm^2). But in the case of time-varying magnetic field exposure, the magnetic pulses are applied to all the cells in the Petri dish located under the coil ($\pi \times 35^2/4$ mm^2). Thus to make the obtained data comparable, the ratio of exposed area was taken into account. This has been accomplished via multiplying the measured fluorescence with the ratio of the Petri dish area and the area between two electrodes.

The laboratory temperature during the experiments was about 25°C. Results were given as a percent of control. The procedures for the control group samples were identical to exposed cells (*i.e.* Lucifer Yellow was added to their medium) except that no pulses were delivered. All results are given as average of 4 to 13 repetitions and are presented

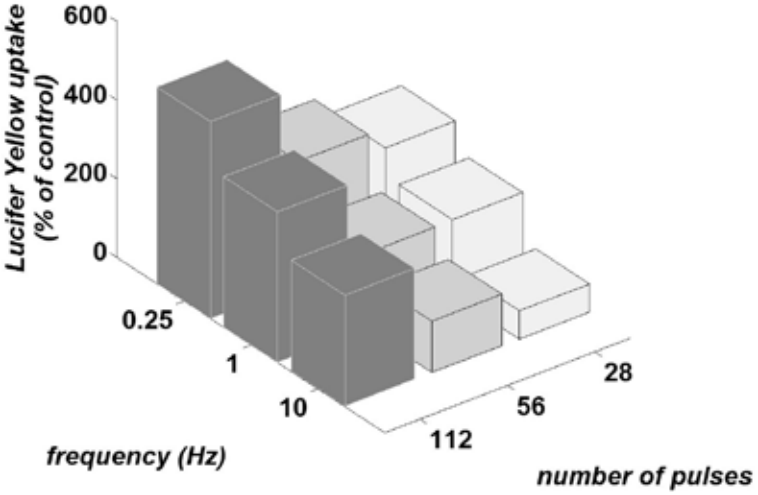

FIGURE 2. Dye uptake of attached CHO cells for three different frequencies 0.25, 1 and 10 Hz with three different numbers of pulses 112, 56 and 28 for each chosen frequency. Attributed number to the control group was chosen 100 and the fluorescence of other groups was computed as the percent of control fluorescence.

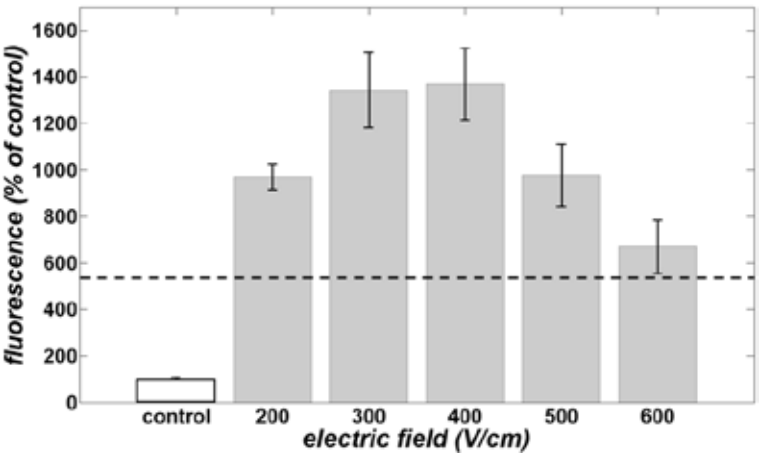

FIGURE 3. Dye uptake of attached CHO cells. The white bar shows the control group normalized to 100. The fluorescence of other groups was computed as the percent of control fluorescence. The gray bars show uptake attributed to different electric field exposure amplitudes of 8 pulses of 100 μs and 1 Hz for electroporation experiments. The dashed line demonstrates the greatest uptake of cells due to magnetic field exposure (112 pulses of 0.25 Hz). Vertical bars represent standard deviation of the mean.

in bar graphs. In order to perform a statistical analysis, Mann-Whitney Rank-Sum test was used.

Results

Figure 2 shows the uptake of Lucifer Yellow for 9 different sets of parameters of magnetic field exposure (three different frequencies of 0.25, 1 and 10 Hz pulses for 112, 56 and 28 pulses). The value of the control group fluorescence was considered as 100 and the fluorescence of experimental groups was normalized to the control group. The comparisons of the uptake between the control group and exposed groups and also between exposed groups were performed using the Mann-Whitney Rank-Sum test. The P-value for the significance level of distinct groups was set equal to 0.05.

The statistical results show that for all frequencies of 0.25, 1 and 10 Hz, exposure of 112 pulses is significantly more efficient in comparison with a control group, 56 and 28 pulses. Moreover, for none of the 0.25, 1 and 10 Hz frequencies, one can observe any significant difference between 28 and 56 pulses groups. For 10 Hz group, there is even no significant difference between the last two groups and the control group.

Exposure to 112 of pulses and frequency of 0.25 Hz result in the highest uptake of Lucifer Yellow. The same number of pulses delivered at frequencies of 1 and 10 Hz shows, however, no significant difference. With 56 pulses, 0.25 Hz frequency is more effective than the two other frequencies while frequency of 10 Hz shows no significant difference with the control group. With 28 number of pulses, 0.25 and 1 Hz make no significant difference at 28 pulses, but they are more efficient relative to the control group; between 10 Hz group and the control group, however, no difference was observed.

Based on above observations, we may state that the dye uptake is greater for lower frequencies and larger number of pulses.

In order to compare cell exposure to magnetic pulses with the conventional method for membrane permeability increase (*i.e.* electroporation), the uptake enhancement of attached CHO cells due to determined applied electric pulses were also investigated. The cells were exposed to 8 pulses of 100 μs duration and 1 Hz pulse repetition frequency of five different electric field intensities (200 to 600 V/cm with 100 V/cm increment). The resulted value for cellular uptake of LY due to electroporation with different pulse amplitudes are displayed in gray in Figure 3. For an easier comparison, the highest measured fluorescence of cells due to the magnetic pulse exposure (112 pulses of 0.25 Hz) is shown with dashed line. The control group is illustrated in white. The comparisons of the uptake between the control group, groups exposed to electric pulses and groups exposed to magnetic pulses were performed using the Mann-Whitney Rank-Sum test. The results of this comparison show that with selected parameters of electric and magnetic exposures, both give rises to the uptake enhancement and have a significant difference with the

control group. Although the results show that all the electric pulse exposure groups, except the one with 600 V/cm field strength, were significantly more effective than magnetic pulse exposure groups (Figure 3).

Discussion

The results of the experimental study on exposing the cells by magnetic pulses show that magnetic pulses can efficiently increase Lucifer Yellow uptake by CHO cells. The amount of florescence measured for the control group not exposed to the pulses was ascribed to the remaining extracellular Lucifer Yellow after washings and also to the uptake due to normal endocytotic process. The results show that all experimental groups except groups exposed to 28 and 56 pulses at 10 Hz have the significantly higher uptake of Lucifer Yellow when compared to the control group. We thus conclude that generally applying magnetic pulses can enhance the uptake of molecules by cells. The results show (Figure 2) that magnetic pulses of the same number but different frequencies to the cells indicate that lower frequencies are more efficient. Furthermore, we observe that increasing the number of pulses enhances dye uptake. It is important to note that the total exposure time for different numbers of pulses used in experiments was different for different frequencies. For example total exposure time for 112 pulses of 0.25, 1 and 10 Hz frequencies were 467, 116 and 11 seconds, respectively.

In addition, the uptake of Lucifer Yellow due to exposure to magnetic pulses of 112 pulses of 0.25 Hz was compared to the exposure of cells electroporated by electric pulses of 1 Hz, duration of 100 μs and electric field amplitudes usually used in electrochemotherapy protocols. The results of this comparison show that with the selected parameters of exposures, both give rises to the uptake enhancement and have a significant difference with the control group, although increase due to exposure of cells to magnetic field is considerably smaller when compared to "classical" electroporation (Figure 3).

The increased permeability in electroporation is believed to be due to exceeding of induced transmembrane voltage from a critical value of few hundred mV. Note that a transmembrane voltage of this amplitude can be by exposing cells to an electric field of few hundred V/cm.[42,43] This high electric field, as suggested in literature, causes structural changes and pore formation in the cell membrane which in turn give rise to an increase of permeability and cellular uptake.[6] In magnetic pulse exposure, the induced electric field due to a time varying magnetic field at the cells position was about 6 V/cm.[31] This field strength is by far much smaller than the electric field needed for electroporation[44] and is unable to form pores in the plasma membrane (although the exposure time in the latter is by far much larger *i.e.* 7 minutes in the latter, contrast to 8 seconds in the former). Therefore, we need to seek an alternative mechanism responsible for the observed increase of dye uptake by the cells in our experiment using magnetic pulses.

Previous studies have shown that long train of low pulsed electric field with a field strength value as low as 2.5-20 V/cm, frequency of a few hundred Hz and total exposure time of 1–10 minutes enhances the uptake of large molecules into the cells.[24,25] The reason for the uptake increase was explained by the imbalance of charge distribution in the two opposite leaflets of the cell membrane due to the electric forces. This charge imbalance was stipulated to stimulate endocytotic-like process named electro-endocytosis. The efficiency of incorporation of macromolecules into the cells depended on the electrical parameters of exposure such as pulse amplitude, duration, frequency and total time of exposure.[25] In another study, the effect of mobile phone electromagnetic fields with envelope frequency of 217 Hz, carrier frequency of 900 MHz and pulse duration of 580 μs were investigated and the uptake increase was reported.[26] Furthermore, it was also demonstrated that the electric component of electromagnetic fields was responsible for this increase. The associated pulsed electric field in their study featured low intensity electric field 1.2-8 V/cm, pulse duration from 75 to 580 μs, frequency from 50 to 400 Hz and total exposure duration from 5 to 90 min.[26] It was demonstrated that the dye uptake in both cases increased due to fluid-phase endocytosis. The exposure of cells to such electric fields results in mV range induced transmembrane voltage – similar to studies reporting electro-endocytosis. In other studies on electroporation, it was proposed that the tangentional component of the field on the external leaflet of the membrane may result in electrophoretic mobility of the charges, proteins and lipids of the membrane, enzyme fluctuation or ruffling. This in turn may induce endocytosis which might last for about one hour after applying pulses.[45-48]

We now discuss the case of magnetic pulse exposure. Pulsed magnetic field induces an electric field. This electric field is circular and tangentional

in the interacellular region. The order of the electric field is comparable with low amplitude electric field in foregoing studies. Thus, the attributed cellular uptake increase can be convincingly explained based on the suggested above mentioned mechanisms with exerting electrophoretic mobility on the outer leaflet of the membrane and inducing endocytosis. We, thus, suggest that electro-endocytosis might facilitate the passage of external substances into the cell.

On the other hand, it is suggested in a survey that magnetic field pulses might create metastable cell membrane pores via interaction with membrane-attached magnetic particles and ubiquitous ferromagnetic contaminant particles exist in solutions and media.[49] Therefore, another possible mechanism for the uptake enhancement due to magnetic pulse exposure is the interaction of transient magnetic field with these particles. This may cause some effects even creating membrane pores due to rotational motion of a membrane-bound particle and transferring enough energy and consequently increasing the cellular uptake.

The purpose of our study was to test enhanced molecular uptake by cells due to the exposure of cells to magnetic pulses. According to the results of our study, with applying time-varying magnetic field the uptake of extracellular molecules to the cells increases significantly. Our results show that this increase is more obvious for lower frequencies and larger number of pulses (also associated with longer time exposure). We also give plausible explanations of the underlying mechanisms. It remains, however, to determine exact mechanisms of this increased uptake of molecules and to test if this technique can be used also *in vivo* for example for the treatment of tumours like electroporation in electrochemotherapy. Considering the fact that magnetic fields *i.e.* transcranial magnetic stimulation are able to focus and pass unhindered through skin, muscle and bone, this approach can potentially be useful in treating deep-seated tumours noninvasively.

Acknowledgement

Part of this work has been done in University of Ljubljana. L.T. wishes to acknowledge kindness of Dr. Marjan Mihelin for providing Magstim device for parts of our experiments. She also thanks Gorazd Pucihar and Tadej Kotnik for several fruitful discussions and Morteza Aslaninejad for critical reading of the manuscript.

References

1. Barnes FS, Greenebaum B. *Biological and medical aspects of electromagnetic fields. Handbook of biological effects of electromagnetic fields.* Third edition. Boca Raton: Taylor and Francis group, CRC Press; 2006.
2. Cameron IL, Short NJ, Markov MS. Safe alternative cancer therapy using electromagnetic fields *The Environmentalist*2007; **27:** 453-6.
3. Pope J. *Medical physics: imaging*. Portsmouth: Heinemann; 1999.
4. Adey WR. *International encyclopedia of neuroscience.* Third edition. New York: Elsevier; 2003.
5. Neumann E, Schaefer-Ridder M, Wang Y, Hofschneider PH. Gene transfer into mouse lyoma cells by electroporation in high electric field. *EMBO J* 1982; **1:** 841-5.
6. Neumann, E, KakorinS, Tönsing K. Fundamentals of electroporative delivery of drugs and genes. *Bioelectrochem Bioenerg* 1999; **48:** 3-16.
7. Teissié J, Rols MP. An experimental evaluation of the critical potential difference inducing cell membrane electropermeabilization. *Biophys J* 1993; **65:** 409-13.
8. Kotnik T, Pucihar G, Rebersek M, Mir LM, Miklavcic D. Role of pulse shape in cell membrane electropermeabilization. *Biochim Biophys Acta* 2003; **1614:** 193-200.
9. Valic B, Golzio M, Pavlin M, Schatz A, Faurie C, Gabriel B, et al. Effect of electric field induced transmembrane potential on spheroidal cells: theory and experiment. *Eur Biophys J* 2003; **32:** 519-28.
10. Miklavcic D, Towhidi L. Numerical study of the electroporation pulse shape effect on molecular uptake of biological cells. *Radiol Oncol* 2010; **44:** 34-41.
11. Faurie C, Golzio M, Phez E, Teissié J, Rols MP. Electric field induced cell membrane permeabilization and gene transfer: theory and experiments. *Eng Life Sci* 2005; **5:** 179-86.
12. Teissie J, Eynard N, Vernhes MC, Bénichou A, Ganeva V, Galutzov B, et al. Recent biotechnological developments of electropulsation. A prospective review. *Bioelectrochem* 2002; **55:** 107-12.
13. Sersa G, Miklavcic D, Cemazar M, Rudolf Z, Pucihar G, Snoj M. Electrochemotherapy in treatment of tumours. *Eur J Surg Oncol* 2008; **34:** 232-40.
14. Mir LM. Bases and rationale of the electrochemotherapy. *Eur J Cancer Suppl* 2006; **4:** 38-44.
15. Miklavčič D, Snoj M, Županič A, Kos B, Čemažar M, Kropivnik M, et al. Towards treatment planning and treatment of deep-seated solid tumors by electrochemotherapy. *Biomed Eng Online* 2010; **9:** 10.
16. He J, Wang X, Guan H, Chen W, Wang M, Wu H, et al. Clinical efficacy of local targeted chemotherapy for triple-negative breast cancer. *Radiol Oncol* 2011; **45:** 123-8.
17. Chiarella P, Fazio VM, Signori E. Application of electroporation in DNA vaccination protocols. *Curr Gene Ther* 2010; **10:** 281-6.
18. Prud'homme GJ, Glinka Y, Khan AS, Draghia-AkliR. Electroporation-enhanced nonviral gene transfer for the prevention or treatment of immunological, endocrine and neoplastic diseases. *Curr Gene Ther*2006; **6:** 243-73.
19. Cemazar M, Golzio M, Sersa G, Rols MP, Teissié J. Electrically-assisted nucleic acids delivery to tissues in vivo: where do we stand? *Curr Pharm Design* 2006; **12:** 3817-25.
20. Andre FM, Mir LM. Nucleic acids electrotransfer in vivo: mechanisms and practical aspects. *Curr Gene Ther* 2010; **10:** 267-80.
21. Pavlin D, Cemazar M, Cör A, Sersa G, Pogacnik A, Tozon N. Electrogene therapy with interleukin-12 in canine mast cell tumors. *Radiol Oncol* 2011; **45:** 30-9.
22. Böckmann RA, Groot BL, Kakorin S, Neumann E, Grubmüller H. Kinetics, statistics, and energetics of lipid membrane electroporation studied by molecular dynamics simulations. *Biophys J* 2008; **95:** 1837-50.
23. Rosemberg Y, Korenstein R. Incorporation of macromolecules into cells and vesicles by low electric fields: induction of endocytotic-like process. *Bioelectrochem Bioenerg* 1997; **42:** 275-81.

24. Antov Y, Barbul A, Korenstein R. Electroendocytosis: stimulation of adsorptive and fluid-phase uptake by pulsed low electric fields. *Exp Cell Res* 2004; **297:** 348-62.

25. Antov Y, Barbul A, Mantsur H, Korenstein R. Electroendocytosis: exposure of cells to pulsed low electric fields enhances adsorption and uptake of macromolecules. *Biophys J* 2005; **88:** 2206-22.

26. Mahrour N, Pologea-Moraru R, Moisescu MG, Orlowski S, Leveque P, Mir LM. In vitro increase of the fluid-phase endocytosis induced by pulsed radiofrequency electromagnetic fields: importance of the electric field component. *Biochim Biophys Acta* 2005; **1668:** 126-37.

27. Marszalek P, Tsong TY. Cell fission and formation of mini cell bodies by high frequency alternating electric field. *Biophys J* 1995; **68:** 1218-21.

28. Hallett M. Transcranial magnetic stimulation and the human brain. *Nature* 2000; **406:** 147-50.

29. Sinclair C, Faulkner D, Hammond G. Flexible real-time control of MagStim 200(2) units for use in transcranial magnetic stimulation studies. *J Neurosci Meth* 2006; **158:** 133-6.

30. Rossi S, Hallett M, Rossini P, Pascual-Leone A. Safety, ethical considerations, and application guidelines for the use of transcranial magnetic stimulation in clinical practice and research. *Clin Neurophys* 2009; **120:** 2008-39.

31. Jalinous R. Technical and practical aspects of magnetic nerve stimulation. *J Clin Neurophysiol* 1991; **8:** 10-25.

32. Roth y, Zangen A, Hallett M. A coil design for transcranial magnetic stimulation of deep brain regions. *J Clin Neurophysiol* 2002; **19:** 361-70.

33. Ravazzani P, Ruohonen J, Grandori F, Tognola G. Magnetic stimulation of the nervous system: induced electric field in unbounded, semi-infinite, spherical, and cylindrical media. *Ann Biomed Eng* 1996; **24:** 606-16.

34. Salinas FS, Lancaster JL, Fox PT. Detailed 3D models of the induced electric field of transcranial magnetic stimulation coils. *Phys Med Biol* 2007; **52:** 2879-92.

35. Macek-Lebar A, Sersa G, Kranjc S, Groselj A, Miklavcic D. Optimisation of pulse parameters in vitro for in vivo electrochemotherapy. *Anticancer Res* 2002; **22:** 1731-6.

36. Towhidi L, Kotnik T, Pucihar G, Firoozabadi SMP, Mozdarani H, Miklavcic D. Variability of the minimal transmembrane voltage resulting in detectable membrane electroporation. *Electromagn Biol Med* 2008; **27:** 372-85.

37. Marjanovič I, Haberl S, Miklavčič D, Kandušer M, Pavlin M. Analysis and comparison of electrical pulse parameters for gene electrotransfer of two different cell lines. *J Membrane Bio* 2010; **236:** 97-105.

38. Usaj M, Torkar D, Kanduser Mm Miklavcic D. Cell counting tool parameters optimization approach for electroporation efficiency determination of attached cells in phase contrast images. *J Microscopy* 2011; **241:** 303-14.

39. Stewart WW. Functional connexions between cells as revealed by dye coupling with a highly fluorescent naphthalamide tracer. *Cell* 1978; **14:** 741-59.

40. Stewart WW. Lucifer dyes highly fluorescent dyes for biological tracing. *Nature* 1981; **292:** 17-21.

41. Puc M, Kotnik T, Mir LM, Miklavčič D. Quantitative model of small molecules uptake after in vitro cell electropermeabilization. *Bioelectrochemistry* 2003; **60:** 1-10.

42. Pucihar G, Kotnik T, Kanduser M, Miklavcic D. The influence of medium conductivity on electropermeabilization and survival of cells in vitro. *Bioelectrochemistry*2001; **54:** 107-15.

43. Kotnik T, Pucihar G, Miklavčič D. Induced transmembrane voltage and its correlation with electroporation-mediated molecular transport. *J Membrane Biol* 2010; **236:** 3-13.

44. Pucihar G, Krmelj J, Reberšek M, Batista Napotnik T, Miklavčič D. Equivalent pulse parameters for electroporation. *IEEE T Biomed Eng* 2011*;* **58:** 3279-88.

45. Rols MP, Femenia P, Teissié J. Long-lived macropinocytosis takes place in electropermeabilized mammalian cells. *Biochem Biophys Res Commun* 1995; **208:** 26-38.

46. Zimmermann U, Schnettler R, Klöck G, Watzka H, Donath E, Glaser RW. Mechanisms of electrostimulated uptake of macromolecules into living cells. *Naturwissenschaften*1990; **77:** 543-5.

47. Glogauer M, Lee W, McCulloch CA. Induced endocytosis in human fibroblasts by electrical fields. *Exp Cell Res* 1993; **208:** 232-40.

48. Escoffre JM, Dean DS, Hubert M. Rols MP, Favard C. Membrane perturbation by an external electric field: a mechanism to permit molecular uptake. *Eur Biophys J* 2007; **36:** 973-83.

49. Timothy EV, Weaver JC. Molecular change due to biomagnetic stimulation and transient magnetic fields: mechanical interference constraints on possible effects by cell membrane pore creation via magnetic particles. *Bioelectrochem Bioenerg* 1998; **46:** 121-8.

research article

The optimization of needle electrode number and placement for irreversible electroporation of hepatocellular carcinoma

Oyinlolu O. Adeyanju, Haitham M. Al-Angari, Alan V. Sahakian

Radiol Oncol 2012; 46(2): 126-135.

Received 16 December 2012
Accepted 7 March 2012

Correspondence to: Oyinlolu O. Adeyanju, PhD student with the Department of Biomedical Engineering, Northwestern University, 2145 Sheridan Rd., Evanston, IL 60208 USA. Phone: 847-467-2297; Fax: 847-491-4455; E-mail: lolu@northwestern.edu

Disclosure: No potential conflicts of interest were disclosed.

Background. Irreversible electroporation (IRE) is a novel ablation tool that uses brief high-voltage pulses to treat cancer. The efficacy of the therapy depends upon the distribution of the electric field, which in turn depends upon the configuration of electrodes used.

Methods. We sought to optimize the electrode configuration in terms of the distance between electrodes, the depth of electrode insertion, and the number of electrodes. We employed a 3D Finite Element Model and systematically varied the distance between the electrodes and the depth of electrode insertion, monitoring the lowest voltage sufficient to ablate the tumor, V_{IRE}. We also measured the amount of normal (non-cancerous) tissue ablated. Measurements were performed for two electrodes, three electrodes, and four electrodes. The optimal electrode configuration was determined to be the one with the lowest V_{IRE}, as that minimized damage to normal tissue.

Results. The optimal electrode configuration to ablate a 2.5 cm spheroidal tumor used two electrodes with a distance of 2 cm between the electrodes and a depth of insertion of 1 cm below the halfway point in the spherical tumor, as measured from the bottom of the electrode. This produced a V_{IRE} of 3700 V. We found that it was generally best to have a small distance between the electrodes and for the center of the electrodes to be inserted at a depth equal to or deeper than the center of the tumor. We also found the distance between electrodes was far more important in influencing the outcome measures when compared with the depth of electrode insertion.

Conclusions. Overall, the distribution of electric field is highly dependent upon the electrode configuration, but the optimal configuration can be determined using numerical modeling. Our findings can help guide the clinical application of IRE as well as the selection of the best optimization algorithm to use in finding the optimal electrode configuration.

Key words: hepatocellular carcinoma; irreversible electroporation; optimization, electrode configuration

Introduction

Hepatocellular carcinoma (HCC), primary liver cancer, is a devastating cancer of the liver resulting in almost 700,000 deaths per year worldwide.[1] HCC is generally caused by hepatitis B or C virus and is secondary to liver cirrhosis, which is most commonly caused by alcoholism and hepatitis C in the West. Hepatitis C infections are rising in western countries, leading to a rise in HCC.[2] The majority of patients who contract HCC die within a year.[3] Although HCC is curable with surgical resection, only 10-15% of patients can undergo surgical resection, and liver transplant waiting lists are prohibitively long.[4]

Many adjuvant therapies have been developed to treat liver tumors. Cryoablation works by freezing the tissue. Radiofrequency ablation (RFA) uses a high frequency (450-500 kHz) alternating current to oscillate cellular ions, inducing the generation of heat to treat the cancer, but RFA is limited in the amount of tissue that it can treat. RFA also suffers from a heat sink effect caused by the presence of blood vessels in the liver that convectively cool the

tissue and thus reduce RFA's efficacy.[5] Also, thermal ablation damages connective tissue and blood vessels.[6]

Irreversible electroporation (IRE) is a novel ablation method to treat HCC.[7] IRE works by applying brief, high amplitude electric pulses to cancerous tissue. The electric field acts on the cellular membrane, raising the cell's transmembrane voltage, which can open semi-permanent to permanent aqueous pores in the membrane through which water soluble substances and ions can traverse the membrane.[5] The permeabilization of the cell membrane disrupts the cell's homeostatic mechanisms and can result in the death of the cell. An advantage of IRE is that it leaves intact large blood vessels, nerves, ducts, etc.[8]

The effectiveness of IRE is highly dependent upon the distribution of the electric field in the tissue[9,10], which in turn is dependent upon the configuration of electrodes and the amplitude of voltage applied. Miklavcic *et al.* demonstrated that tumor coverage with an adequate electric field is important for the effectiveness of the therapy.[11] Various studies have looked into the effects of varying the electrode configuration for reversible electroporation applications.[5, 9, 10, 12-23] The majority of these were electrochemotherapy studies aiming to maximize the reversibly electroporated zones and to minimize the regions that were irreversibly electroporated. We are aware of only a few studies to date examining the effects of electrode configuration specifically for IRE therapy (Davalos *et al*. briefly reviewed some 2D simulated configurations in [5] and Zupanic and Miklavcic looked at a treatment plan for IRE in [24] and [25]), but the results for the reversible electroporation studies are useful in designing IRE treatments. Corovic *et al.* showed that the voltage, distance between electrodes, and the depth of electrode insertion were important parameters for the distribution of the electric field.[18]

There is a great deal of flexibility in terms of the configuration of electrodes. One could vary the number, shape, and size of electrodes, etc. as well as their placement. This study utilizes 3D finite element modeling studies to further develop knowledge in optimizing the needle electrode configuration for the purpose of treating liver cancer. We chose to study needle electrodes for their flexibility in placement and ability to treat both surface and deep-tissue tumors. That said, studies have shown that parallel plate electrodes may be more effective for surface tumors due to their ability to produce more uniform electric fields.[26] Although the results are specific to HCC, our hope is that the developed electrode configuration results would be useful for the ablation of other types of cancer and for motivating the use of different optimization algorithms.

Materials and Methods

Finite Element Model

We employed a 3D Finite Element Model using COMSOL ® 4.2 (COMSOL, Stockholm, Sweden) with MATLAB™ on a 64 bit 2.61 GHz Dell Optiplex with an AMD™ 64X2 Dual Core Processor 5200+ with 3.93 GB of RAM running Microsoft Windows XP Professional Version 2003 Service Pack 2. We modeled the liver as a 3D rectangular object with dimensions (18 cm width x 10 cm depth x 15 cm height), which was set to be the approximate dimensions of a human liver. The tumor was modeled as a sphere with a 2.5 cm diameter, which can be considered an average size for liver tumors[27]. The electrical potential was calculated using the Laplace equation for potential distribution:

$$\nabla(\sigma\nabla\phi) = 0 \quad [1]$$

σ represents tissue conductivity and ϕ represents the electric potential. The electric field was calculated from the electric potential.

$$E = -\nabla\phi \quad [2]$$

E represents the electric field.

The boundaries of the cube were also set to be electrically insulating:

$$-n \cdot J = 0 \quad [3]$$

n represents the unit outward normal vector and J represents the current density. The tissue density was set to be 1050 kg/m^3, [28] and the electrode conductivity was set to be 4x10^6 S/m.[29] The active electrode(s) were set to an electric potential $\phi = \phi_0$, and the electrode(s) that were not active were set to ground. A bounding box around the tumor was used in the FEM simulations to improve the quality of the meshing and computations. The mesh consisted of 29,505 elements.

The electrodes modeled in the study were platinum-iridium (90%/10%) electrodes represented by cylinders with 2.0 cm exposed length and 1 mm diameter with insulated portions above the exposed regions of the electrode. The normal liver was given a relative permittivity of 8.2x10^4, while the tumor relative permittivity was set to 9.9x10.[430] We modeled the nonlinear change in the electrical conductivity due to the process of membrane permeabilization with a sigmoid relationship depending upon the electric field magnitude as according to Sel *et al*.[31] for the liver and Ivorra *et al*.[32] for the tumor.

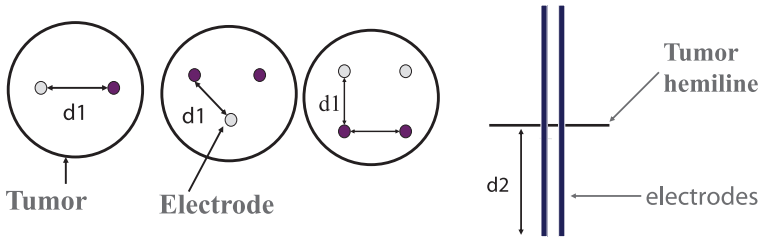

FIGURE 1. Depiction of the electrode configurations. (left) The purple circles represent active electrodes, and the lighter shaded electrodes are set to ground. The distance (d1) between electrodes and the depth of insertion (d2) was varied in the study.

The fit equation for the liver was:

$$\sigma(E) = 0.075 + (0.27 - 0.075) * (\frac{1}{1 + 10e^{(-1/3000*(E-58000))}})$$

The fit equation for the tumor was:

$$\sigma(E) = 0.166(2.154 * \exp(-e^{(-0.001234*(|E/100|-1500))}) + 1)$$

E represents the electric field in V/m. Since the liver model from Sel *et al*. was determined from rabbit data, we changed the baseline value to 0.075 S/m to coincide with human data derived from Haemmerich *et al*. 2009.[33] The fit equation for the tumor was derived from mouse data, so the baseline conductivity was selected from Laufer *et al*.[30] to be 0.166 S/m. The value from Laufer *et al*. was closer to the tumor fit equation's original baseline than the value from Haemmerich *et al*. for tumors, and conversely the chosen baseline value for the normal liver was closer to the original fit equation value from Sel *et al*. than that found in Laufer *et al*. It is well known that liver tumor conductivities tend to be higher than normal liver conductivities, and the ratio of 0.166/0.075≈2.21 is a reasonable ratio between the tumor and the liver.[18,28,34]

Mainly three different parameters of electrode configurations were analyzed for the study: 1) distance between electrodes 2) depth of electrode insertion 3) the number of electrodes. Basically, the parameter space for the distance between electrodes and the depth of electrode insertion was explored for three different electrode numbers: two, three, and four electrodes. The means of optimizing this was to increment the applied voltage at the active electrode(s) by 100 V intervals to the minimum value necessary to cover 95% of the tumor with an electric field sufficient to irreversibly electroporate the tumor tissue: V_{IRE}. This electric field was set at 680 V/cm, as derived from Davalos *et al*..[5] The voltage was iterated, and the criterion for tumor ablation was determined via the MATLAB™ environment. Also, we were able to visualize the region of irreversible electroporation (tissue ablation) using an isosurface plotted in the COMSOL® 3D environment. V_{IRE} was determined at several electrode distances and depths, and the results were tabulated for two, three, and four electrodes. The seven different distances between the electrodes that were measured were 1 cm, 1.5 cm, 2 cm, 2.5 cm, 3 cm, 4 cm, and 5 cm. A distance of 1.9 cm was used for three electrodes as opposed to 2 cm to allow meshing with the electrodes close to the tumor border. The depths of insertion of the electrodes, as measured from the tumor's spherical hemiline to the bottom of the electrodes, were 0.5 cm, 1 cm, 1.25 cm, and 1.5 cm (Figure 1). In previous studies (data not shown), we tested shallower depths, but they had exorbitantly large V_{IREs} and thus were not included for these experiments.

The applied pulse duration was selected to be 20 μs, which is at the lower end of the spectrum of pulse durations.[35] This minimizes computational time and would also be useful for minimizing tissue resistive heating, which is directly related to pulse duration. A shorter pulse was not selected also because there should be an adequate amount of time to charge the membrane for IRE to be effective, and the membrane has a charge time of about 1 μs.[36] There has been no rigorous study as of yet examining the use of shorter versus longer pulses in the irreversible electroporation ablation of liver cancer cells as far as monitoring the size of the ablation zone. However, ultra-short pulses have been employed with very high electric fields (up to 300 kV/cm) to induce apoptosis by irreversibly electroporating inner organelles of the cell.[37]

The volume of normal (non-cancerous) tissue that was irreversibly electroporated—the Volume of Ablated Normal Tissue (V_{ANT})—was calculated in COMSOL® by integrating the volume of normal liver tissue in the simulated environment at or above 680 V/cm. V_{IRE} and V_{ANT} were plotted versus distance at several depths, and some summary statistics were determined (mean, min, max).

Results

V_{IRE}

The V_{IRE} results for two, three, and four electrodes are graphically depicted in Figure 2 A-C. The highest V_{IRE} values consistently occur at the largest distances for all three sets of electrodes. The two electrode data show a parabolic minimum at a distance of 2 cm. We can observe two regions from the results in Figure 2A, the first where the electrodes

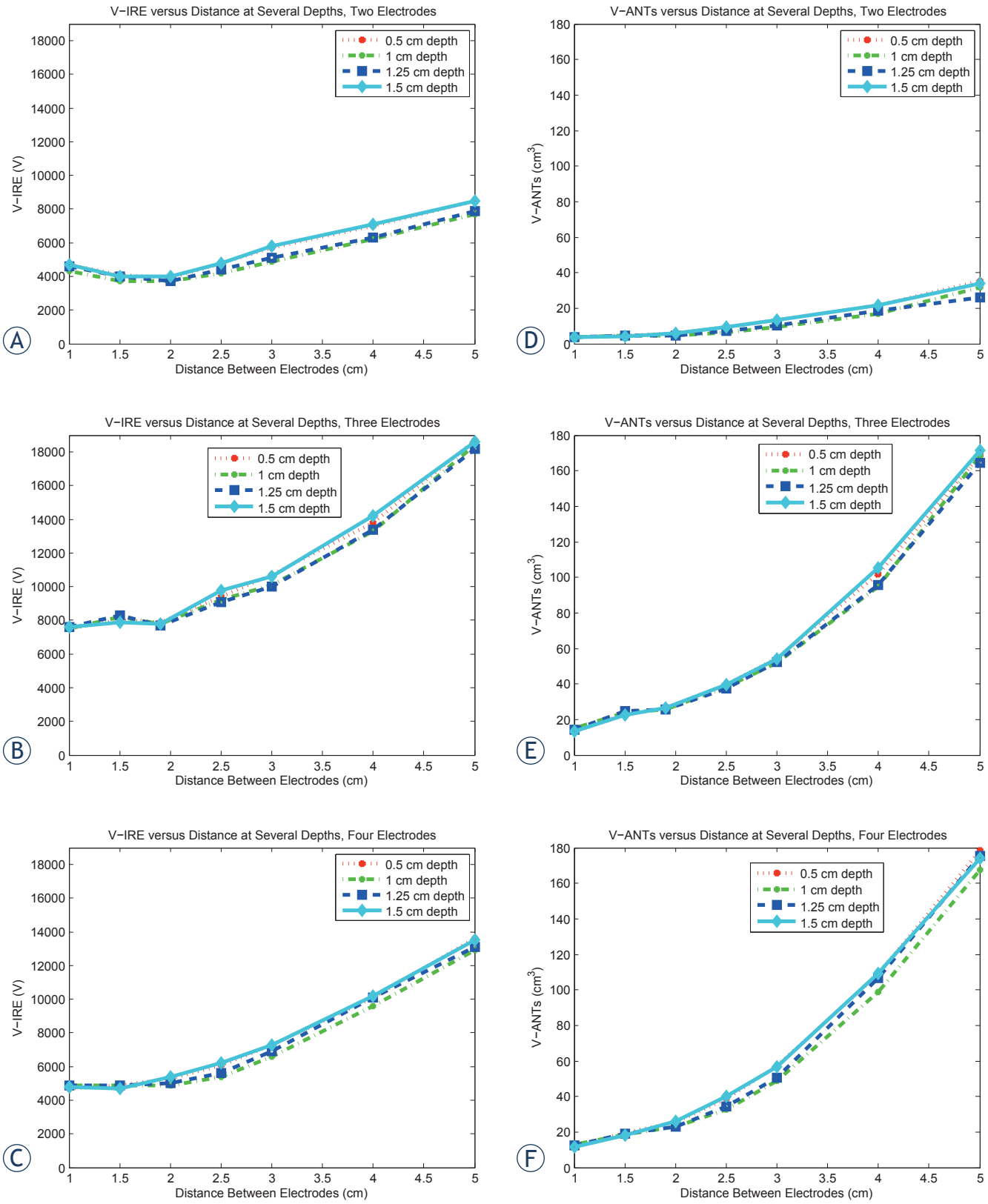

FIGURE 2 A-C. Graphical depiction of VIRE values upon distance at several depths. There appears to be a parabolic minima at 2 cm distance between the electrodes for the two electrode set, whereas the VIRE values for both three and four electrodes decrease linearly with the distance between the electrodes. D-F Graphical depiction of the dependence of the VANT values upon distance at several depths. The VANT values decrease with distance for all electrode setups. Two electrodes overall have the lowest VANT values, followed by four electrodes and then three electrodes.

TABLE 1: Summary statistics from the three V_{IRE} tables (V)

Number of Electrodes	Minimum V_{IRE}	Mean V_{IRE}	Maximum V_{IRE}
Two	3700	5296	8500
Three	7500	10761	18700
Four	4700	7279	13600
summed V_{IRE} standard deviations while varying either distance or depth (V)			
Parameter varying	Two electrodes	Three electrodes	Four electrodes
Distance	6343	16036	12873
Depth	2133	1616	1762

TABLE 2: Summary statistics from the three V_{ANT} tables (cm^3)

Electrode #	Minimum	Mean	Maximum
Two	3.53	12.1	35.1
Three	13.2	60.5	171.3
Four	11.5	60.7	178.6
summed V_{ANT} Standard Deviations while varying either Distance or Depth			
Parameter varying	Two electrodes	Three electrodes	Four electrodes
Distance	41.2	221	236
Depth	11.4	12.5	20.0

are placed inside the tumor and the second where the electrodes are outside the tumor. The two-electrode data show a drop in the voltage as the distance increases from 1 cm, before it rises again near the tumor-tissue boarder at a distance of 2.5 cm. This behavior is observed for all electrode depths. The lowest V_{IRE} values occur at depths of 1 cm and 1.25 cm, which correspond to the center of the electrode overlapping with the center of the tumor. The higher V_{IRE} values generally occur at a depth of 1.5 cm and then 0.5 cm, indicating the highest V_{IRE} values are at the shallowest depth of insertion, and the deepest insertions (lower overlap) produce lower V_{IRE} values.

The lowest V_{IRE} values for three and four electrodes appear to occur at the shortest distances between the electrodes. However, the three-electrode configuration showed an increase in the voltage as the distance increased, before it dropped again near the tumor-tissue boarder. Again this observation is independent of the electrode depth.

For the four-electrode configuration, there was either no change in the voltage (with 1 cm and 1.25 cm depth), an increase (0.5 cm depth), or a decrease in the voltage (with 1.5 cm depth) as a function of distance. When the electrodes were placed outside of the tumor, there was a monotonic increase in the required voltage for ablation as a function of distance for all of the electrode configurations and with all choices of depth. Overall, for all the different electrode configurations, there appears to be a smaller dependence of the V_{IRE} values upon the depth of electrode insertion as compared to the distance between electrodes.

To visualize the differing ablation zones for the different electrode configurations, we examined a cross section of the center of the tumor, demarcating regions that were greater than or equal to 680 V/cm for two, three, and four electrodes at a distance of 2.5 cm and a depth of 1 cm and plotted the ablation zones in Figure 3. Due to the asymmetric ablation shape with three-electrode configuration we tried moving the center of the electrode array and checked whether this would lower V_{IRE} and V_{ANT} (Figure 3D). In fact this, lowered V_{IRE} and V_{ANT} from 9200 V and 38.4 cm^3 to 4600 V and 16.3 cm^3 respectively when moving the center of the electrode array 1 cm to the right of the center of the tumor.

Summary statistics for V_{IRE} and influence of parameters (distance, depth) on V_{IRE}

Overall, the V_{IRE} values were lowest for two electrodes, followed by four electrodes and then three electrodes. Table 1 below shows some summary statistics concerning the three V_{IRE} tables as well as information about the influence of the different parameters upon the V_{IRE}. The minimum, mean, and maximum V_{IRE} were lowest for two electrodes followed by four electrodes and then three electrodes. The summed standard deviations for varying the distance were consistently greater for two, three, and four electrodes as compared to the summed standard deviations while varying the depth.

V_{ANT} results

The V_{ANT} results for two three, and four electrodes are depicted in Figure 2 D-F. The V_{ANT} values increase monotonically with distance for all electrode configurations and show the same variation with depth of electrode insertion as with the V_{IRE} values where the depths of 1 cm and 1.25 cm consistently have the lower V_{ANT} values relative to depths of 0.5 cm and 1.5 cm. The two electrode setups have the lowest V_{ANT} values, followed by four electrodes and three electrodes. The summary statistics are shown for V_{ANT} values in Table 2. As with the V_{IRE} values, the summed standard deviations are greater, when varying distance as opposed to depth.

The best configuration for the a) two b) three and c) four electrode setups, as according the lowest V_{IRE} are: a) a distance of 2 cm and a depth of 1 cm (V_{IRE} =3700 V) b) a distance of 1 cm and a depth of 1 cm (V_{IRE} =7500 V) and c) a distance of 2 cm and a depth of 1 cm (V_{IRE} =4900 V). The overall, global best choice for all electrode configurations was: the two-electrode configuration with a distance of 2 cm and a depth of 1 cm with V_{IRE} 3700 V.

Discussion

The overall goal of our study was to find the optimal distance, depth, and number of electrodes for a simulated irreversible electroporation therapy of a subcutaneous HCC tumor. We systematically varied the distance and depth for three different sets of electrodes (two, three, and four electrodes) and looked at the outcome measures V_{IRE} and V_{ANT}. The currently used Angiodynamics™ system uses only two electrodes at a time, but our study helps explore the potential benefits of different electrode

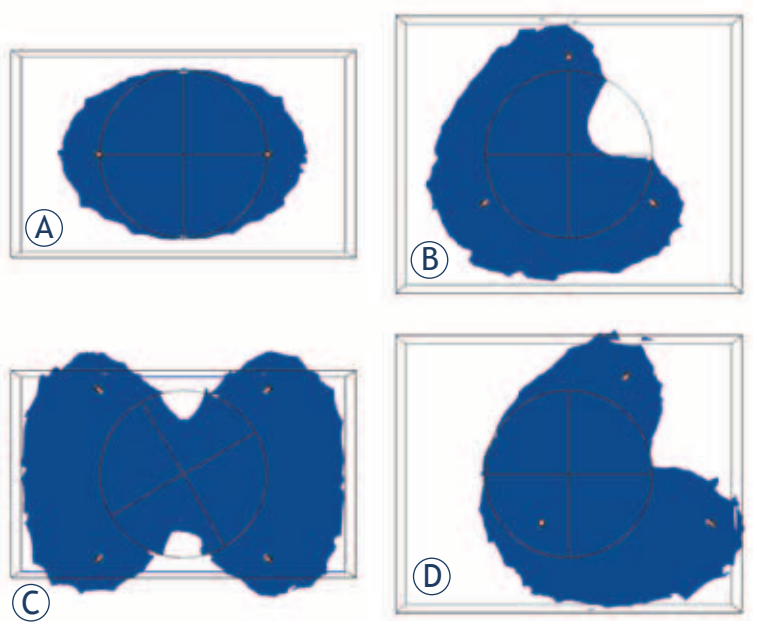

FIGURE 3. Cross section of the tumor (circle) and its ablation zone (blue) at an applied voltage of 5.05 kV, which corresponds to the VIRE for two electrodes at a distance of 2.5 cm and depth of 1 cm for A) two electrodes B) three electrodes C) four electrodes D) three electrodes with the center of the electrodes shifted to the right 1 cm Note the asymmetry in B and the narrowing of the ablation zone in C. A bounding box around the tumor was used in the FEM simulations to improve the quality of the meshing and computations.

configuration patterns, particularly with the three electrode configurations.[35] Our study builds upon findings from Zupanic *et al*.[16] in that we include the possibility of electrodes within the tumor in our 3D simulations, which is advantageous, because the electric fields are highest near the electrodes and rapidly drop off with distance (*i.e.*, the greatest amount of therapy occurs near the electrodes). It must be considered, however, that for some tumor cases it may not be possible to have the electrodes within the tumor.[22]

In looking at V_{IRE}, two electrodes produced the lowest V_{IRE}, at a value of 3700 V. It was unexpected that the two-electrode configuration produced the lowest outcome measure values (V_{IRE} and V_{ANT}) whereas the three electrode configurations produced the highest, and the four electrode configuration outcome measures were in the middle. We expected that the greater surface area provided by a higher number of electrodes would cause the four-electrode configuration to have the lowest V_{IRE} values. This observation could be explained by a number of factors that played a role in the simulated tumor ablation process: a) the number of electrodes clearly plays a role as exhibited in Figure 3 B) the high threshold of 95% tumor abla-

tion c) the symmetry of electrode positioning and d) the distribution of the electric fields between the electrodes that occurred in the study.

The number of electrodes alters the shape of the ablated zone, as exhibited in Figure 3 where we visualize the difference in the ablation zone for two, three, and four electrode setups at a distance of 2.5 cm and depth of 1 cm with the same voltage of 5050 V. For example, the two-electrode configuration in Figure 3A has an elliptic ablation shape while the three-electrode has the most asymmetric shape. Another factor to consider is the different rise in the conductivity of the tissue and tumor due to the different nonlinear response to the rise in the electric field. As the electrodes are place outside and away from the tumor, the ablation shape has less effect as the whole tumor becomes more encompassed by the overall ablated zone, while the applied pulse has less effect on raising the tumor conductivity and more effect on raising the tissue conductivity.

The three-electrode configuration was the most asymmetric of the ones studied (relative to the tumor), as we used a symmetrical spherical tumor. Thus, it is reasonable to deduce that having an outcome whereby the tumor must be 95% ablated rather than 80% or 90% ablated can lead to using high voltages for configurations that use more than two electrodes. If one uses a threshold of 100% tumor ablation, the V_{IRE} values increase significantly. For example, the V_{IRE} becomes 4300 V instead of 3700 V for two electrodes with a distance of 2 cm and depth of 1 cm, and V_{IRE} becomes 16450 V instead of 4900 V for four electrodes with 2 cm distance and 1 cm depth. The asymmetric distribution of electrodes for three electrodes can more easily lead to incomplete tumor coverage (Figure 3B). This would explain why four electrodes, with greater symmetry of electrode patterning, would have lower outcome measures than that for three electrodes. The effect of moving the electrode center with respect to the tumor center in improving V_{IRE} and V_{ANT} make us consider this feature when searching for the optimum electrode position, especially for configurations that result in asymmetric ablation zones. We noted the appearance of slightly higher V_{IRE} values for three electrodes at 1.5 cm relative to the other nearby distances and reasoned that it may be caused by some effect due to both asymmetry and the nonlinear distribution of electric fields due to electrode positioning.

As for two electrodes versus four electrodes, we visualized the differing ablation zone shapes in Figure 3A,C. We saw that the four electrodes had a narrowing of the ablation zone near the center of the tumor, which would account for the higher V_{IRE} values for the four electrodes as compared with the two electrodes. Also, the best choice for depth between 1 and 1.25 cm can be explained as more electrode surface area is facing the tumor with these depths. These findings suggest that clinicians applying IRE for subcutaneous tumors may find the use of two electrodes more beneficial. This information is also useful, because an increase in the number of electrodes can also lead to increased pain and discomfort for the patient and a greater risk of tumor seeding.[38, 39]

The lowest V_{ANT} values occur roughly at the same distances and depths as the lowest V_{IRE} values. The monotonic increase in the V_{ANT} values as a function of distance is expected as more normal tissue volume experiences higher electric field intensities as the electrodes are placed further from the tumor. It is desirable in the application of IRE to minimize both the ablated normal tissue as well as the thermally ablated tissue, for the sake of preserving tissue structural elements (*e.g.*, extracellular matrix, blood vessels, *etc*.). There appears to be a curvilinear relationship between the V_{ANT} values and the distance between the electrodes, and thus clinicians should be careful to minimize the distance between the electrodes when applying the electric field across the tumor tissue to avoid the destruction of normal tissue.

We found that the distance between the electrodes held greater significance for determining what the optimal electrode configuration was, as compared with the depth of electrode insertion. This is apparent visually in Figure 2. Noting the greater influence of distance upon V_{IRE} and the volume of normal and thermally ablated tissue could allow for more leeway in the electrode positioning as far as the depth of electrode insertion as compared to the distance between electrodes. It appeared that the dependence of the outcome measures with depth was greater for two and four electrodes as compared with three electrodes. Also, it seemed that the optimal depth was to have the center of the electrodes inserted close to or deeper than the center of the tumor. This finding corroborates what Zupanic *et al*.[16] However, we build upon Zupanic *et al*. in that we include configurations where the electrodes were inserted into the tumor, and we simulated a greater tumor size (Zupanic *et al*. used sizes: 2 mm, 4 mm, 8 mm radii).

It would be interesting to conduct similar studies with different tumor sizes and to explore the effects of tumor size on the results. However, a tumor

with a diameter of 2.5 cm is within the desired size range of <3.0 cm preferred by clinicians who apply the therapy[40], and it could be considered an average size.[27] Also, it may not be practical to record results for every feasible tumor size. However, these findings and similar studies, besides serving as a reference for clinicians, has the value of better informing the use of dedicated optimization algorithms. Rather than having one sole output from an optimization algorithm, one gains a better understanding of how the fitness function (V_{IRE}) changes over the parameter space. In other words, the plots of V_{IRE} over parameter space provide a better understanding of how the desired optimal value can vary with designated parameters. Thus, one can determine an optimization algorithm that best fits the fitness landscape, whether it is a gradient descent or genetic algorithm. Each algorithm has its strengths and weaknesses, and one could evaluate what the best optimization algorithm would be based upon these results. Also, by plotting the value of the objective function over the parameter space, one can know with greater certainty where the global minima versus local minima are. This is opposed to the use of an optimization method that would only output one or a limited number of values for the parameters, and one may not know if it is a local versus a global minima.

In the use of a dedicated optimization algorithm, it may be beneficial to relax the stringent standard of 95% ablation to 80-90% ablation to increase the diversity of potential solutions and utilize overlapping ablation zones. In clinical practice it may be better to attempt to ablate the tumor all at once to prevent future seeding. It would also be difficult to have overlapping IRE ablation zones due to the difficulty in visualizing the development of the ablation zone with high resolution in real time. Research in visualizing the ablation zone in real time has been done via electrical impedance tomography[41], but significant advances must be made for this to become a reality. Some researchers have suggested that MRI may be a viable route for visualizing the ablation zone during IRE therapy.[42-44]

Limitations

The liver and tumor are assumed to be isotropic and homogenous. Future studies could also implement liver and tumor geometries from medical images. We do not account for the dependence of permeabilization on cell size, shape, and interaction with surroundings.[31] Also, we did not study different electrode pulse sequence patterns or shapes, which can have a significant impact on the efficacy of the therapy.[45] If electrode sequence activation patterns had been used, the four-electrode configurations could have been more efficacious, due to improved tumor coverage.[46] Adjustments of the voltage to reach V_{IRE} were done in increments of 50 V, and thus there is the possibility that some of the measurements were overestimated. Also, although we thought V_{IRE} to occur at 680 V/cm, it is possible that it occurs at a different cutoff value. However, the results would be expected to scale accordingly with a higher or lower threshold value for V_{IRE}.

The voltage amplitudes recorded from the study are higher than the maximum voltage supplied by NanoKnife (3000 V)[35], but the information gleaned from the efficacy of different positions would still be useful to clinicians, and hopefully as technology improves, the observed voltages would become more feasible. Our optimum electrode position with two electrodes and a distance of 2.5 cm and 1 cm depth would ablate 82% of the tumor at the maximum system voltage of 3000 V (data not shown). It would also be useful to know thermal information about the electrode configurations used, but IRE pulse sequences use somewhere on the order of 90-100 pulses[47], which would be impractical to examine for each electrode configuration with current computational capabilities.

Conclusion

We demonstrated that the optimal electrode configuration for applying IRE therapy for the ablation of HCC tumors could be determined using numerical modeling. We determined that it may be better to use two electrodes rather than three or four electrodes and that it is more important to be mindful of the distance between the electrodes rather than the depth of insertion of the electrodes to minimize the thermally ablated volume of tissue and the affected normal tissue. All of this information could serve as useful guidelines for physicians attempting to employ irreversible electroporation for the treatment of liver cancers. Although the model parameters we employed were specifically for liver cancer, the findings could be similar for other types of cancer e.g. kidney, breast, lung, etc. Our results corroborated previous findings that the distribution of the electric field in the tissue is highly dependent upon the electrode configuration, and future studies could further explore different electrode configurations with patient-generated tumor geometries and tissue properties.

Acknowledgements

This work was supported by F31 CA150658 fellowship for PhDs from the National Cancer Institute of the NIH.

References

1. World health organization: Cancer. World Health Organization. 2012. Accessed: March 12, 2012. Available from: http://www.who.int/mediacentre/factsheets/fs297/en/index.html
2. Gomaa AI, Khan SA, Toledano MB, Waked I, Taylor-Robinson SD. Hepatocellular carcinoma: Epidemiology, risk factors and pathogenesis. *World J Gastroenterol* 2008; **14:** 4300-8
3. Medicine Net: Liver cancer. Stoppler, M. 2011. Accessed: March 12, 2012. Available from: http://www.medicinenet.com/liver_cancer/article.htm
4. Forner A, Llovet JM, Bruix J. Hepatocellular carcinoma. *Lancet* 2012; Epub ahead of print.
5. Davalos RV, Mir IL, Rubinsky B. Tissue ablation with irreversible electroporation. *Ann Biomed Eng* 2005; **33:** 223-31.
6. Daniels C, Rubinsky B. Electrical field and temperature model of nonthermal irreversible electroporation in heterogeneous tissues. *J Biomech Eng* 2009; **131:** 071006.
7. Rubinsky B. Irreversible electroporation in medicine. *Technol Cancer Res Treat* 2007; **6:** 255-60.
8. Rubinsky B, Onik G, Mikus P. Irreversible electroporation: A new ablation modality--clinical implications. *Technol Cancer Res Treat* 2007; **6:** 37-48.
9. Hofmann GA. Instrumentation and electrodes for in vivo electroporation. In. Jaroszeski MJ, Heller R, Gilbert R, editors. *Electrochemotherapy, electrogenetherapy, and transdermal drug delivery. Electrically mediated delivery of molecules to cells.* Totowa, New Jersey: Humana Press, 2000. p. 37-61.
10. Sel D, Mazeres S, Teissie J, Miklavcic D. Finite-element modeling of needle electrodes in tissue from the perspective of frequent model computation. *IEEE Trans Biomed Eng* 2003; **50:** 1221-32.
11. Miklavcic D, Beravs K, Semrov D, Cemazar M, Demsar F, Sersa G. The importance of electric field distribution for effective in vivo electroporation of tissues. *Biophys J* 1998; **74:** 2152-8.
12. Gilbert RA, Jaroszeski MJ, Heller R. Novel electrode designs for electrochemotherapy. *Biochim Biophys Acta* 1997; **1334:** 9-14.
13. Sersa G, Cemazar M, Semrov D, Miklavcic D. Changing electrode orientation improves the efficacy of electrochemotherapy of solid tumors in mice. *Bioelectrochem Bioenerg* 1996; **39:** 61-6.
14. Corovic S, Pavlin M, Miklavcic D. Analytical and numerical quantification and comparison of the local electric field in the tissue for different electrode configurations. *Biomed Eng Online* 2007; **6:** 37.
15. Cındea NBF, Gournay F, Poignard C. Optimal placement of electrodes in an electroporation process. *ESAIM: Proceedings* 2010; **30:** 34-43.
16. Zupanic A, Corovic S, Miklavcic D. Optimization of electrode position and electric pulse amplitude in electrochemotherapy. *Radiol Oncol* 2008; **42:** 93-101.
17. Brandisky K, Daskalov I. Electrical field and current distributions in electrochemotherapy. *Bioelectrochem Bioenerg* 1999; **48:** 201-8.
18. Corovic S, Zupanic A, Miklavcic D. Numerical modeling and optimization of electric field distribution in subcutaneous tumor treated with electrochemotherapy using needle electrodes. *IEEE Transactions on Plasma Science* 2008; 36: 1665-72.
19. Miklavcic D, Semrov D, Mekid H, Mir LM. A validated model of in vivo electric field distribution in tissues for electrochemotherapy and for DNA electrotransfer for gene therapy. *Biochim Biophys Acta* 2000; **1523:** 73-83.
20. Zupanic A, Corovic S, Miklavcic D, Pavlin M. Numerical optimization of gene electrotransfer into muscle tissue. *Biomed Eng Online* 2010; **9:** 66.
21. Kos B, Zupanic A, Kotnik T, Snoj M, Sersa G, Miklavcic D. Robustness of treatment planning for electrochemotherapy of deep-seated tumors. *J Membr Biol* 2010; **236:** 147-53.
22. Miklavcic D, Snoj M, Zupanic A, Kos B, Cemazar M, Kropivnik M, Bracko M, Pecnik T, Gadzijev E, Sersa G. Towards treatment planning and treatment of deep-seated solid tumors by electrochemotherapy. *Biomed Eng Online* 2010; **9:** 10.
23. Sel D, Lebar AM, Miklavcic D. Feasibility of employing model-based optimization of pulse amplitude and electrode distance for effective tumor electropermeabilization. *IEEE Trans Biomed Eng* 2007; **54:** 773-81.
24. Rubinsky B. Irreversible electroporation. Springer. *Series in biomedical engineering*. 2009. pp 203-217
25. Zupanic A, Miklavcic D. Method for treatment planning of tissue ablation by irreversible electroporation. In: Dössel O, Schlegel WC, eds. *World congress on medical physics and biomedical engineering, september 7 - 12, 2009, Munich, Germany*. Springer Berlin Heidelberg; 2009:150-153.
26. Edd JF, Horowitz L, Davalos RV, Mir LM, Rubinsky B. In vivo results of a new focal tissue ablation technique: Irreversible electroporation. *IEEE Trans Biomed Eng* 2006; **53:** 1409-15.
27. Arrive L, Rosmorduc O, Dahan H, Fartoux L, Monnier-Cholley L, Lewin M, et al. Percutaneous acetic acid injection for hepatocellular carcinoma: Using ct fluoroscopy to evaluate distribution of acetic acid mixed with an iodinated contrast agent. *AJR Am J Roentgenol*. 2003; **180:** 159-62.
28. Duck FA. *Physical properties of tissue*. San Diego: Academic Press Inc; 1990. p. 138
29. Elwassif MM, Kong Q, Vazquez M, Bikson M. Bio-heat transfer model of deep brain stimulation-induced temperature changes. *J Neural Eng* 2006; **3:** 306-15.
30. Laufer S, Ivorra A, Reuter VE, Rubinsky B, Solomon SB. Electrical impedance characterization of normal and cancerous human hepatic tissue. *Physiol Meas* 2010; **31:** 995-1009.
31. Sel D, Cukjati D, Batiuskaite D, Slivnik T, Mir LM, Miklavcic D. Sequential finite element model of tissue electropermeabilization. *IEEE Trans Biomed Eng* 2005; **52:** 816-27.
32. Ivorra A, Al-Sakere B, Rubinsky B, Mir LM. In vivo electrical conductivity measurements during and after tumor electroporation: Conductivity changes reflect the treatment outcome. *Phys Med Biol* 2009; **54:** 5949-63.
33. Haemmerich D, Schutt DJ, Wright AW, Webster JG, Mahvi DM. Electrical conductivity measurement of excised human metastatic liver tumours before and after thermal ablation. *Physiol Meas* 2009; **30:** 459-66.
34. Deng ZS, Liu, J. Blood perfusion-based model for characterizing the temperature fluctuation in living tissues. *Physica A: Statistical Mechanics and its Applications* 2001; **300:** 521-30.
35. Bertacchini C, Margotti PM, Bergamini E, Lodi A, Ronchetti M, Cadossi R. Design of an irreversible electroporation system for clinical use. *Technol Cancer Res Treat* 2007; **6:** 313-20.
36. Edd JF, Davalos RV. Mathematical modeling of irreversible electroporation for treatment planning. *Technol Cancer Res Treat* 2007; **6:** 275-86.
37. Gundersen M, Vernier PT, Marcu L, Li A, Zhu X, Gallam AZ, et al. Ultrashort pulse electroporation: Applications of high pulsed electric fields to induced caspase activation of human lymphocytes. *Power Modulator Symposium, 2002 and 2002 High-Voltage Workshop. Conference Record of the Twenty-Fifth International* 2002
38. Cabibbo G, Craxi A. Needle track seeding following percutaneous procedures for hepatocellular carcinoma. *World J Hepatol* 2009; **1:** 62-6.
39. Tezcan Y, Mehmet, K. Hepatocellular carcinoma with subcutaneous metastasis of the scalp. *Radiol Oncol* 2011; **45:** 292-5.
40. Narayanan G. Irreversible electroporation for treatment of liver cancer. *Gastroenterol Hepatol (N Y)* 2011; **7:** 313-6.
41. Granot Y, Ivorra A, Maor E, Rubinsky B. In vivo imaging of irreversible electroporation by means of electrical impedance tomography. *Phys Med Biol* 2009; **54:** 4927-43.
42. Zhang Y, Guo Y, Ragin AB, Lewandowski RJ, Yang GY, Nijm GM, et al. Mr imaging to assess immediate response to irreversible electroporation for targeted ablation of liver tissues: Preclinical feasibility studies in a rodent model. *Radiology* 2010; **256:** 424-32.

43. Kranjc M, Bajd F, Sersa I, Miklavcic D. Magnetic resonance electrical impedance tomography for monitoring electric field distribution during tissue electroporation. *IEEE Trans Med Imaging* 2011; **30:** 1771-8.

44. Hjouj M, Rubinsky B. Magnetic resonance imaging characteristics of nonthermal irreversible electroporation in vegetable tissue. *J Membr Biol* 2010; **236:** 137-46.

45. Miklavcic D, Towhidi, L. Numerical study of the electroporation pulse shape effect on molecular uptake of biological cells. *Radiol Oncol* 2010; **44:** 34-41.

46. Sahakian AV, Al-Angari HM, Adeyanju OO. Electrode activation sequencing employing conductivity changes in irreversible electroporation tissue ablation. *IEEE Trans Biomed Eng* 2012; **59:** 604-7.

47. Zupanic A, Miklavcic, D. Tissue heating during tumor ablation with irreversible electroporation. *Elektrotehniski Vestnik* 2011; **78:** 42-7.

research article

Improved survival after introduction of chemotherapy for malignant pleural mesothelioma in Slovenia: Population-based survey of 444 patients

Viljem Kovac[1], Matjaz Zwitter[1], Tina Zagar[2]

[1] Department of Radiotherapy, [2] Cancer Registry of Republic of Slovenia, Institute of Oncology, Ljubljana, Slovenia

Radiol Oncol 2012; 46(2): 136-144.

Received 15 January 2012
Accepted 10 February 2012

Correspondence to: Viljem Kovač, MD, PhD, Institute of Oncology, Zaloška 2, 1000 Ljubljana, Slovenia. Phone: +386 1 5879 504; Fax: +386 1 5879 400; E-mail: vkovac@onko-i.si

Disclosure: No potential conflicts of interest were disclosed.

Background. Malignant pleural mesothelioma is a rare tumour with increasing frequency throughout the world. Due to long latency after exposure to asbestos, restrictions in the production and use of asbestos have not yet alleviated the burden of mesothelioma. During the last decade, several trials confirmed the benefit of systemic treatment with drugs such as doublets with cisplatina and gemcitabine or pemetrexed for carefully selected patients in good performance status. The purpose of this survey was to assess the impact of systemic treatment for the whole national population of patients with mesothelioma.

Patients and methods. A retrospective study included all patients in Slovenia with histologically confirmed diagnosis of malignant pleural mesothelioma in the period from 1974 till 2008. Data from the Cancer Registry of Slovenia were supplemented by review of clinical records of the Institute of Oncology in Ljubljana where virtually all non-surgical treatment for mesothelioma was performed. We analysed the incidence, treatment, and survival of patients treated in the era of infrequent chemotherapy (1974-2003, the first period) and after it (2004-2008, the second period).

Results. The survey included 444 patients, of whom 325 and 119 were diagnosed in the first and second period, respectively. Joinpoint regression analysis showed that after 1995 the trend in crude incidence rates increased more rapidly; the annual change was 0.03 per 100,000 per year before 1995 and 0.06 per 100,000 per year after. There was clear male predominance (70%) throughout the period covered by the survey. The proportion of patients above 65 years of age increased from 41.8% to 54.6% for the first and second period, respectively (p = 0.02). With a total of 52 (11.7%) operated patients, surgical treatment was rare and used only for selected patients with early disease and without comorbidity, leading to their relatively long median survival of 13.6 months. Chemotherapy was applied to 56 (17.2%) and to 96 (80.7%) patients during the first and second period, respectively. While a variety of older drugs were used in the first period, the most common regimen in the second period (applied to 91 patients) was doublet of low-dose gemcitabine in prolonged infusion and cisplatin. For the whole population of patients regardless the mode of treatment, median survival was 7.4 and 12.6 months (p-value = 0.037) for the first and second period, respectively.

Conclusions. Increasing incidence, male predominance and increased proportion of older patients confirm that the burden of mesothelioma persists in spite of a 15-years old ban in the production of asbestos. Modern chemotherapy, and in particular treatment with low-dose gemcitabine in prolonged infusion and cisplatin significantly prolonged median survival of patients with malignant pleural mesothelioma in Slovenia.

Key words: malignant pleural mesothelioma; incidence; survival; chemotherapy; gemcitabine in prolonged infusion

Introduction

Malignant pleural mesothelioma (MPM) is a rare and highly aggressive tumour arising from mesothelial surfaces of pleura.[1,2]

After recognizing asbestos as the most important factor in the pathogenesis of mesothelioma, the production and use of asbestos were banned in most developed countries. However, due to the long latent period between exposure to asbestos and the development of the disease, the incidence of mesothelioma is expected to increase for at least another decade. Since the risk for development of mesothelioma persists for several decades after professional or environmental exposure, the burden of the disease will shift to the older population.[2-6]

In spite of all efforts to find an effective treatment, the prognosis of mesothelioma remains poor and over 90% of patients die from the disease.[7] For the few patients in good performance status, without significant co-morbidity and with apparently limited disease, magnetic resonance (MR) and positron emission tomography-computerised tomography (PET-CT) are helpful in selecting patients with early stages for surgery and/or multimodality therapy with curative intent.[8-12] However, even most aggressive treatment rarely leads to cure. In several series of early-stage mesothelioma treated with multi-modality approach including surgery, median survival rarely exceeds two years. The optimal selection of the surgical procedure remains to be defined and the standard treatment for early stage of MPM remains unclear.[12-15]

At the time of diagnosis, most patients have advanced disease. In this situation, systemic treatment is the only modality with a potential to influence survival. Due to scepticism regarding clinical benefit of chemotherapy for patients with mesothelioma, a randomised clinical study was conducted in England, comparing chemotherapy with navelbine to best supportive care alone. While the trial did not confirm a statistical significant difference, it did show a clear trend for an improved survival for patients treated with chemotherapy, in comparison to the control arm.[16]

During the past 15 years, dozens of trials of chemotherapy for patients with mesothelioma have been reported. Since all these trials were performed on selected populations of patients and none of them included a control arm without chemotherapy, the real value of chemotherapy remains unknown. This is especially true for patients in poor performance status or with significant co-morbidity who are not eligible for large multi-center clinical trials.[17]

In Slovenia, we had two distinct periods of treatment of mesothelioma. Until 2003, occasional patients with early disease were treated with surgery, some patients received palliative irradiation, and very few patients received any form of systemic treatment. In 2003, we activated a Phase II clinical trial of low-dose gemcitabine in prolonged infusion and cisplatin.[18] Due to the national policy of referral of all patients with mesothelioma to the Institute of Oncology Ljubljana, virtually all patients with mesothelioma eligible for treatment with platin-based chemotherapy were included in the trial.

So far, we found only one population-based report, which has been published to prove that chemotherapy can improve survival for patients with mesothelioma.[19] We therefore did the following survey, aiming to evaluate the role of chemotherapy for pleural mesothelioma on a population basis in Slovenia.

Patients and methods

The survey included all patients with permanent residence in Slovenia with a diagnosis of malignant pleural mesothelioma in the period from 1974 till 2008 and reported to the Cancer Registry of Republic of Slovenia. Data were derived from individual hospital reports to the Cancer Registry. For patients who received any form of specific anticancer treatment, additional data were obtained from the clinical documentation of the Institute of Oncology Ljubljana. Eligible patients had biopsy-proven malignant mesothelioma regardless the histologic subtype. Almost all patients had thoracoscopy or CT-guided biopsy as well as US-guided needle biopsy.[18,20,21] Stage of disease was not consistently recorded in the clinical documentation and was therefore omitted from the analysis. Data on surgery and on the type of chemotherapy were recorded. During the period covered by the survey, radiotherapy was exclusively applied for palliation, using a wide spectrum of fractionation schedules. Since palliative radiotherapy does not influence survival, data on radiotherapy were not included in the analysis.

The two periods of treatment were defined as the era of infrequent chemotherapy (1974-2003) and of frequent use of chemotherapy (2004-2008). These were further divided into 5-year periods. December 1, 2011 was the close-out date for data collection.

Overall survival time was calculated from the day of diagnosis to the death from all causes or

TABLE 1. Demographic data for malignant pleural mesothelioma, Slovenia 1974-2008

	1974-2003	2004-2008	Total
Males: number (%)	223 (68.6%)	91 (76.5%)	314 (70.7%)
Females: number (%)	102 (31.4%)	28 (23.5%)	130 (29.3%)
Age: range (mean)	22-89 (61.7)	33-87 (64.4)*	22-89 (62.4)
Age above 65: number (%)	136 (41.8%)	65 (54.6%)	201 (45.3%)
Total	**325**	**119**	**444**

*p = 0.021

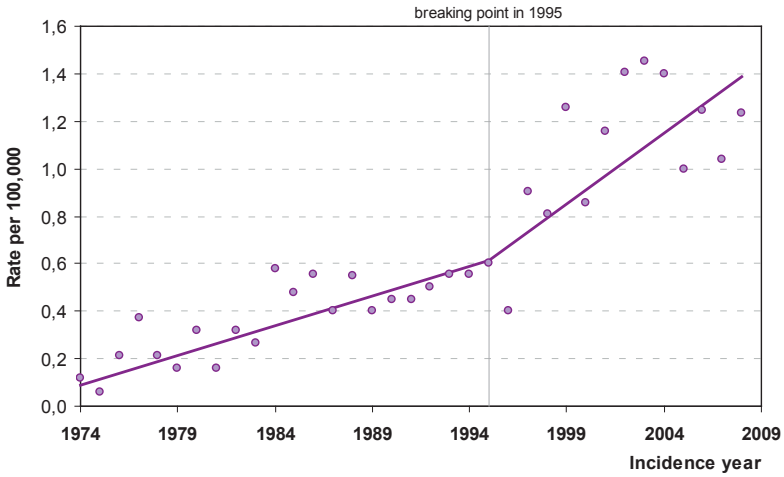

FIGURE 1. The crude incidence rates of patients with malignant pleural mesothelioma with results of trend analysis, Slovenia 1974-2008.

when censored. Kaplan-Meier method was used for estimation of survival and log-rank test was used to compare survival distributions between samples. A p-value lower than 0.05 was considered statistically significant. The data were analysed using SPSS statistical package (Release 13.0, SPSS Inc., Chicago, IL).

The investigators strictly followed recommendations of the Helsinki Declaration (1964, with later amendments) and of the European Council Convention on Protection of Human Rights in Bio-Medicine (Oviedo 1997).

To assess trend in cancer rates, joinpoint regression analysis[22] was performed with software Joinpoint Regression Program, Version 3.0.

Results

Patients

The survey included 444 patients, of whom 325 had the diagnosis of malignant pleural mesothelioma in the first period (January 1974 – December 2003) and 119 in the second period (January 2004 – December 2008). The incidence increased throughout the analyzed time period (Figure 1, Table 1). Joinpoint regression analysis showed that after 1995, the trend in crude incidence rates increased more rapidly. The annual change in crude rates was 0.03 per 100,000 per year for the 1974-1995 period and 0.06 per 100,000 per year for the 1995-2008 period. Both regression slopes and the difference between the slopes are statistically significant with p-values smaller than 0.05 (Figure 1).

Demographic data are presented in Table 1. Male predominance was obvious (70.7%). Difference in gender distribution in two periods 1974-2003 and 2004-2008 was not statistically significant (Pearson Chi-Square test gives p-value of 0.107). However, the mean age was statistically significant different between the two time periods (t-test gave p-value of 0.021, normal distribution for age was confirmed by Kolmogorov-Smirnov Test). Furthermore, the proportion of patients over 65 years of age at the date of diagnosis increased from 41.8% for the first half of the survey period to 54.6% for the later years.

Surgery was rarely used, except for one of the 5-year periods (1999-2003) when the surgical procedures were more frequent (Figure 2).

Fifty-six (17.2%) patients were treated by systemic therapy in the 1974-2003 period and 96 (80.7%) in the years 2004-2008 (Table 2, Figure 2). Two hundreds and sixty-two patients were treated neither by systemic therapy nor by surgery, while 22 patients were treated by both.

The choice of chemotherapy clearly depended on the period. Prior to 2003, only rare patients in unusually good performance status received mono-therapy or doublets with older drugs (cisplatin, doxorubicin, methotrexate, etoposide, or interferon). Exception was 5-year period 1999-2003, when we began with clinical trial and the first 10 patients were treated with a new approach. In the second

TABLE 2. Number of newly diagnosed malignant pleural mesothelioma cases, number of patients treated by chemotherapy and by surgery, Slovenia 1974-2008

	No. of new cases	No. of treated by systemic therapy (%)	No. of treated by surgery (%)
1974-1978	18	6 (33.3%)	1 (5.6%)
1979-1983	23	4 (17.4%)	4 (17.4%)
1984-1988	50	1 (2.0%)	6 (12.0%)
1989-1993	47	2 (4.3%)	2 (4.3%)
1994-1998	65	4 (6.2%)	6 (9.2%)
1999-2003	122	39 (32.0%)	25 (20.5%)
2004-2008	119	96 (80.7%)	8 (6.7%)
Total	**444**	**152 (34.2%)**	**52 (11.7%)**

period, after 2003, 68 patients were enrolled in a Phase II clinical trial and received the doublet of low-dose gemcitabine in prolonged infusion (250 mg/m^2/6 hours on days 1 and 8) and cisplatin (75 mg/m^2 on day 2). The similar schedule of treatment was given to 4 patients in another clinical trial Agili. Additional, 19 patients with impaired organ function or in poor performance status who did not meet the eligibility criteria for the trial received a modified treatment schedule. For these poor-risk patients, we usually applied gemcitabine at even a lower dose of 200 mg/m^2/6 hours and either cisplatin at 60 mg/m^2 or carboplatin at AUC 5 and omitted gemcitabine on day 8 of a 3-weekly cycle. Finally, 5 patients treated in the last 5 year of survey received other forms of the first line chemotherapy, the doublet of pemetrexed and cisplatin.

Overall survival

Median survival increased from 7.4 months (95% confidence interval [CI] was 5.9-23.8) for the period of 1974-2003 to 12.6 months (95% CI 10.7-14.5) for the period 2004-2008. The difference between the two periods was statistically significant (p = 0.037) (Figure 3).

Regarding surgery, the median survival for surgical patients was 13.6 months (95% CI 10.6-16.7), as compared to 8.4 months (95% CI 7.0-9.9) for non-surgical patients (p = 0.000; Figure 4).

Patients treated by systemic therapy had significantly longer survival than those who did not receive chemotherapy. Median survival times for patients who did receive or did not receive chemotherapy were 14.5 months (95% CI 11.4-15.8) and 5.6 months (95% CI 3.9-7.3), respectively (p = 0.000; Figure 5).

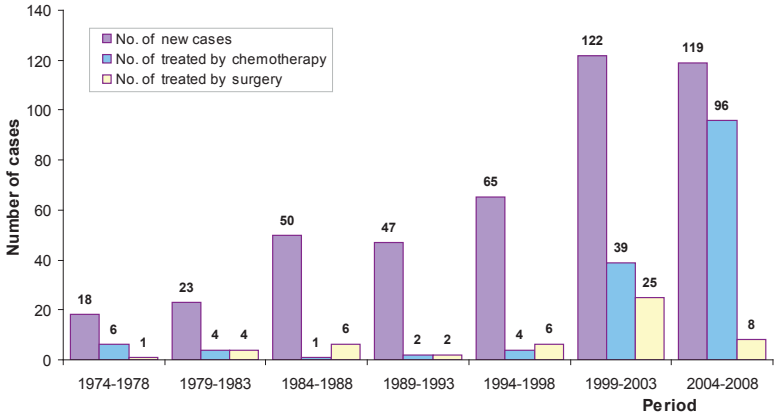

FIGURE 2. Number of newly diagnosed malignant pleural mesothelioma cases, number of patients treated by chemotherapy and by surgery, Slovenia 1974-2008.

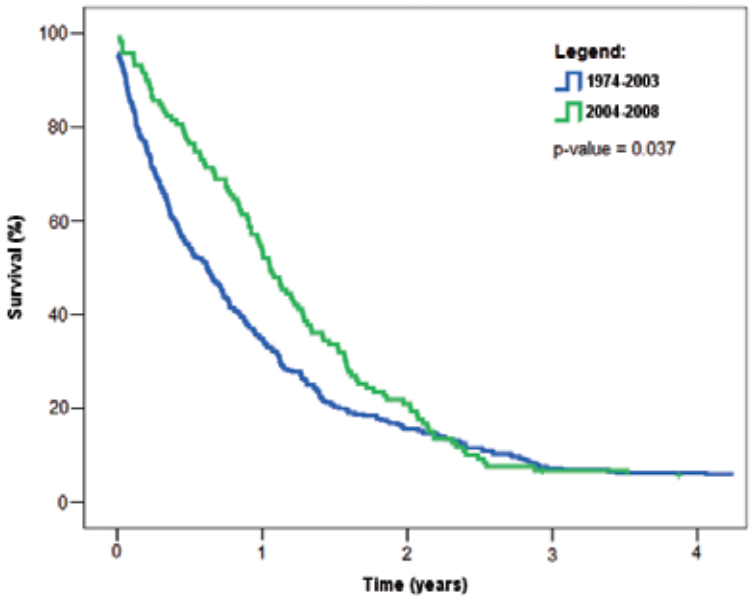

FIGURE 3. Overall survival of Slovenian patients with malignant pleural mesothelioma by two time periods, 1974-2003 and 2004-2008. P-value refers to log-rank test used to compare survival distributions in the two periods.

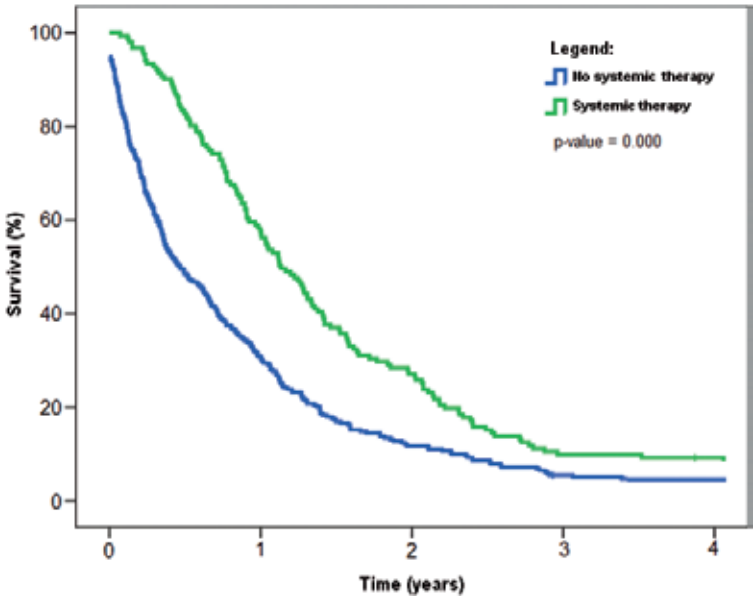

FIGURE 4. Overall survival of patients with malignant pleural mesothelioma with respect to surgery, Slovenia 1974-2008. P-value refers to log-rank test used to compare survival distributions between the two data samples.

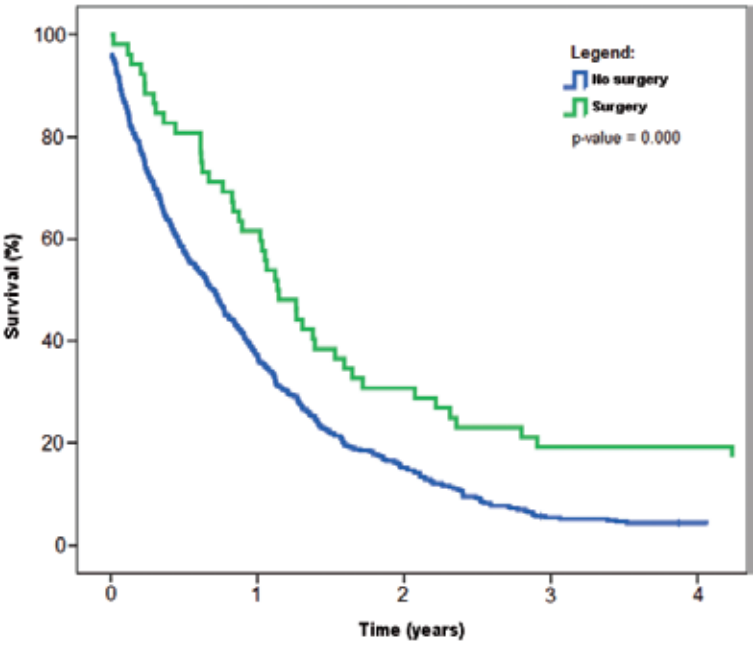

FIGURE 5. Overall survival of patients with malignant pleural mesothelioma with respect to systemic therapy, Slovenia 1974-2008. P-value refers to log-rank test used to compare survival distributions between the two data samples.

Discussion

Our survey is the first one, worldwide, to confirmed that systematic introduction of chemotherapy leads to longer survival for the national population of patients with malignant pleural mesothelioma. The whole unselected population as the basis of our survey confirms the validity of the data and makes our survey distinct to reports on clinical trials which typically include only patients in good performance status and without significant co-morbidity.

Slovenia has the privilege of an excellent national cancer registry with a long tradition covering more than 60 years. Moreover, the country is compact, national health policy is well defined, migration of the population is relatively limited, and vital national statistics are complete and reliable. These circumstances further support the validity of the data presented in this survey.

In spite of a ban in the production and use of asbestos implemented in 1996, the incidence of mesothelioma in Slovenia is still rising. Joinpoint regression analysis showed that after 1995 the trend in crude incidence rates increased more rapidly (Figure 1). While better diagnostic possibilities in recent years might contribute to the observation of the rising incidence, we nevertheless believe that the data reflect a real persistent and increasing risk for the disease. Furthermore, our data support the concept of a long latency period between exposure to asbestos and development of mesothelioma. In this respect, we see a persistent and markedly increased risk in the local communities at close proximity to the former asbestos factory.[18] Also notable is an increasing proportion of elderly patients with mesothelioma and clear male predominance in recent cohorts covered by our survey. At 73 years after the beginning of production of asbestos in Slovenia and 15 years after the facility closed its production of asbestos, these observations additionally indicate that the latency period from the exposure to asbestos to the development of disease is really long.

The other putative aetiological factor, Semian virus 40, was not implicated in pathogenesis of malignant pleural mesothelioma in Slovenia.[23,24]

So far, all efforts to implement screening and early diagnosis of mesothelioma for the high-risk populations have failed, or are still in the investigative phase.[2] Our survey proves that very few patients are diagnosed at an early stage when multi-modality treatment with a curative intent is a realistic option. We believe that carefully selected patients do benefit from surgery; indeed, patients treated with surgery had significantly better survival than those who were not operated (p-value = 0.000) (Figure 4). In the interpretation of these data, one should consider that the surgical patients are usually those with good prognostic factors: good performance

TABLE 3. Effectiveness of different chemotherapy schemes in the treatment of the patients with malignant pleural mesothelioma

Trial	Phase of study	Drugs	N	RR, %	MOS, months	MPFS, months	1-year survival, %
Byrne MJ *et al.*[30], 1999	Phase II	Gemcitabine + cisplatin	21	48	10.0	NA	NA
Aversa SM *et* Favaretto AG[31], 1999	Phase II	Gemcitabine + carboplatin	20	20	NA	4-21	NA
van Haarst JMW *et al.*[32], 2002	Phase II	Gemcitabine + cisplatin	32	16	9.6	6.0	36
Nowak AK *et al.*[33], 2002	Phase II	Gemcitabine + cisplatin	52	17	11.2	6.4	NA
Mikulski SM *et al.*[34], 2002	Phase II	Ranpirnase	105	5	8.3	3.4	34
Vogelzang NJ *et al.*[28], 2003	Phase III	Pemetrexed + cisplatin	226	41	12.1	5.7	50
		cisplatin	222	17	9.3	3.9	38
Favaretto AG *et al.*[35], 2003	Phase II	Gemcitabine + carboplatin	50	26	14.7	8.9	53
Andreopoulou E *et al.*[36], 2004	Phase II	Mitomycin C + vinblastine + cisplatin	150	15	7.0	NA	31
van Meerbeeck JP *et al.*[37], 2005	Phase III	Raltitrexed + cisplatin	126	24	11.4	5.3	46
		cisplatin	124	14	8.8	4.0	40
Castagneto B *et al.*[38], 2005	Phase II	Gemcitabine + cisplatin	35	26	13.0	8.0	NA
Berghmans T *et al.*[39], 2005	Phase II	Epirubicin + cisplatin	69	19	13.3	NA	50
Jänne PA *et al.*[40], 2005	Phase II	Pemetreksed+gemcitabine	108	17	10.1	7.4	46
Ceresoli GL *et al.*[41], 2006	Phase II	Pemetrexed + carboplatin	102	19	12.7	6.5	52
Obasaju CK *et al.*[42], 2007	Phase IV (EAP)	Pemetrexed + cisplatin	728	21	10.8	NA	45
Santoro A *et al.*[43], 2007	Phase IV (EAP)	Pemetrexed + cisplatin or carboplatin	861	22	NA	NA	64
Castagneto B *et al.*[44], 2008	Phase II	Pemetrexed + carboplatin	76	25	14.0	NA	NA
Kalmadi SR *et al*[45], 2008	Phase II	Gemcitabine + cisplatin	50	12	10.0	6.0	30
Hillerdal G *et al*[46], 2008	Phase II	Gemcitabine + carboplatin + liposomized doxorubicin	173	32	13.0	8.6	NA
Sørensen JB *et al*[47], 2008	Phase II	Vinorelbin + cisplatin	54	30	16.8	7.2	61
Muers M *et al.*[16], 2008	Phase III	Vinorelbin	136	16	9.5	6.2	34
		Mitomycin + vinblastine + cisplatin	132	10	7.6	5.6	31
Ralli M *et al.*[48], 2009	Phase II	Docetaxel + gemcitabine	25	28	15.0	7.0	NA
Sørensen JB *et al*[49], 2011	Phase II	Vinorelbin + carboplatin	47	30	14.6	7.2	55
Kovac V *et al.*[18], 2012	Phase II	Gemcitabine* + cisplatin	78	50	17.0	8.0	67

N = number of patients included in the trial; RR = response rate; MOS = median overall survival; MPFS = median progression-free survival, NA = not available; EAP = expanded access program

* applied in low dose in 6-hours infusion

status, low comorbidity, low stage of disease, low weight loss and epitheloid subtype of mesothelioma.[18,20,25,26] A bias in the selection for surgery precludes any comparison to other patients.[18,20]

Our survey revealed a statistically superior survival for patients treated after 2004 when we introduced chemotherapy as a standard treatment modality for mesothelioma. Regarding this finding, two possible factors leading to a bias should be discussed. The first one is earlier diagnosis in recent cohorts of patients. This seems unlikely, since there was no program for early diagnostics of mesothelioma and since the number of patients with early operable stages remained constantly low. The second possible bias is improved supportive care in recent years. While this possibility cannot be entirely rejected[27], we believe that better supportive care alone cannot be responsible for a prolongation of the median survival for more than 5 months. Hence, it seems reasonable to link improved survival to the new treatment policy and to introduction of chemotherapy.

After the trial conducted in England and discussed in the introduction[16] and after our survey[18], the question of benefit of chemotherapy for most patients with mesothelioma appears to be solved. However, the choice of a particular chemotherapeutic schedule is a distinct question. The three parameters determining the choice are efficacy; side effects, quality of life and convenience for the pa-

tients; and costs. We will first discuss the published experience with other scheduled of chemotherapy and later return to low-dose gemcitabine in prolonged infusion and cisplatin as our preferred combination during the last five years of our survey.

In 2003, Vogelzang published experience from a landmark trial which compared pemetrexed and cisplatin against monotherapy with cisplatin and demonstrated a statistically significant advantage for the doublet.[28] On the basis of this trial, pemetrexed was the first drug to be specifically registered for the treatment of mesothelioma, leading to its wide acceptance as the standard treatment. A critical look reveals that the superiority of pemetrexed may be attributable to suboptimal control arm: cisplatin alone is was never the standard treatment for mesothelioma, and certainly not at the turn of the century when several other drugs and their combinations were available. In that period, the doublet of gemcitabine and cisplatin or carboplatin was the most widely used systemic treatment for mesothelioma patients.[29] Pooled data of 7 studies lead to an estimated median survival of 11.7 months, which is comparable with median survival of 12.1 months in pemetrexed study.[18,28] A large spectrum of other combinations from various Phase II clinical trials reported results which are at least comparable to the doublet of pemetrexed and cisplatin, and superior to cisplatin alone (Table 3).

Superior survival of the national pool of patients with mesothelioma during the last five years of our survey should be attributable to low-dose gemcitabine in prolonged infusion and cisplatin as our preferred combination. On the basis of a favourable experience in several trials for non-small cell lung cancer[50-52], we decided to use this combination also for patients with mesothelioma and included 78 patients in a Phase II clinical trial (10 patients in the 5-year period 1999-2003 and 68 patients in the 5-year period 2004-2008).[18] In the last 5-year period, additional 19 patients in poor performance status or with organ dysfunction who were not eligible for the aforementioned trials received a less intensive modification of the same schedule. After completing a Phase II trial for mesothelioma, our research continues with an on-going randomised Phase II trial which compares this combination to the doublet of pemetrexed and cisplatin (**A**limta vs. **G**emcitabin **I**n **L**ong **I**nfusion – AGILI trial).[53]

During the last 5 years of the survey, treatment with low-dose gemcitabine in long infusion and cisplatin was applied to a total of 91 patients. This figure represents 94.8% of the total number of patients who received any form of chemotherapy and 76.5% of the total number of patients with mesothelioma during this period (91 out of 119). Future clinical research on mesothelioma should address several important questions. One of them is to compare different chemotherapy schedules for their efficacy and tolerability, a question already addressed in our on-going AGILI trial.[53] The second one is the question of maintenance treatment. This concept got wide acceptance in the treatment of advanced non-small cell lung cancer.[54,55] Regarding mesothelioma, several trials (including our Phase II trial of low-dose gemcitabine in prolonged infusion and cisplatin) showed that patients who responded to first-line treatment have fair chances to benefit either from re-induction of the same treatment, or from a different combination of drugs.[18,56,57] Finally, research should focus on genetic polymorphisms which influence DNA damage[58], leading to individualised systemic treatment. A key issue in the development of individualized therapy is identification of biomarkers to predict chemotherapeutics' efficacy and toxicity.[59,60] Thus, our research on patients with mesothelioma confirmed that the nucleotide excision repair (NER) pathway polymorphisms influence platinum-treatment efficacy and toxicity[26] and that ribonucleotide reductase subunit 1 (RRM1) polymorphisms as well as haplotypes are associated with gemcitabine treatment efficacy and toxicity.[60]

In conclusion, our survey showed superior survival of patients with mesothelioma during the last five years when a new national policy was implemented and virtually all eligible patients received chemotherapy. Our success should be attributable to our preferred schedule of low-dose gemcitabine in prolonged infusion which proved to be effective, with acceptable toxicity also for patients in poor performance status, and linked to reasonable costs.

Acknowledgement

We are most thankful for the invaluable help of Slovenian pulmologists for diagnostic procedures, to the staff of the Cancer Registry of Slovenia and to our devoted nursing team.

References

1. Robinson BW, Lake RA. Advances in malignant mesothelioma. *N Engl J Med* 2005; **353:** 1591-603.
2. Franko A, Dolzan V, Kovac V, Arneric N, Dodic-Fikfak M. Soluble mesothelin-related peptides levels in patients with malignant mesothelioma. *Dis Markers* 2012; **32:** 123-31.

3. Robinson BWS, Musk AW, Lake RA. Malignant mesothelioma. *Lancet* 2005; **366:** 397-408.
4. Hodgson JT, McElvenny DM, Darnton AJ, Price MJ, Peto J. The expected burden of mesothelioma mortality in Great Britain from 2002 to 2050. *Br J Cancer* 2005; **92:** 587-93.
5. Marinaccio A, Binazzi A, Cauzillo G, Cavone D, Zotti RD, Ferrante P, et al; Italian Mesothelioma Register (ReNaM) Working Group. Analysis of latency time and its determinants in asbestos related malignant mesothelioma cases of the Italian register. *Eur J Cancer* 2007; **43:** 2722-8.
6. Rake C, Gilham C, Hatch J, Darnton A, Hodgson J, Peto J. Occupational, domestic and environmental mesothelioma risks in the British population: a case-control study. *Br J Cancer* 2009; **100:** 1175-83.
7. Milano MT, Zhang H. Malignant pleural mesothelioma. A population-based study of survival. *J Thorac Oncol* 2010; **5:** 1841-8.
8. Podobnik J, Kocijancic I, Kovac V, Sersa I. 3T MRI in evaluation of asbestos-related thoracic diseases – preliminary results. *Radiol Oncol* 2010; **44:** 92-6.
9. Gill RR. Imaging of mesothelioma. *Recent Results Cancer Res* 2011; **189:** 27-43.
10. Peake MD, Entwisle J, Gray SG. Malignant pleural mesothelioma: clinical presentation, radiological evaluation and diagnosis. In: O'Byrne K, Rusch V, editors. *Malignant pleural mesothelioma*. Oxford: Oxford University Press; 2006. p. 35-60.
11. Zauderer MG, Krug LM. The evolution of multimodality therapy for malignant pleural mesothelioma. *Curr Treat Options Oncol* 2011; **12:** 163-72.
12. Okada M, Mimura T, Ohbayashi C, Sakuma T, Soejima T, Tsubota N. Radical surgery for malignant pleural mesothelioma: results and prognosis. *Interact Cardiovasc Thorac Surg* 2008; **7:** 102-6.
13. Scherpereel A, Astoul P, Baas P, Berghmans T, Clayson H, de Vuyst P, et al; European Respiratory Society/European Society of Thoracic Surgeons Task Force. Guidelines of the European Respiratory Society and the European Society of Thoracic Surgeons for the management of malignant pleural mesothelioma. *Eur Respir J* 2010; **35**: 479-95.
14. Eržen J, Vidmar S, Sok M, Debeljak A, Kecelj P, Kovač V, et al. Surgical treatment of malignant pleural mesothelioma. Experience in Slovenia in the interdisciplinary approach. *Radiol Oncol* 2005; **39:** 123-31.
15. Krug LM, Pass HI, Rusch VW, Kindler HL, Sugarbaker DJ, Rosenzweig KE, et al. Multicenter phase II trial of neoadjuvant pemetrexed plus cisplatin followed by extrapleural pneumonectomy and radiation for malignant pleural mesothelioma. *J Clin Oncol* 2009; **27:** 3007-13.
16. Muers MF, Stephens RJ, Fisher P, Darlison L, Higgs CM, Lowry E, et al**.** Active symptom control with or without chemotherapy in the treatment of patients with malignant pleural mesothelioma (MS01): a multicentre randomised trial. *Lancet* 2008; **371**: 1685-94.
17. Zwitter M. Dutch statistics on lung cancer: sobering experience for a new approach. *J Thorac Oncol* 2012; **7:** 269-71.
18. Kovac V, Zwitter M, Rajer M, Marin A, Debeljak A, Smrdel U, et al. A phase II trial of low-dose gemcitabine in prolonged infusion and cisplatin for malignant pleural mesothelioma. *Anticancer Drugs* 2012; **23:** 230-8.
19. Damhuis RA, Schroten C, Burgers JA. Population-based survival for malignant mesothelioma after introduction of novel chemotherapy. *Eur Respir J* 2011; Dec 1. [Epub ahead of print]
20. Debevec M, Kovač V, Debeljak A, Eržen J, Remškar Z, Kern I. [Malignant pleural mesothelioma. Analysis of patients in Slovenia 1980-1997]. [Slovenian]. *Zdrav Vest* 2000; **69:** 599-606.
21. Debeljak A, Kecelj P, Kern I, Eržen J, Kovač V, Rott T. Medical thorascopy in pleural malignant mesothelioma. In: Zaltloukal P, Petruželka L, editors. *Lung Cancer. Current Topics.* Prague: Monduzzi Editore; 2001. p. 81-6.
22. Kim HJ, Fay MP, Feuer EJ, Midthune DN. Permutation tests for joinpoint regression with applications to cancer rates. *Stat Med* 2000; **19:** 335-51.
23. Hmeljak J, Coer A. Presence and role of Simian virus 40 (SV40) in malignant pleural mesothelioma. *Radiol Oncol* 2009; **43:** 9-16.
24. Hmeljak J, Kern I, Cor A. No implication of Simian virus 40 in pathogenesis of malignant pleural mesothelioma in Slovenia. *Tumori* 2010; **96:** 667-73.
25. Fennell DA, Gaudino G, O'Byrne KJ, Mutti L, van Meerbeeck J. Advances in the systemic therapy of malignant pleural mesothelioma. *Nat Clin Pract Oncol* 2008; **5:** 136-47.
26. Erculj N, Kovac V, Hmeljak J, Dolzan V. The influence of platinum pathway polymorphisms on the outcome in patients with malignan pleural mesothelioma. *Ann Oncol* 2012; **23:** 961-7.
27. Temel JS, Greer JA, Muzikansky A, Gallagher ER, Admane S, Jackson VA, et al. Early palliative care for patients with metastatic non-small-cell lung cancer. *N Engl J Med* 2010; **363:** 733-42.
28. Vogelzang NJ, Rusthoven JJ, Symanowski J, Denham C, Kaukel E, Ruffie P, et al. Phase III study of pemetrexed in combination with cisplatin versus cisplatin alone in patients with malignant pleural mesothelioma. *J Clin Oncol* 2003; **21:** 2629-30.
29. Lee CW, Murray N, Anderson H, Rao SC, Bishop W. Outcomes with first-line platinum-based combination chemotherapy for malignant pleural mesothelioma: A review of practice in British Columbia. *Lung Cancer* 2009; **64:** 308-13.
30. Byrne MJ, Davidson JA, Musk AW, Dewar J, van Hazel G, Buck M, et al. Cisplatin and gemcitabine treatment for malignant mesothelioma: a phase II study. *J Clin Oncol* 1999; **17:** 25-30.
31. Aversa *SM*, Favaretto AG. Carboplatin and gemcitabine chemotherapy for malignant pleural mesothelioma: a phase II study of the GSTPV. *Clin Lung Cancer* 1999; **1:** 73-7.
32. van Haarst JMW, Baas P, Manegold C, Schouwink JH, Burgers JA, de Bruin HG, et al. Multicentre phase II study of gemcitabine and cisplatin in malignant pleural mesothelioma. *Br J Cancer* 2002; **86:** 342-5.
33. Nowak AK, Byrne MJ, Williamson R, Ryan G, Segal A, Fielding D, Mitchell P, Musk AW, Robinson BW. A multicentre phase II study of cisplatin and gemcitabine for malignant mesothelioma. *Br J Cancer* 2002; **87:** 491-6.
34. Mikulski SM*,* Costanzi JJ, Vogelzang NJ, McCachren S, Taub RN, Chun H, et al. Phase II trial of a single weekly intravenous dose of ranpirnase in patients with unresectable malignant mesothelioma. *J Clin Oncol* 2002; **20:** 274-81.
35. Favaretto *AG*, Aversa SM, Paccagnella A, Manzini Vde P, Palmisano V, Oniga F, et al. Gemcitabine combined with carboplatin in patients with malignant pleural mesothelioma: a multicentric phase II study. *Cancer* 2003; **97:** 2791-7.
36. Andreopoulou E, Ross PJ, O'Brien ME, Ford HE, Priest K, Eisen T, et al. The palliative benefits of MVP (mitomycin C, vinblastine and cisplatin) chemotherapy in patients with malignant mesothelioma. *Ann Oncol* 2004; **15:** 1406-12.
37. van Meerbeeck JP, Gaafar R, Manegold C, van Klaveren RJ, van Marck EA, Vincent M, et al. Randomized phase III study of cisplatin with or without raltitrexed in patients with malignant pleural mesothelioma: an intergroup study of the European Organisation for Research and Treatment of Cancer, Lung Cancer Group and the National Cancer Institute of Canada. *J Clin Oncol* 2005; **23:** 6881-9.
38. Castagneto B, Zai S, Dongiovanni D, Muzio A, Bretti S, Numico G, et al. Cisplatin and gemcitabine in malignant pleural mesothelioma: a phase II study. *Am J Clin Oncol* 2005; **28:** 223-6.
39. Berghmans T, Lafitte JJ, Paesmans M, Stach B, Berchier MC, Wackenier P, et al. A phase II study evaluating the cisplatin and epirubicin combination in patients with unresectable malignant pleural mesothelioma. *Lung Cancer* 2005; **50:** 75-82.
40. Jänne PA, Simon GR, Langer CJ, Taub RN, Dowlati A, Fidias P, et al. Phase II trial of pemetrexed and gemcitabine in chemotherapy-naive malignant pleural mesothelioma. *J Clin Oncol* 2008; **26:** 1465-71.
41. Ceresoli GL, Zucali PA, Favaretto AG, Grossi F, Bidoli P, Del Conte G, et al. Phase II study of pemetrexed plus carboplatin in malignant pleural mesothelioma. *J Clin Oncol* 2006; **24:** 1443-8.
42. Obasaju CK, Ye Z, Wozniak AJ, Belani CP, Keohan ML, Ross HJ, et al; Pemetrexed Expanded Access Program Investigators. Single-arm, open label study of pemetrexed plus cisplatin in chemotherapy naïve patients with malignant pleural mesothelioma: outcomes of an expanded access program. *Lung Cancer* 2007; **55:** 187-94.
43. Santoro A, O'Brien ME, Stahel RA, Nackaerts K, Baas P, Karthaus M, et al. Pemetrexed plus cisplatin or pemetrexed plus carboplatin for chemonaïve patients with malignant pleural mesothelioma: results of the International Expanded Access Program. *J Thorac Oncol* 2008; **3:** 756-63.
44. Castagneto B, Botta M, Aitini E, Spigno F, Degiovanni D, Alabiso O, et al. Phase II study of pemetrexed in combination with carboplatin in patients with malignant pleural mesothelioma (MPM). *Ann Oncol* 2008; **19:** 370-3.

45. Kalmadi SR, Rankin C, Kraut MJ, Jacobs AD, Petrylak DP, Adelstein DJ, et al. Gemcitabine and cisplatin in unresectable malignant mesothelioma of the pleura: a phase II study of the Southwest Oncology Group (SWOG 9810). *Lung Cancer* 2008; **60:** 259-63.

46. Hillerdal G, Sorensen JB, Sundström S, Riska H, Vikström A, Hjerpe A. Treatment of malignant pleural mesothelioma with carboplatin, liposomized doxorubicin, and gemcitabine: a phase II study. *J Thorac Oncol* 2008; **3:** 1325-31.

47. Sørensen JB, Frank H, Palshof T. Cisplatin and vinorelbine first-line chemotherapy in non-resectable malignant pleural mesothelioma. *Br J Cancer* 2008; **99:** 44-50.

48. Ralli M, Tourkantonis I, Makrilia N, Gkini E, Kotteas E, Gkiozos I, et al. Docetaxel plus gemcitabine as first-line treatment in malignant pleural mesothelioma: a single institution phase II study. *Anticancer Res* 2009; **29:** 3441-4.

49. Sørensen JB, Bech C, Sorensen P, Frank H. Phase II study of carboplatin and vinorelbine 1st line treatment in advanced malignant pleural mesothelioma. [Abstract]. *J Thorac Oncol* 2011; **6(6 Suppl):** S1354-5.

50. Zwitter M, Kovac V, Smrdel U, Kocijancic I, Segedin B, Vrankar M. Phase I-II trial of low-dose gemcitabine in prolonged infusion and cisplatin for advanced non-small cell lung cancer. *Anticancer Drugs* 2005; **16:** 1129-34.

51. Zwitter M, Kovac V, Smrdel U, Vrankar M, Zadnik V. Gemcitabine in brief versus prolonged low-dose infusion, both combined with cisplatin, for advanced non-small cell lung cancer: a randomized phase II clinical trial. *J Thorac Oncol* 2009; **4:** 1148-55.

52. Zwitter M, Kovac V, Rajer M, Vrankar M, Smrdel U. Two schedules of chemotherapy for patients with non-small cell lung cancer in poor performance status: a phase II randomized trial. *Anticancer Drugs* 2010; **21:** 662-8.

53. Kovac V. Zwitter M. Cisplatin with Alimpta or gemcitabine in long infusion for mesothelioma (AGILI). Available: http://clinicaltrials.gov/ct2/show/NCT01281800

54. Brodowicz T, Krzakowski M, Zwitter M, Tzekova V, Ramlau R, Ghilezan N, et al; Central European Cooperative Oncology Group CECOG. Cisplatin and gemcitabine first-line chemotherapy followed by maintenance gemcitabine or best supportive care in advanced non-small cell lung cancer: a phase III trial. *Lung Cancer* 2006; **52:** 155-63.

55. Velez M, Arango BA, Perez CA, Santos ES. Safety and efficacy of pemetrexed in maintenance therapy of non-small cell lung cancer. *Clin Med Insights Oncol* 2012; **6:** 117-24.

56. Ceresoli GL, Zucali PA, De Vincenzo F, Gianoncelli L, Simonelli M, Lorenzi E, et al. Retreatment with pemetrexed-based chemotherapy in patients with malignant pleural mesothelioma. *Lung Cancer* 2011; **72:** 73-7.

57. Zucali PA, Simonelli M, Michetti G, Tiseo M, Ceresoli GL, Collovà E, et al. Second-line chemotherapy in malignant pleural mesothelioma: Results of a retrospective multicenter survey. *Lung Cancer* 2012; **75:** 360-7.

58. Goricar K, Erculj N, Zadel M, Dolzan V. Genetic polymorphisms in homologous recombination repair genes in healthy Slovenian population and their influence on DNA damage. *Radiol Oncol* 2012; **46:** 46-53.

59. Zimling ZG, Sørensen JB, Gerds TA, Bech C, Andersen CB, Santoni-Rugiu E. Low ERCC1 expression in malignant pleural mesotheliomas treated with cisplatin and vinorelbine predicts prolonged progression-free survival. *J Thorac Oncol* 2012; **7:** 249-56.

60. Erculj N, Kovac V, Hmeljak J, Franko A, Dodič-Fikfak M, Dolzan V. The influence of gemcitabine pathway polymorphisms on treatment outcome in patients with malignant mesothelioma. *Pharmacogenet Genomics* 2012; **22:** 58-68.

research article

Long term outcome after combined modality treatment for anal cancer

Irena Oblak, Primoz Petric, Franc Anderluh, Vaneja Velenik, Peter Albert Fras

Department of Radiotherapy, Institute of Oncology Ljubljana, Ljubljana, Slovenia

Radiol Oncol 2012; 46(2): 145-152.

Received 23 December 2011
Accepted 25 January 2012

Correspondence to: doc. dr. Oblak Irena, MD, PhD, Department of Radiology, Institute of Oncology Ljubljana, Zaloška 2, 1000 Ljubljana, Slovenia. Phone: +386 1 5879 293; Fax: +386 1 5879 304; E-mail: ioblak@onko-i.si

Disclosure: No potential conflicts of interest were disclosed.

Background. The aim of the retrospective study was to evaluate the effectiveness and toxicity of radiochemotherapy in patients with squamous cell carcinoma of the anal canal treated at a single institution.

Patients and methods. Between 1/2003 and 9/2010, 84 patients were treated with radical radiochemotherapy at the Institute of Oncology Ljubljana, Slovenia. The treatment consisted of 3-dimensional conformal external beam radiotherapy with concurrent chemotherapy (5-fluorouracil and mytomycin C), followed by brachytherapy or external beam boost. The toxicity of therapy and its effectiveness were assessed.

Results. The treatment was completed according to the protocol in 79.8% of patients. The median follow-up time of 55 survivors was 53 months (range: 16-105 months). The 5-year locoregional control (LRC), disease-free survival (DFS), disease-specific survival (DSS), overall survival (OS) and colostomy-free survival (CFS) rates were 71%, 68%, 81%, 67% and 85%, respectively. No treatment-related mortality was observed. The most frequent acute side-effect of the treatment was radiodermatitis (grade 3-4 in 58.2% of patients). LENT-SOMA grade 3-4 late radiation side effects were observed in 15 (18%) patients. In patients with brachytherapy boost a trend of less late side effects was observed compared to patients with external beam boost (P=0.066). On multivariate analysis, complete clinical disease response was identified as an independent prognostic factor for LRC, DFS and DSS, the salvage surgery for LRC and DFS, whereas Hb below 120 g/l retained its independent prognostic value for OS.

Conclusions. Radiochemotherapy provides an excellent disease control and the survival with preserving anal sphincter function in majority of patients. Surgical salvage with abdominoperineal resection for persistent or recurrent disease has curative potential.

Key words: anal cancer; radiochemotherapy; salvage surgery; outcome

Introduction

Anal cancer is a relatively rare tumour, representing 2-4% of all cancers of colorectum and anus.[1] Women are more often affected than men. During the past decades, the incidence in developing countries has increased, mostly in young homosexual men, perhaps due to sexual transmission of human papilloma virus (HPV) and human immunodeficiency virus (HIV), which are known causal factors in this and other cancers.[1,2] Anal cancer is predominantly a locoregional disease and distant metastases are found in 5-10% of the patients.[1,3-8] Following publications on organ preserving treatment in the eighties[9], the treatment paradigm has shifted from abdomino-perineal resection (APE) with permanent colostomy to radical radiochemotherapy, resulting in sphincter preservation rates of around 80%, even in cases with locally advanced disease. Surgery is indicated only in cases of residual or recurrent tumour and for complications of radiotherapy.[1,10]

Numerous trials have demonstrated complete response rates of 80-90%, with high local control, survival and sphincter preservation rates following radical radiochemotherapy.[3,10-12] The purpose

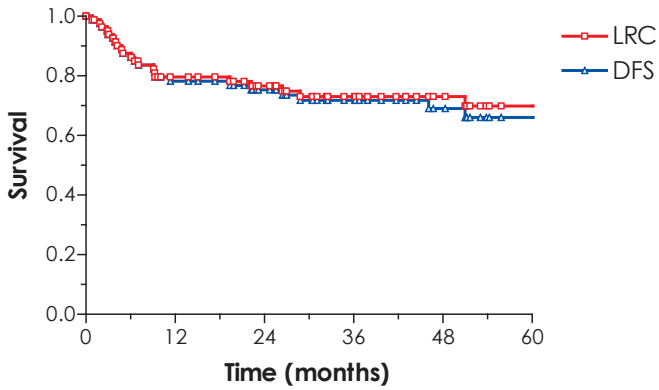

FIGURE 1. Locoregional control (LRC) and disease-free survival (DFS).

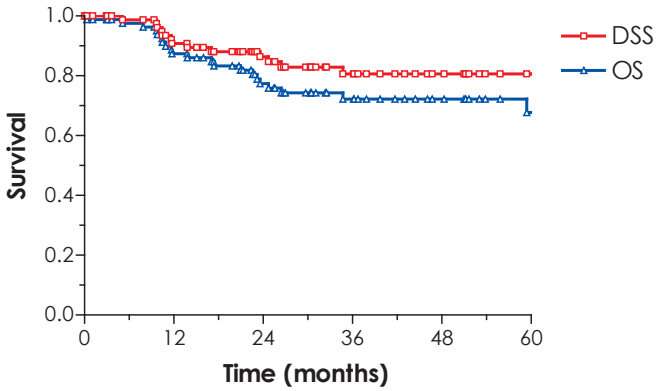

FIGURE 2. Disease-specific survival (DSS) and overall survival (OS).

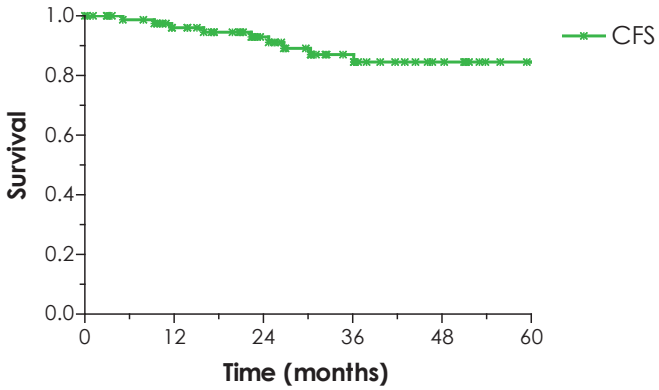

FIGURE 3. Colostomy-free survival (CFS).

of our retrospective study was to evaluate the effectiveness and toxicity of radiochemotherapy in a single-centre prospective cohort of patients with squamous cell carcinoma of the anal canal.

Patients and methods

Patients and tumour characteristics

Eighty-six patients with biopsy proven cancer of the anal canal were treated at the Institute of Oncology Ljubljana between January 2003 and September 2010. Two patients with distant metastases were treated with palliative intent and were excluded from present analysis. The remaining 84 patients (48 females and 36 males) were treated with curative intent. Mean age was 63 years (range: 34-87 years). According to the UICC TNM staging criteria, 6 (7.1%) patients had stage I, 48 (57.1%) stage II, 14 (16.7%) stage IIIA and 16 (19%) stage IIIB disease.[13]

Investigations before and during therapy

The multidisciplinary approach is the policy of treatment for all cancer patients at the Institute of Oncology Ljubljana[14]; therefore, all patients were presented to a multidisciplinary advisory team, consisting of a surgeon, radiation oncologist and medical oncologist, in order to assess the prospects of the treatment. All patients underwent a general clinical examination, blood tests, chest radiography and abdominopelvic computed tomography (CT). Locoregional extent of the disease was evaluated with anorectal examination (performed by a surgeon and a radiation oncologist), rectoscopy, endoscopic ultrasound (US) and magnetic resonance imaging (MRI) of the pelvis. In cases, suspicious for inguinal lymph node involvement, fine needle aspiration biopsy was performed. Detailed pre-treatment clinical drawings and photographs were taken and tumour borders tattooed on perianal skin for the purpose of brachytherapy (BT) treatment planning.

During the treatment, weekly clinical examination and blood tests were performed. The acute treatment related toxicity was assessed according to National Cancer Institute Common Toxicity Criteria (NCI-CTC) version 2.0.[15]

Treatment

A planned treatment schedule consisted of 3-dimensional (3D) conformal external beam radiotherapy (EBRT) with concurrent chemotherapy (ChT), followed by brachytherapy (BT) or EBRT boost. 3D conformal EBRT was delivered using a four-field box technique at a 15 MV linear accelerator. Clinical target volume (CTV) included the gross tumour volume with a safety margin of

1.5-2 cm in all directions and the regional lymph node areas. To arrive at a planning target volume (PTV), an additional margin of 0.7 cm in all directions was applied to the CTV. A nominal dose of 45 Gy (1.8 Gy daily fractions, five fractions a week) was prescribed to ≥95% of the PTV. Prophylactic bilateral inguinal EBRT was given to 45-50 Gy by anterior photon beam and adequate additional electron beam complements of adequate energy to reach the deepest portion of these nodes. In cases with inguinal lymph node metastases, the involved areas were irradiated with separate electron fields to a total dose of 60 Gy.

Concurrent ChT was planned in all but stage I patients and patients with significant medical comorbidities. ChT consisted of two cycles of 5-fluorouracil (5-FU) (daily dose of 1000 mg/m^2 in 96-hours continuous infusion), given during weeks 1 and 5 of EBRT. Mitomycin C (10 mg/m^2 in bolus intravenous injection) was administered on day 1 of the first ChT cycle.

After delivery of 45 Gy of EBRT+/-ChT, a boost dose was planned. In tumours, larger than 5 cm or N2-3 disease, the boost was applied with EBRT, whereas in all other cases an interstitial pulsed-dose rate BT boost was delivered. CTV at the time of BT corresponded to initial tumour extension, as documented by pre-treatment clinical drawings, imaging examinations, photographs and tattooed markings of tumour borders on perianal skin. Metal needles were implanted through a perineal template homogeneously in the CTV, respecting the rules of the Paris system. The distance between needles and ano-rectal mucosa was kept above 5 mm. This was assured by palpation during the needle insertion and by transrectal US. The anal cylinder was inserted to displace uninvolved ano-rectal mucosa from the high dose region. Until 2006, treatment planning was based on two orthogonal radiographs. From then on, CT based treatment planning was introduced. A biologically equivalent dose of 15-30 Gy was prescribed to the reference isodose line, corresponding to the 85% of mean basal dose (linear quadratic model, assuming an α/β of 10 Gy and 3 Gy for the tumour and late reacting normal tissues, respectively, sublethal damage repair half time of 1.5 hours, reference dose rate of 0.5 Gy per hour). The prescribed dose was chosen depending on initial tumour burden and extent of regression during EBRT. After introduction of CT into treatment planning, subtle individualized 3D-optimization of dose distribution was performed to increase the dose to the CTV while respecting the normal tissues tolerance.

In cases of severe treatment-related toxicity, irradiation and/or ChT doses were modified and adapted to the patient's physical condition or laboratory findings. When necessary, ChT application was delayed, or EBRT was temporarily interrupted or terminated.

Follow-up after treatment

The first post-treatment follow-up visit was performed by a senior radiation oncologist 6 weeks after the completion of radiotherapy. A response to the treatment was evaluated by clinical examination, appropriate imaging studies (MRI, US) and biopsies, when indicated. In patients with clinical complete remission, follow-up investigations were carried out at 3 month-intervals thereafter. In cases of the incomplete response, the clinical evaluation was repeated every 6 weeks until the complete remission was recorded. In cases with evidence of progression or recurrence after the end of the treatment, surgery (APE) was recommended.

Late normal tissue side effects (events occurring 3 months or more after the end of the treatment) were assessed at time of each follow-up evaluation, employing the LENT-SOMA scoring system.[16]

Statistical analysis and ethical consideration

A statistical analysis was performed using personal computer and software statistical package SPSS, version 18 (SPSS Inc., USA).

The main endpoints of the study were as follows: response to therapy, locoregional control (LRC, the event was local or regional recurrence), disease-free survival (DFS, the event was local, regional or systemic recurrence), disease-specific survival (DSS, the event was death due to the carcinoma of the anal canal), overall survival (OS, the event was death from any cause) and colostomy-free survival (CFS, the event is need for colostomy).

The survival of patients was computed from the date of the treatment start to December 1, 2011 (close-out date). Survival probability was calculated using Kaplan-Meier estimate, and log-rank test was used to evaluate the influence of individual prognostic factors (age, performance status, T-, N- and overall stage, radiotherapy and chemotherapy dose), on the analysed endpoints.[17,18] Independent prognostic values of the factors that appeared statistically significant on the univariate analysis, were tested by the multivariate Cox regression analysis model.[19] Two-sided tests were used and

TABLE 1. Acute treatment toxicities

Toxicity	NCI[12] grade (%)					
	0	1	2	3	4	Total
Stomatitis	61	19	12	8	0	100
Nausea, vomiting	82	10	6	2	0	100
Diarrhoea	61	18	11	9	1	100
Radiodermatitis	12	14	16	57	1	100
Infection	55	17	18	7	3	100
Leucocyte count	43	31	18	7	1	100
Haemoglobin level	46	46	7	0	1	100
Platelet count	69	27	3	1	0	100

the differences at $P<0.05$ were considered as statistically significant.

The retrospective study was carried out according to the Declaration of Helsinki.

Results

Course of treatment

Median duration of EBRT and total treatment time was 36 days (range: 29-72 days) and 57 days (range: 30-98 days), respectively. Sixty-seven (79.8%) patients completed the treatment according to the protocol. Total EBRT dose of 45 Gy was applied in 82 (97.6%) patients. In two, due to acute side effects, EBRT was stopped at 18 and 25 Gy, respectively, but the treatment was completed with BT (TD: 30-35 Gy).

During EBRT, two cycles of 5-FU were administered as planned in 67 (79.8%) patients. Eight (14%) patients received one cycle only due to adverse side effects during the treatment. Concomitant capecitabine was administered in one patient who was primarily operated for locoregionally advanced colon carcinoma and in who during preoperative investigations synchronous anal carcinoma was found. Chemotherapy was omitted in 6 (7.1%) and 3 (3.6%) patients due to stage I disease and severe comorbidity, respectively.

Boost with the median dose of 14.4 Gy (range: 6-20 Gy) to the primary tumour was applied through reduced photon fields in 33 (39.3%) patients. Interstitial BT boost was performed in 49 (58.3%) patients after EBRT with a mean interval of 27 days (range: 6-57 days). Boost was omitted in two (2.4%) patients because of treatment side effects in one case and the other patient refused the further treatment.

Acute side effects

The treatment was well tolerated in the majority of patients and no treatment-related mortality was observed. Frequency and intensity of acute adverse side effects are listed in Table 1. The most frequent grade 3 side-effect was radiodermatitis, occurring in 48 (57%) patients during EBRT. One patient developed grade 4 radiodermatitis. All cases of radiodermatitis healed without consequences.

Outcome

Median follow-up time was 43 months (range: 8-105 months) in all patients and 53 months (range: 16-105 months) in survivors.

At the first follow-up evaluation, which was done 6 weeks after the treatment, the complete clinical remission of the tumour was found in 55 (65.5%) patients. At 18 weeks after the end of the treatment, complete remission, partial response and stable disease were recorded in 67 (79.8%), 12 (14.3%) and 4 (4.8%) patients, respectively. In one patient, there was evidence of tumour progression during the treatment.

Five patients with complete response later developed local or locoregional recurrence after a median period of 8 months (range: 4-26 months). In two patients with complete response, distant metastases without local recurrence occurred.

Of 24 (28.6%) patients with persistent disease or locoregional recurrence, 12 (14.3%) were treated surgically. In 11 patients, APE was performed and one patient had inguinal dissection due to a recurrence in inguinal lymph nodes. Other 12 (14.3%) patients had unresectable disease. Three of the operated patients died of the recurrent disease, others are alive without evidence of the disease.

TABLE 2. Univariate and multivariate analysis of survival

Prognostic factor	N	Locoregional control			Disease free survival			Disease specific survival			Overall survival			Colostomy free survival		
		UVA		MVA	UVA		MVA	UVA		MVA	UVA		MVA	UVA		MVA
		%	p-value	p-value	%	p-value	p-value	%	p-value	p-value	%	p-value	p-value	%	p-value	p-value
T-stage																
T1+2	45	80.3			80.3			92.3			75			94.4		
T3+4	39	55	0.016		46.6	0.004		65.2	0.009		57.5	0.049		45.9	0.01	
N-stage																
N0	56	78.6			75			90.8			73.7			89.8		
N+	28	50.6	0.028		47.8	0.018		59.4	0.002		56.9	0.059		71.7	0.015	
Overall stage																
Stage I+II	54	78.5			74.9			90.8			73.6			89.8		
Stage III	30	50.8	0.031		48	0.02		59.4	0.002		56.9	0.061		71.7	0.015	
PS																
0	58	75.2			75.2			81.3			77.9			84.4		
1+2	26	54,5			43.4			78.9			39.4	0.041		84.7		
OTT																
<73 days	70	73.4			69			83			72.3			70.6		
≥ 73 days	14	56.3	0.043		56.3	0.062		67.5			44.2	0.062		60.9	0.086	
CR																
Yes	67	91.1			85.6			95.9			80			66.8		
No	17	5.9	<0.001	<0.001	5.9	<0.001	<0.001	22.4	<0.001	<0.001	21	<0.001		59.3	0.014	
Hb																
< 120 g/l	47	58.5			52.6			68			45.5			78.7		
≥ 120 g/l	37	82.7	0.016	0.061	80	0.017		94	0.015		90.7	0.001	0.007	89.6		
SS																
Yes	13	30.8			30.8			71.9			67.3			10.1		
No	71	77.9	<0.001	0.01	73.3	<0.001	0.003	82.4			71.9			100	<0.001	

N, number of patients; UVA, univariate analysis; MVA, multivariate analysis; PS, performance status; OTT, overall treatment time; CR, complete response; Hb, hemoglobin; SS, salvage surgery.

On the study close-out date, 55 (65.5%) patients were alive, 51 (92.7%) of them being disease free. Fifteen (17.9%) patients died from the anal canal cancer. One (1.2%) patient, who experienced locoregional recurrence, died from metachronous bronchus cancer, four (4.8%) patients died from metastatic breast cancer, metastatic colon cancer, metastatic bronchus cancer and metastatic malignant melanoma, six patients (7.1%) died from vascular events and in three (3.5%) patients the cause of death could not be determined.

The 5-year LRC, DFS, DSS, OS and CFS rates for all patients are 71%, 68%, 81%, 67% and 85%, respectively (Figure 1-3).

Late side effects

Grade 3-4 late radiation side effects according to the LENT-SOMA scoring system[13] were observed in 15 (18%) patients. Three (4%) patients experienced post-treatment anal stenosis, requiring repeated dilatations and two (2%) developed chronic non-healing ulcer at the anal verge. Nine (11%) patients had grade 3 incontinence of anal sphincter. In one patient without disease recurrence, colostomy was performed due to severe anal sphincter disfunction. In one patient with anal stenosis, hematuria was observed, as well. Forty-nine (58.3%) patients with BT boost on primary tumour had less late site effects compared to 33 (39.3%) patients with EBRT boost, but the difference was not significant (P=0.066).

Prognostic Factors

On the univariate analysis, patients with locally advanced disease (T3-4) and incomplete response had worse LRC and all studied survival endpoints when compared to their counterparts.

Patients with the involvement of lymph nodes and patients with overall disease stage III had worse LRC, DFS, DSS and CFS in comparison with patients with N0 and overall stage I or II and patients with Hb below 120 g/l had worse LRC, DFS, DSS and OS in comparison with patients with Hb 120 g/l or higher. In addition, patients with poor performance status (WHO 1 or 2) had worse OS and patients with overall treatment time over 73 days had worse LRC. The patients with salvage surgery (APE or nodal dissection) for residual disease or tumour and/or regional lymph node recurrence had worse LRC, DFS and CFS, but not DSS and OS compared to complete responders.

For other analysed factors (sex, age, treatment intensity and the method of radiotherapy boost) no impact on the outcome was found.

On the multivariate analysis, a complete clinical disease response was identified as an independent prognostic factor for LRC, DFS and DSS, the salvage surgery for LRC and DFS, whereas Hb below 120 g/l retained its independent prognostic value for OS, and for LRC it was on the threshold of statistical significance (P=0.061) (Table 2).

Discussion

Before Negro *et al.* in 1974 reported that a complete tumour response can be achieved with radiochemotherapy, APE was the standard of the treatment in patients with anal cancer.[9] Nowadays, radiotherapy with concomitant ChT represents a standard treatment of anal cancer. Complete response rates and 5-year OS in patients with early stage disease range from 80-90% and 95-100%, respectively, and in patients with tumours larger than 5 cm from 50-75% and 35-70%.[1,3,11,20] In our study the complete response was recorded in 67 (79.8%) patients, regardless of the stage. Results of our analysis compare favourably to other published studies.[1,3,19,20-22] According to the data of the Cancer Registry of Slovenia, 24 (24%) patients were not referred to the treatment with radiotherapy in the period between 2003 and 2007.[4-8] We can only speculate that these patients were treated with local excision and were not presented to multidisciplinary advisory board. It could be debated if all these patients had an appropriate treatment, since it is well known that the local excision should be reserved only for small, well differentiated mucosal or submucosal tumours (<2 cm) and without sphincter involvement.[1]

Although in 24 (28.6%) patients the complete clinical response could not be achieved or they had recurrent disease, in only 12 (50%) patients salvage surgery was possible and only 8 (66.7%) of these operated patients were free of the disease. APE was performed in 11 patients and in one patient bilateral nodal dissection was carried out due to a solitary lymph node involvement. In one patient, APE was necessary due to severe sphincter incontinence after the end of the treatment. Our results on the salvage surgery rate are comparable to results of Ajani *et al*. and Peiffert *et al.* with salvage APE rate of 16% and 10%, respectively.[22,23] In the study of Akbari *et al.*, where salvage surgery was performed in 57 patients with persistent

or recurrent disease, the 5-year OS for all patients was 33%, whereas in our study it was 67%.[24] As the median follow-up time in Akbari´s study was 34.1 months, whereas in ours it was 43 months (range: 8-105 months), the direct comparison of reported results of these two studies could be misleading. However, the observed 75% rate of disease-free patients after salvage surgery is without doubt encouraging.

It is well known that patients with a complete tumour response following radiochemotherapy have a better local control and survival, which was demonstrated in our series, as well.[3,23,25] We found out that a complete clinical disease response was an independent prognostic factor for LRC, DFS and DSS.

The patients who had salvage surgery had worse LRC and DFS but it is encouraging that no statistically significant difference in DSS and OS was found. We can conclude that patients in whom salvage surgery was performed had similar OS as patients with the complete tumour remission. In some, but not all series, they reported that residual or recurrent carcinoma of anal canal after radiochemotherapy was associated with poor outcome after the attempted salvage surgery.[25] Furthermore, they found out that APE is successful as salvage therapy in about 50% of patients with local disease only but salvage rate is very poor in patients that have nodal involvement or residual or recurrent carcinoma which is fixed to the pelvic sidewall.[26-27]

In our study Hb below 120 g/l was identified as an independent prognostic factor for OS. It is not surprising, because anaemia is namely a well known prognostic factor for the lower tumour control and the survival in patients who are treated with radiotherapy.[28] It may be related with hypoxia and consequent development of tumour cells' radioresistency.[29]

At first evaluation at 6 weeks after the end of the treatment, the complete tumour remission was found in only 55 (65.5%) of patients, while another 12 (14.3%) patients reached the complete remission at 18 weeks post treatment. There are several other reports of very slow disease regression, with a complete response observed even up to 6-9 months after the treatment was completed.[1,30,31] The evaluation recommendations suggest that if there is no progression of the disease, a careful »wait and see« policy with repeated biopsies may be advocated. However, in cases of persistent disease or tumour progression, APE is recommended following the histological confirmation of the presence of viable malignant cells.

In our study, the profile and frequency of acute and late treatment-related toxic side effects were comparable to reports of other researchers.[2,10,32] The most frequently reported acute side effect was radiodermatitis with grade 3 or 4 occurring in 58% of patients during EBRT, whereas 15 (18%) patients experienced grade 3 or 4 late radiation side effects. Three (4%) patients experienced post-treatment anal stenosis, two (2%) developed chronic non-healing ulcer at the anal verge, 9 (11%) patients had grade 3 incontinence of anal sphincter and in one patient without disease recurrence, colostomy was performed due to the severe anal sphincter dysfunction. The rate of our late side effects is similar to other reports.[3,11,22,32,33]

The patients with BT boost on primary tumour had less late side effects (P=0.066). We should emphasize that these patients had less advanced tumours and, correspondingly, smaller tissue volumes were irradiated during boost phase of the treatment. Furthermore, it is well known that patients with BT boost have less late toxicity when compared to EBRT boost, because the use of interstitial implant has the advantage of more focused escalation of irradiation dose, resulting in more efficient sparing of the surrounding normal tissues.[34]

There are several possibilities for the improvement in the disease control and the survival in the future. In locally advanced disease, innovative approaches with 3D image-based BT boost and intensity modulated radiotherapy offer a potential for the individualised escalation of the target dose while respecting normal tissue tolerance.[35] For the treatment of unresectable recurrences and distant metastases, the development of more active new anti-cancer drugs, for example epidermal growth factor receptor (EGFR) inhibitors may represent an option. Finally, the majority of the anal cancers are causally connected to the persistent HPV infection, so it can be assumed that the HPV vaccines may become an important prevention measure against anal cancer in the future.

To conclude, radiochemotherapy provides an excellent disease control and the survival with preserving anal sphincter function in majority of patients which were evidenced also by our results. Surgical salvage with APE for persistent or recurrent disease should be considered whenever applicable as it can be curative in substantial proportion of such patients.

References

1. Rousseau DL, Thomas CR, Petrelli NJ, Kahlenberg MS. Sqamous cell carcinoma of the anal canal. *Surg Oncol* 2005; **14:** 121-32.
2. But-Hadzic J, Jenko K, Poljak M, Kocjan BJ, Gale N, Strojan P. Sinonasal inverted papilloma associated with squamous cell carcinoma. *Radiol Oncol* 2011; **45:** 267-72.
3. Chapet O, Gerard JP, Riche B, Alessio A, Mornex F, Romestaing P. Prognostic value of tumour regression evaluated after first course of radiotherapy for anal canal cancer. *Int J Radiat Oncol Biol Phys* 2005; **63:** 1316-24.
4. Cancer incidence in Slovenia 2003. Ljubljana: Institute of Oncology Ljubljana, Cancer Registry of Republic of Slovenia; 2006.
5. Cancer incidence in Slovenia 2004. Ljubljana: Institute of Oncology Ljubljana, Cancer Registry of Republic of Slovenia; 2007.
6. Cancer incidence in Slovenia 2005. Ljubljana: Institute of Oncology Ljubljana, Cancer Registry of Republic of Slovenia; 2008.
7. Cancer incidence in Slovenia 2006. Ljubljana: Institute of Oncology Ljubljana, Cancer Registry of Republic of Slovenia; 2009.
8. Cancer incidence in Slovenia 2007. Ljubljana: Institute of Oncology Ljubljana, Cancer Registry of Republic of Slovenia; 2010.
9. Nigro ND, Vaitkevicius VK, Considine D. Combined therapy for cancer of the anal canal. *Dis Colon Rectum* 1974; **27:** 763-6.
10. Fraunholz I, Rebeneck D, Weiß C, Rödel C. Combined-modality treatment for anal cancer. *Strahlenther Oncol* 2010; **186:** 361-6.
11. Ferrigno R, Nakamura RA, Dos Santos Novaes PE, Pellizzon AC, Maia MA, Fogarolli RC, et al. Radiochemotherapy in the conservative treatment of anal canal carcinoma: Retrospective analysis of the results and radiation dose effectiveness. *Int J Radiat Oncol Biol Phys* 2005; **61:** 1136-42.
12. Oblak I, Petric P, Anderluh F, Velenik V, Hudej R, Fras AP. Anal cancer chemoirradiation with curative intent - a single institution experience. *Neoplasma* 2009; **56:** 150-5.
13. Sobin LH, Gospodarowitcz MK, Wittekind C. International Union Against Cancer (UICC): TNM classification of malignant tumours. 7th edition. New York: Wiley-Liss; 2009.
14. Strojan P. Role of radiotherapy in melanoma management. *Radiol Oncol* 2010; **44:** 1-12.
15. Ajani JA, Welch SR, Raber MN, Fiels WS, Krakoff IM. Comprehensive criteria for assessing therapy-induced toxicity. *Cancer Invest* 1990; **8:** 147-59.
16. LENT-SOMA scales for all anatomic sites. *Int J Radiat Oncol Biol Phys* 1995; **31:** 1049-91.
17. Kaplan EL, Meier P. Nonparametric estimation from incomplete observations. *J Am Stat Assoc* 1958; **53:** 457-81.
18. Peto R, Pike MC, Armitage P, Breslow NE, Cox DR, Howard SV, et al. Design and analysis of randomized clinical trials requiring prolonged observation of each patient. II. Analysis and examples. *Br J Cancer* 1977; **35:** 1-39.
19. Cox DR. Regression models and life-tables. *J R Stat Soc Bull* 1972; **34:** 187-220.
20. Gerard JP, Ayzac L, Hun D, Romestaing P, Coquard R, Ardiet JM, et al. Treatment of anal canal carcinoma with high dose radiation therapy and concomitant fluorouracil-cisplatinum. Long-term results in 95 patients. *Radiother Oncol* 1998; **46:** 249-56.
21. Flam M, John M, Pajak TF, Petrelli N, Myerson R, Doggett S, et al. Role of mitomycin in combination with florouracil and radiotherapy, and a salvage chemoradiotherapy in the definitive nonsurgical treatment of the epidermoid carcinoma of the anal canal: results of a phase III randomized intergroup study. *J Clin Oncol* 1996; **14:** 2527-39.
22. Ajani JA, Winter KA, Gunderson LL, Pedersen J, Benson AB 3rd, Thomas CR Jr, et al. Fluorouracil, mitomycin, and radiotherapy vs fluorouracil, cisplatin, and radiotherapy for carcinoma of the anal canal: a randomized controlled trial. *JAMA* 2008; **299:** 1914-21.
23. Peiffert D, Bey P, Pernot M, Guillemin F, Luporsi E, Hoffstetter S, et al. Conservative treatment by irradiation of epidermoid cancers of the anal canal. Prognostic factors of tumoural control and complications. *Int J Radiat Oncol Biol Phys* 1997; **37:** 313-24.
24. Akbari RP, Paty PB, Guillem JG, Weiser MR, Temple LK, Minsky BD, et al. Oncologic outcomes of salvage surgery for epidermoid carcinoma of the anus initially managed with combined modality therapy. *Dis Colon Rectum* 2004; **47:** 1136-44.
25. Cummings BJ, Brierley JD. Anal Cancer. In: Halperin EC, Perez CA, Brady LW, editors. *Principles and Practice of Radiation Oncology*. 5th edition. Philadelphia: Lippincott Williams& Wilkins, 2008. p. 1383-96.
26. Schiller DE, Cummings BJ, Rai S, Le LW, Last L, Davey P, et al. Outcomes of salvage surgery for squamous cell carcinoma of the anal canal. *Ann Surg Oncol* 2007; **14:** 2780-9.
27. Pocard M, Tiret E, Nugent K, Dehni N, Parc R. Results of salvage abdominoperineal resection for anal cancer after radiotherapy. *Dis Colon Rectum* 1998; **41:** 1488-93.
28. Oblak I, Strojan P, Zakotnik B, Budihna M, Smid L. Hemoglobin as a factor influencing the outcome in inoperable oropharyngeal carcinoma treated by concomitant radiochemotherapy. *Neoplasma* 2003; **50:** 452-8.
29. Horsman MR, Van der Kogel A. Therapeutic approaches to tumour hypoxia. In: Joiner M, Van der Kogel A, editors. *Basic Clinical Radiobiology*. 4th edition. London: Hodder Arnold, 2009. p. 233-45.
30. Sato H, Koh PK, Bartolo DCC. Management of anal canal cancer. *Dis Colon Rectum* 2005; **48:** 1301-15.
31. Cummings BJ, Keane TJ, O´Sullivan B, Wong CS, Catton CN. Epidermoid anal cancer: treatment by radiation alone or by radiation and 5-fluorouracil with and without mitomycin C. *Int J Radiat Oncol Biol Phys* 1991; **21:** 1115-25.
32. Marshall DT, Thomas CR. Carcinoma of the anal canal. *Oncol Rev* 2009; **3:** 27-40.
33. Mitchell SE, Mendenhal WM, Zlotecki RA, Carroll RR. Squamous cell carcinoma of the anal canal. *Int J Radiat Oncol Biol Phys* 2001; **45:** 1007-13.
34. Hwang JM, Rao AR, Cosmatos HA, Wang R, Kaptein JS, Kagan RA, et al. Treatment of T3 and T4 anal carcinoma with combined chemotharapy and interstitial 192-Ir implantation: a 10-year experience. *Brachytherapy* 2004; **3:** 95-100.
35. Bailey DW, Kumaraswamy L, Podgorsak MB. A fully electronic intensity-modulated radiation therapy quality assurance (IMRT QA) process implemented in a network comprised of independent treatment planning, record and verify, and delivery systems. *Radiol Oncol* 2010; **44:** 124-30.

research article

The diffuse large B-cell lymphoma – where do we stand now in everyday clinical practice

Brigita Gregoric[1], Vesna Zadnik[2], Barbara Jezersek Novakovic[1]

[1] Division of Medical Oncology and [2] Department of Epidemiology, Institute of Oncology Ljubljana, Ljubljana, Slovenia

Radiol Oncol 2012; 46(2): 153-159.

Received 3 September 2011
Accepted 2 November 2011

Correspondence to: Assist. Prof. Barbara Jezeršek Novaković, MD, PhD, Department of Medical Oncology, Institute of Oncology Ljubljana, Zaloška2, SI-1000 Ljubljana, Slovenia. Phone: +386 15879280; Fax: +386 15879305; E-mail: bjezersek@onko-i.si

Disclosure: No potential conflicts of interest were disclosed.

Background. Due to superior results observed with the addition of rituximab into treatment of patients with the diffuse large B-cell lymphoma (DLBCL),the R-CHOP (rituximab, cyclophosphamide, doxorubicin, vincristine, and prednisolone) regimen and its variants became the standard initial treatment of these patients. However, the treatment recommendations are based on results of clinical studies while the conditions of routine treatment are far different from the ones in clinical studies. The aim of this retrospective study was therefore to compare the treatment results of routinely treated patients with the DLBCL to results reported by some larger studies.

Patients and methods. Two hundred and ninety five patients with the DLBCL were treated between 2004 and 2008 according to the then protocol with R-CHOP or R-CHOP-like regimens at the Institute of Oncology Ljubljana. Treatment response was evaluated according to Cheson's criteria and the disease-free and overall survival by means of Kaplan Meier survival curves.

Results. Response to treatment in our evaluation diverged from the reported one predominately in the low risk group (international prognostic index [IPI] categorisation) and in the very good prognosis group (revised international prognostic index (R-IPI) categorisation). The determined complete response (CR) rates in other IPI and R-IPI groups were generally within expectations. Also in the disease-free survival the largest discrepancy occurred in the low-risk patient group (3 year disease-free survival rate of 75%) and in the very good prognosis group (4 year disease-free survival rate of 59%). In all other IPI risk groups, the disease-free survival at 3 years (low intermediate risk 76%, high intermediate risk group 57%, and high risk group 53%) agreed very well with the quoted ones. Slightly worse was the compliance of the 4 year disease-free survival rates (72% in the good prognosis and 51% in the poor prognosis group) with the results from the literature. The 3 year overall survival rates (low risk patients 87%, high intermediate risk 61% and high risk patients 51%) were somewhat worse than the reported ones in all IPI subgroups except in the low intermediate risk group (82%). On the other hand, the 4 year overall survival rates of the R-IPI categories (94% in the very good prognosis group, 80% in the good prognosis group, 56% in the poor prognosis group) were much better correlated with the data from the literature.

Conclusions. In total, the treatment outcomes of routinely treated patient with the DLBCL at our institute are quite encouraging when compared to results of some larger studies. There are probably no dilemmas about how to treat young good prognosis patients and patients aged over 60 years at present. However, the 5 year overall survival rate of 76% for the young poor prognosis group is unsatisfying and needs to be improved. At present, quite a few studies are underway to clarify which of the regimens will perform best in this population.

Key words: diffuse large B-cell lymphoma; R-CHOP; treatment result; routine treatments

Introduction

The diffuse large B-cell lymphoma (DLBCL) is the most common histologic subtype of non-Hodgkin's lymphomas.[1,2] However, the disease is quite heterogeneous in terms of morphology, genetics, biologic behaviour, and consequently response to treatment and prognosis.[1] Beside histopathology and genetics, similar like in other malignancies, clinical parameters have been identified that

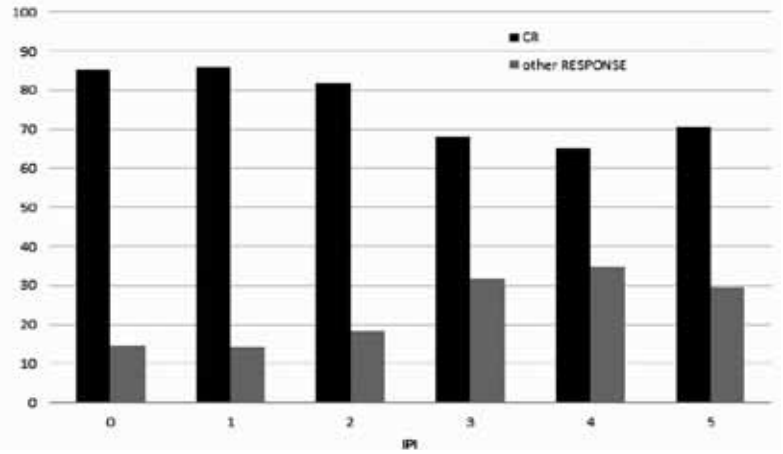

FIGURE 1. Percentage of patients achieving complete and other responses according to various IPI categories.
IPI = international prognostic index. CR = complete response

influence the prognosis of patients with DLBCL.[3-5] Namely, the age above 60 years, serum lactate dehydrogenase concentration above normal, ECOG performance status of 2 or more, Ann Arbor stage III or IV and number of involved extranodal sites above 1 have been shown to correlate significantly with a shorter disease-free and overall survival of patients treated with anthracycline containing regimen. These five factors have been included in the original international prognostic index (IPI).[3]

The addition of rituximab to standard chemotherapy (cyclophosphamide, doxorubicin, vincristine, and prednisolone [CHOP] and CHOP-like) in patients with DLBCL has resulted in significant improvements of the disease-free and overall survival rates.[6-8] Beside the original IPI that has been later on validated also in patients receiving rituximab containing treatment[9] similarly the revised international prognostic index (R-IPI)[10] has been proposed to predict outcome in patients with the DLBCL receiving R-CHOP or R-CHOP-like regimens. It is still unclear which of the two indexes is more appropriate for presentation of study results in this population.

Due to superior results with rituximab, the R-CHOP and variants have become the standard initial treatment of patients with the DLBCL.[11] However, the conditions of routine treatment are far different from the ones in clinical studies where the study population is highly selected, the histopathology and staging procedures are thoroughly revised and treatment and side effects are strictly controlled. The aim of our retrospective study was therefore to analyse and to compare the treatment results of routinely treated patients with the DLBCL at the Institute of Oncology Ljubljana to results reported by some larger studies.

TABLE 1. Distribution of patients according to the selected regimens

	Number	%
R-ACVBP	19	6.4
R-CHOP	253	85.8
R-CHOP+MTX	12	4.1
R-CHOP/R-other	11	3.7
Total	295	100.0

R-ACVBP = rituximab, doxorubicin, cyclophosphamide, vincristine, bleomycin, prednisolone; R-CHOP = rituximab, doxorubicin, cyclophosphamide, vincristine, prednisolone; R-CHOP+MTX = rituximab, doxorubicin, cyclophosphamide, vincristine, prednisolone, middle-dose methotrexate; R-CHOP/R-other = R-CHOP with reduced doses of doxorubicin + etoposide

Patients and methods

Two hundred and ninety five patients with the DLBCL were treated between 2004 and 2008 according to the then protocol with R-CHOP or R-CHOP-like regimens at the Institute of Oncology Ljubljana. The patients' characteristics, patohistological diagnosis, disease stage, response to treatment and survival data were taken from patients' records. Treatment response was evaluated according to Cheson' criteria[12,13] and the disease-free and overall survival by means of Kaplan Meier survival curves. For the determination of statistical differences the log rank test and Chi-square test were applied.

Results

Patients' characteristics and treatment

Among 295 patients, there were 132 males (44.7%) and 163 females (55.3%). Their median age was 64 years (range from 19 to 86 years). One hundred and sixteen patients (39.3%) were aged below 60 years and 179 patients (60.7%) were aged 60 or more years. Ninety three (31.5%) patients had limited disease (stage I or II) and 198 (67.1%) patients had advanced disease (stages III and IV) at presentation. The stage of disease could not be defined in 4 patients. According to the IPI categories, there were 34 (11.5%) patients with IPI 0, 63 (21.4%) patients with IPI 1, 66 (22.4%) patients with IPI 2, 69 (23.4%) patients with IPI 3, 46 (15.6%) patients with IPI 4 and 17 (5.7%) patients with IPI 5, respectively.

All patients were treated with R-CHOP or R-CHOP-like regimens (Table 1). The selection of regimen was influenced only by adverse prognostic factors (*e.g.* massive infiltration of bone marrow and/or bones where middle dose MTX was added to R-CHOP). In just few young poor-prognosis

TABLE 2. Response to treatment according to different IPI categories

	All patients		Low risk IPI=0,1		Low intermediate risk IPI=2		High intermediate risk IPI=3		High risk IPI=4-5	
	N	%	N	%	N	%	N	%	N	%
CR	226	76,6	83	85,6	54	81,8	47	68,1	42	66,7
CRu	4	1,4	1	1,0	0	0,0	0	0,0	3	4,8
PR	36	12,2	10	10,3	4	6,1	14	20,3	8	12,7
SD	2	0,7	0	0,0	0	0,0	1	1,4	1	1,6
PD	13	4,4	1	1,0	4	6,1	4	5,8	4	6,3
Unclassified	14	4,7	2	2,1	4	6,1	3	4,3	5	7,9
Total	295	100,0	97	100,0	66	100,0	69	100,0	63	100,0

CR = complete response; CRu= complete response unconfirmed; PR = partial response; SD = stable disease; PD = progressive disease; unclassified – unclassified response to treatment; IPI = international prognostic index; N = number of patients

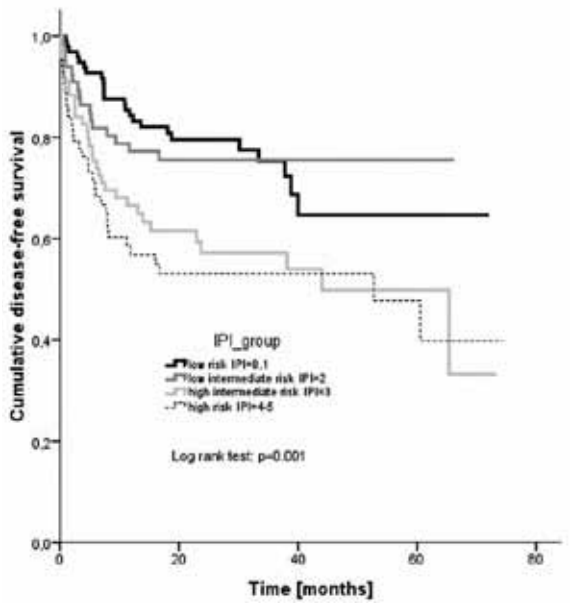

FIGURE 2. Disease-free survival according to different IPI risk groups. IPI = international prognostic index.

patients, the more dose-intensive R-ACVBP$_{21}$ regimen was used instead of the R-CHOP$_{21}$ regimen. The R-CHOP$_{14}$ regimen has never been applied. In patients with compromised cardiac function, reduced doses of anthracyclines were applied and were sometimes compensated for with the addition of etoposide (reduced intensity R-CHOEP). Patients with stage I or II of the disease received 6 cycles while patients with stage I.X, II.X, III and IV received 8 cycles of rituximab containing treatment. Patients treated with R-ACVBP received 6 cycles at maximum.

Response to treatment

The response to treatment for all patients and for distinct IPI categories is presented in Table 2. The difference in response between the low risk group and low intermediate risk group was statistically insignificant as was the difference between the high intermediate and high risk groups. But the significant Chi-square for the entire table (p=0.045) indicates the significant difference between both low risk and both high risk groups.

The response to treatment is given also for distinct R-IPI categories (Table 3). In this case, the difference between the very good and good prognosis groups was statistically insignificant, as well as the entire table Chi-square p value (p=0,088). A statistically significant difference in the response was observed between the IPI 2 and IPI 3 categories which was detected by both indexes – namely by the IPI and the R-IPI and is also clearly presented in Figure 1.

The disease-free survival according to IPI and R-IPI categories

With the median observation period of 22 months, the estimated 3 year disease-free survival rates were 75.3% for low risk, 75.6% for low intermediate risk, 57.2% for high intermediate risk, and 53.1% for high risk group, respectively (Figure 2). The difference between the groups was statistically significant (log rank, p = 0.001).

The progression-free survival was plotted also according to the R-IPI categories - the estimated 4 year disease-free survival rates were 59.4% for very good prognosis, 71.6% for good prognosis, and 51.1% for bad prognosis group, respectively (Figure 3). Again, the difference between the groups was statistically significant (log rank, p= 0.000).

The overall survival according to IPI and R-IPI categories

With the median observation period of 31 months, the estimated 3 year overall survival rates were

TABLE 3. Response to treatment according to different R-IPI categories

	All patients		Very good prognosis IPI=0		Good prognosis IPI=1,2		Bad prognosis IPI=3-5	
	N	%	N	%	N	%	N	%
CR	226	76,6	29	85,3	108	83,7	89	67,4
CRu	4	1,4	0	0,0	1	0,8	3	2,3
PR	36	12,2	5	14,7	9	7,0	22	16,7
SD	2	0,7	0	0,0	0	0,0	2	1,5
PD	13	4,4	0	0,0	5	3,9	8	6,1
Unclassifed	14	4,7	0	0,0	6	4,6	8	6,1
Total	295	100,0	34	100,0	129	100,0	132	100,0

CR = complete response; CRu= complete response unconfirmed; PR = partial response; SD = stable disease; PD = progressive disease; unclassified = unclassified response to treatment; R-IPI = revised international prognostic index; IPI = international prognostic index; N = number of patients

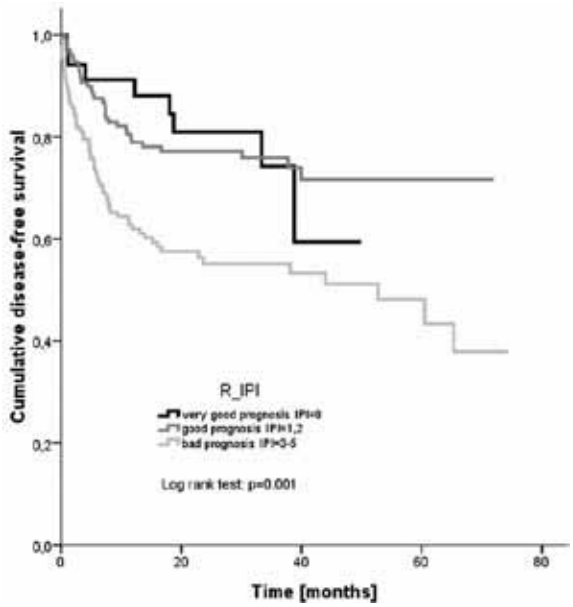

FIGURE 3. Disease-free survival according to different R-IPI risk groups. R-IPI = revised international prognostic index.

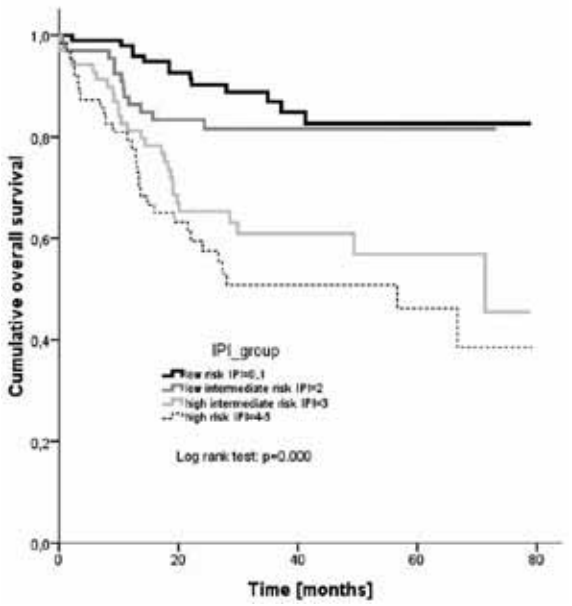

FIGURE 4. Overall survival according to different IPI risk groups. IPI = international prognostic index.

86.9% for low risk, 81.6% for low intermediate risk, 60.9% for high intermediate risk, and 50.9% for high risk group, respectively (Figure 4). The difference between the groups was statistically significant (log rank, p = 0.000).

The overall survival was plotted also according to the R-IPI categories - the estimated 4 year overall survival rates were 93.7% for very good prognosis, 79.5% for good prognosis, and 55.9% for bad prognosis group, respectively (Figure 5). Again, the difference between the groups was statistically significant (log rank, p= 0.000).

Treatment outcomes according to clinical categories of patients

Treatment outcomes were evaluated also according to clinical categories – namely, response to treatment, disease-free survival and overall survival were followed separately for young good prognosis patients (younger than 60 years with IPI 0 or 1), young poor prognosis patients (younger than 60 years with IPI of 2 or more), and older patients (aged over 60 years regardless of IPI), respectively.

The response to treatment is given in Table 4, while the disease-free and overall survivals are plotted in Figures 6 and 7, respectively. The difference in the disease-free survival between all three groups was statistically significant (log rank, p = 0.005), but it was insignificant when only young good prognosis and young poor prognosis groups were compared (p = 0.365). Also the difference in the overall survival between all there groups was significant (p = 0.000) as was the difference between young good prognosis and young poor prognosis group (p = 0.005).

TABLE 4. Response to treatment according to different clinical categories. The difference among groups was insignificant (p=0.150)

	All patients		<60years, IPI=0,1		<60years, IPI>1		>60years	
	N	%	N	%	N	%	N	%
CR	226	76,6	58	85,3	34	70,8	134	74,9
CRu	4	1,4	1	1,5	0	0,0	3	1,7
PR	36	12,2	8	11,8	7	14,6	21	11,7
SD	2	0,7	0	0,0	1	2,1	1	0,6
PD	13	4,4	0	0,0	5	10,4	8	4,5
Unclassified	14	4,7	1	1,5	1	2,1	12	6,7
Total	295	100,0	68	100,0	48	100,0	179	100,0

CR = complete response; CRu= complete response unconfirmed; PR = partial response; SD = stable disease; PD = progressive disease; unclassified = unclassified response to treatment; IPI = international prognostic index; N = number of patients

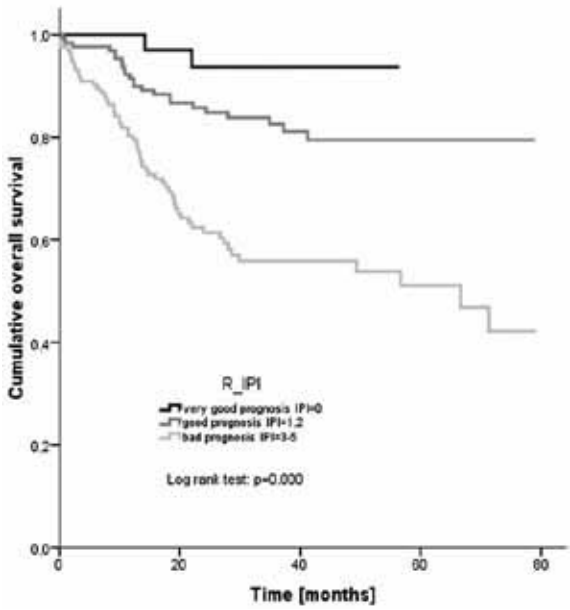

FIGURE 5. Overall survival according to different R-IPI risk groups. R-IPI = revised international prognostic index.

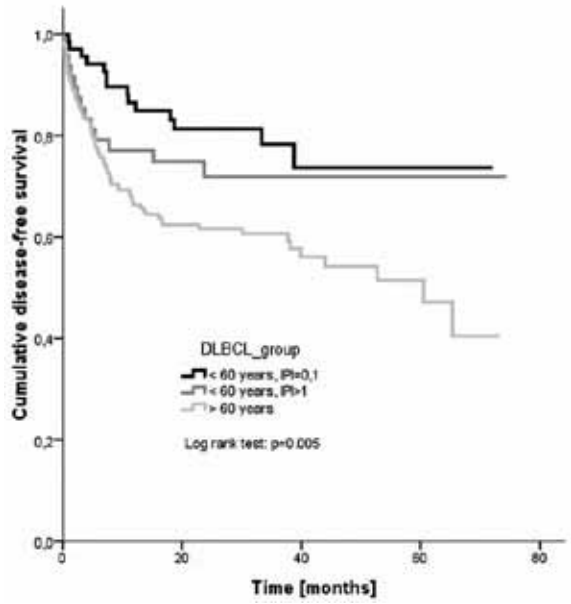

FIGURE 6. Disease-free survival of different clinical categories of patients. DLBCL = diffuse large B-cell lymphoma. IPI = international prognostic index.

Discussion

The treatment outcomes in patients with the DLBCL have been significantly improved with the addition of rituximab to standard anthracycline containing chemotherapies both in terms of the disease-free as well as the overall survival. This has been demonstrated by various researchers during the last decade[14-21], which resulted in the introduction of rituximab into standard first-line treatment of these patients. However, it is somewhat difficult to compare the results of different studies due to variable study designs and regimens applied and therefore we are still uncertain about the optimal therapy for a given patient or for a given group of patients.[22] Consequently, quite problematic is also the evaluation of treatment outcomes in patients treated in everyday clinical practice. The introduction of the standard IPI by Shipp *et al.*[3], its validation in patients receiving rituximab containing treatments by Ziepert *et al.*[9] and the proposal of R-IPI by Sehn *et al.*[10], beside determining the patients' prognosis at least partially facilitated the comparison of study results as well as the comparison of routine treatment outcomes with the study results.

Response to treatment in our evaluation diverged from the reported one predominately in the low risk group (CR rate of 85.6%) where it was even lower than the reported 87% CR rate in the original IPI study where patients received chemotherapy without rituximab.[3] The same observation holds true for the very good prognosis group in the R-IPI categorisation in which a higher CR

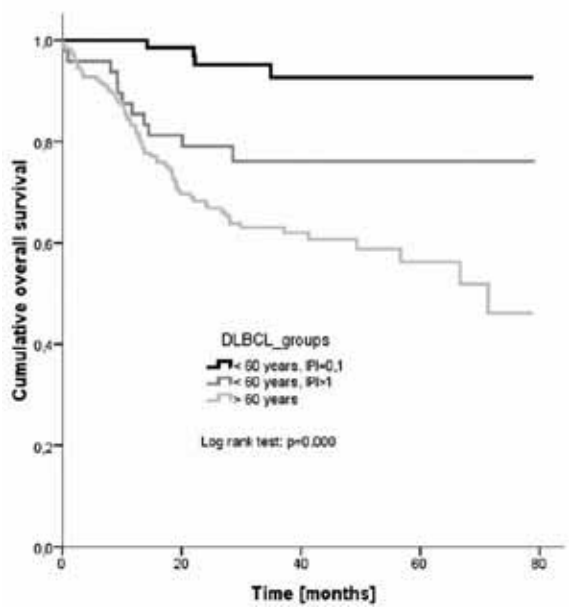

FIGURE 7. Overall survival of different clinical categories of patients. DLBCL = diffuse large B-cell lymphoma. IPI = international prognostic index

rate from the observed 85.3% could have been expected. The determined CR rates in other IPI and R-IPI groups were generally within expectations. The CR rates observed in the group of young good prognosis patients (86.8% of patients achieving CR or CRu) are completely in agreement with the results reported by Pfreundschuh *et al*. in the MInT study.[19] However, the overall response rate of 88.3% achieved in our patients aged over 60 years was much better than the 77% overall response rate reported by Habermann *et al*.[18]

Regarding the duration of response given by the disease-free survival, again the largest discrepancy occurred in the low-risk patient group where the 3 year disease-free survival rate was 75% compared to 87% reported by Ziepert *et al*.[9] In all other risk groups the disease-free survival at 3 years (low intermediate risk 76%, high intermediate risk group 57%, high risk group 53%, respectively) agreed very well with the reported ones (75%, 59% and 50%, respectively).[9] An even larger discrepancy was noted in case of the R-IPI categories – namely, the 4 year disease-free survival rate was 59% in the very good prognosis, 72% in the good prognosis and 51% in the poor prognosis group, respectively, as compared to the reported 94%, 80%, and 53%, respectively.[10] The 3 year disease-free survival of young good prognosis patients in our evaluation was 78% while Pfreundshuh *et al*.[19] reported of 85% rate in equivalent population. On the other hand, Habermann *et al*.[18] achieved a 53% 3 year disease-free survival rate in older patients as compared to the 61% rate in our study.

The 3 year overall survival rate of the low risk patients (87%) in our analysis was somewhat worse than the 91% reported by Ziepert *et al*.[9] Equivalent or slightly worse were also the 3 year overall survival rates of low intermediate risk, high intermediate risk and high risk patients (82%, 61%, 51%, respectively) as compared to the reported rates (81%, 65%, 59%, respectively).[9] On the other hand, the 4 year overall survival rates of the R-IPI categories (94% in the very good prognosis group, 80% in the good prognosis group, and 56% in the poor prognosis group, respectively) were much better correlated with the reported ones of 94%, 79%, and 55%, respectively.[10] The 3 year overall survival of young good prognosis patients in our evaluation was 93% which completely corresponds to the rate reported by Pfreundshuh *et al*.[19] in equivalent population. Then again, Habermann *et al*.[18] achieved a 67% 3 year overall survival rate in older patients (aged over 60 years) as compared to the 63% rate in our study.

The repeating pattern of worst results achieved in our low risk and/or the very good prognosis group raises the question of whether those patients have been in some way "understaged". Another possible explanation is the existence of some not yet determined aspect that negatively influenced response to treatment, disease-free survival and to some extent also the overall survival of these patients. This aspect could be of patohistological origin – *e.g*. the inclusion of patients with immunoblastic variants of the DLBCL which are no longer recognized as a separate entity in the WHO classification but have been associated with a worse outcome even after treatment with R-CHOP[23] or of genetic origin – namely patients with the activated B-cell type gene expression profile have a much worse 5 year overall survival compared to patients with the germinal centre type gene expression profile.[24,25] It is, however, quite unlikely that patients with immunoblastic lymphomas or activated B-cell type lymphomas would have been gathered prevailingly in the low risk and/or very good prognosis groups.

In total, the treatment outcomes of routinely treated patient with the DLBCL at our institute are quite encouraging when compared to results of some larger studies. There are probably no dilemmas about how to treat young good prognosis patients at present – it is with 6 cycles of R-CHOP$_{21}$.[19] On the other hand, for patients aged over 60 years

the Ricover-60 study reported the best results with 6 cycles of R-CHOP$_{14}$ (and total 8 applications of rituximab).[26] This regimen is unfortunately associated with serious toxicity and therefore not applicable in the routine setting. Regarding our results also the treatment with 6 or 8 cycles (considering the stage of the disease) of R-CHOP$_{21}$ will be appropriate for everyday management of the DLBCL in this fragile population. As for the young poor prognosis group – the 5 year overall survival rate of 76% is unsatisfying and needs to be improved. At present, quite a few studies are underway to clarify which of the regimens will perform best in this population. Most probably this will have to include routine determination of the gene expression profile in each patient in order to tailor his individual treatment.

Acknowledgement

This research was partially supported by Slovenian Ministry of Science (research program J3-0321).

References

1. Swerdlow SH, Campo E, Harris NL, Pileri SA, Stein H, Thiele J, et al, editors. *WHO classification of tumours of haematopoietic and lymphoid tissues.* 4th edition. Lyon, France: International Agency for Research on Cancer; 2008.
2. Žakelj Primic M, Bračko M, Pompe-Kirn V, Zakotnik B, editors. *Rak v Sloveniji 2007.* Ljubljana: Onkološki inštitut Ljubljana, Epidemiologija in register raka, Register raka Republike Slovenije, 2010.
3. Shipp M, Harrington D, Anderson J, Armitage JO, Bonadonna G, Brittinger G, et al. A predictive model for aggressive non-Hodgkin¢s lymphomas. *N Engl J Med* 1993; **329:** 987-94.
4. Strojan-Flezar M, Lavrencak J, Zganec M, Strojan P. Image cytometric nuclear texture features in inoperable head and neck cancer: a pilot study. *Radiol Oncol* 2011; **45:** 40-50.
5. Velnar T, Smrdel U, Popovic M, Bunc G. Genetic markers in oligodendroglial tumours. *Radiol Oncol* 2010; **44:** 13-8.
6. Cvetkovic RS, Perry CM. Rituximab: a review of its use in non-Hodgkin's lymphoma and chronic lymphocytic leukemia. *Drugs* 2006; **66:** 791-820.
7. Molina A. A decade of rituximab: improving survival outcomes in non-Hodgkin's lymphoma. *Annu Rev Med* 2008; **59:** 237-50.
8. Jezeršek Novaković B, Benigar A. Treatment of non-Hodgkin's lymphomas with rituximab in Slovene patients. *Med Oncol* 2010; **27:** 167-76.
9. Ziepert M, Hasenclever D, Kuhnt E, Glass B, Schmitz N, Pfreundschuh M, et al. Standard International prognostic index remains a valid predictor of outcome for patients with aggressive CD20+ B-cell lymphoma in the rituximab era. *J Clin Oncol* 2010; **28:** 2373-80.
10. Sehn LH, Berry B, Chhanabhai M, Fitzgerald C, Gill K, Hoskins P, et al. The revised International Prognostic Index is a better predictor of outcome than the standard IPI for patients with diffuse large B-cell lymphoma treated with R-CHOP. *Blood* 2007; **109:** 1857-61.
11. Tilly H, Dreyling M. Diffuse large B-cell non-Hodgkin's lymphoma: ESMO Clinical Practice Guidelines for diagnosis, treatment and follow-up. *Ann Oncol* 2010; **21(Suppl 5):** 172-4.
12. Cheson BD, Horning SJ, Coiffier B, Shipp MA, Fisher RI, Connors JM, et al. Report of an international workshop to standardize response criteria for non-Hodgkin's lymphomas. *J Clin Oncol* 1999: **17:** 1244-53.
13. Cheson BD. New staging and response criteria for non-Hodgkin lymphoma and Hodgkin lymphoma. *Radiol Clin North Am* 2008; **46:** 213-23.
14. Pettengell R, Linch D. Position paper on the therapeutic use of rituximab in CD20-positive diffuse large B-cell non-Hodgkin's lymphoma. *Br J Haematol* 2003; **121:** 44-8.
15. Coiffier B, Lepage E, Briere J, Herbrecht R, Tilly H, Bouabdallah R, et al. CHOP chemotherapy plus rituximab compared with CHOP alone in elderly patients with diffuse large-B-cell lymphoma. *N Engl J Med* 2002; **346:** 235-42.
16. Sehn LH, Donaldson J, Chhanabhai M, Fitzgerald C, Gill K, Klasa R, et al. Introduction of combined CHOP plus rituximab therapy dramatically improved outcome of diffuse large B-cell lymphoma in British Columbia. *J Clin Oncol* 2005; **23:** 5027-33.
17. Feugier P, Van Hoof A, Sebban C, Solal-Celigny P, Bouabdallah R, Fermé C, et al. Long-term results of the R-CHOP study in the treatment of elderly patients with diffuse large B-cell lymphoma: a study by the Groupe d'Etude des Lymphomes de l'Adulte. *J Clin Oncol* 2005; **23:** 4117-26.
18. Habermann TM, Weller EA, Morrison VA, Gascoyne RD, Cassileth PA, Cohn JB, et al. Rituximab-CHOP versus CHOP alone or with maintenance rituximab in older patients with diffuse large B-cell lymphoma. *J Clin Oncol* 2006; **24:** 3121-7.
19. Pfreundschuh M, Trümper L, Osterborg A, Pettengell R, Trneny M, Imrie K, et al. CHOP-like chemotherapy plus rituximab versus CHOP-like chemotherapy alone in young patients with good-prognosis diffuse large-B-cell lymphoma: a randomised controlled trial by the MabThera International Trial (MInT) Group. *Lancet Oncol* 2006; **7:** 379-91.
20. Coiffier B, Thieblemont C, Van Den Neste E, Lepeu G, Plantier I, Castaigne S, et al. Long-term outcome of patients in the LNH-98.5 trial, the first randomized study comparing rituximab-CHOP to standard CHOP chemotherapy in DLBCL patients: a study by the Groupe d'Etudes des Lymphomes de l'Adulte. *Blood* 2010; **116:** 2040-5.
21. Horvat M, Jezeršek Novaković B. Effect of response quality and line of treatment with rituximab on overall and disease-free survival of patients with B-cell lymphoma. *Radiol Oncol* 2010, **44:** 232-8.
22. Kovač V, Smrdel U. Meta-analyses of clinical trials in patients with non-small cell lung cancer. *Neoplasma* 2004; **51:** 334-40.
23. Ott G, Ziepert M, Klapper W, Horn H, Szczepanowski M, Bernd HW, et al. Immunoblastic morphology but not the immunohistochemical GCB/nonGCB classifier predicts outcome in diffuse large B-cell lymphoma in the RICOVER-60 trial of the DSHNHL. *Blood* 2010; **116:** 4916-25.
24. Alizadeh AA, Eisen MB, Davis RE, Ma C, Lossos IS, Rosenwald A, et al. Distinct types of diffuse large B-cell lymphoma identified by gene expression profiling. *Nature* 2000; **403:** 503-11.
25. Lenz G, Wright G, Dave SS, Xiao W, Powell J, Zhao H, et al. Stromal gene signatures in large-B-cell lymphomas. *N Engl J Med* 2008; **359:** 2313-23.
26. Pfreundschuh M, Schubert J, Ziepert M, Schmits R, Mohren M, Lengfelder E, et al. Six versus eight cycles of bi-weekly CHOP-14 with or without rituximab in elderly patients with aggressive CD20+ B-cell lymphomas: a randomised controlled trial (RICOVER-60). *Lancet Oncol* 2008; **9:** 105-16.

research article

Effectiveness of L-thyroxine treatment on TSH suppression during pregnancy in patients with a history of thyroid carcinoma after total thyroidectomy and radioiodine ablation

Blaz Krhin[1] and Nikola Besic[2]

[1] Department of Laboratory Diagnostics, Institute of Oncology Ljubljana, Ljubljana, Slovenia
[2] Department of Surgical Oncology, Institute of Oncology Ljubljana, Ljubljana, Slovenia

Radiol Oncol 2012; 46(2): 160-165.

Received 29 September 2011
Accepted 24 November 2011

Correspondence to: Prof. Nikola Bešič MD, PhD, Dept. of Surgical Oncology, Institute of Oncology Ljubljana, Zaloška 2, SI-1000 Ljubljana, Slovenia. Phone: +386 1 5879 953; Fax:+386 1 5879400; E-mail: nbesic@onko-i.si

Disclosure: No potential conflicts of interest were disclosed.

Introduction. There are scarce data about the optimal increase of L-thyroxine dose during pregnancy in patients with a history of thyroid carcinoma. The first aim of the study was to find out if routine therapeutic measures enable adequate TSH suppression in pregnancy. The other aim was to find out the optimal dose of L-thyroxine for TSH suppression in pregnant women.

Patients and methods. In this retrospective observational study, we analysed 36 pregnancies of 32 women with a history of thyroid carcinoma. Before pregnancy, all of them underwent total thyroidectomy and radioiodine ablation of thyroid remnant, and they were on suppressive doses of L-thyroxine. Thyroid function tests were obtained before, during and after pregnancy.

Results. Mean L-thyroxine dose before pregnancy, in the first, second and, third trimester and after delivery was 149, 147, 155, 165 and 158 micrograms daily, respectively. TSH concentration remained suppressed in 9 pregnancies, it was within normal range in 22 and elevated in 5 pregnancies. The mean dose of L-thyroxine in patients with suppressed TSH before pregnancy, in the first, second and, third trimester and after delivery was 154, 154, 164, 160 and 161 micrograms daily, respectively. When the dose had to be changed, the mean increase of the dose was 31.5 micrograms daily.

Conclusions. The range of changes in TSH concentration during pregnancy in the patients who have been on suppressive L-thyroxine therapy before conception is quite wide. TSH was adequately suppressed in only 25% of pregnancies. The dose of L-thyroxine in patients with suppressed TSH in the first, second and third trimester was 154, 164 and 160 micrograms daily, respectively.

Key words: pregnancy; TSH suppression; L-thyroxine; thyroid carcinoma.

Introduction

Thyroid hormones are important for normal pregnancy and the foetal development.[1,2] During pregnancy, maternal thyroid hormones requirements increase.[3,4] It is well known that the reference values of TSH, free T_3 and free T_4 for healthy the non-pregnant population are not the same as during pregnancy. Dashe *et al*.[5] published the data about the TSH concentration in 13,599 pregnancies. They found out that the normal physiological concentration of TSH during the first trimester of pregnancy was as low as 0.1 mU/L. According to the trimester-specific reference ranges of serum, TSH concentrations above 2.3 mU/L in the first trimester and 3.1-3.5 mU/L in the second and third trimester may already be indicative of subclinical hypothyroidism.[1,6] Safety of pregnancy during subclinical hyperthyroidism was reported by Casey *et al*.[7] They found out that the subclinical hyperthyroidism was not associated with the adverse outcome of pregnancy.[7]

The patients having undergone thyroidectomy and radioiodine therapy are dependent on exogenous L-thyroxine.[8] Some authors advocate that the increase of dose of L-thyroxine during pregnancy should be determined from the results of thyroid function tests[8-11], while others propose to increase L-thyroxine dose as soon as pregnancy is confirmed.[12,13]

There are very limited data in the literature about the changes of TSH and thyroid hormones during pregnancy in patients with a history of thyroid carcinoma. To our knowledge, these studies included only a small number of patients[8, 12-15] with the largest study group of 18 such cases reported by Loh *et al*.[8] There are scarce data about the optimal increase of L-thyroxine dose during pregnancy in the patients with thyroid carcinoma after total thyroidectomy and radioiodine ablation of thyroid remnant. The first aim of the study was to find out if routine therapeutic measures enable adequate TSH suppression in pregnancy. The other aim was to find out the optimal dose of L-thyroxine for TSH suppression in pregnant women.

Material and methods

In this retrospective observational study we analysed 36 pregnancies of 32 women (mean age at conception 29.9 ± 0.6 years) with a history of thyroid carcinoma during the period from 2000 to 2009. T1, T2 and T3 tumour was diagnosed in 15, 7 and 10 patients, respectively. In 23 and 9 patients, the tumour stage was assessed as N0 and N1, respectively. None of the patients had distant metastases. All of them had no evidence of disease at conception and after delivery. Histopathology of bioptic specimen revealed the presence of Hashimoto's thyroiditis in 11/36 (=31%) of patients. Before pregnancy, all of them underwent total thyroidectomy and radioiodine ablation of the thyroid remnant and they were all on suppressive doses of L-thyroxine. All patients were advised to take L-thyroxine four hours before vitamins, iron or calcium drugs.

At conception, the age of patients was 22 to 37 years (mean age 29.9 ± 0.6 years). Among our patients, 28 women were pregnant once and four twice. Pregnancy passed without any events in 30 cases and with complications in six cases (premature delivery in two cases, preeclampsia in one, increased blood pressure in one, high serum glucose concentration in two, vaginal bleeding in the seventh month of gestation in one case).

Thyroid function tests were performed before, during and after pregnancy. The last test of thyroid function before pregnancy was done 1-12 (median 3) months before conception. During pregnancy, a clinical exam and thyroid function tests were performed every 6-8 weeks. When more than one set of tests was performed in any one trimester, the highest TSH concentration with the corresponding free T_3 and free T_4 concentrations were used in the statistical analysis in order to minimize any bias towards avoidance of dose change. The median number of thyroid function tests performed during pregnancy in each woman was four (range3-6). L-thyroxine dose was modified to maintain serum TSH below 0.3 mU/L. Suppression dose was adequate if TSH was 0.01-0.29 mU/L and free T_3 was within normal range.

From 2000-2006, TSH was measured by the two-site immunoluminometric assay (sandwich principle) LIASON TSH (Byk-Sangtec Diagnostica, Dietzenbach, Germany). Free T_3 and free T_4 were measured by commercially available kits (LIAISON FT_3, LIAISON FT_4) with "LIAISON" Immunoassay System (Byk-Sangtec, Germany later DiaSorin, Italy). Reference values for TSH, free T_3 and free T_4 were 0.27-4.2 mU/L, 2.93-6.8 pmol/L and 7.7-23.2 pmol/L, respectively. From 2007 onwards, TSH, free T_3 and free T_4 were measured by commercially available kits (TSH, FT_3, FT_4) with "Modular Analytics E170" Immunoassay System (Roche Diagnostics, Mannheim, Germany). Reference values for TSH, free T_3 and free T_4 were 0.27-4.20 mIU/L, 3.1-6.8 pmol/L and 12-22 pmol/L, respectively.

The study was reviewed by the appropriate medical ethics committee. The Institute's Protocol Review Board approved the study, which was performed in accordance with the medical ethics standards laid down in an appropriate version of the 1964 Declaration of Helsinki. The participants gave informed consent.

Statistical analysis

Changes in the results of thyroid-function tests, and L-thyroxine doses throughout pregnancy were analysed by repeated measures ANOVA or Friedman's test, followed by Wilcoxon signed rank test in case of non-normal data distribution. P-values of less than 0.05 were considered to indicate statistical significance. The software package SPSS 16.0 for Windows (SPSS Inc., Chicago, IL USA) was used.

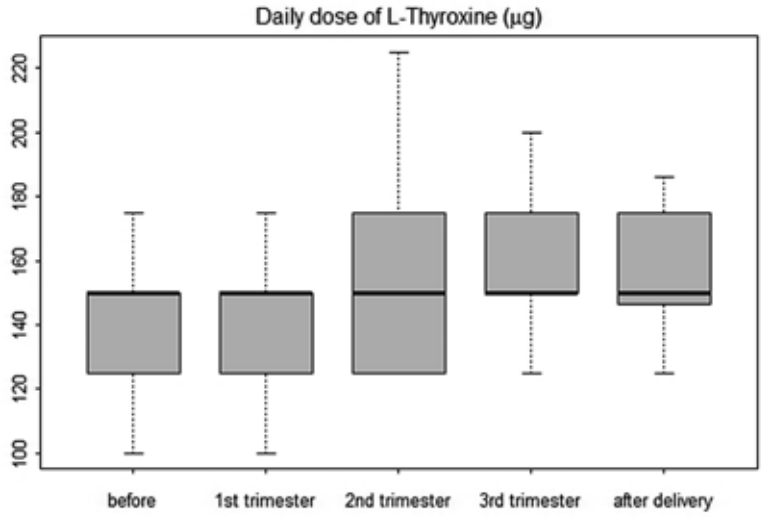

FIGURE 1. Changes of TSH during 36 pregnancies. The bottom and top of the box are the 25th and 75th percentile (the lower and upper quartiles, respectively), and the band near the middle of the box is the 50th percentile (the median). The ends of the whiskers represent the minimum and maximum of all the data.

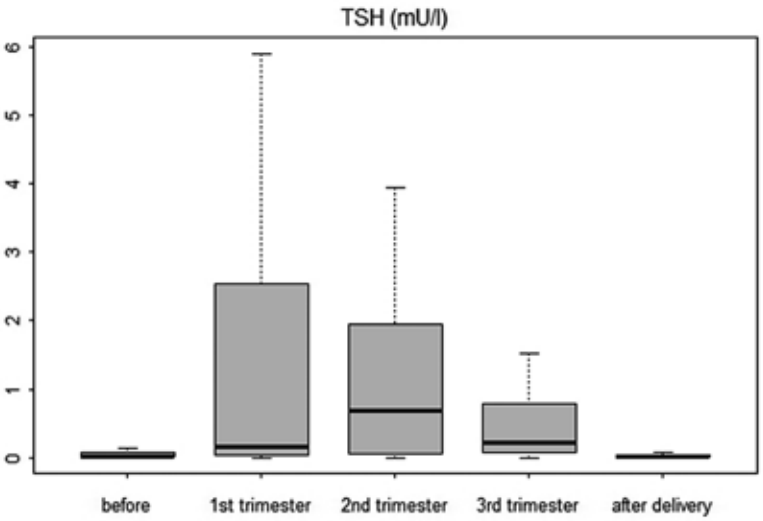

FIGURE 2. Changes of dose of L-thyroxine during 36 pregnancies. The bottom and top of the box are the 25th and 75th percentile (the lower and upper quartiles, respectively), and the band near the middle of the box is the 50th percentile (the median). The ends of the whiskers represent the minimum and maximum of all the data.

Results

The mean concentration of TSH, freeT_4 and free T_3 before pregnancy, in the first, second and third trimester and after delivery are presented in Table 1. The concentration of TSH during the first, second and third trimester were higher in comparison to the TSH concentration before pregnancy ($p<0.001$). The changes of TSH concentration during pregnancy are presented in Figure 1. In none of our patients, a decrease of TSH was observed in the first 16 weeks of pregnancy.

The doses of L-thyroxine during the second and the third trimester were higher than the doses before pregnancy ($p<0.05$). The changes of dose of L-thyroxine during pregnancy are presented in Figure 2. Obese patients had larger dose of L-thyroxine in comparison to patients with normal body mass index (BMI) or underweight patients before conception as well as during pregnancy. However, BMI had no impact on the proportion of patients with adequate TSH suppression during pregnancy. The time period from the last test before pregnancy to the first test in pregnancy did not differ in women with adequate TSH suppression and women with inadequate TSH suppression ($p=0.377$).

Changes of the mean TSH concentration and dose of L-thyroxine before and during pregnancy and after delivery in patients with suppressed and not suppressed TSH concentration are presented in Table 2. The mean dose of L-thyroxine in patients with suppressed TSH before pregnancy, in the first, second and, third trimester and after delivery was 154, 154, 164, 160 and 161 micrograms daily, respectively.

In 36 pregnancies, the TSH concentration remained suppressed during 9 pregnancies. In 22 pregnancies the TSH concentration was within normal range,whilein5 pregnancies it was elevated. A dose of L-thyroxine was not changed in 14 pregnancies (mean dose 159 micrograms daily); TSH was suppressed in 5 pregnancies and within normal range in 9 pregnancies.

The dose of L-thyroxine had to be increased in 22 pregnancies. The TSH concentration in 22 pregnancies remained suppressed in 4, within normal range in 13 and elevated in 5 of them. TSH was over 5.0 mU/L during the first trimester and second trimester in 5/22 (23%) cases and 3/22 (14%) cases, respectively.

The dose of L-thyroxine was increased 30 times and decreased four times during the course of pregnancy. The dose was changed 9, 11 and 14 times in the second, third and the fifth month, respectively. The mean increase of L-thyroxine dose in these 22 cases was 32.15 (range 25-75) micrograms.

Discussion

According to the current American Thyroid Association and European Thyroid Association guidelines[16,17], the patients with a history of thyroid

TABLE 1. Mean L-thyroxine dose and mean TSH concentration before pregnancy, in the first trimester, the second trimester, the third trimester and after delivery.

	Daily dose of L-thyroxine Mean (±SD; range) Micrograms	Mean TSH (±SD; range) mU/L	FT4 (±SD; range) pmol/L	FT3 (±SD; range) pmol/L
Before pregnancy	149 (±32; 100-300)	0.07 (±0.12; 0.001-0.29)	20.13 (±5.08; 13.9-28.4)	5.16 (±0.86; 3.91-6.61)
1. trimester	147 (±34; 100-300)	1.96 (±3.60; 0.001-14.54)	16.72 (±4.32; 9.29-27.6)	4.15 (±1.08; 2.41-7.6)
2. trimester	155 (±35; 125-300)	1.43 (±1.96; 0.001-7.64)	14.79 (±3.39; 8.95-24.1)	4.00 (±0.85; 2.72-5.5)
3. trimester	165 (±34; 125-300)	0.63 (±0.95; 0.001-4.60)	14.04 (±3.15; 5.07-23.1)	3.83 (±0.69; 2.52-5.2)
After pregnancy	158 (±34; 100-300)	0.05 (± 0.11; 0.001-0.59)	22.15 (±3.94; 14.6-31.9)	5.41 (±1.08; 3.18-7.83)

carcinoma are either on substitution or suppressive doses of L-thyroxine. Our study group consisted of 36 pregnancies in 32 patients with a history of thyroid carcinoma. Before conception they were treated by total thyroidectomy and radioiodine ablation of thyroid remnant and were on the suppressive dose of L-thyroxine. So, in all of our patients there was no viable thyroid tissue to produce thyroid hormones. These patients were, therefore, entirely dependent on exogenous L-thyroxine.

In healthy women, a transient decrement of serum TSH concentration occurs during the first two months of pregnancy, which is a result of the elevation of human chorionic gonadotropin (hCG) having similar molecular structure as TSH.[1,18,19] In none of our patients, lower concentration of TSH was detected during the first two months of pregnancy. In the absence of viable thyroid tissue, there was no effect of elevated concentration of hCG on the synthesis and secretion of thyroid hormones from thyroid and on the consequent decrease of TSH concentration.

According to Endocrine Society Clinical Practice Guideline[1], L-thyroxine dose often needs to be increased within 4-6 weeks of gestation and may require a 30-50% addition of dosage.[3,4] But we observed that there was no need to increase the dose during pregnancy in 25% of our cases who were on suppressive doses of L-thyroxine before conception. Also Loh *et al*.[8] observed that there was no need to change the dosage in some of the patients with thyroid carcinoma who were on TSH suppression therapy before pregnancy. Based on our results, we believe that an increment of dose immediately after conception as advocated by some authors[12] is not appropriate for all the patients who are on suppressive doses of L-thyroxine. We agree with Loh *at al*.[8] that these patients may be over treated by an empiric increase of L-thyroxine dose and may develop overt hyperthyroidism.

The other important finding of our study is that TSH suppression was not achieved in 75% of cases when thyroid testing was performed each 6-8 weeks. Furthermore, an elevation of TSH level above normal was observed in 14% of our patients. Possibly, this could be avoided, if thyroid function tests would be obtained every 4-6 weeks as recommended by Endocrine Society Clinical Practice Guideline[1], or every 4 weeks as recommended by Yassa *et al*..[13] In a recent study Yassa *et al*.[13] performed serum testing every two weeks until the 20th week of pregnancy and at the 30th week of pregnancy. If blood samples were obtained every four weeks, 92% of abnormal TSH concentrations were detected. But, if an every six week testing protocol had been followed, only 73% of abnormal TSH concentrations would have been detected.[10] So, they concluded that the thyroid function tests should be repeated every four weeks during the first half of pregnancy.

It is still not known when it is most appropriate to increase the dose of L-thyroxine[20]: before pregnancy[21], immediately after conception[12,13] or when elevation of TSH is observed.[8-11] Rotondi *et al*.[21] suggested the increase of L-thyroxine dose to "partially suppressive" dose before pregnancy. The patients who underwent thyroidectomy because of multinodular goitre or Hashimoto's thyroiditis and who were on substitution therapy were randomized in two groups before conception: one group continued with substitution doses, while the other was on partially suppressive dose.[21] Before conception, the average dose in the substitution group and the partially suppressive group of patients was 143 and 178 micrograms, while the average TSH was 1.84 and 0.48 (0.32-0.7) mU/L, respectively.[21] TSH level above 3.5 mU/L was found to be more common in the substitution group in comparison to the "partially suppressive" group of patients (36% vs. 14%).

TABLE 2. Adequacy of suppression, mean L-thyroxine dose and mean TSH concentration before pregnancy, in the first trimester, the second trimester, the third trimester and after delivery.

		Before pregnancy	First trimester	Second trimester	Third trimester	After pregnancy
Adequatelly supressed	Daily dose of L-thyroxine Mean (±SD) Micrograms	154 (±32)	154 (±28)	164 (±47)	160 (±21)	161 (±33)
	Daily dose of L-thyroxine/kg Mean (±SD) Micrograms/kg	2.37 (±0.31)	-	-	2.17 (±0.30)	-
	Daily dose of L-thyroxine/BMI Mean (±SD) Micrograms/kg/m2	6.64 (±0.90)			6.03 (±0.80)	
	Mean TSH (±SD) mU/L	0.049 (±0.07)	0.07 (±0.07)	0.057 (±0.07)	0.12 (±0.08)	0.03 (±0.06)
	Number of patients	34	21	12	22	34
Not adequatelly supressed	Daily dose of L-thyroxine Mean (±SD) Micrograms	125 (±0)	154 (±28)	152 (±27)	173 (±48)	112 (±18)
	Daily dose of L-thyroxine/kg Mean (±SD) Micrograms/kg	1.88 (±0.50)			2.35 (±0.36)	
	Daily dose of L-thyroxine/BMI Mean (±SD) Micrograms/kg/m2	5.13 (±1.46)			6.00 (±0.90)	
	Mean TSH (±SD) mU/L	0.5 (±0.21)	4.6 (±4.4)	2.2 (±2.08)	1.43 (±1.13)	0.49 (±0.14)
	Number of patients (% of patients with TSH over 5 mU/L)	2 (0%)	15 (33%)	24 (8%)	14 (0%)	2 (0%)

Another approach, *i.e.* increment of the dose as soon as pregnancy is confirmed, was proposed by Alexander *et al*..[12] They studied precisely the timing and amount of L-thyroxine adjustment in 20 pregnancies in 19 women.[12] Eight patients had Hashimoto's disease, six thyroid carcinoma, three Graves disease and two were after the treatment for benign thyroid nodule. L-thyroxine requirements increased as early as the fifth week of gestation.[12] That is why they recommended an increase of L-thyroxine dose as soon as possible.[12] Their opinion is that the dose should be increased by about 30%.[12] Yassa *et al*.[13] performed a prospectively randomized study in which women were receiving an increased L-thyroxine dose at the beginning of pregnancy. The dose in the first group was increased by 29%, and in the second group, by 43%. The mean dose before and after the change in the first and the second group was 112, 145, 109 and 156 micrograms, respectively.[13] After the change of dose, TSH suppression was present in 32% of women from the first group and in 65% of women from the second group; but less than 0.1 mU/L of TSH was found in only one patient (8%) from the first group and in six patients from the second group (26%).[13] They found out that a 29% increase of dose (from 112 to 145 micrograms) prevented maternal TSH elevation over 2.5 and 5.0 mU/L in 85% and 100% of patients, respectively. But the majority of their patients had Hashimoto's disease, while our patients had a history of thyroid carcinoma and were without any functional thyroid tissue. In our patients, the mean dose before pregnancy was 149 micrograms of L-thyroxine. When a dosage during pregnancy remained the same, the mean dose was 159 micrograms. This dosage prevented the elevation of TSH over 5.0 mU/L in all the cases. On the other hand, when a dosage during pregnancy had

to be changed, the mean dose before conception was 125 micrograms only. In the latter cases, TSH was over 5.0 mU/L during the first and second trimester in 23% of cases and 14%, respectively.

The third approach, increment of a dose based on thyroid function tests was reported by Loh *et al*..[8] In 18 cases with a history of thyroid carcinoma, the average daily L-thyroxine dose before conception was 153 micrograms. During pregnancy they required an increase of dose by 26%.[8] In our patients, the average dose was 149 micrograms before conception. But during pregnancy our patients required an increase of dose by 11% only. Obviously the range of changes in TSH concentration during pregnancy in the patients who have been on suppressive L-thyroxine therapy before conception is quite wide.

As a conclusion, the patients with thyroid carcinoma who are on high doses of L-thyroxine require close monitoring of thyroid function tests during pregnancy. TSH was adequately suppressed in only 25% of pregnancies. The dose of L-thyroxine in patients with suppressed TSH in the first, second and third trimester was 154, 164 and 160 micrograms daily, respectively. When the dose had to be changed, the mean increase of the dose was 31.5 (range 25-75) micrograms daily.

Acknowledgments

Research studies P3-0289 supported by the Ministry of Education, Science and Sport of Slovenia. This work was presented in part at the 14th International Thy roid Congress, held in Paris, France, September 11-16 2011.

References

1. Abalovich M, Amino N, Barbour LA, Cobin RH, De Groot LJ, Glinoer D, et al. Management of thyroid dysfunction during pregnancy and postpartum: an Endocrine Society Clinical Practice Guideline. *J Clin Endocrinol Metab* 2007; **92:** S1-47.
2. Haddow JE, Palomaki GE, Allan WC, Williams JR, Knight GJ, Gagnon J, et al. Maternal thyroid deficiency during pregnancy and subsequent neuropsychological development of the child. *N Engl J Med* 1999; **341:** 549-55.
3. Kaplan MM. Monitoring thyroxine treatment during pregnancy. *Thyroid* 1992; **2:** 147-52
4. Mandel SJ, Larsen PR, Seely EW, Brent GA. Increased need for thyroxine during pregnancy in women with primary hypothyroidism. *N Engl J Med* 1990; **323:** 91-6.
5. Dashe JS, Casey BM, Wells CE, McIntire DD, Byrd EW, Leveno KJ, et al. Thyroid-stimulating hormone in singleton and twin pregnancy: importance of gestational age-specific reference ranges. *Obstet Gynecol* 2005; **106:** 753-7.
6. Panesar NS, Li CY, Rogers MS. Reference intervals for thyroid hormones in pregnant Chinese women. *Ann Clin Biochem* 2001; **38:** 329-32.
7. Casey BM, Dashe JS, Wells CE, McIntire DD, Leveno KJ, Cunningham FG. Subclinical hyperthyroidism and pregnancy outcomes. *Obstet Gynecol* 2006; **107:** 337-41.
8. Loh JA, Wartofsky L, Jonklaas J, Burman KD. The magnitude of increased levothyroxine requirements in hypothyroid pregnant women depends upon the etiology of the hypothyroidism. *Thyroid* 2009; **19:** 269-75.
9. Girling JC, de Swiet M. Thyroxine dosage during pregnancy in women with primary hypothyroidism. *Br J Obstet Gynaecol* 1992; **99:** 368-70.
10. Verga U, Bergamaschi S, Cortelazzi D, Ronzoni S, Marconi AM, Beck-Peccoz P. Adjustment of L-T4 substitutive therapy in pregnant women with subclinical, overt or post-ablative hypothyroidism. *Clin Endocrinol (Oxf)* 2009; **70:** 798-802.
11. Hallengren B, Lantz M, Andreasson B, Grennert L. Pregnant women on thyroxine substitution are often dysregulated in early pregnancy. *Thyroid* 2009; **19:** 391-4.
12. Alexander EK, Marqusee E, Lawrence J, Jarolim P, Fischer GA, Larsen PR. Timing and magnitude of increases in levothyroxine requirements during pregnancy in women with hypothyroidism. *N Engl J Med* 2004; **351:** 241-9.
13. Yassa L, Marqusee E, Fawcett R, Alexander EK. Thyroid hormone early adjustment in pregnancy (the THERAPY) trial. *J Clin Endocrinol Metab* 2010; **95:** 3234-41.
14. Chopra IJ, Baber K. Treatment of primary hypothyroidism during pregnancy: is there an increase in thyroxine dose requirement in pregnancy? *Metabolism* 2003; **52:** 122-8.
15. Dobrenic M, Huic D, Zuvic M; Grosev D, Petrovic R, Samardzic T. Usefulness of low iodine diet in managing patients with differentiated thyroid cancer - initial results. *Radiol Oncol* 2011; **45:** 189-95.
16. Cooper DS, Doherty GM, Haugen BR, Kloos RT, Lee SL, Mandel SJ, et al. Management guidelines for patients with thyroid nodules and differentiated thyroid cancer. *Thyroid* 2006; **16:** 109-142.
17. Pacini F, Schlumberger M, Dralle H, Elisei R, Smit JW, Wiersinga W. The European Thyroid Cancer Taskforce: European consensus for the management of patients with differentiated thyroid carcinoma of the follicular epithelium. *Europ J Endocrinol* 2006; **154:** 787-803.
18. Glinoer D. The regulation of thyroid function in pregnancy: pathways of endocrine adaptation from physiology to pathology. *Endocr Rev*1997; **18:** 404-33.
19. Gaberscek S, Zaletel K. Thyroid physiology and autoimmunity in pregnancy and after delivery. *Expert Rev Clin Immunol* 2011;**7:** 697–707.
20. Toft A. Increased levothyroxine requirements in pregnancy--why, when, and how much? *N Engl J Med* 2004; **351:** 292-4.
21. Rotondi M, Mazziotti G, Sorvillo F, Piscopo M, Cioffi M, Amato G, et al. Effects of increased thyroxine dosage pre-conception on thyroid function during early pregnancy. *Eur J Endocrinol* 2004; **151:** 695-700.

research article

What sampling device is the most appropriate for vaginal vault cytology in gynaecological cancer follow up?

Del Pup Lino[1], Canzonieri Vincenzo[2], Serraino Diego[3], Campagnutta Elio[1]

[1] Gynaecology Oncology Department,
[2] Pathology Department and
[3] Epidemiology Unit, National Cancer Institute CRO, Aviano, PN, Italy

Radiol Oncol 2012; 46(2): 166-169.

Received 1 August 2011
Accepted 8 February 2012

Correspondence to: Del Pup Lino, Oncologia Ginecologica, Istituto Nazionale Tumori, Centro di Riferimento Oncologico, Aviano, Pordenone, Via F. Gallini 2, Aviano, Pordenone, Italy, Phone: +39 0434 659051; Fax: +39 0434 659439; ldelpup@cro.it

Disclosure: No potential conflicts of interest were disclosed.

Background. In women with cancer-related hysterectomy, the vaginal vault cytology has a low efficacy - when performed by conventional methods – for the early detection of vaginal recurrence. The amount of exfoliated cells collected is generally low because of atrophy, and the vaginal vault corners can be so narrow that the commonly used Ayres spatula cannot often penetrate deeply into them. This prospective study aimed at identifying the advantages obtained in specimens collection using the cytobrush, as compared to the Ayres's spatula.

Patients and methods. 141 gynaecologic cancer patients were studied to compare samplings collected with Ayre's spatula or with cytobrush. In a pilot setting of 15 patients, vaginal cytology samples obtained by both Ayre's spatula and cytobrush were placed at the opposite sites of a single slide for quali-quantitative evaluation. Thereafter, the remaining 126 consecutive women were assigned to either group A (spatula) or B (cytobrush) according to the order of entry. The same gynaecologist performed all the procedures.

Results. In all 15 pilot cases, the cytobrush seemed to collect a higher quantity of material. The comparative analysis of the two complete groups indicated that the cytobrush technique was more effective than the spatula one. The odds ratio (OR) for an optimal cytology using the cytobrush was 2.8 (95% confidence interval -C.I. 1.3-6.2; chi-square test, p=0.008).

Conclusions. Vaginal vault cytology with cytobrush turned out to better perform than the traditional Ayre's spatula to obtain an adequate sampling in gynecological cancer patients.

Key words: Ayre's spatula; cytobrush; female cancer; vaginal cytology

Introduction

The main aim of post-treatment surveillance in oncology is to improve the survival through early detection of recurrent tumours.[1] The cytopathologic examination is a one of the valuable method to detect an early recurrence of malignancy or new primary carcinoma during the follow-up of patients after the treatment of a different cancer.[2] However, the vaginal vault cytology is considered a surveillance method with low efficacy for the early detection of vaginal recurrence in patients with a malignancy-related hysterectomy.[3,4] This is partially caused either by cytologic artefacts due to inflammation or by vaginal effects of previous chemotherapy, radiotherapy, or surgery. The amount of exfoliated cells collected is generally low because of atrophy. In addition, the vaginal vault corners can be so narrow that the commonly used Ayres spatula is often unable to penetrate deeply into them. These two latter factors could further reduce the probability of the early detection of a local recurrence, though they can be improved by different sampling methods.

Extended-tip spatulas improve the collection of exfoliated cells, with a nearly 2-fold higher odds ratio (OR) -in comparison with Ayre's spatula. However, the available data refer to endocervical samples, not to vaginal vault cytology of hysterectomized cancer patients.[5]

To evaluate the best spatula for obtaining adequate vaginal samplings, we reviewed the available literature in PubMed using the following strategy: ("Vaginal Smears/instrumentation"[MeSH] OR "Vaginal Smears/methods"[MeSH] OR "Vaginal Smears/standards"[MeSH] OR "Vaginal Smears/utilization"[MeSH]) AND "Genital Neoplasms, Female"[MeSH] AND "Hysterectomy"[MeSH]. Then we searched for indications on the methods in Plumbed with the strategy: "Follow up" AND "Genital Neoplasms, Female"[Mesh] AND "Hysterectomy"[Mesh] as well as in the main guidelines. We could not find adequate randomized trials regarding the optimal method to perform vaginal vault cytology during the follow-up of hysterectomized women.

Patients and methods

At the Gynaecology Oncology Department of the National Cancer Institute "Centro di Riferimento Oncologico", Aviano, North East of Italy, 141 gynaecologic cancer patients in follow-up were included in prospective study. The study design complied with national regulations and institutional policies and the study was carried out according to the Helsinki Declaration.

The survey was conducted in two steps. In a preliminary study of 15 patients, we performed vaginal cytology with both Ayres and cytobrush and the cells samples were placed on the same slide, half of the slide area for each device. In order to prevent bias due to the greater amount of cells collected by the first device used, the first sample was obtained initially with Ayres spatula and subsequently with cytobrush. For every subsequent patient this order was changed. Cytobrush samples were placed on the half of the slide far from patient's identification data. Criteria of adequacy for vaginal vault cytology consisted in the evaluation of enough cellularity of squamous type. However, since the goal of our work was to identify the best method to collect more vaginal cells for smears, some differences in the amount of cells available for comparisons between the two studied methods were expected. This first step of the study aimed to describe the cytology differences between the two sampling devices analysing the cells on the same slide. The study continued with a methodology that allowed an improved assessment of the differences.

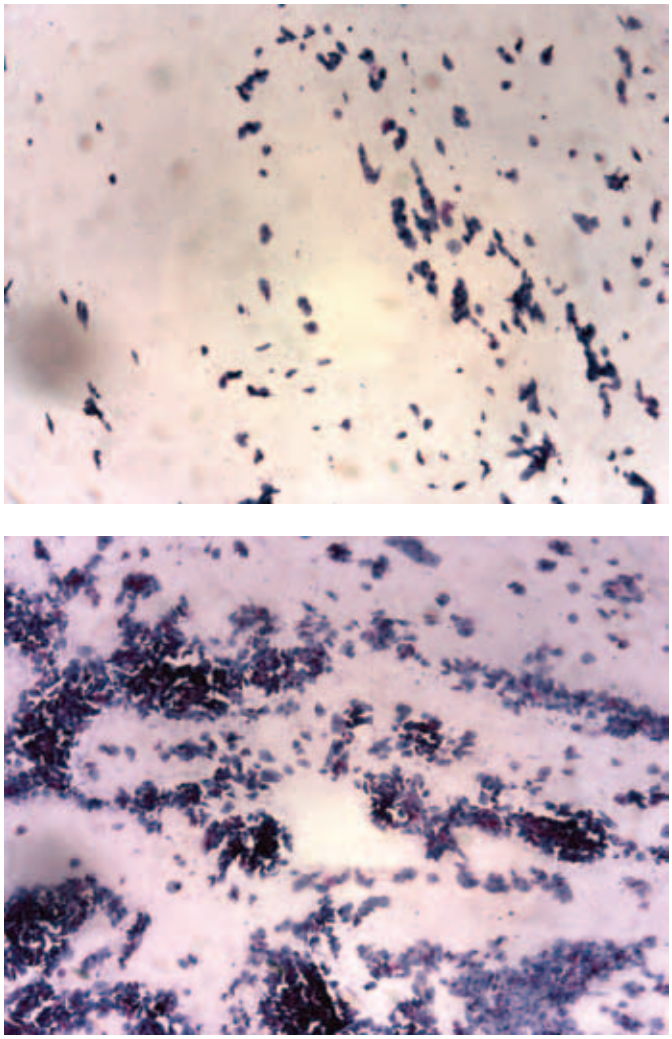

FIGURE 1. Cytological sample collected from vaginal vault with Ayre's spatula (A) and cytobrush (B) (Papanicolau; mag. 100X).

In the second and most important step of the study, 126 consecutive hysterectomized cancer patients who underwent vaginal vault cytology were investigated. Fifty-nine (47%) of them had cervical cancer, 53 (42%) endometrial cancer, nine (8%) had ovarian cancer, four (3%) had vulvar cancer, and one uterine sarcoma. These women were alternatively assigned either to group A (*i.e.*, classical Ayres spatula) or B (*i.e.*, cytobrush) according to the order of entry, starting from group A. Vaginal vault cytology collection was performed in group A with the classical Ayres spatula and in group B with cytobrush. The same gynaecologist (DPL) performed all the procedures with exactly the

TABLE 1. Differences in cytologic adequate sampling (optimal and suboptimal) between the two sampling devices: Ayre's spatula and cytobrush

		Optimal		Suboptimal		Total
		n	%	n	%	n
Group A:	Ayre's spatula	23	35.9	41	64.1	64
Group B:	Cytobrush	38	61.3	24	38.7	62
		65		61		126

(Chi square test, p= 0.008)

same approach. Smears were immediately fixed by cytofix spray with uniform distribution over the smear without artifacts. Staining was conducted by standard Papanicolau method. One pathologist (CV), blinded to the sampling method, analysed all the samples. The cellularity was considered suboptimal when scanty and/or showing an unsuitable morphology for diagnosis. Criteria of adequacy for vaginal vault cytology consisted in the evaluation of adequate cellularity of squamous type. However, since the goal of the work was to establish the best method to collect more vaginal cells for smears, some differences in the amount of cells available for evaluation between the two methods were expected. The Chi-square test for heterogeneity, OR and their 95% CI were computed to assess statistical associations.

Results

All samples were accepted as adequate. In the preliminary study, fifteen specimens showed a higher cellularity using cytobrush (Figure 1). In the second part of the study, among patients where the vaginal cytology with Ayres spatula was performed, 41 patients had a suboptimal quantity of collected cells and 23 of them an optimal one. Among patients who underwent vaginal cytology with cytobrush, 24 had a suboptimal cytology and 38 an optimal one. This difference was statistically significant (p= 0.008), while the OR for an optimal cytology using the cytobrush was 2.8 (95% C.I. 1.3-6.2) (Table 1). There were no side effects, such as bleeding, in both sampling groups.

Discussion

Our data suggested that the cytobrush is a more efficient sampling device than the traditional Ayre's spatula btain from vaginal vault. Indeed, it allows collecting 2.8 times the amount of optimal specimen, as it enables more efficient cell scraping from the vaginal epithelium, which is almost invariably atrophic in hysterectomized gynaecologic cancer patients. The cytobrush device carries also the advantage of a deeper sampling by reaching the narrow corners sometimes produced by surgical interventions in the vaginal vault. In these hidden spaces, an initial recurrence can also be difficult to be visualized or palpated. Furthermore, plastic materials tend to have a lower adherence than wooden spatulas, allowing more cells to be smeared to the slide for the analysis.

The Ayre's spatula is the device commonly used for cervical cytology and the one used in previous vaginal vault cytology studies that are summarized below. Vaginal vault cytology is generally performed during follow-up, after hysterectomy for cervical cancer. Only one patient, out of 79 completing a 15-year follow-up study[6], had an abnormal smear and a vaginal intraepithelial neoplasia (VAIN) later diagnosed and no patient developed invasive vaginal carcinoma. A French study[7], conducted over a 10-year period on 2152 patients, reported only four cases of invasive cancer of the vagina of which one occurring after radical hysterectomy for invasive cancer of the cervix and three after total hysterectomy for cervical intraepithelial neoplasia (CIN). The follow-up of endometrial cancer does not seem to improve the survival. A Canadian study[8] concluded that the routine use of vaginal vault smears was not cost effective during the follow-up. A detection of each asymptomatic vaginal recurrence requires 1067 Pap-smear tests, producing benefits for only 0.5% of patients.[9] Neither recurrence free nor the overall survival are improved in these cases compared to those detected at clinical presentation.[10,11] Only in non-irradiated patients, a strong case can be made for regular follow-up to detect vaginal recurrence at the earliest opportunity, given the high salvage rate following radiotherapy.[12,13] In a systematic review, the detection of asymptomatic recurrences of endometrial cancer ranged from 0% to 4% with vaginal vault cytology, as compared to 5% to 33% with physical examination.[14]

The effectiveness of vaginal vault cytology in the above mentioned studies could have been different, if performed with the cytobrush. We used both the cytobrush and the Ayre's spatula for vaginal vault sampling. Smear preparation was made according to standard pathological operative procedures. In our study, we did not use liquid based cytology to increase the whole number of collected cells because the main goal of the study was to compare two sampling methods conducted by means of two different devices.

In conclusion, our data revealed that, in women with gynecological cancers, vaginal vault cytology conducted with the cytobrush appeared more efficient than its conventional counterpart, the Ayre's spatula, as it allowed the collection of a more adequate sample.

References

1. Velenik V. Post-treatment surveillance in colorectal cancer. *Radiol Oncol* 2010; **44:** 135-41.
2. Strojan Flezar M. Urine and bladder washing cytology for detection of urothelial carcinoma: standard test with new possibilities. *Radiol Oncol* 2010; 44: 207-14.
3. Cooper AL, Dornfeld-Finke JM, Banks HW, Davey DD, Modesitt SC Is cytologic screening an effective surveillance method for detection of vaginal recurrence of uterine cancer? *Obstet Gynecol* 2006; **107:** 71-6.
4. Kew FM, Roberts AP, Cruickshank DJ. The role of routine follow-up after gynecologic malignancy. *Int J Gynecol Cancer* 2005; **15:** 413-9.
5. Martin-Hirsch P, Lilford R, Jarvis G, Kitchener HC. Efficacy of cervical-smear collection devices: a systematic review and meta-analysis. *Lancet* 1999; **354:** 1763-70.
6. Gemmell J, Holmes DM, Duncan I. How frequently need vaginal smears be taken after hysterectomy for cervical intraepithelial neoplasia? *Br J Obstet Gynaecol* 1990; **97:** 58-61.
7. Mouithys P, Papadopoulos C, Allier G, Lanta S, Delpierre C, Najas S, et al. Faut-il poursuivre les frottis de dépistage après hystérectomie? *Gynecol Obstet Fertil* 2003; **31:** 620-3.
8. Agboola O, Grunfeld E, Coyle D, Perry GA Costs and benefits of routine follow-up after curative treatment for endometrial cancer. *Can Med Assoc* 1997; **157:** 879-86.
9. Bristow RE, Purinton SC, Santillan A. Cost-effectiveness of routine vaginal cytology for endometrial cancer surveillance. *Gynecol Oncol* 2006; **103:** 709-13.
10. Allsop JR, Preston J, Crocker S. Is there any value in the long term follow up of women treated for endometrial cancer? *Br J Obstet Gynaecol* 1997; **104:** 119-22.
11. Shumsky AG, Stuart G., Brasher PM, Nation JG, Robertson DI, Sangkarat S. An evaluation of routine follow-up of patients treated for endometrial carcinoma. *Gynecol Oncol* 1994; **55:** 229-33.
12. Ackerman I, Malone S, Thomas G, Franssen E, Balogh J, Dembo A. Endometrial carcinoma - relative effectiveness of adjuvant irradiation vs therapy reserved for relapse. *Gynecol Oncol* 1996; **60:** 177-83.
13. Ball HG. Do we know the best therapy for early endometrial cancer? *Gynecol Oncol* 1996; **60:** 173-5.
14. Fung-Kee-Fung M, Dodge J, Elit L, Lukka H, Chambers A, Oliver T. Follow-up after primary therapy for endometrial cancer: A systematic review. *Gynecol Oncol* 2006; **101:** 520-9.

research article

Dosimetric characterizations of GZP6 ^{60}Co high dose rate brachytherapy sources: application of superimposition method

Mohammad Taghi Bahreyni Toossi[1], Mahdi Ghorbani[2], Ali Asghar Mowlavi[3] and Ali Soleimani Meigooni[4]

[1] Medical Physics Research Center, Medical Physics Department, Faculty of Medicine, Mashhad University of Medical Sciences, Mashhad, Iran
[2] North Khorasan University of Medical Sciences, Bojnurd, Iran
[3] Physics Department, School of Sciences, Hakim Sabzevari University, Sabzevar, Iran
[4] Comprehensive Cancer Center of Nevada, 3730 S. Eastern Avenue, Las Vegas, Nevada, USA

Radiol Oncol 2012; 46(2): 170-178.

Received 2 October 2011
Accepted 21 November 2011

Correspondence to: Mahdi Ghorbani, Vice Chancellery of Research and Technology, North Khorasan University of Medical Sciences, South Shariati No. 7, Bojnurd, North Khorasan, Iran. Phone: +98 584 2247124; Fax: +98 584 2247124; E-mail: mhdghorbani@gmail.com

Disclosure: No potential conflicts of interest were disclosed.

Background. Dosimetric characteristics of a high dose rate (HDR) GZP6 Co-60 brachytherapy source have been evaluated following American Association of Physicists in MedicineTask Group 43U1 (AAPM TG-43U1) recommendations for their clinical applications.

Materials and methods. MCNP-4C and MCNPX Monte Carlo codes were utilized to calculate dose rate constant, two dimensional (2D) dose distribution, radial dose function and 2D anisotropy function of the source. These parameters of this source are compared with the available data for Ralstron ^{60}Co and microSelectron^{192}Ir sources. Besides, a superimposition method was developed to extend the obtained results for the GZP6 source No. 3 to other GZP6 sources.

Results. The simulated value for dose rate constant for GZP6 source was 1.104±0.03 cGyh^{-1}U^{-1}. The graphical and tabulated radial dose function and 2D anisotropy function of this source are presented here. The results of these investigations show that the dosimetric parameters of GZP6 source are comparable to those for the Ralstron source. While dose rate constant for the two ^{60}Co sources are similar to that for the microSelectron^{192}Ir source, there are differences between radial dose function and anisotropy functions. Radial dose function of the ^{192}Ir source is less steep than both ^{60}Co source models. In addition, the ^{60}Co sources are showing more isotropic dose distribution than the ^{192}Ir source.

Conclusions. The superimposition method is applicable to produce dose distributions for other source arrangements from the dose distribution of a single source. The calculated dosimetric quantities of this new source can be introduced as input data to the GZP6 treatment planning system (TPS) and to validate the performance of the TPS.

Key words: brachytherapy; GZP6; TG-43; superimposition method; Monte Carlo simulation

Introduction

Recently, the GZP6 high dose rate (HDR) ^{60}Co brachytherapy unit, manufactured byNuclear Power Institute of China (Chengdu, China), has been introduced for brachytherapy procedures.[1] Although not as common as ^{192}Ir source, ^{60}Co has been used in past as a brachytherapy source in the treatment of various malignancies[2-4], and a brachytherapy technique remains a frequent treatment in clinical praxis.[5] There are also potential logistical advantages for ^{60}Co sources for HDR systems over ^{192}Ir[6], including less frequency of source exchange which provides longer duration of clinical use and reduced operating costs. Different geometric designs of ^{60}Co radionuclide have been used in radiotherapy clinics in the past with limited traditional dosimetric information.[7,8] Dose cal-

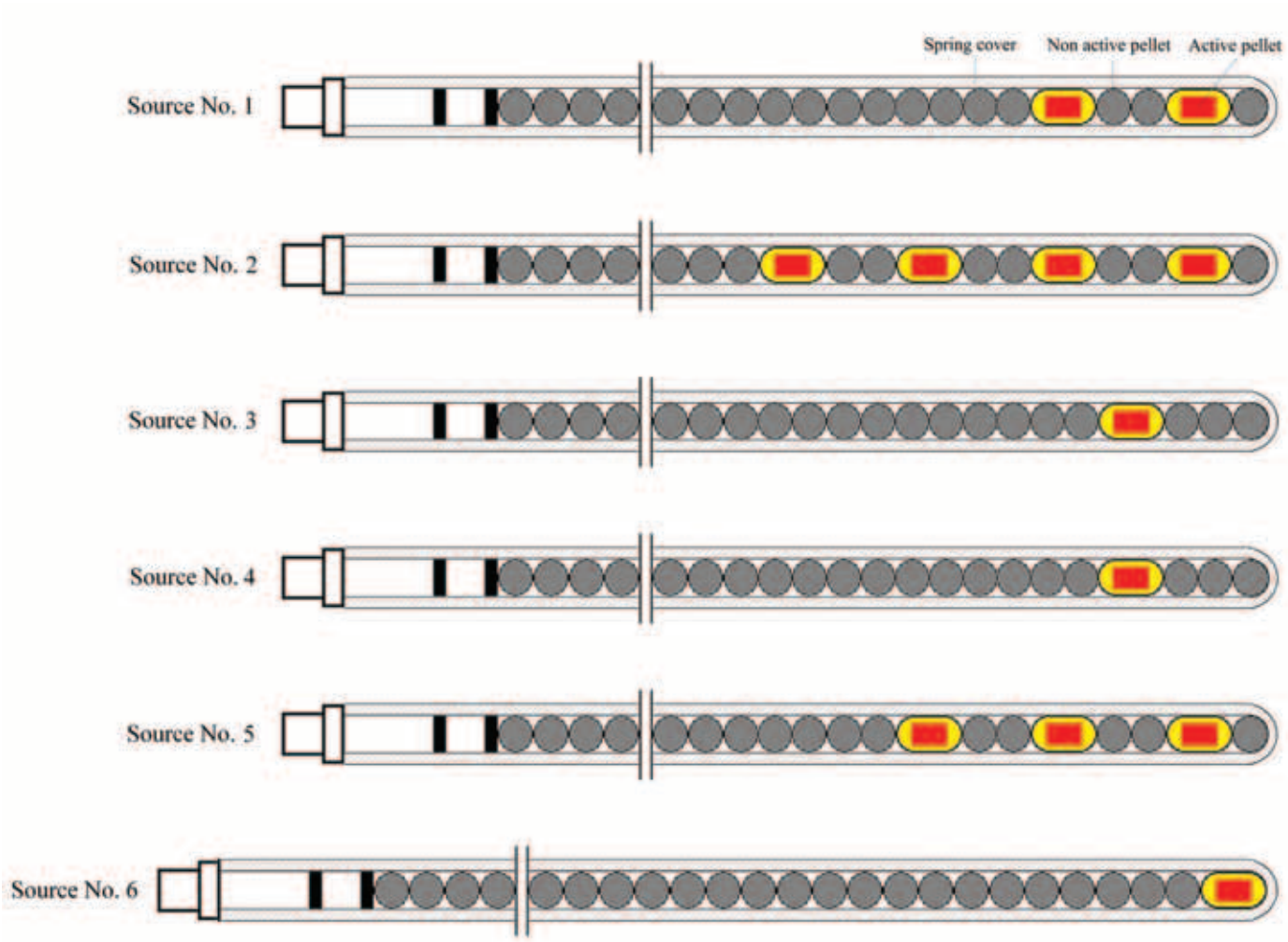

FIGURE 1. Schematic diagram illustrating six GZP6 source braids, containing active and nonactive pellets. Each source is allocated to one separate channel. The sources 1-5 are stationary while the source No. 6 is stepper.

culations around these implants were performed using the traditional dose calculation technique. However, presently, the Task Group 43 (TG-43) report of American Association of Physicists in Medicine(AAPM) has recommended determination of dosimetric parameters, such as radial dose function, anisotropy function (ANF), etc., of any brachytherapy sourcebefore its clinical use.[9] Also according to the AAPM TG-56 such parameters are required as input data and for verification of the treatment planning system.[10]

The newly designed GZP6 HDR ^{60}Co brachytherapy unit has been recently employed for the clinical practice in Iran. Unlike the HDR ^{192}Ir systems, which contain one source, the GZP6 unit includes six different sources (Figure 1). Each source is designated to a separate channel in the HDR unit. Five of these six sources are stationary, and the 6th source (*i.e.* source number 6) has stepping (dwelling) capability that could be used for treatment of patients with longer active length. As shown in Figure 1, each source is composed of a source-braid or packing, consist of 1, 2, 3 or 4 radioactive source pellets as well as a number of non active steel pellets. In order to make these source

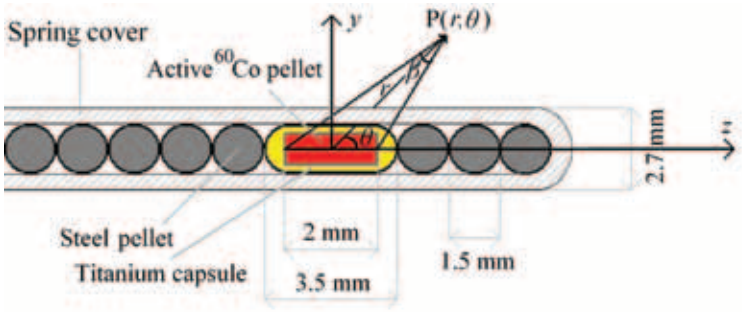

FIGURE 2. A schematic view of the GZP6 source braid number 3 illustrating the dimensions of active cylindrical ^{60}Co and non-active steel pellets as well as TG43U1 coordinate systems. This diagram is schematic and is not to scale.

geometries reproducible, at the same time flexible as it moves within the transfer tube and applicator, the active and non-active pellets are fitted within a steel spring cover. Dimensions and components of the active and non-active pellets of these sources are provided in the schematic diagram of source number 3 (Figure 2). In their first publication on this system, Mesbahi *et al.* measured the air kerma strengthsof source numbers 1, 2 and 5.[11] In a separate investigation, Mesbahi has also calculated radial dose function for these three sources.[12] Naseri *et al*. have examined the accuracy of the dose distributions calculated by the GZP6 treatment planning system by Monte Carlo simulation of these sources.[13] Monte Carlo simulation is widely used in radiophysics[14], however, to our knowledge the GZP6 unit has not been studied before, based on a comprehensive determination of TG-43U1 dosimetric parameters.[15] Since the GZP6 unit has six sources with different fixed configurations, each source has been individually evaluated for their clinical applications.

The goal of this project is to investigate the dosimetric parameters (*i.e.* dose rate constant, radial dose function and anisotropy function) of source number 3, which has not been studied before, following the TG-43U1 recommendation through Monte Carlo simulations. The results of these investigations will be compared with the corresponding data available for Ralstron (type 2) ^{60}Co and microSelectron ^{192}Ir sources.[4,16] The dose distribution for the source No. 3 is used to produce dose distributions for the other GZP6 sources using a superimposition method developed in this study.

Materials and methods

Radioactive source structure

The GZP6 high dose rate afterloading unit comprises of different six ^{60}Co sources affixed to six different channels in the system. In this study dosimetric characteristic of the source number 3 of the unit, which is a non-stepping source and includes one active cylindrical ^{60}Co pellet, is being evaluated. As illustrated schematically in Figure 2, this source braid consists of an active nickel-plated cobalt pellet and a number of inactive spherical pellets which are made of steel. The active ^{60}Co cylinder has a radius of 0.5 mm and length of 2 mm (including the nickel-plating), in which the ^{60}Co radionuclide was distributed uniformly throughout the core. The nickel plating has a thickness of 0.05 mm, which has not been illustrated in the Figure 2. The active cobalt pellet is additionally encapsulated in a titanium capsule, with 0.25 mm in thickness and consisting of two hemispheres with 0.75 mm in radius at the two ends, sealed by Argon arc welding. The whole pellets are accommodated in a steel spring cover with an external diameter of 2.7 mm. ^{60}Co is emitting two gamma photons with 1.17 and 1.33 MeV energies and β^- particles with E_{max}=0.318 MeV. It has a half-life of 5.271 years. The latter particle is attenuated effectively with the titanium capsule.

TG 43 formalism

The formalism of TG-43U1 was followed to compute the dosimetric parameters of the source.[15] According to this formalism the dose rate at the point P(r, θ) from the source center is defined by the following equation (as illustrated in Figure 2):

$$D(r,\theta) = S_k \Lambda \frac{G(r,\theta)}{G(r_0,\theta_0)} g(r,\theta) F(r,\theta) \quad [1]$$

Where r is the radial distance (in cm) from the source center and θ is the polar angle. $r_0$is the reference radial distance of 1 cm and θ_0 is the reference polar angle of 90º. S_k is air kerma strength of the source (in U, where 1 U=1 μGym^{2}h^{-1}), Λ is dose rate constant, $G(r,\theta)$ is geometry function, $g(r,\theta)$ is radial dose function and $F(r,\theta)$ is two-dimensional (2D) anisotropy function.

The dose rate constant is the ratio of dose rate at the reference point (r_0,θ_0) and air kerma strength:

$$\Lambda = \frac{\dot{D}(r_0,\theta_0)}{S_k} \quad [2]$$

Dose rate constant has a unit of cGyh^{-1}U^{-1}.

In this study the line-source approximation was used for calculation of geometry function. By using this approximation, for the geometry function can be obtained from the following equation:

$$G(r,\theta) = (r^2 - L^2/4)^{-1} \quad [3]$$

If $\theta \neq 0^\circ$ the geometry function is obtained from equation [4]:

$$G(r,\theta) = \frac{\beta}{Lr\sin\theta} \quad [4]$$

As denoted by Awan *et al.*[17], considering the source active length L, the radial distance r and the angles θ and β as showed in the Figure 2, equation [5] can be resulted from the above equation:

$$G(r,\theta) = \frac{\tan^{-1}[(r\cos\theta + L/2)/r\sin\theta] - \tan^{-1}[(r\cos\theta - L/2)/r\sin\theta]}{Lr\sin\theta} \quad [5]$$

Thus if $\theta \neq 0^\circ$, the geometry function can be calculated directly in terms of r and θ from equation [5].

TABLE 1. Mass density and compostion of the materials used in the Monte Carlo simulations

Material: description	Mass density (g/cm³)	Composition (element/weight fraction)
Cobalt: source core	8.85	Co/1
Nickel: source plating	8.902	Ni/1
Titanium: source capsule	4.54	Ti/1
Steel pellets: spacers in the source braid	7.9	Fe/0.71994, C/0.0005, Si/0.0072, Mn/0.0137, S/0.00011, P/0.00025, Cr/0.17, Ni/0.0822, Mo/0.0013, V/0.0006, Ti/0.0042
Steel: spring cover	6.999	Fe/0.7416, Ni/0.069, S/0.0001, Cr/0.167, C/0.0006, Mn/0.0062, Cu/0.0026, Al/0.0062, Mo/0.0015, Si/0.0052
Air	0.001205	C/0.000124, N/0.7555267, O/0.231781, Ar/0.012827
Water: phantom material	1	H/0.111894, O/0.888106

TABLE 2. Two dimensional geometry function () for GZP6 source number 3

	θ (°)									
r(cm)	0°	10°	20°	30°	40°	50°	60°	70°	80°	90°
0.5	1.037	1.036	1.031	1.024	1.016	1.008	1.000	0.994	0.990	0.988
0.75	1.016	1.016	1.014	1.011	1.007	1.003	1.000	0.997	0.995	0.995
1	1.009	1.009	1.008	1.006	1.004	1.002	1.000	0.998	0.997	0.997
1.5	1.004	1.004	1.003	1.003	1.002	1.001	1.000	0.999	0.999	0.999
2	1.002	1.002	1.002	1.002	1.001	1.000	1.000	1.000	0.999	0.999
2.5	1.001	1.001	1.001	1.001	1.001	1.000	1.000	1.000	1.000	1.000
3	1.001	1.001	1.001	1.001	1.000	1.000	1.000	1.000	1.000	1.000
3.5	1.001	1.001	1.001	1.000	1.000	1.000	1.000	1.000	1.000	1.000
4	1.001	1.001	1.000	1.000	1.000	1.000	1.000	1.000	1.000	1.000
4.5	1.000	1.000	1.000	1.000	1.000	1.000	1.000	1.000	1.000	1.000
5	1.000	1.000	1.000	1.000	1.000	1.000	1.000	1.000	1.000	1.000

The radial dose function, $g(r)$, and anisotropy function, $F(r, \theta)$ are defined as:

$$g(r) = \frac{\dot{D}(r,\theta_0)}{\dot{D}(r_0,\theta_0)} \frac{G(r_0,\theta_0)}{G(r,\theta_0)} \quad [6]$$

$$F(r,\theta) = \frac{\dot{D}(r,\theta)}{\dot{D}(r,\theta_0)} \frac{G(r,\theta_0)}{G(r,\theta)} \quad [7]$$

In which $\dot{D}(r,\theta)$ denotes the dose rate at the point P(r, θ) from the source.

Monte Carlo calculations

The MCNP-4C Monte Carlo code was employed to estimate absorbed dose towards obtaining TG-43U1 parameters.[18] Since it has the option of defining the mesh grids, the MCNPX version 2.4.0 Monte Carlo code was also utilized to obtain 2D dose distribution for the source.[19] When this option is used it would be easier to score tally values in a large number of scoring volumes. Table 1 lists the mass density and chemical composition of the materials used in our Monte Carlo calculations.

In calculations of dose rate constant and 2D dose distributions, the value of air kerma strength was taken from our previous work.[20]

The source braid was centered in a cylindrical water of dimensions R=25 cm and L=50 cm in the simulations. A cutoff energy of 10 keV was used for both photons and electrons. To speed up the Monte Carlo calculations, the absorbed dose was approximated as kerma to estimate dose at points where the electronic equilibrium exists. For a ^{60}Co source, the dose build up region affects only points in close vicinity from the ^{60}Co pellet. The f6 tally was used to score collision kerma (in MeV/g/photon). At the points in the vicinity of the source, in which the electronic equilibrium may not exist, dose was scored using *f8

TABLE 3. Dose rate constant (Λ) values for GZP6 ^{60}Co (number 3), Ralstron (type 2) ^{60}Co (Ref. 4) and microSelectron ^{192}Ir (Ref. 16) sources

Source Type	GZP6 (This Study)	Ralstron (type 2) (Papagiannis *et al.*[4])	microSelectron (Karaiskos *et al.* [16])
Λ (cGyh^{-1}U^{-1})	1.104±0.03	1.101±0.005	1.116±0.006

tally (in MeV/photon). Toroid tally cells of 0.05 cm in thickness were used to score the tally values. The numbers of photon histories simulated were 1.6×10^7, 1.6×10^7 and 1.45×10^8 respectively to obtain dose rate constant, radial dose function, and 2D anisotropy function. The corresponding statistical errors were respectively equal to 1.58, 0.5 and 0.88 percent for the Monte Carlo calculations in the used tally cells. Dose values at different radial distances and angles from the source (required for calculation of radial dose function and anisotropy function) were obtained through Monte Carlo simulations for a water phantom. The data for radial dose function and anisotropy function then were calculated respectively using equations [6] and [7]. Dose rate constant, radial dose function and 2D anisotropy function values for GZP6 source number 3 were compared with corresponding data for Ralstron (type 2) ^{60}Co source, reported by Papagiannis *et al.*[4], and microSelectron ^{192}Ir source, reported by Karaiskos *et al.*.[16]

To obtain 2D dose rate table, a cylindrical grid of 14 cm×14 cm in *y*-*z* plane, with resolution of 0.05 cm in both longitudinal and radial directions was overlaid on the geometry. The thin grid was used to reduce the Monte Carlo computation time. 3.5×10^8 photon histories were followed, resulting an average error of 0.44% over the mesh cells. MCNPX tally type 1 with the option of depth for photons was used to determine energy deposition per volume per photon in terms of per photon. The tally value then was converted to the dose rate per U by introducing the activity, air kerma strength of the source and appropriate conversion factors in the calculations.

Superimposition method

A superimposition algorithm was developed to produce the dose distributions of the GZP6 sources No. 1, 2 and 5 from the dose distribution data of the source No. 3. The algorithm was consisted of four steps:

(a) The dose distribution data for each pellet in the sources 1, 2 and 5 was obtained from the dose distribution matrix of source 3 through application of matrix shift method.[21] The shifting distance was equal to the inter-pellets distance (6.5 mm).

(b) The dose distribution data for each pellet was multiplied by normalized activity of that pellet to the activity of source No. 3.

(c) A summation was then performed over the matrixes of all pellets in each source of 1, 2 ad 5.

(d) Dose contours were plotted from the dose distribution matrix of sources 1, 2 and 5.

The results of the mentioned algorithm were verified to examine its accuracy. For this purpose the sources 1, 2 and 5 were simulated separately and the obtained dose distributions were compared by the dose distributions resulted from the above algorithm.

Results and discussion

TG-43 dosimetric parameters

The calculated values of geometry function for 0.5-5 cm radial distance and 0°-90° angles are presented in the Table 2. The calculated values for geometry function were equal to unity at 6-10 cm distance. To summarize the results, these values were not presented in the Table 2. The geometry function is symmetrical with reference to the angle of 90°. On the other hand the angular values of the on the either side of the 90° angle, for the angles 100°-180°, are mirror images of the values for 80°-0° angles.[22] So as showed in Table 2, the two dimensional geometry function is presented only for angles 0°-90°.

Monte Carlo calculated value of air kerma strength is $S_{k=}$17240.01 cGyh^{-1}U^{-1} as worked out earlier for the GZP6 source number three.[20] The value was used for the calculation of dose rate constant in the present study. Monte Carlo calculated dose rate constants for GZP6 and Ralstron (type 2) and microSelectron sources are presented in Table 3.

The dose rate results, in terms of cGyh^{-1}U^{-1}, in Cartesian away (*y*) and along (*z*) coordinates are presented in the Table 4. It should be noted that the source center is assumed to be in the origin of the Cartesian coordinates.

Radial dose function (RDF) computed values for GZP6 source number 3 are presented in Table 5. The tabulated $g(r)$ data presented in the Table 5 were fitted to a fifth order polynomialin form of:

$$g(r) = a_5r^5 + a_4r^4 + a_3r^3 + a_2r^2 + a_1r + a_0, \quad R^2=0.9989 \quad [8]$$

TABLE 4. Dose rate values (in cGyh-1U-1) for GZP6 source number 3

z (cm)	y (cm)														
	0	0.25	0.5	0.75	1	1.5	2	2.5	3	4	5	6	8	10	14
14	0.00366	0.00348	0.00349	0.00351	0.00355	0.00360	0.00362	0.00364	0.00361	0.00356	0.00346	0.00330	0.00293	0.00251	0.00179
10	0.00776	0.00747	0.00753	0.00762	0.00775	0.00782	0.00783	0.00779	0.00765	0.00731	0.00683	0.00627	0.00512	0.00408	0.00257
8	0.01268	0.01233	0.01242	0.01259	0.01268	0.01272	0.01271	0.01249	0.01216	0.01122	0.01007	0.00893	0.00679	0.00517	0.00301
6	0.02344	0.02289	0.02322	0.02358	0.02372	0.02358	0.02300	0.02212	0.02088	0.01808	0.01534	0.01284	0.00901	0.00640	0.00347
5	0.03438	0.03373	0.03461	0.03494	0.03486	0.03422	0.03282	0.03072	0.02829	0.02343	0.01902	0.01544	0.01029	0.00706	0.00369
4	0.05513	0.05436	0.05559	0.05558	0.05527	0.05295	0.04905	0.04425	0.03936	0.03047	0.02357	0.01838	0.01156	0.00768	0.00387
3	0.10007	0.09995	0.10120	0.10029	0.09802	0.08880	0.07717	0.06576	0.05547	0.03962	0.02874	0.02139	0.01277	0.00825	0.00404
2.5	0.14581	0.14691	0.14702	0.14424	0.13804	0.11895	0.09868	0.08070	0.06597	0.04472	0.03140	0.02291	0.01334	0.00848	0.00411
2	0.23037	0.23371	0.23087	0.22057	0.20321	0.16323	0.12726	0.09901	0.07780	0.04994	0.03406	0.02428	0.01382	0.00869	0.00416
1.5	0.41507	0.42096	0.40432	0.36373	0.31538	0.22747	0.16335	0.11957	0.09008	0.05494	0.03631	0.02549	0.01423	0.00886	0.00421
1	0.96404	0.95030	0.82069	0.65489	0.51070	0.31436	0.20414	0.14060	0.10142	0.05909	0.03812	0.02642	0.01452	0.00897	0.00424
0.75	-	1.64251	1.25332	0.90067	0.64913	0.36206	0.22361	0.14951	0.10613	0.06068	0.03887	0.02673	0.01461	0.00903	0.00426
0.5	-	3.24317	1.98378	1.22459	0.80260	0.40566	0.23943	0.15679	0.10993	0.06193	0.03931	0.02696	0.01469	0.00905	0.00427
0.25	-	7.37207	3.01733	1.55687	0.93343	0.43739	0.25079	0.16130	0.11215	0.06268	0.03962	0.02714	0.01475	0.00907	0.00427
0	-	12.32321	3.63819	1.71023	0.98796	0.44908	0.25446	0.16313	0.11306	0.06297	0.03976	0.02718	0.01481	0.00910	0.00427
-0.25	-	7.37187	3.01661	1.55670	0.93376	0.43736	0.25056	0.16142	0.11212	0.06262	0.03961	0.02716	0.01476	0.00907	0.00427
-0.5	-	3.24423	1.98345	1.22515	0.80214	0.40577	0.23968	0.15661	0.10981	0.06196	0.03935	0.02695	0.01470	0.00905	0.00426
-0.75	-	1.64362	1.25309	0.90124	0.64938	0.36188	0.22361	0.14959	0.10621	0.06073	0.03882	0.02675	0.01466	0.00903	0.00425
-1	-	0.95463	0.82232	0.65543	0.51092	0.31428	0.20416	0.14068	0.10151	0.05911	0.03812	0.02639	0.01452	0.00897	0.00424
-1.5	-	0.41756	0.40609	0.36472	0.31569	0.22760	0.16345	0.11980	0.09005	0.05499	0.03636	0.02548	0.01421	0.00885	0.00420
-2	-	0.22359	0.23240	0.22150	0.20379	0.16334	0.12738	0.09904	0.07777	0.04997	0.03406	0.02431	0.01383	0.00869	0.00416
-2.5	-	0.13517	0.14677	0.14507	0.13834	0.11910	0.09893	0.08086	0.06605	0.04477	0.03147	0.02295	0.01334	0.00849	0.00411
-3	-	0.08853	0.09925	0.10101	0.09848	0.08899	0.07729	0.06578	0.05563	0.03965	0.02878	0.02145	0.01280	0.00825	0.00405
-4	-	0.04431	0.05223	0.05502	0.05557	0.05320	0.04907	0.04429	0.03938	0.03057	0.02360	0.01836	0.01156	0.00768	0.00388
-5	-	0.02532	0.03133	0.03368	0.03451	0.03434	0.03291	0.03077	0.02835	0.02347	0.01907	0.01545	0.01028	0.00706	0.00369
-6	-	0.01587	0.02029	0.02213	0.02306	0.02367	0.02307	0.02216	0.02090	0.01808	0.01534	0.01289	0.00902	0.00641	0.00348
-8	-	0.00756	0.00999	0.01126	0.01192	0.01256	0.01270	0.01251	0.01219	0.01124	0.01008	0.00894	0.00683	0.00516	0.00302
-10	-	0.00423	0.00571	0.00654	0.00701	0.00753	0.00771	0.00777	0.00768	0.00734	0.00683	0.00627	0.00511	0.00408	0.00257
-14	-	0.00183	0.00244	0.00279	0.00305	0.00333	0.00346	0.00355	0.00358	0.00356	0.00347	0.00331	0.00293	0.00251	0.00178

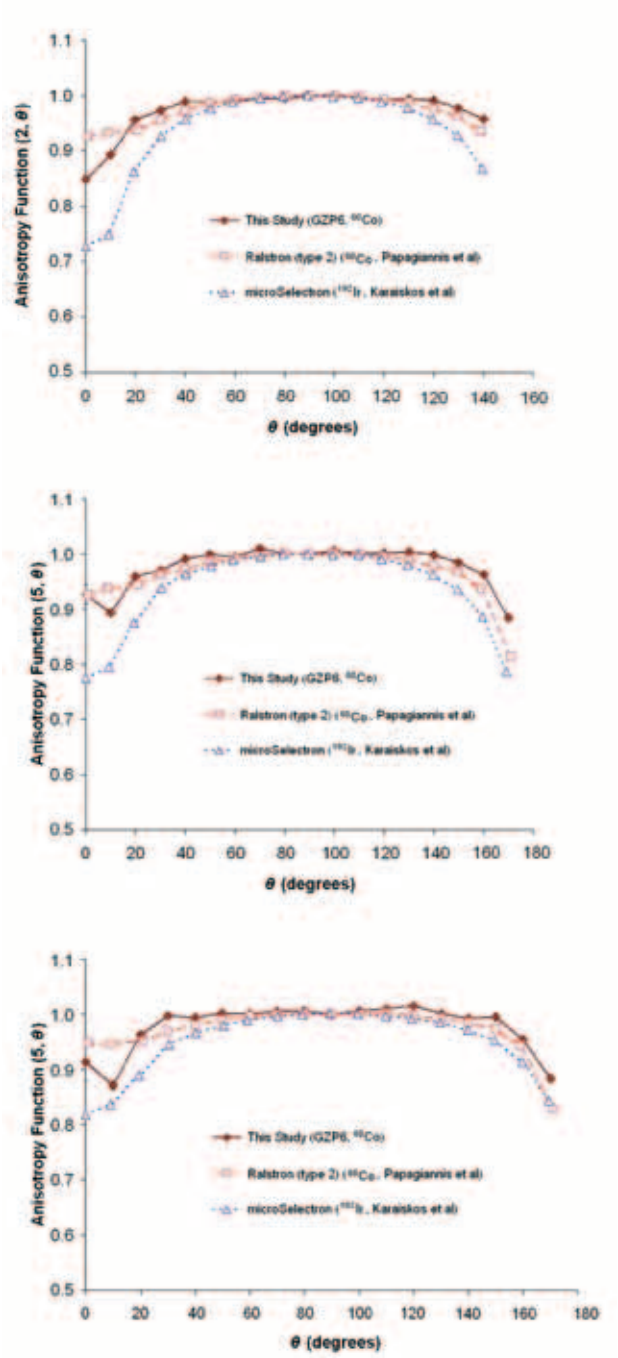

A

B

C

FIGURE 4. Anisotropy functions of GZP6 ^{60}Co (number 3), Ralstron (type 2) ^{60}Co (by Papagiannis *et al.*[4]) and microSelectron ^{192}Ir (by Karaiskos *et al.*[16]) sources: (A) for *r*=2 cm; (B) for *r*=5 cm; (C) for *r*=10 cm.

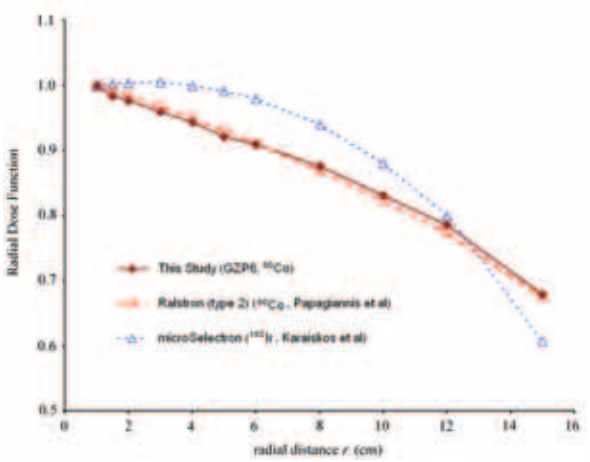

FIGURE 3. Radial dose function versus radial distance from the source for GZP6 ^{60}Co (number 3), Ralstron (type 2) ^{60}Co (by Papagiannis *et al.*[4]) and microSelectron ^{192}Ir (by Karaiskos *et al.*[16]) sources.

TABLE 5. Monte Carlo calculated radial dose functions of GZP6 source number 3

Radial distance r (cm)	g_L (r)
1	1.000
1.5	0.983
2	0.976
2.5	0.968
3	0.959
3.5	0.950
4	0.943
4.5	0.932
5	0.921
6	0.909
7	0.890
8	0.876
9	0.851
10	0.831
12	0.785
13	0.767
15	0.679
20	0.539

The parameters of the fitted polynomial are as follows:

a_5=1.000×10^{-6}, a_4=-5.000×10^{-5}, a_3=0.0007, a_2=-0.0039, a_1=-0.01, a_0=1.0087.

A graphical representation of $g(r)$ values for the GZP6 source is presented in Figure 3 and compared with the corresponding data for the Ralstron (type 2) ^{60}Co source reported by Papagiannis *et al.*[4] and microSelectron ^{192}Ir source reported by Karaiskos *et al.*.[16]

Table 6 presents the anisotropy function data for GZP6 ^{60}Co source number 3. $F(r, \theta)$ values of the GZP6, Ralstron and microSelectron sources for distances of 2, 5 and 10 cm are presented in Figure 4 A-C.

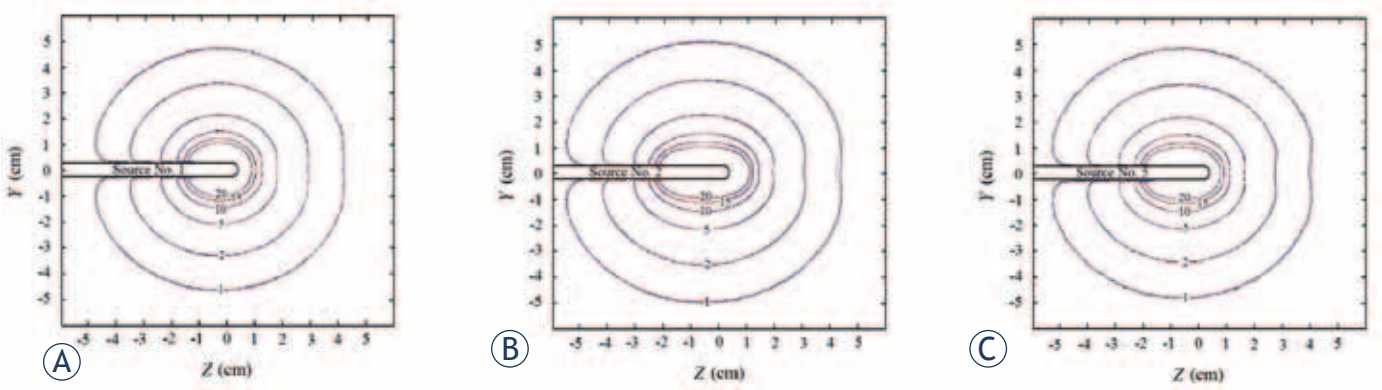

FIGURE 5. Dose distributions (Gy) obtained by MC simulations (blue lines) and superimposition method (red lines) for GZP6 sources: (a) source No. 1; (b) source No. 2 and (c) source No. 5. Isodoses of 1-20 Gy are contoured in the figure and since the contours by the two methods are overlapped in many points, are almost not distinguishable.

TABLE 6. 2D anisotropy functions for GZP6 ^{60}Co source (number 3) calculated by Monte Carlo code

θ (degrees)	r (cm)					
	1	2	3	4	5	10
0	0.858	0.849	0.863	0.904	0.927	0.913
10	...	0.893	0.898	0.901	0.893	0.870
20	0.990	0.956	0.957	0.957	0.959	0.963
30	...	0.973	0.974	0.970	0.970	0.998
40	0.992	0.990	0.988	0.989	0.991	0.994
50	...	0.989	0.986	0.990	0.999	1.002
60	1.011	0.990	0.985	0.982	0.995	1.001
70	...	0.995	1.000	1.002	1.010	1.005
80	1.025	0.994	0.995	0.992	1.001	1.007
90	1.000	1.000	1.000	1.000	1.000	1.000
100	0.995	1.000	1.004	1.004	1.007	1.006
110	...	0.998	1.001	0.999	1.001	1.010
120	0.978	0.993	0.995	0.993	1.001	1.015
130	...	0.995	0.998	0.998	1.004	1.000
140	1.019	0.992	0.992	0.990	0.998	0.993
150	...	0.977	0.979	0.978	0.984	0.995
160	...	0.958	0.958	0.956	0.963	0.954
170	...	...	0.881	0.876	0.884	0.883

Our results are indicating that the dose rate constant, radial dose function and anisotropy function for GZP6 and Ralstron (type 2) ^{60}Co sources are comparable. While the value of dose rate constant for the GZP6 and Ralstron (type 2) ^{60}Co sources are close to that for the microSelectron ^{192}Ir source (Table 3), radial dose function fall off for the ^{192}Ir source is less steep compared to the cobalt sources especially for lower radial distances from the source (in Figure 3). It can be also noticed from the Figure 4 that the two cobalt sources have more isotropic anisotropy functions than the iridium source.

The dosimetric data presented in this study for GZP6 source (number 3) can be utilized in clinical practice of the source and towards the improvement of its treatment planning system.

Dose distributions from the superimposition method

The dose distributions for the GZP6 source No. 1, 2 and 5 which was obtained by MC simulations of the sources and the superimposition method described are presented in the Figure 5. The dose contours of 1, 2, 5, 10, 15 and 20 Gy were plotted. As it can be observed the dose distributions obtained by the two methods for the sources 1, 2 and 5 are equal.

The superimposition algorithm developed in this study is able to produce dose distributions for the GZP6 sources No. 1, 2 and 5 from the dose distribution of the source No. 3. The algorithm is also applicable for other bracytherapy units in which an arrangement of sources is used in the treatment process. These results may provide comprehensive dosimetric information that could be clinically more applicable for dose calculations around different implants by superimposition method.

Acknowledgments

The authors would like to thank Dr. Yasha Makhdoomi and Mr. Mojtaba Taheri for their valuable assistances in this study. This project was fully funded by Mashhad University of Medical Sciences (MUMS).

References

1. Nuclear Power Institute of China (NPIC), 2010, Available at:www.npic.ac.cn/. Accessed October 24, 2010.
2. Ito H. Radiotherapy for cervical cancer: A multi-institutional comparison. *Nippon Igaku Hoshasen Gakkai Zasshi* 1999; **59:** 745-9.
3. Kim WC, Kim GE, Suh CO, Loh JJK. High versus low dose rate intracavitary irradiation for adenocarcinoma of the uterine cervix. *Jpn J Clin Oncol* 2001; **31:** 432-7.
4. Papagiannis P, Angelopoulos A, Pantelis E, Sakelliou L, Karaiskos P, Shimizu Y Monte Carlo dosimetry of 60Co HDR brachytherapy sources. *Med Phys* 2003; **30:** 712-21.
5. Vranic A. New developments in surgery of malignant gliomas. *Radiol Oncol* 2011; **45:** 159-65.
6. Richter J, Baier K, Flentje M. Comparison of 60Cobalt and 192Iridium sources in high dose rate afterloading brachytherapy. *Strahlenther Onkol* 2008; **184:** 187-92.
7. Meisberger LL, Keller R, Shalek RJ. The effective attenuation in water of the gamma rays of 198Au, 192Ir, 137Cs, 226Ra, and 60Co. *Radiology* 1968; **90:** 953-7.
8. Sakelliou L, Sakellariou K, Sarigiannis K, Angelopoulos A, Perris A, Zarris G. Dose rate distributions around 60Co, 137Cs, 198Au, 192Ir, 241Am, 125I (models 6702 and 6711) brachytherapy sources and the nuclide 99mTc. *Phys Med Biol* 1992; **37:** 1859-72.
9. Nath R, Anderson LL, Luxton G, Weaver KA, Williamson JF, Meigooni AS. Dosimetry of interstitial brachytherapy sources: Recommendations of the AAPM Radiation Therapy Committee Task Group No. 43. *Med Phys* 1995; **22:** 209-34.
10. Nath R, Anderson LL, Meli JA, Olch AJ, Stitt JA, Williamson JF. Code of practice for brachytherapy physics: Report of the AAPM Radiation Therapy Committee Task Group 56. *Med Phys* 1997; **24:** 1557-98.
11. MesbahiA, Naseri A. In-air calibration of new high dose rate 60Co brachytherapy sources: results of measurements on a GZP6 brachytherapy afterloading unit. *Rep Pract Oncol Radiother* 2008; **13:** 69-73.
12. Mesbahi A. Radial dose functions of GZP6 intracavitary brachytherapy 60Co sources: treatment planning system versus Monte Carlo calculations. *Iran J Radiat Res* 2008; **5:** 181-6.
13. Naseri A, Mesbahi A. Application of Monte Carlo calculations for validation of atreatment planning system in high dose rate brachytherapy.*Rep Pract Oncol Radiother* 2009; **14:** 200-4.
14. Mowlavi AA, Fornasier MR, de Denaro M. Thyroid volume's influence on energy deposition from 131I calculated by Monte Carlo (MC) simulation. *Radiol Oncol* 2011; **45:** 143-6.
15. Rivard MJ, Coursey BM, DeWerd LA, Hanson WF, Huq MS, Ibbott GS, et al. Update of AAPM Task Group No. 43 Report: A revised AAPM protocol for brachytherapy dose calculations. *Med Phys* 2004; **31:** 633-74.
16. Karaiskos P, Angelopoulos A, Sakelliou L, Sandilos P, Antypas C, Vlachos L, et al. Monte Carlo and TLD dosimetry of an 192Ir high dose-rate brachytherapy source. *Med Phys* 1998; **25:** 1975-84.
17. Awan ShB, Dini ShA, Hussain M, Meigooni DS, and Meigooni AS. Cylindrical coordinate-based TG-43U1 parameters for dose calculation around elongated brachytherapy sources. *J Appl Clin Med Phys* 2008; **9:** 123-42.
18. Briesmeister JF. MCNP-A general Monte Carlo N-particle transport code, Version 4C. *Report LA-13709-M* 2000; Los Alamos National Laboratory, NM.
19. Waters LS. MCNPX User's Manual, Version 2.4.0. *Report LA-CP-02-408* 2002; Los Alamos National Laboratory.
20. Bahreyni Toossi MT, Ghorbani M, Mowlavi AA, Taheri M, Layegh M, Makhdoumi Y, et al. Air kerma strength characterization of a GZP6 Cobalt-60 brachytherapy source. *Rep Pract Oncol Radiother* 2010; **15:** 190-4.
21. Bahreyni Toossi MT, Abdollahi M, Ghorbani M. Monte Carlo dose calculation of GZP6 60Co stepping source based on a matrix shift technique. *Rep Pract Oncol Radiother* 2010; **16:**10-3.
22. Baltas D, Sakelliou L, Zamboglou N. *The physics of modern brachytherapy for oncology.* Boca Raton, FL: Taylor and Francis Group; 2007. p. 312.

RadiolOncol 2012; 46(2): 89-96.
doi:10.2478/v10019-012-0029-8

Dvojni BioDisk: nov biološki pripomoček za znotrajžilno zapiranje defekta preddvornega pretina - raziskava pri ovcah

Pavčnik D, Tekulve K, Uchida BT, Luo ZH, Jeromel M, Van Alstine WG, Keller FS, Rösch J

Izhodišča. Z raziskavo smo proučevali dolgoročno učinkovitost in varnost novega dvojnega BioDiska (DBD), pripomočka za zapiranje defekta preddvornega pretina (ASD).

Materiali in metode. Pri 12-ih ovcah smo v raziskovalne namene izvedli ASD s pomočjo transseptalne (TS) igle ob dodatni balonski razširitvi. Telesna teža živali je bila od 40,1 do 64,0 kg, srednja vrednost pa 55,2 ± 7,1 kg. Premer ASD smo izmerili neposredno po posegu in čez 14 dni, preden smo vsadili DBD, ki sta ga sestavljala dva obroča iz nitinola. Velika sta bila 18 in 28 mm, povezana z majhnimi spoji in prekrita s submukozo tankega črevesa (SIS) prašiča. DBD smo vstavili preko žilnega uvajala velikosti 10 Fr. Učinkovitost DBD smo ocenjevali angiokardiografsko in z znotrajsrčnim dopplerskim ultrazvokom (ICE). Dve živali smo proučevali neposredno po vsaditvi, preostale pa v različnih obdobjih po vsaditvi (2 čez 6 tednov, 3 čez 3 mesece, 3 čez 6 mesecev in 2 čez 12 mesecev).

Rezultati. S TS iglo smo uspešno izvedli ASD pri 10 ovcah. V ostalih dveh primerih smo ASD izvedli z razširitvijo obstoječega odprtega ovalnega okna (PFO). Premer ASD je po začetni balonski razširitvi znašal od 13-15 mm (srednja vrednost 14,1 ± 0,73 mm), po dveh tednih pa od 9-13 mm (srednja vrednost 10,06 ± 1,37 mm). Ob vsaditvi DBD in ob sledenju v nobenem primeru ni prišlo do spontane embolizacije. S sledenjem z ICE nismo prikazali nikakršnega puščanja ob robovih vsajenih DBD. Po 6, 12, 24 in 52 tednih smo tako makroskopsko kot histološko potrdili dobro vraščen DBD in s tem popolno zaprtje pretoka preko preddvornega pretina poskusnih živali. Ugotavljali smo postopno remodeliranje SIS s celicami poskusnih živali in preraščanje endotela na površini DBD.

Zaključki. Dvojni BioDisk je varen in učinkovit pripomoček za zapiranje ASD pri ovcah.

Radiol Oncol 2012; 46(2): 97-105.
doi:10.2478/v10019-012-0016-0

Magnetnoresonančno (MR) vodena vakuumska biopsija (VAB) dojke. Začetne izkušnje na Onkološkem inštitutu v Ljubljani

Zebič-Šinkovec M, Hertl K, Kadivec M, Čavlek M, Podobnik G, Snoj M

Izhodišča. Magnetnoresonančna mamografija (MRM) ima kot ostale slikovne metode določeno specifičnost. Pozitivna napovedna vrednost za spremembe, ki jih odkrijemo samo z magnetnoresonančnim slikanjem, se giblje med 15% in 50%. MR vodeni posegi (biopsije, lokalizacije) so nujni pri sumljivih spremembah, ki jih odkrijemo samo z magnetnoresonančnim slikanjem. Cilj retrospektivne raziskave je bil ovrednotiti naše začetne izkušnje z MR-VAB. Želeli smo tudi opredeliti korelacijo med histološkimi izvidi biopsij in značilnostmi sprememb na magnetnoresonančni mamografiji.

Bolniki in metode. Pri 14 bolnicah (srednja starost 51 let) smo opravili vakuumsko biopsijo dojke pod kontrolo magnetne resonance. Punktirali smo 14 sprememb, ki so bile odkrite z magnetnoresonančnim slikanjem. Preučili smo značilnosti sprememb in indikacije za biopsijo, histološke izvide biopsij in končne histološke izvide.

Rezultati. Biopsija je bila tehnično uspešna pri 14 od 15 bolnic (93%). V 6 primerih je smo s histologija preiskavo odkrili malignom (6/14, 43%), 6 sprememb je bilo benignih (6/14, 43%), 2 spremembi pa sta bili opredeljeni kot spremembi nejasnega biološkega potenciala (2/14, 14%). Od 6 odkritih rakih so bili 3 invazivni duktalni karinomi in 3 duktalni karcinomi *in situ*. Pozitivna napovedna vrednost je bila višja za spremembe, ki so se barvale po vzorcu NMLE ("*nonmasslike enhancement*"). Višja napovedna vrednost je bila tudi za kinetični krivulji, ki v kasnejši fazi kažeta plato ali "*wasout*".

Zaključki. Naše začetne izkušnje potrjujejo, da je MR vodena VAB hitra, varna in zanesljiva alternativa kirurški biopsiji za lezije, ki jih odkrijemo samo z magnetnoresonančno mamografijo.

Radiol Oncol 2012; 46(2): 106-113.
doi:10.2478/v10019-012-0021-3

Razlikovanje malignih in benignih pljučnih sprememb s pomočjo difuzijskega magnetnoresonančnega slikanja

Gümüştaş S, Inan N, Akansel G, Çiftçi E, Demirci A, Özkara KS

Izhodišča. Namen raziskave je bil ugotoviti pomen difuzijskega magnetnoresonančnega slikanja pri diferencialni diagnozi pljučnih sprememb.

Bolniki in metode. V prospektivno raziskavo smo vključili 67 bolnikov s pljučnimi spremembami (48 malignih, 19 benignih). Izmerili smo intenzitete signala difuzijskega magnetnoresonančnega slikanja dobljene za vrednosti b = 0, 500 in 1000 s/mm^2. Vrednosti izračunanega difuzijskega koeficienta (IDK) pa so bile pridobljene s pomočjo slik z vrednostjo b = 0 in 1000 s/mm^2. Statistično značilnost razlik smo analizirali s pomočjo Studentovega testa T.

Rezultati. Intenziteta signala malignih sprememb je bila statistično značilno višja od benignih sprememb (p<0,004 za vrednost b = 0 s/mm^2 in p<0,000 za ostale vrednosti b). V primerih, ko je bil b = 500 s/mm^2, so vrednosti intenziteta signala ≥391 pomenile maligno spremembo, pri čemer je bila občutljivost metode 95%, specifičnost 73% ter pozitivna napovedna vrednost 87%. Če pa je bil b = 1000 s/mm^2, je bila intenziteta signala ≥277 kriterij za maligno spremembo, pri čemer je bila občutljivost metode 93%, specifičnost 69% in pozitivna napovedna vrednost 85%. Glede na IDK se maligne in benigne lezije niso statistično značilno razlikovale (p = 0,675). Prav tako ni bilo statistično značilnih razlik v intenziteti signala in IDK med drobnoceličnim in nedrobnoceličnim rakom pljuč. V primerjavi z dobro ali delno diferenciranimi raki so bile vrednosti intenzitete signala pri slabo diferenciranih karcinomih višje pri vseh vrednostih b, vendar pa so bile razlike statistično značilne samo pri vrednosti b = 1000 s/mm^2 (p<0,04).

Zaključki. Difuzijsko magnetnoresonančno slikanje je uporabna metoda za razlikovanje malignih od benignih pljučnih sprememb.

Radiol Oncol 2012; 46(2): 114-118.
doi:10.2478/v10019-012-0012-4

Ugotavljanje rigidnosti spolnega uda med erekcijo z uporabo ultrazvočne kvantifikacije

Zheng X, Ji P, Mao H, Wu J

Izhodišča. Namen raziskave je bil s hitrostjo strižnih valov ("*shear wave velocity*") ugotoviti stopnjo nabrekanja moškega spolnega uda. Želeli smo z ultrazvočno kvantifikacijo oz. virtualnim dotikom proučiti klinično uporabnost te metode pri ugotavljanju sprememb rigidnosti pri erekciji.

Bolniki in metode. Ultrazvočno kvantifikacijo smo naredili pri 37 zdravih prostovoljcih. Med erekcijo smo ultrazvočno izmerili stopnjo nabrekanja glavice, telesa in korena spolnega uda. Ultrazvočno izmerjene vrednosti smo primerjali s stopnjo (gradusom) ugotovljene erekcije.

Rezultati. Vse vrednosti aksialnega in radialnega nabrekanja glavice, telesa in korena spolnega uda so se statistično značilno zniževale od stopnje erekcije gradus 0 do gradus 4. Pri erekciji gradus 4 so bile vrednosti le še približno tretjino vrednosti izmerjenih pri gradusu 0 (aksialno: 0,79 ± 0,13 proti 2,79 ± 0,32 za glavico spolnega uda, *P*<0,001; 0,77 ± 0,19 proti 2,84 ± 0,30 za telo spolnega uda, *P*<0,001 in 0,76 ± 0,15 proti 2,81 ± 0,34 za koren spolnega uda, *P*<0.001; radialno 0,82 ± 0,15 proti 2,83 ± 0,31 za glavico spolnega uda, *P*<0,001; 0,79 ± 0,18 proti 2,81 ± 0,27 za telo spolnega uda, *P*<0,001in 0,81 ± 0,16 proti 2,82 ± 0,33 za koren spolnega uda, *P*<0,001).

Zaključki. Ultrazvočna kvantifikacija oz. virtualni dotik nam omogoča numerično merjenje rigidnosti spolnega uda. Metoda učinkovito in občutljivo pokaže spremembe v aksialni in radialni rigidnosti spolnega uda in predstavlja nov način ugotavljanja erektilne funkcije.

Radiol Oncol 2012; 46(2): 119-125.
doi:10.2478/v10019-012-0014-2

Vnos barvila Lucifer Yellow v CHO celice izpostavljene magnetnim in električnim pulzom

Towhidi L, Firoozabadi SMP, Mozdarani H, Miklavčič D

Izhodišča. Za večino hidrofilnih molekul je celična membrana nepremagljiva ovira za njihov vstop v celico. Številne aplikacije na področju medicine, biologije in biotehnologije pa zahtevajo vnos hidrofilnih molekul v biološke celice. Ena od najbolj znanih metod na področju vnosa hidrofilnih molekul v celice je elektroporacija, pri kateri celice izpostavimo električnim pulzom visoke napetosti, vendar zelo kratkega trajanja. Cilj naše raziskave je bil raziskati učinek časovno spremenljivega magnetnega polja na molekularni transport prek membrane.

Materiali in metode. Primerjali smo vnos barvila Lucifer Yellow v celice pri njihovi izpostavitvi časovno spremenljivemu magnetnemu polju in elektroporacijskim električnim pulzom. Celice CHO smo izpostavili magnetnim pulzom amplitude 2,2 T vršne amplitude, trajanja 250 mikrosekund. Za izpostavitev magnetim pulzom smo uporabili Magstim stimulator in dvojno 70 mm tuljavo. Uporabili smo tri različne frekvence 0,25, 1 in 10 Hz pulzov z različnim številom, t.j. 112, 56 in 28 pulzov (skupaj devet eksperimentalnih skupin). Poleg tega smo vnos barvila Lucifer Yellow v celice izpostavljene magnetnimi pulzom primerjali z izmerjenim vnosom barvila v elektroporirane CHO celice, ki smo jih izpostavili tipičnim elektroporacijskim električnim pulzom: 8 pulzov dolžine 100 mikrosekund ponavljalne frekvence 1 Hz in električnega polja amplitude od 200 do 600 V/cm.

Rezultati in zaključki. Rezultati dobljeni v naši raziskavi kažejo, da časovno spreminjajoče magnetno polje poveča molekularni transmembranski transport. Vnos barvila Lucifer Yellow v celice, ki so bile izpostavljene časovno spremenljivemu magnetnemu polju, je višji pri nižjih ponavljalnih frekvencah in večjem številu dovedenih pulzov. Poleg tega primerjava vnosa barvila Lucifer Yellow v celice pri njihovi izpostavitvi časovno spremenljivemu magnetnemu polju in poracijskim električnim pulzom kaže, da je elektroporacija bolj učinkovita odmagnetnega polja, vendar pa je vnos barvila Lucifer Yellow zaradi izpostavljenosti celic magnetnemu polju še vedno znaten.

Radiol Oncol 2012; 46(2): 126-135.
doi:10.2478/v10019-012-0026-y

Optimizacija postavitve in števila elektrod za ireverzibilno elektroporacijo hepatocelularnega raka

Adeyanju OO, Al-Angari HA, Sahakian AV

Izhodišča. Ireverzibilna elektroporacija (IRE) je nova ablacijska metoda, ki uporablja visokonapetostne električne pulze za zdravljenje raka. Njena učinkovitost je odvisna od razporeditve električnega polja, ta pa od razporeditve uporabljenih elektrod.

Metode. V raziskavi predstavljamo poskus optimalne razporeditve elektrod glede na njihovo medsebojno razdaljo, globino vstavitve in njihovega števila. Uporabili smo model 3D neskončnih elementov, pri katerem smo sistematično spreminjali parametrične razdalje med elektrodami in njihovo globino vstavitve ter izračunali najnižje vrednosti napetosti za ireverzibilno elektroporacijo V_{ire}. Ob tem smo izmerili količino poškodb normalnega tkiva. Meritve smo naredili za par elektrod ter za tri in štiri elektrode. Optimalna konfiguracija elektrod je bila tista, kjer je bila V_{ire} najnižja in najmanjša poškodba normalnega tkiva.

Rezultati. Za 2,5 cm sferoidni tumor je bila optimalna postavitev dveh elektrod z razmikom med njima 2 cm, vstavljenih 1 cm pod sredino tumorja. Ob taki postavitvi je bila V_{ire} 3700 V. Na splošno smo ugotovili, da je bolj ugodna mala razdalja med elektrodami, centralni del elektrode pa mora segati do centralnega dela tumorja ali malo nižje. Ugotovili smo tudi, da je za učinkovito zdravljenje pomembnejša razdalja med elektrodami, kot globina njihove ustavitve.

Zaključki. Razporeditev električnega polja je odvisna od konfiguracije elektrod, kar lahko določimo z numeričnim modeliranjem. Rezultati so pomembni za načrtovanje ireverzibilne elektroporacije v klinični praksi, kot tudi za izbor najboljšega algoritma za postavitev elektrod.

Radiol Oncol 2012; 46(2): 136-144.
doi:10.2478/v10019-012-0032-0

Izboljšanje preživetja po uvedbi kemoterapije pri bolnikih z malignim plevralnim mezoteliomom v Slovenji: populacijska raziskava 444 bolnikov

Kovač V, Zwitter M, Žagar T

Izhodišča. Maligni plevralni mezoteliom je redek tumor, njegova incidenca pa še vedno narašča pri nas in v svetu. Znatne omejitve proizvodnje in uporabe azbesta še niso zmanjšale bremena te bolezni, ker je latentni čas med izpostavljenostjo azbestu in obolevnostjo zelo dolg. V zadnjem desetletju so različne klinične raziskave potrdile učinkovitost sistemskega zdravljenja kot sta kombinaciji cisplatina in gemcitabina ter cisplatina in premetrekseda, vendar le pri izbranih bolnikih z dobrim splošnim stanjem zmogljivosti. Namen pričujoče raziskave je bil oceniti morebitni vpliv sistemskega zdravljenja na celotno slovensko populacijo bolnikov z mezoteliomom.

Bolniki in metode. V retrospektivno raziskavo smo vključili vse bolnike s histološko potrjenim malignim plevralnim mezoteliomom v Sloveniji od leta 1974 do 2008. Podatke iz Registra raka Republike Slovenije smo dopolnili s klinično dokumentacijo Onkološkega inštituta Ljubljana, kjer smo nekirurško zdravili skoraj vse bolnike. Primerjali smo incidenco, zdravljenje in preživetje bolnikov iz obdobja, ko smo kemoterapijo redko uporabljali (1974-2003, prvo obdobje) ter po njem (2004-2008, drugo obdobje).

Rezultati. Pregled podatkov je pokazal 444 bolnikov, v prvem obdobju jih je bilo diagnosticiranih 325, v drugem pa 119. Z regresijsko analizo Joinpoint smo ugotovili, da je groba letna incidenčna stopnja naraščala hitreje po letu 1995; povprečna letna sprememba grobe incidenčne stopnje je bila 0,03 na 100.000 pred letom 1995 in 0,06 na 100.000 po njem. Prav tako smo ugotovili prevlado moškega spola (70%) skozi celotno obdobje, ki ga pokriva raziskava. Delež bolnikov starejših od 65 let je narastel z 41,8% v prvem obdobju na 54,6% v drugem (p = 0,02). Operiranih je bilo le 52 (11,7%) izbranih bolnikov, ki so imeli zgodnjo obliko bolezni, so bili brez resnih spremljajočih bolezni, njihovo srednje celokupno preživetje pa je bilo sorazmerno daljše (13,6 mesecev, p = 0,000). Kemoterapevtsko je bilo zdravljenih 56 (17,2%) bolnikov iz prvega obdobja in 96 (80,7%) iz drugega. V prvem obdobju smo uporabljali različne starejše citostatike, v drugem pa je bil najbolj pogost način zdravljenja (dobilo ga je 91 bolnikov) kombinacija gemcitabina v podaljšani infuziji in v nizkem odmerku ter cisplatina. V prvem obdobju je bilo ne glede na zdravljenje srednje preživetje bolnikov 7,4 mesecev, v drugem pa 12,6 mesecev (p = 0,037).

Zaključki. Čeprav je v Sloveniji že 15 let prepovedana proizvodnja in uporaba azbesta, incidenca malignega plevlarnega mezotelioma še vedno narašča in s tem tudi breme te bolezni. V novejšem obdobju še vedno pogosteje obolevajo moški, bolniki pa so ob diagnozi starejši. Sodobno kemoterapevtsko zdravljenje, zlasti gemcitabin v podaljšani infuziji in v nizkem odmerku je statistično značilno podaljšalo srednje celokupno preživetje bolnikov s to boleznijo v Sloveniji.

Radiol Oncol 2012; 46(2): 145-152.
doi:10.2478/v10019-012-0022-2

Dolgoročni rezultati kombiniranega zdravljenja raka analnega kanala

Oblak I, Petrič P, Anderluh F, Velenik V, Fras PA

Izhodišča. V retrospektivni raziskavi smo želeli analizirati učinkovitost in toksičnost radiokemoterapije pri bolnikih s ploščatoceličnim rakom analnega kanala zdravljenih na Onkološkem inštitutu Ljubljana.

Bolniki in metode. V obdobju med januarjem 2003 in septembrom 2010 smo na Onkološkem inštitutu v Ljubljani zdravili 84 bolnikov z radikalno radiokemoterapijo. Zdravili smo jih s 3-dimenzionalno konformno teleradioterapijo ter sočasno kemoterapijo (5-fluorouracil in mitomicin C), nato pa smo jim dodatno obsevali predel tumorja z varnostnim robom z brahi- ali teleterapijo. Ocenjevali smo učinkovitost in toksičnost takšnega zdravljenja.

Rezultati. Zdravljenje smo po protokolu zaključili pri 79,8% bolnikih. Srednji čas sledenja je bil pri 55 živih bolnikih bil 53 mesecev (razpon: 16-105 mesecev). Petletna lokoregionalna ozdravitev (LRO), preživetje brez bolezni (PBB), bolezensko specifično preživetje (BSP), celokupno preživetje (CP) in preživetje brez kolostome (PBK) so znašali 71%, 68%, 81%, 67% in 85%. Nobeden od bolnikov ni umrl zaradi zapletov samega zdravljenja. Najbolj pogost akutni sopojav zdravljenja je bil radiodermatitis (stopnja 3-4 pri 58,2% bolnikov). Kasne sopojave LENT-SOMA zaradi obsevanja smo zabeležili pri 15 (18%) bolnikih. Pri bolnikih, ki smo jih dodatno obsevali z brahiterapijo na tumor z varnostnim robom, je bilo manj kasnih stranskih učinkov (P=0,066), kot pri tistih, ki smo jih dodatno obsevali s teleterapijo. V multivariatni analizi smo ugotovili, da je bil neodvisni napovedni dejavnik za boljšo LRO, PBB in BSP popolni klinični odgovor na zdravljenje, za LRO in PBB je bila "rešilna" operacija (angl. *salvage surgery*) ter za boljše CP nivo hemoglobina 120g/l ali več.

Zaključki. Z radiokemoterapijo lahko pri večini bolnikov zagotovimo odlično kontrolo bolezni in preživetje ob ohranitvi funkcije analne mišice zapiralke. Pri ostanku ali ponovitvi bolezni pa lahko ozdravitev zagotovimo z "rešilno" operacijo (abdominoperinealna resekcija).

Radiol Oncol 2012; 46(2): 153-159.
doi:10.2478/v10019-012-0002-6

Difuzni velikocelični limfom B - današnja vsakodnevna klinična praksa

Gregorič B, Zadnik V, Jezeršek Novaković B

Izhodišča. Ko so pri zdravljenju bolnikov z difuznim velikoceličnim limfomom B (DVCLB) dodali h kemoterapiji rituksimab, so dosegli boljše rezultate. Tako je sistemsko zdravljenje z R-CHOP (rituksimab, ciklofosfamid, doksorubicin, vinkristin, prednisolon) ali različicami postalo standardno začetno zdravljenje teh bolnikov. Priporočila za zdravljenje temeljijo na rezultatih kliničnih raziskav, pogoji rutinskega zdravljenja bolnikov pa se precej razlikujejo od pogojev obravnave bolnikov v kliničnih raziskavah. Namen pričujoče retrospektivne raziskave je bila zato primerjava rezultatov rutinskega zdravljenja bolnikov z DVCLB z rezultati nekaterih večjih kliničnih raziskav.

Bolniki in metode. Med letoma 2004 in 2008 smo na Onkološkem inštitutu Ljubljana v skladu s tedanjimi priporočili 295 bolnikov z DVCLB zdravili z R-CHOP ali R-CHOP-u podobnimi shemami. Odgovor na zdravljenje smo ocenili v skladu s Chesonovimi kriteriji, preživetje brez bolezni in celokupno preživetje pa s Kaplan Meier-jevimi krivuljami preživetja.

Rezultati. Odgovor na zdravljenje se je v naši raziskavi razlikoval od rezultatov drugih raziskav, predvsem v skupini z nizkim tveganjem (kategorizacija po mednarodnem prognostičnem indeksu – IPI) in v skupini z zelo dobro napovedjo poteka bolezni (kategorizacija po revidiranem mednarodnem prognostičnem indeksu – R-IPI). Delež bolnikov s popolnim odgovorom (CR) v ostalih IPI in R-IPI skupinah je bil večinoma v skladu s pričakovanji. Tudi v primeru preživetja brez bolezni smo največje neskladje z rezultati iz literature ugotovili v skupini z nizkim tveganjem (delež preživelih brez bolezni po 3 letih 75%) in v skupini z zelo dobro napovedjo poteka bolezni (delež preživelih brez bolezni po 4 letih 59%). V ostalih IPI skupinah se je delež preživelih brez bolezni po 3 letih (srednje nizko tveganje 76%, srednje visoko tveganje 57%, visoko tveganje 53%) dobro skladal z navedenimi deleži v primerjalnih raziskavah. Nekoliko slabše ujemanje s citiranimi rezultati pa smo ugotavljali v deležu preživelih brez bolezni po 4 letih za preostali dve R-IPI skupini (72% za skupino z dobro prognozo in 51% za skupino s slabo napovedjo poteka bolezni). Deleži preživelih po 3 letih (bolniki z nizkim tveganjem 87%, s srednje visokim tveganjem 61% in visokim tveganjem 51%) so bili nekoliko slabši od primerjalnih v vseh IPI skupinah, razen v skupini s srednje nizkim tveganjem (82%). Po drugi strani pa so deleži preživelih po 4 letih v vseh R-IPI skupinah (94% v skupini z zelo dobro napovedjo poteka bolezni, 80% v skupini z dobro in 56% v skupini s slabo napovedjo poteka bolezni) dobro korelirali s podatki iz literature.

Zaključki. Rezultati zdravljenja bolnikov z DVCLB na našem inštitutu so dokaj spodbudni v primerjavi z rezultati nekaterih večjih raziskav. Trenutno verjetno ni dilem o tem, kako zdraviti mlade bolnike z dobro prognozo in starejše bolnike. Delež preživelih po 5 letih za skupino mladih bolnikov s slabo prognozo (76%) pa je zaskrbljujoč, zaradi česar je potrebno rezultate izboljšati. Na tem področju poteka precej raziskav, ki bodo razjasnile, katera vrsta zdravljenja je za to skupino bolnikov najbolj primerna.

Radiol Oncol 2012; 46(2): 160-165.
doi:10.2478/v10019-012-0003-5

Uspešnost zdravljenja z L-tiroksinom, s katerim smo zavrli izločanje TSH med nosečnostjo pri bolnicah, ki so prebolele raka ščitnice in bile zdravljene s totalno tiroidektomijo in ablacijo ostanka ščitnice z radiojodom

Krhin B, Bešič N

Izhodišča. V literaturi je zelo malo podatkov o tem, kakšno je optimalno povečanje odmerka L-tiroksina med nosečnostjo pri bolnicah, ki so prebolele raka ščitnice. Z našo raziskavo smo želeli ugotoviti, kako uspešno smo spremenili odmerek L-tiroksina, da je bilo med nosečnostjo še vedno ustrezno zavrto izločanje TSH. Drugi naš namen je bil ugotoviti, kateri odmerek L-tiroksina pri nosečnicah je ustrezen, da je izločanje TSH zavrto.

Bolniki in metode. V retrospektivni raziskavi smo analizirali podatke o 36 nosečnostih pri 32 bolnicah, ki so prebolele raka ščitnice. Vsem smo pred zanositvijo napravili totalno tiroidektomijo in vse so imele ablacijo ostanka ščitnice z radiojodom. Vse bolnice so jemale L-tiroksin v takih odmerkih, da so imele pred zanositvijo zavrto izločanje TSH. Funkcijske teste za ščitnico smo napravili pred, med in po nosečnosti.

Rezultati. Aritmetična sredina dnevnega odmerka L-tiroksina pred zanositvijo, v času prvega, drugega in tretjega tromesečja in po porodu je bila 149, 147, 155, 165 in 158 mikrogramov. Izločanje TSH je ostalo zavrto pri devetih nosečnostih. Koncentracija TSH je bila znotraj referenčnega območja pri 22 nosečnostih in zvišana pri petih nosečnostih. Pri nosečnicah, ki so imele v času celotne nosečnosti ustrezno zavrt TSH, je bila aritmetična sredina dnevnega odmerka L-tiroksina pred zanositvijo, v času prvega, drugega in tretjega tromesečja in po porodu: 154, 154, 164, 160 in 161 mikrogramov. Pri nosečnicah, katerim smo spremenili odmerek, smo ga v povprečju povečali za 31,5 mikrogramov.

Zaključki. Bolnice, ki so imele pred zanositvijo zavrto izločanje TSH, so imele med nosečnostjo zelo velik razpon sprememb vrednosti TSH. Ustrezno zavrto izločanje TSH med nosečnostjo je imelo le 25% nosečnic. Nosečnice, ki so imele ustrezno zavrto izločanje TSH v času prvega, drugega in tretjega tromesečja, so jemale odmerek 154, 164 in 160 mikrogramov L-tiroksina.

RadiolOncol 2012; 46(2): 166-169.
doi:10.2478/v10019-012-0019-x

Kateri je najprimernejši način odvzema citoloških vzorcev iz nožničnega oboka za spremljanje bolnic z ginekološkimi raki

Del Pup L, Canzonieri V, Serraino D, Campagnutta E

Izhodišča. Za zgodnje odkrivanje ponovitve rakave bolezni v vaginalnem oboku pri ženskah po histerektomiji uporabljamo citološko analizo. Njena uspešnost je zelo majhna pri vzorcih odvzetih z običajno metodo z Ayresovim loparčkom. Število dobljenih celic je majhno zaradi atrofije, ali pa zato, ker sta kota vaginalnega oboka tako tesno skupaj, da s pomočjo Ayresovega loparčka ne prodremo dovolj globoko. Namen raziskave je bil ugotoviti prednosti in slabosti odvzema citološkega vzorca s pomočjo citološke krtačke ter tak odvzem primerjati s klasičnim odvzemom s pomočjo Ayresovega loparčka.

Bolniki in metode. V raziskavo smo vključili 141 bolnic z ginekološkim rakom. V prvem delu raziskave smo pri 15 bolnicah odvzeli citološke vzorce tako z Ayresovim loparčkom kot s citološko krtačko. Vzorca iste bolnice smo nanesli na različna dela istega objektnega stekelca. V vsakem vzorcu sta bili nato naredili kvalitativno in kvantitativno analizo. Pri ostalih 126 bolnicah smo citološki vzorec odvzeli bodisi z Ayersovim loparčkom (skupina A) ali s citološko krtačko (skupina B). Vse vzorce je odvzel isti ginekolog.

Rezultati. V vseh 15 vzorcih prvega dela raziskave smo s pomočjo citološke krtačke odvzeli večje število celic kot pri klasičnem odvzemu. Primerjava skupin A in B v drugem delu raziskave pa je potrdila, da je jemanje citološkega vzorca s pomočjo citološke krtačke učinkovitejše kot je jemanje s pomočjo Ayresovega loparčka. Razmerje uspešnosti je bilo pri jemanju vzorcev s pomočjo citološke krtačke 2,8 (95% interval zaupanja od 1,3 do 6,2; hi-kvadrat p=0,008).

Zaključki. Tehnika odvzema citoloških vzorcev iz vaginalnega oboka s pomočjo citološke krtačke je učinkovitejša od običajne tehnike s pomočjo Ayersovega loparčka.

RadiolOncol 2012; 46(2): 170-178.
doi:10.2478/v10019-012-0005-3

Dozimetrična značilnost brahiterapijskega izvira ^{60}Co GZP6 z visoko hitrostjo doze (HDR). Uporaba superpozicijske metode

Toossi MTB, Ghorbani M, Mowlavi AS, Meigooni AS

Izhodišča. Želeli smo ovrednotili dozimetrične značilnosti brahiterapijskega izvira ^{60}Co GZP6 z visoko hitrostjo doze (HDR) po priporočilih Ameriškega združenja za medicinsko fiziko (AAPM TG43U1) ter uporabo v klinični praksi.

Materiali in metode. S kodami Monte Carlo MCNP-4C in MCNPX smo izračunali konstanto hitrosti doze, dvodimenzionalno (2D) porazdelitev doze, radialno dozno funkcijo in 2D anizotropično funkcijo izvira. Dobljene parametre smo primerjali s podatki izvirov Ralstron ^{60}Co in microSelectron ^{192}Ir. Razvili smo superpozicijsko metodo za razširitev rezultatov izvira GZP6 št. 3 na druge GZP6 izvire.

Rezultati. Simulirana vrednost konstante hitrosti doze je 1,104±0,03 cGyh^{-1}U^{-1}. Radialno dozno funkcijo in 2D anizotropično funkcijo smo predstavili grafično in tabelarično. Rezultati raziskave kažejo, da so dozimetrični parametri izvira GZP6 primerljivi s tistimi od izvira Ralstron. Konstanti hitrosti doz dveh ^{60}Co izvirov so podobne tistim od izvira microSelectron ^{192}Ir, medtem ko sta radialna dozna funkcija in anizotropična funkcija različni. Radialna dozna funkcija ^{192}Ir izvira je bolj položna, kot jo imata ^{60}Co izvira. Poleg tega ^{60}Co izviri kažejo bolj izotropično dozno porazdelitev kot ^{192}Ir izvir.

Zaključki. Superpozicijska metoda lahko proizvede dozne porazdelitve za drugačne razporeditve posameznih izvirov. Izračunane dozimetrične količine tega novega izvira lahko uvedemo v GZP6 planirni sistem (TPS), ki ga tako usposobimo za uporabo.

Fundacija "Docent dr. J. Cholewa"
je neprofitno, neinstitucionalno in nestrankarsko
združenje posameznikov, ustanov in organizacij, ki želijo
materialno spodbujati in poglabljati raziskovalno
dejavnost v onkologiji.

Dunajska 106
1000 Ljubljana

ŽR: 02033-0017879431

Activity of "Dr. J. Cholewa" Foundation for Cancer Research and Education – a report for the second quarter of 2012

The Dr. J. Cholewa Foundation for Cancer Research and Education aims to search for and support novel initiatives and forward thinking in all of the activities in any way associated with cancer. It is a non-profit, non-government and non-political association of experts, institutions and organisations associated with cancer research, cancer education, cancer treatment and prevention.

The Foundation continues to support the publication of "Radiology and Oncology", an international medical scientific journal that is edited, published and printed in Ljubljana, Slovenia. "Radiology and Oncology" publishes scientific articles, reviews, case reports, short reports and letters to the editor about problems in experimental and clinical research in radiology, radiophyics, experimental and clinical oncology, supportive therapy, prevention and early diagnostics of different types of cancer. Radiology and Oncology is an open access journal with a Science Citation Index impact factor. In the year 2011 and in the first quarter of 2012 the Foundation gave its support to a number of lay associations and organizations that are involved in the fight against cancer in Slovenia. The Foundation also supports a number of activities with long term effect and is thus involved in activities in all three levels of prevention of cancer.

The Dr. J. Cholewa Foundation for Cancer Research and Education helps professional and other associations in Slovenia to organise scientific and other meetings of specific interest in different fields of advanced cancer research and education.

The Foundation has continued with its activities throughout 2011 and the first and second quarter of 2012 with the aim to spread as much knowledge as possible about cancer and related problems in Slovenia, an important part of this activities being the education and information of the lay public.

Borut Štabuc, MD, PhD
Andrej Plesničar, MD, MSc
Tomaž Benulič, MD

Prvi na poti individualnega zdravljenja bolnikov z napredovalim nedrobnoceličnim pljučnim rakom.

Iressa je prva in edina tarčna monoterapija, ki dokazano podaljša preživetje brez napredovanja bolezni v primerjavi z dvojno kemoterapijo kot zdravljenje prvega reda pri bolnikih z napredovalim nedrobnoceličnim pljučnim rakom z mutacijo EGFR.

IRESSA® (GEFITINIB)
SKRAJŠAN POVZETEK GLAVNIH ZNAČILNOSTI ZDRAVILA

Sestava: Filmsko obložene tablete vsebujejo 250 mg gefitiniba.
Indikacije: zdravljenje odraslih bolnikov z lokalno napredovalim ali metastatskim nedrobnoceličnim pljučnim rakom z aktivacijskimi mutacijami EGFR-TK
Odmerjanje in način uporabe: Zdravljenje z gefitinibom mora uvesti in nadzorovati zdravnik, ki ima izkušnje z uporabo zdravil proti raku. Priporočeno odmerjanje zdravila IRESSA je ena 250-mg tableta enkrat na dan. Tableto je mogoče vzeti s hrano ali brez nje, vsak dan ob približno istem času.
Kontraindikacije: preobčutljivost za zdravilno učinkovino ali katerokoli pomožno snov, dojenje
Opozorila in previdnostni ukrepi: Pri 1,3 % bolnikov, ki so dobivali gefitinib, so opažali intersticijsko bolezen pljuč (IBP). Ta se lahko pojavi akutno in je bila v nekaterih primerih smrtna. Če se bolniku poslabšajo dihalni simptomi, npr. dispneja, kašelj in zvišana telesna temperatura, morate zdravljenje z zdravilom IRESSA prekiniti in bolnika takoj preiskati. Če je potrjena IBP, morate terapijo z zdravilom IRESSA končati in bolnika ustrezno zdraviti. Opažene so bile nepravilnosti testov jetrnih funkcij, občasno zabeležene kot hepatitis. Opisani so bili posamezni primeri odpovedi jeter. Zato so priporočljive redne kontrole delovanja jeter. V primeru blagih do zmernih sprememb v delovanju jeter je treba zdravilo IRESSA uporabljati previdno. Če so spremembe hude, pride v poštev prekinitev zdravljenja. Zdravilo IRESSA vsebuje laktozo. Bolniki z redko dedno intoleranco za galaktozo, laponsko obliko zmanjšane aktivnosti laktaze ali malabsorpcijo glukoze/galaktoze ne smejo jemati tega zdravila. Bolnikom naročite, da morajo takoj poiskati zdravniško pomoč, če se jim pojavijo kakršnikoli očesni simptomi, huda ali dolgotrajna driska, navzea, bruhanje ali anoreksija, ker lahko vse te posredno povzročijo dehidracijo.
Medsebojno delovanje zdravil: Sočasna uporaba močnih zaviralcev CYP3A4 lahko poveča koncentracijo gefitiniba v plazmi. Močni zaviralci CYP2D6 lahko pri izrazitih metabolizatorjih CYP2D6 povečajo koncentracijo gefitiniba v plazmi za približno 2-krat. Induktorji CYP3A4 lahko povečajo presnovo gefitiniba in zmanjšajo njegovo koncentracijo v plazmi. Zato lahko sočasna uporaba induktorjev CYP3A4 zmanjša učinkovitost zdravljenja in se ji je treba izogniti. Snovi, ki občutno in dolgotrajno zvišajo pH v želodcu, lahko zmanjšajo koncentracijo gefitiniba v plazmi in tako zmanjšajo njegovo učinkovitost. Veliki odmerki kratkodelujočih antacidov, uporabljenih blizu časa jemanja gefitiniba, imajo lahko podoben učinek. Pri nekaterih bolnikih, ki so jemali varfarin skupaj z gefitinibom, so se pojavili zvišanje internacionalnega normaliziranega razmerja (INR) in/ali krvavitve. Bolnike, ki sočasno jemljejo varfarin in gefitinib, morate redno kontrolirati glede sprememb protrombinskega časa (PČ) ali INR.
Neželeni učinki: V kumulativnem naboru podatkov kliničnih preskušanj III. faze so bili najpogosteje opisani neželeni učinki, ki so se pojavili pri več kot 20 % bolnikov, driska in kožne reakcije (vključno z izpuščajem, aknami, suho kožo in srbenjem). Neželeni učinki se ponavadi pojavijo prvi mesec zdravljenja in so praviloma reverzibilni. Ostali pogostejši neželeni učinki so: anoreksija, konjunktivitis, blefaritis in suho oko, krvavitev, npr. epistaksa in hematurija, intersticijska bolezen pljuč (1,3 %), navzea, bruhanje, stomatitis, dehidracija, suha usta, nepravilnosti testov jetrnih funkcij, bolezni nohtov, alopecija, asimptomatično laboratorijsko zvišanje kreatinina v krvi, proteinurija, cistitis, astenija, pireksija.
Vrsta in vsebina ovojnine: škatla s 30 tabletami po 250 mg gefitiniba
Način izdajanja zdravila: samo na recept
Datum priprave besedila: januar 2011
Imetnik dovoljenja za promet: AstraZeneca AB, S-151 85, Sodertalje, Švedska
Pred predpisovanjem, prosimo, preberite celoten povzetek glavnih značilnosti zdravila.
Dodatne informacije so na voljo pri:
AstraZeneca UK Limited, Podružnica v Sloveniji, Verovškova 55, 1000 Ljubljana, telefon: 01/51 35 600.

Samo za strokovno javnost.
Informacija pripravljena: avgust 2011

AstraZeneca
ONKOLOGIJA

IRESSA®
gefitinib

Merck Serono Onkologija | ključ je v kombinaciji

Erbitux 5 mg/ml raztopina za infundiranje (Skrajšan povzetek glavnih značilnosti zdravila)

Sestava: En ml raztopine za infundiranje vsebuje 5 mg cetuximaba in pomožne snovi. Cetuksimab je himerno monoklonsko IgG1 protitelo. **Terapevtske indikacije:** Zdravilo Erbitux je indicirano za zdravljenje bolnikov z metastatskim kolorektalnim rakom z ekspresijo receptorjev EGFR in nemutiranim tipom KRAS v kombinaciji s kemoterapijo na osnovi irinotekana, kot primarno zdravljenje v kombinaciji s FOLFOX in kot samostojno zdravilo pri bolnikih, pri katerih zdravljenje z oksaliplatinom in irinotekanom ni bilo uspešno ter pri bolnikih, ki ne prenašajo irinotekana. Zdravilo Erbitux je indicirano za zdravljenje bolnikov z rakom skvamoznih celic glave in vratu v kombinaciji z radioterapijo za lokalno napredovalo bolezen in v kombinaciji s kemoterapijo na osnovi platine za ponavljajočo se in/ali metastatsko bolezen. **Odmerjanje in način uporabe:** Zdravilo Erbitux pri vseh indikacijah infundirajte enkrat na teden. Pred prvo infuzijo mora bolnik prejeti premedikacijo z antihistaminikom in kortikosteroidom. Začetni odmerek je 400 mg cetuksimaba na m^2 telesne površine. Vsi naslednji tedenski odmerki so vsak po 250 mg/m^2. **Kontraindikacije:** Zdravilo Erbitux je kontraindicirano pri bolnikih z znano hudo preobčutljivostno reakcijo (3. ali 4. stopnje) na cetuksimab. Kombinacija zdravila Erbitux s kemoterapijo, ki vsebuje oksaliplatin, je kontraindicirana pri bolnikih z metastatskim kolorektalnim rakom z mutiranim tipom KRAS ali kadar status KRAS ni znan. **Posebna opozorila in previdnostni ukrepi:** Če pri bolniku nastopi blaga ali zmerna reakcija, povezana z infundiranjem, lahko zmanjšate hitrost infundiranja. Priporočljivo je, da ostane hitrost infundiranja na nižji vrednosti tudi pri vseh naslednjih infuzijah. Če se pri bolniku pojavi huda kožna reakcija (≥ 3. stopnje po kriterijih US NCI-CTC), morate prekiniti terapijo s cetuksimabom. Z zdravljenjem smete nadaljevati le, če se je reakcija izboljšala do 2. stopnje. Zaradi možnosti pojava znižanja nivoja magnezija v serumu se pred in periodično med zdravljenjem priporoča določanje koncentracije elektrolitov. Če se pojavi sum na nevtropenijo, je potrebno bolnika skrbno nadzorovati. Potrebno je upoštevati kardiovaskularno stanje bolnika in sočasno dajanje kardiotoksičnih učinkovin kot so fluoropirimidini. Cetuksimab je treba uporabljati previdno pri bolnikih z anamnezo keratitisa, ulcerativnega keratitisa ali zelo suhih oči. **Interakcije:** Farmakokinetične značilnosti cetuksimaba ostanejo nespremenjene po sočasni uporabi enkratnega odmerka irinotekana, tudi farmakokinetika irinotekana je nespremenjena pri sočasni uporabi cetuksimaba. Pri kombinaciji s fluoropirimidini se je povečala pogostnost srčne ishemije, vključno z miokardnim infarktom in kongestivno srčno odpovedjo ter pogostnost sindroma dlani in stopal. V kombinaciji s kemoterapijo na osnovi platine se lahko poveča pogostnost hude levkopenije ali hude nevtropenije. **Neželeni učinki:** Zelo pogosti (≥ 1/10): hipomagneziemija, povečanje ravni jetrnih encimov, kožne reakcije, blage ali zmerne reakcije povezane z infundiranjem, blag do zmeren mukozitis. Pogosti (≥ 1/100, < 1/10): dehidracija, hipokalciemija, anoreksija, glavobol, konjunktivitis, driska, navzeja, bruhanje, hude reakcije povezane z infundiranjem, utrujenost. **Posebna navodila za shranjevanje:** Shranjujte v hladilniku (2 °C - 8 °C). **Pakiranje:** 1 viala z 20 ml ali 100 ml raztopine. **Način in režim izdaje:** H. **Imetnik dovoljenja za promet:** Merck KGaA, 64271 Darmstadt, Nemčija. **Datum zadnje revizije besedila:** Januar 2012.

Pred predpisovanjem zdravila natančno preberite celoten Povzetek glavnih značilnosti zdravila.

Podrobnejše informacije so na voljo pri predstavniku imetnika dovoljenja za promet z zdravilom: Merck d.o.o., Ameriška ulica 8, 1000 Ljubljana, tel.: 01 560 3810, faks: 01 560 3830, el. pošta: info@merck.si

www.merckserono.net

www.Erbitux-international.com

Merck Serono

Merck Serono is a division of Merck.

MERCK

Samo za strokovno javnost PM-ONC-1/12-30.01.2012

SKRAJŠAN POVZETEK GLAVNIH ZNAČILNOSTI ZDRAVILA

Samo za strokovno javnost.

Ime zdravila: Tarceva 25 mg/100 mg/150 mg filmsko obložene tablete
Kakovostna in količinska sestava: Ena filmsko obložena tableta vsebuje 25 mg, 100 mg ali 150 mg erlotiniba (v obliki erlotinibijevega klorida).
Terapevtske indikacije: Nedrobnocelični rak pljuč: Zdravilo Tarceva je indicirano za prvo linijo zdravljenja bolnikov z lokalno napredovalim ali metastatskim nedrobnoceličnim rakom pljuč z EGFR-aktivirajočimi mutacijami. Zdravilo Tarceva je indicirano tudi za samostojno vzdrževalno zdravljenje bolnikov z lokalno napredovalim ali metastatskim nedrobnoceličnim rakom pljuč s stabilno boleznijo po 4 ciklih standardne kemoterapije na osnovi platine v prvi liniji zdravljenja. Zdravilo Tarceva je indicirano tudi za zdravljenje bolnikov z lokalno napredovalim ali metastatskim nedrobnoceličnim rakom pljuč po neuspehu vsaj ene predhodne kemoterapije. Pri predpisovanju zdravila Tarceva je treba upoštevati dejavnike, povezane s podaljšanim preživetjem. Koristnega vpliva na podaljšanje preživetja ali drugih klinično pomembnih učinkov zdravljenja niso dokazali pri bolnikih z EGFR-negativnimi tumorji (glede na rezultat imunohistokemije). Rak trebušne slinavke: Zdravilo Tarceva je v kombinaciji z gemcitabinom indicirano za zdravljenje bolnikov z metastatskim rakom trebušne slinavke. Pri predpisovanju zdravila Tarceva je treba upoštevati dejavnike, povezane s podaljšanim preživetjem. Koristnega vpliva na podaljšanje preživetja niso dokazali za bolnike z lokalno napredovalo boleznijo.
Odmerjanje in način uporabe: Zdravljenje z zdravilom Tarceva mora nadzorovati zdravnik z izkušnjami pri zdravljenju raka. Pri bolnikih z lokalno napredovalim ali metastatskim nedrobnoceličnim rakom pljuč, ki še niso prejeli kemoterapije, je treba testiranje za določanje mutacij EGFR opraviti pred začetkom zdravljenja z zdravilom Tarceva. Zdravilo Tarceva vzamemo najmanj eno uro pred zaužitjem hrane ali dve uri po tem. Kadar je potrebno odmerek prilagoditi, ga je treba zmanjševati v korakih po 50 mg. Pri sočasnem jemanju substratov in modulatorjev CYP3A4 bo morda potrebna prilagoditev odmerka. Pri dajanju zdravila Tarceva bolnikom z jetrno okvaro je potrebna previdnost. Če se pojavijo hudi neželeni učinki, pride v poštev zmanjšanje odmerka ali prekinitev zdravljenja z zdravilom Tarceva. Uporaba zdravila Tarceva pri bolnikih s hudo jetrno ali ledvično okvaro ter pri otrocih ni priporočljiva. Bolnikom kadilcem je treba svetovati, naj prenehajo kaditi, saj so plazemske koncentracije erlotiniba pri kadilcih manjše kot pri nekadilcih. Nedrobnocelični rak pljuč: Priporočeni dnevni odmerek zdravila Tarceva je 150 mg. Rak trebušne slinavke: Priporočeni dnevni odmerek zdravila Tarceva je 100 mg, v kombinaciji z gemcitabinom. Pri bolnikih, pri katerih se kožni izpuščaj v prvih 4 do 8 tednih zdravljenja ne pojavi, je treba ponovno pretehtati nadaljnje zdravljenje z zdravilom Tarceva.
Kontraindikacije: Preobčutljivost za erlotinib ali katero koli pomožno snov.
Posebna opozorila in previdnostni ukrepi: Pri določanju bolnikovega statusa mutacij EGFR je pomembno izbrati dobro validirano in robustno metodologijo, da se izognemo lažno negativnim ali lažno pozitivnim rezultatom. Močni induktorji CYP3A4 lahko zmanjšajo učinkovitost erlotiniba, močni zaviralci CYP3A4 pa lahko povečajo toksičnost. Sočasnemu zdravljenju s temi zdravili se je treba izogibati. Bolnikom, ki kadijo, je treba svetovati, naj prenehajo kaditi, saj so plazemske koncentracije erlotiniba pri kadilcih zmanjšane v primerjavi s plazemskimi koncentracijami pri nekadilcih. Verjetno je, da je velikost zmanjšanja klinično pomembna. Pri bolnikih, pri katerih se akutno pojavijo novi in/ali poslabšajo nepojasnjeni pljučni simptomi, kot so dispneja, kašelj in vročina, je treba zdravljenje z zdravilom Tarceva prekiniti, dokler ni znana diagnoza. Bolnike, ki se sočasno zdravijo z erlotinibom in gemcitabinom, je treba skrbno spremljati zaradi možnosti pojava toksičnosti, podobni intersticijski bolezni pljuč. Če je ugotovljena intersticijska bolezen pljuč, zdravilo Tarceva ukinemo in uvedemo ustrezno zdravljenje. Pri približno polovici bolnikov, ki so se zdravili z zdravilom Tarceva, se je pojavila driska (vključno z zelo redkimi primeri, ki so se končali s smrtnim izidom). Zmerno do hudo drisko zdravimo z loperamidom. V nekaterih primerih bo morda potrebno zmanjšanje odmerka. V primeru hude ali dolgotrajne driske, navzeje, anoreksije ali bruhanja, povezanih z dehidracijo, je treba zdravljenje z zdravilom Tarceva prekiniti in dehidracijo ustrezno zdraviti. O hipokaliemiji in ledvični odpovedi so poročali redko. Posebno pri bolnikih z dejavniki tveganja (sočasno jemanje drugih zdravil, simptomi, bolezni ali drugi dejavniki, vključno z visoko starostjo) moramo, če je driska huda ali dolgotrajna oziroma vodi v dehidracijo, zdravljenje z zdravilom Tarceva prekiniti in bolnikom zagotoviti intenzivno intravensko rehidracijo. Dodatno je treba pri bolnikih s prisotnim tveganjem za razvoj dehidracije spremljati ledvično delovanje in serumske elektrolite, vključno s kalijem. Pri uporabi zdravila Tarceva so poročali o redkih primerih jetrne odpovedi. K njenemu nastanku je lahko pripomogla predhodno obstoječa jetrna bolezen ali sočasno jemanje hepatotoksičnih zdravil. Pri teh bolnikih je treba zato premisliti o rednem spremljanju jetrnega delovanja. Dajanje zdravila Tarceva je treba prekiniti, če so spremembe jetrnega delovanja hude. Bolniki, ki prejemajo zdravilo Tarceva, imajo večje tveganje za razvoj perforacij v prebavilih, ki so jih opazili občasno (vključno z nekaterimi primeri, ki so se končali s smrtnim izidom). Pri bolnikih, ki sočasno prejemajo zdravila, ki zavirajo angiogenezo, kortikosteroide, nesteroidna protivnetna zdravila (NSAID) in/ali kemoterapijo na osnovi taksanov, ali so v preteklosti imeli peptični ulkus ali divertikularno bolezen, je tveganje večje. Če pride do tega, je treba zdravljenje z zdravilom Tarceva dokončno ukiniti. Poročali so o primerih kožnih bolezni z mehurji in luščenjem kože, vključno z zelo redkimi primeri, ki so nakazovali na Stevens-Johnsonov sindrom/toksično epidermalno nekrolizo in so bili v nekaterih primerih smrtni. Zdravljenje z zdravilom Tarceva je treba prekiniti ali ukiniti, če se pri bolniku pojavijo hude oblike mehurjev ali luščenja kože. Bolniki, pri katerih se pojavijo znaki in simptomi, ki nakazujejo na keratitis in so lahko akutni ali se poslabšujejo: vnetje očesa, solzenje, občutljivost na svetlobo, zamegljen vid, bolečine v očesu in/ali rdeče oči, se morajo takoj obrniti na specialista oftalmologije. V primeru, da je diagnoza ulcerativnega keratitisa potrjena, je treba zdravljenje z zdravilom Tarceva prekiniti ali ukiniti. V primeru, da se postavi diagnoza keratitisa, je treba skrbno razmisliti o koristih in tveganjih nadaljnega zdravljenja. Zdravilo Tarceva je pri bolnikih, ki so v preteklosti imeli keratitis, ulcerativni keratitis ali zelo suhe oči, uporabljati previdno. Uporaba kontaktnih leč je prav tako dejavnik tveganja za keratitits in ulceracijo. Med uporabo zdravila Tarceva so zelo redko poročali o primerih perforacije ali ulceracije roženice. Tablete vsebujejo laktozo in jih ne smemo dajati bolnikom z redkimi dednimi stanji: intoleranco za galaktozo, laponsko obliko zmanjšane aktivnosti laktaze ali malabsorpcijo glukoze/galaktoze.
Medsebojno delovanje z drugimi zdravili in druge oblike interakcij: Erlotinib se pri ljudeh presnavlja v jetrih z jetrnimi citokromi, primarno s CYP3A4 in v manjši meri s CYP1A2. Presnova erlotiniba zunaj jeter poteka s CYP3A4 v črevesju, CYP1A1 v pljučih in CYP1B1 v tumorskih tkivih. Z zdravilnimi učinkovinami, ki se presnavljajo s temi encimi, jih zavirajo ali pa so njihovi induktorji, lahko pride do interakcij. Erlotinib je srednje močan zaviralec CYP3A4 in CYP2C8, kot tudi močan zaviralec glukuronidacije z UGT1A1 *in vitro*. Pri kombinaciji ciprofloksacina ali močnega *zaviralca CYP1A2* (npr. fluvoksamina) z erlotinibom je potrebna previdnost. V primeru pojava neželenih učinkov, povezanih z erlotinibom, lahko odmerek erlotiniba zmanjšamo. Predhodno ali sočasno zdravljenje z zdravilom Tarceva ni spremenilo očistka prototipov *substratov CYP3A4,* midazolama in eritromicina. Inhibicija glukoronidacije lahko povzroči interakcije z zdravili, ki so *substrati UGT1A1* in se izločajo samo po tej poti. Močni *zaviralci aktivnosti CYP3A4* zmanjšajo presnovo erlotiniba in zvečajo koncentracije erlotiniba v plazmi. Pri sočasnem jemanju erlotiniba in močnih zaviralcev CYP3A4 je zato potrebna previdnost. Če je treba, odmerek erlotiniba zmanjšamo, še posebno pri pojavu toksičnosti. Močni *spodbujevalci aktivnosti CYP3A4* zvečajo presnovo erlotiniba in pomembno zmanjšajo plazemske koncentracije erlotiniba. Sočasnemu dajanju zdravila Tarceva in induktorjev CYP3A4 se je treba izogibati. Pri bolnikih, ki potrebujejo sočasno zdravljenje z zdravilom Tarceva in močnim induktorjem CYP3A4, je treba premisliti o povečanju odmerka do 300 mg ob skrbnem spremljanju njihove varnosti. Zmanjšana izpostavljenost se lahko pojavi tudi z drugimi induktorji, kot so fenitoin, karbamazepin, barbiturati ali šentjanževka. Če te zdravilne učinkovine kombiniramo z erlotinibom, je potrebna previdnost. Kadar je mogoče, je treba razmisliti o drugih načinih zdravljenja, ki ne vključujejo močnega spodbujanja aktivnosti CYP3A4. Bolnikom, ki jemljejo *kumarinske antikoagulante*, je treba redno kontrolirati protrombinski čas ali INR. Sočasno zdravljenje z zdravilom Tarceva in *statinom* lahko poveča tveganje za miopatijo, povzročeno s statini, vključno z rabdomiolizo; to so opazili redko. Sočasna uporaba *zaviralcev P-glikoproteina,* kot sta ciklosporin in verapamil, lahko vodi v spremenjeno porazdelitev in/ali spremenjeno izločanje erlotiniba. Za erlotinib je značilno zmanjšanje topnosti pri pH nad 5. *Zdravila, ki spremenijo pH v zgornjem delu prebavil,* lahko spremenijo topnost erlotiniba in posledično njegovo biološko uporabnost. Učinka antacidov na absorpcijo erlotiniba niso proučevali, vendar je ta lahko zmanjšana, kar vodi v nižje plazemske koncentracije. Kombinaciji erlotiniba in zaviralca protonske črpalke se je treba izogibati. Če menimo, da je uporaba antacidov med zdravljenjem z zdravilom Tarceva potrebna, jih je treba jemati najmanj 4 ure pred ali 2 uri po dnevnem odmerku zdravila Tarceva. Če razmišljamo o uporabi ranitidina, moramo zdravili jemati ločeno: zdravilo Tarceva je treba vzeti najmanj 2 uri pred ali 10 ur po odmerku ranitidina. V študiji faze Ib ni bilo pomembnih učinkov *gemcitabina* na farmakokinetiko erlotiniba, prav tako ni bilo pomembnih učinkov erlotiniba na farmakokinetiko gemcitabina. Erlotinib poveča koncentracijo platine. Pomembnih učinkov *karboplatina* ali paklitaksela na farmakokinetiko erlotiniba ni bilo. *Kapecitabin* lahko poveča koncentracijo erlotiniba. Pomembnih učinkov erlotiniba na farmakokinetiko kapecitabina ni bilo.
Neželeni učinki: *Zelo pogosti neželeni učinki* so kožni izpuščaj in driska, kot tudi utrujenost, anoreksija, dispneja, kašelj, okužba, navzea, bruhanje, stomatitis, bolečina v trebuhu, pruritus, suha koža, suhi keratokonjunktivitis, konjunktivitis, zmanjšanje telesne mase, depresija, glavobol, nevropatija, dispepsija, flatulenca, alopecija, okorelost, pireksija, nenormalnosti testov jetrne funkcije. *Pogosti neželeni učinki* so krvavitve v prebavilih, epistaksa, keratitis, paronihija, fisure na koži. *Občasno* so poročali o perforacijah v prebavilih, hirzutizmu, spremembah obrvi, krhkih nohtih, odstopanju nohtov od kože, blagih reakcijah na koži (npr. hiperpigmentacija), spremembah trepalnic, hudi intersticijski bolezni pljuč (vključno s smrtnimi primeri). *Redko* pa so poročali o jetrni odpovedi. *Zelo redko* so poročali o Stevens-Johnsonovem sindromu/toksični epidermalni nekrolizi ter o ulceracijah in perforacijah roženice.
Režim izdaje zdravila: H/Rp. **Imetnik dovoljenja za promet:** Roche Registration Limited, 6 Falcon Way, Shire Park, Welwyn Garden City, AL7 1TW, Velika Britanija. **Verzija:** 1.0/11. **Informacija pripravljena:** April 2012.

013-12-TAR

DODATNE INFORMACIJE SO NA VOLJO PRI:
Roche farmacevtska družba d.o.o.
Vodovodna cesta 109, 1000 Ljubljana.
Povzetek glavnih značilnosti zdravila je dosegljiv na www.roche.si ali www.onkologija.si.

Tarceva®
erlotinib

ČAS ZA ŽIVLJENJE.

DOKAZANO PODALJŠA PREŽIVETJE PRI BOLNIKIH:

- z lokalno napredovalim ali metastatskim nedrobnoceličnim rakom pljuč[1]
- z metastatskim rakom trebušne slinavke[1]

[1] Povzetek glavnih značilnosti zdravila TARCEVA, www.ema.europa.eu

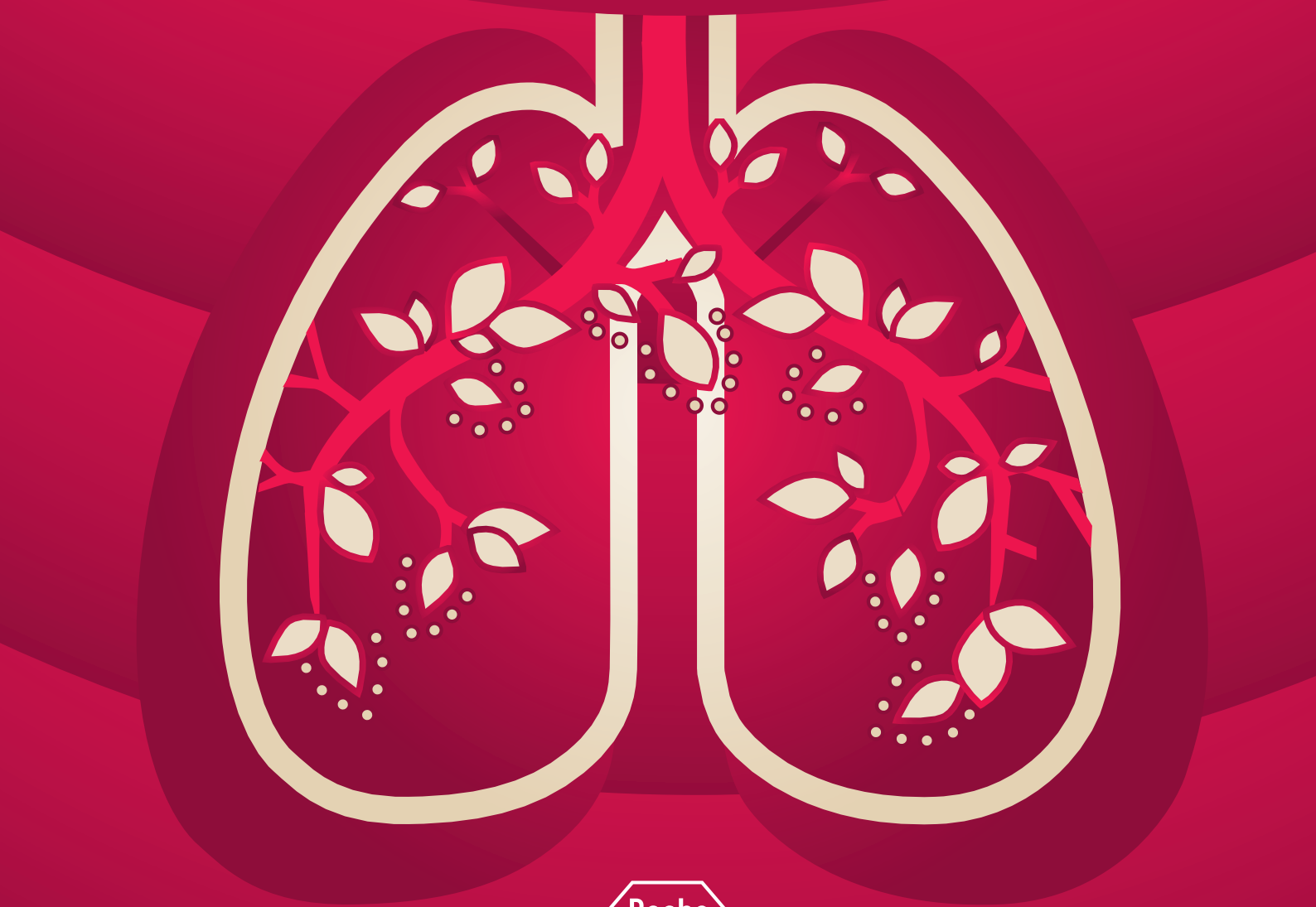

Roche

odprto

Novartis Oncology prinaša spekter inovativnih zdravil, s katerimi poskuša spremeniti življenje bolnikov z rakavimi in hematološkimi obolenji.

Ta vključuje zdravila kot so Glivec® (imatinib), Tasigna® (nilotinib), Afinitor® (everolimus), Zometa® (zoledronska kislina), Femara® (letrozol), Sandostatin® LAR® (oktreotid/i.m. injekcije) in Exjade® (deferasiroks).

Novartis Oncology ima tudi obširen razvojni program, ki izkorišča najnovejša spoznanja molekularne genomike, razumskega načrtovanja in tehnologij za odkrivanje novih učinkovin.

glivec imatinib

Tasigna (nilotinib)

AFINITOR (everolimus) tablete

ZOMETA zoledronska kislina

Femara (letrozol)

Sandostatin LAR oktreotid/i.m. injekcije

EXJADE deferasiroks

NOVARTIS ONCOLOGY

Novartis Pharma Services Inc. • Podružnica v Sloveniji • Verovškova 57 • 1000 Ljubljana

Samo za strokovno javnost.

NV-JA-08/11-SI

KEMOMED

Prinašamo rešitve

Z vami že 15 let

Iščete rešitve na področju znanosti o življenju?
Potrebujete ustrezna orodja za analitiko?

Mi vam jih ponujamo!

- Reagenti za diagnostiko in biomedicino
- Instrumenti in tehnična podpora
- Potrošni material
- Aplikativna pomoč
- Pipetni program in akreditirane kalibracije
- Plastika

KEMOMED d.o.o., Svetovanje, trgovina in trženje • Kališka 9 • **PE:** Stritarjeva 5, 4000 KRANJ, Slovenija
T: 04 20 15 050 • **F:** 04 20 15 055 • **E:** info@kemomed.si • **W:** **www.kemomed.si**

Novo, učinkovito zdravilo

za zdravljenje metastatskega raka prostate, odpornega na kastracijo pri odraslih bolnikih, z napredovalo obliko bolezni ali po osnovni kemoterapevtski shemi z docetakselom[1]

V placebo-nadzorovani klinični raziskavi III. faze so imeli bolniki, ki so prejeli zdravilo ZYTIGA® v kombinaciji z prednizonom:

- 35,4% manjše tveganje za smrt (HR=0,65)[2]
- 33% manjše tveganje za radiografsko potrjeno napredovanje bolezni[2]
- pomembno manj bolečin[2]
- primerljiv pojav neželenih učinkov kot v skupini, ki je prejemala placebo[2]
- možnost jemanja zdravila na domu (peroralno zdravljenje)[1]

Samo za strokovno javnost

Zdravilo je v postopku pridobitve financiranja s strani ZZZS.

SKRAJŠANO NAVODILO ZA PREDPISOVANJE ZDRAVILA:

Ime zdravila: ZYTIGA® 250 mg tablete **Kakovostna in količinska sestava:** 250 mg abirateronacetata; pomožne snovi: laktoza monohidrat, mikrokristalna celuloza, premreženi natrijev karmelozat, povidon, natrijev lavrilsulfat, magnezijev stearat in koloidni silicijev dioksid. **Indikacije:** uporaba skupaj s prednizonom ali prednizolonom za zdravljenje metastatskega raka prostate, rezistentnega na kastracijo pri odraslih bolnikih, z napredovalo obliko bolezni ali po osnovni kemoterapevtski shemi z docetakselom. **Odmerjanje:** priporočeni odmerek: 1.000 mg (štiri 250 mg tablete v enem odmerku), 10 mg prednizona ali prednizolona/dan, najmanj dve uri po obroku. Pri bolnikih s hudo okvaro jeter ali ledvic je potrebna previdnost. **Kontraindikacije:** preobčutljivost za zdravilno učinkovino ali katerokoli pomožno snov, uporaba zdravila pri ženskah. **Posebna opozorila:** Pri uporabi zdravila pri bolnikih z anamnezo kardiovaskularne bolezni je potrebna previdnost. Pri bolnikih z iztisnim deležem levega prekata < 50% ali s srčnim popuščanjem razreda III ali IV po NYHA varnost uporabe zdravila ni dokazana. Pred začetkom zdravljenja je treba urediti hipertenzijo in odpraviti hipokaliemijo. Če kadarkoli med zdravljenjem pride do pojava hude hepatotoksičnosti je treba z zdravljenjem prenehati in se ga ne sme ponovno uvesti. Pri bolnikih, ki prejemajo prednizon ali prednizolon in so v stresni situaciji, je lahko pred in med stresno situacijo ter po njej indiciran zvečan odmerek kortikosteroidov. Pri bolnikih z napredovanim metastatskim rakom prostate (rezistentnim na kastracijo) lahko pride do zmanjšanja kostne gostote. Jemanje zdravila v kombinaciji z glukokortikoidi lahko ta učinek poveča. Pri bolnikih z rakom prostate, zdravljenih s ketokonazolom, lahko pričakujemo nižjo stopnjo odziva na zdravljenje. Bolniki z redko dedno intoleranco za galaktozo, laponsko obliko zmanjšane aktivnosti laktaze ali malabsorpcijo glukoze/galaktoze ne smejo jemati tega zdravila. Zdravilo vsebuje tudi več kot 1 mmol (oziroma 27,2 mg) natrija na odmerek (v štirih tabletah), kar je treba upoštevati pri bolnikih na dieti z nadzorovanim vnosom natrija. **Interakcije:** zdravila se ne sme jemati s hrano, ker se bistveno poveča absorpcija abirateronacetata. Pri sočasni uporabi z zdravili, ki jih aktivira ali presnavlja CYP2D6, zlasti tistih z majhno terapevtsko širino je potrebna previdnost. In vitro podatki kažejo, da je zdravilo substrat CYP3A4. Med zdravljenjem se uporabi močnih zaviralcev in induktorjev CYP3A4 izogibajte ali bodite še posebej previdni. **Nosečnost in dojenje:** Ženske, ki so noseče in ženske, ki bi lahko bile noseče, morajo v primeru stika ali rokovanja z zdravilom, nositi zaščitne rokavice. **Neželeni učinki:** periferni edemi, hipokaliemija, hipertenzija, okužbe sečil, adrenalna insufucienca, hipertrigliceridemija, srčno popuščanje, angina pektoris, aritmija, atrijska fibrilacija, tahikardija, hepatotoksičnost z zvišanimi vrednostmi ALT, AST in celokupnega bilirubina. **Imetnik dovoljenja za promet:** Janssen-Cilag International NV, Turnhoutseweg 30, 2340 Beerse, Belgija, Predstavnik v Sloveniji: Johnson & Johnson d.o.o., Šmartinska 53, Ljubljana **Režim izdajanja zdravila:** Rp.Spec. **Datum zadnje revizije besedila:** 05.09.2011

Viri:

1. ZYTIGA® – Povzetek glavnih značilnosti zdravila: 05. 09. 2011
2. de Bono JS et al. Abiraterone and increased survival in metastatic prostate cancer. N Engl J Med 2011; 364: p1995-2005.

janssen
PHARMACEUTICAL COMPANIES OF Johnson&Johnson

ZYT-SLO-A-015-051011

Zytiga®
abirateronacetat

TANTUM® VERDE

Benzidamin

Lajšanje bolečine in oteklin pri vnetju v ustni votlini in žrelu, ki nastanejo zaradi okužb in stanj po operaciji in kot posledica radioterapije (t.i. radiomukozitis).

CSC ANGELINI

Imetnik dovoljenja za promet
CSC Pharma d.o.o.
Jana Husa 1a
1000 Ljubljana

www.tantum-verde.si

Tantum Verde 1,5 mg/ml oralno pršilo, raztopina

Kakovostna in količinska sestava
1 ml raztopine vsebuje 1,5 mg benzidaminijevega klorida, kar ustreza 1,34 mg benzidamina. V enem razpršku je 0,17 ml raztopine. En razpršek vsebuje 0,255 mg benzidaminijevega klorida, kar ustreza 0,2278 mg benzidamina. En razpršek vsebuje 13,6 mg 96 odstotnega etanola, kar ustreza 12,728 mg 100 odstotnega etanola, in 0,17 mg metilparahidroksibenzoata (E218).

Terapevtske indikacije
Samozdravljenje: lajšanje bolečine in oteklin pri vnetju v ustni votlini in žrelu, ki so lahko posledica okužb in stanj po operaciji. Po nasvetu in navodilu zdravnika: lajšanje bolečine in oteklin v ustni votlini in žrelu, ki so posledica radiomukozitisa.

Odmerjanje in način uporabe
Uporaba 2- do 6-krat na dan (vsake 1,5 do 3 ure). Odrasli: 4 do 8 razprškov 2- do 6-krat na dan. Otroci od 6 do 12 let: 4 razprški 2- do 6-krat na dan. Otroci, mlajši od 6 let: 1 razpršek na 4 kg telesne mase; do največ 4 razprške 2 do 6-krat na dan.

Kontraindikacije
Znana preobčutljivost za zdravilno učinkovino ali katerokoli pomožno snov.

Posebna opozorila in previdnostni ukrepi
Pri manjšini bolnikov lahko resne bolezni povzročijo ustne/žrelne ulceracije. Če se simptomi v treh dneh ne izboljšajo, se mora bolnik posvetovati z zdravnikom ali zobozdravnikom, kot je primerno. Zdravilo vsebuje aspartam (E951) (vir fenilalanina), ki je lahko škodljiv za bolnike s fenilketonurijo. Zdravilo vsebuje izomalt (E953) (sinonim: izomaltitol (E953)). Bolniki z redko dedno intoleranco za fruktozo ne smejo jemati tega zdravila. Uporaba benzidamina ni priporočljiva za bolnike s preobčutljivostjo za salicilno kislino ali druga nesteroidna protivnetna zdravila. Pri bolnikih, ki imajo ali so imeli bronhialno astmo, lahko pride do bronhospazma. Pri takih bolnikih je potrebna previdnost.

Medsebojno delovanje z drugimi zdravili in druge oblike interakcij
Pri ljudeh raziskav o interakcijah niso opravljali.

Nosečnost in dojenje
Tantum Verde z okusom mentola 3 mg pastile se med nosečnostjo in dojenjem ne smejo uporabljati.

Vpliv na sposobnost vožnje in upravljanja s stroji
Uporaba benzidamina lokalno v priporočenem odmerku ne vpliva na sposobnost vožnje in upravljanja s stroji.

Neželeni učinki
Bolezni prebavil Redki: pekoč občutek v ustih, suha usta.
Bolezni imunskega sistema Redki: preobčutljivostna reakcija.
Bolezni dihal, prsnega koša in mediastinalnega prostora Zelo redki: laringospazem.
Bolezni kože in podkožja Občasni: fotosenzitivnost. Zelo redki: angioedem.

Rok uporabnosti
4 leta. Zdravila ne smete uporabljati po datumu izteka roka uporabnosti, ki je naveden na ovojnini. Posebna navodila za shranjevanje Za shranjevanje pastil niso potrebna posebna navodila. Plastenko z raztopino shranjujte v zunanji ovojnini za zagotovitev zaščite pred svetlobo. Shranjujte pri temperaturi do 25°C. Shranjujte v originalni ovojnini in nedosegljivo otrokom.

CLINIPORATOR

LEADING CLINICAL ELECTROPORATION

Electrochemotherapy

Effective, safe, simple.

For local tumours control

Before electrochemotherapy

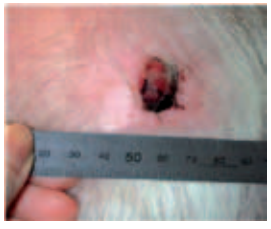

10 weeks after electrochemotherapy

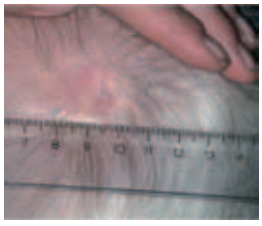

Gehl J, EJC Supplements, Volume 4, N° 11:35-37, 2006

Before electrochemotherapy

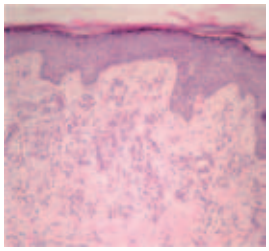

60 days after electrochemotherapy

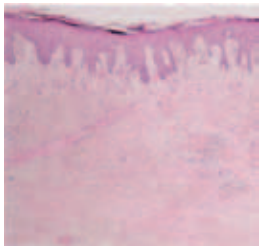

Quaglino P, Annals Of Surgical Oncology. 15 (8):2215-2222. 2008

CLINICAL INDICATIONS
Melanoma and other skin tumors
Local recurrences and cutaneous metastases from breast cancer
Head and neck cancers

High response rate
Preservation of normal tissue and organ function
Efficacy in areas previously treated with radiation therapy
Palliation of painful, ulcerated or bleeding lesions
Improved quality of life and cosmetic results

IGEA SpA, Carpi, Italy | www.igeamedical.com | info@igeamedical.com

IGEA®
CLINICAL BIOPHYSICS

Kakovost • Izbira • Zadovoljstvo

THE

Natrelle™

COLLECTION

Prsni vsadki in ekspanderji tkiv

Individualne ženske

Individualen izbor

ALLERGAN

DISTRIBUCIJA IN PRODAJA:
SANOLABOR, d.d.,
Leskoškova 4, 1000 Ljubljana, Slovenija
Tel:+386 (0)1 585-42-11
Fax:+386 (0)1 585-42-98
www.sanolabor.si

Sanolabor

PROMOCIJA, MARKETING IN STROKOVNA PODPORA:
EWOPHARMA d.o.o., Cesta 24.junija 23, 1000 Ljubljana, Slovenija
Jurij Pivka, vodja poslovne enote -Medicinska estetika
Tel: +386 (0) 59 084 845, mobilnik: +386 (0) 51 326 058
Fax: +386 (0) 59 084 849

Instructions for authors

The editorial policy

Radiology and Oncology is a multidisciplinary journal devoted to the publishing original and high quality scientific papers, professional papers, review articles, case reports and varia (editorials, short communications, professional information, book reviews, letters, etc.) pertinent to diagnostic and interventional radiology, computerized tomography, magnetic resonance, ultrasound, nuclear medicine, radiotherapy, clinical and experimental oncology, radiobiology, radiophysics and radiation protection. Therefore, the scope of the journal is to cover beside radiology the diagnostic and therapeutic aspects in oncology, which distinguishes it from other journals in the field.

The Editorial Board requires that the paper has not been published or submitted for publication elsewhere; the authors are responsible for all statements in their papers. Accepted articles become the property of the journal and, therefore cannot be published elsewhere without the written permission of the editors.

Submission of the manuscript

The manuscript written in English should be submitted to the journal via online submission system Editorial Manager available for this journal at: www.radioloncol.com.

In case of problems, please contact Sašo Trupej at saso.trupej@computing.si or the Editor of this journal at gsersa@onko-i.si

All articles are subjected to the editorial review and the review by independent referees.

Authors are requested to suggest persons competent to review their manuscript. However, please note that this will be treated only as a suggestion, the final selection of reviewers is exclusively the Editor's decision. The authors' names are revealed to the referees, but not vice versa.

Manuscripts which do not comply with the technical requirements stated herein will be returned to the authors for the correction before peer-review. The editorial board reserves the right to ask authors to make appropriate changes of the contents as well as grammatical and stylistic corrections when necessary. Page charges will be charged for manuscripts exceeding the recommended page number, as well as additional editorial work and requests for printed reprints.

All articles are published printed and on-line as the open access. To support the open access policy of the journal, the authors are encouraged to pay the open access charge of 500 EUR.

Manuscripts submitted under multiple authorship are reviewed on the assumption that all listed authors concur in the submission and are responsible for its content; they must have agreed to its publication and have given the corresponding author the authority to act on their behalf in all matters pertaining to publication. The corresponding author is responsible for informing the coauthors of the manuscript status throughout the submission, review, and production process.

Preparation of manuscripts

Radiology and Oncology will consider manuscripts prepared according to the Uniform Requirements for Manuscripts Submitted to Biomedical Journals by International Committee of Medical Journal Editors (www.icmje.org). The manuscript should be typed double-spaced with a 3-cm margin at the top and left-hand side of the sheet. The manuscript should be written in grammatically and stylistically correct language. Abbreviations should be avoided. If their use is neccessary, they should be explained at the first time mentioned. The technical data should conform to the SI system. The manuscript, including the references, must not exceed 15 typewritten pages, and the number of figures and tables is limited to 8. If appropriate, organize the text so that it includes: Introduction, Materials and methods, Results and Discussion. Exceptionally, the results and discussion can be combined in a single section. Start each section on a new page, and number each page consecutively with Arabic numerals.

The Title page should include a concise and informative title, followed by the full name(s) of the author(s); the institutional affiliation of each author; the name and address of the corresponding author (including telephone, fax and E-mail), and an abbreviated title. This should be followed by the abstract page, summarizing in less than 250 words the reasons for the study, experimental approach, the major findings (with specific data if possible), and the principal conclusions, and providing 3-6 key words for indexing purposes. Structured abstracts are preferred. Slovene authors are requested to provide title and the abstract in Slovene language in a separate file. The text of the research article should then proceed as follows:

Introduction should summarize the rationale for the study or observation, citing only the essential references and stating the aim of the study.

Materials and methods should provide enough information to enable experiments to be repeated. New methods should be described in detail.

Results should be presented clearly and concisely without repeating the data in the figures and tables. Emphasis should be on clear and precise presentation of results and their significance in relation to the aim of the investigation.

Discussion should explain the results rather than simply repeating them and interpret their significance and draw conclusions. It should discuss the results of the study in the light of previously published work.

Charts, Illustrations, Photographs and Tables must be numbered and referred to in the text, with the appropriate location indicated. Charts, illustrations and photographs, provided electronically, should be of appropriate quality for good reproduction. Illustrations and charts must be vector image, created in CMYK colour space, used font familie are encouraged "Century Gothic" and saved as .AI, .EPS or .PDF format. Color charts, illustrations and photographs are encouraged. Picture (image) size must be 2.000 pixels on the longer side and saved as .JPG (maximum quality) format. In photographs, mask the identities of the patients. Tables should be typed double-spaced, with a descriptive title and, if appropriate, units of numerical measurements included in the column heading. The files with the figures can be uploaded as separate files.

References must be numbered in the order in which they appear in the text and their corresponding numbers quoted in the text. Authors are responsible for the accuracy of their references. References to the Abstracts and Letters to the Editor must be identified as such. Citation of papers in preparation or submitted for publication, unpublished observations, and personal communications should not be included in the reference list. If essential, such material may be incorporated in the appropriate place in the text. References follow the style of Index Medicus. All authors should be listed when their number does not exceed six; when there are seven or more authors, the first six listed are followed by "et al.". The following are some examples of references from articles, books and book chapters:

Dent RAG, Cole P. *In vitro* maturation of monocytes in squamous carcinoma of the lung. *Br J Cancer* 1981; **43:** 486-95.

Chapman S, Nakielny R. *A guide to radiological procedures.* London: Bailliere Tindall; 1986.

Evans R, Alexander P. Mechanisms of extracellular killing of nucleated mammalian cells by macrophages. In: Nelson DS, editor. *Immunobiology of macrophage.* New York: Academic Press; 1976. p. 45-74.

Authorization for the use of human subjects or experimental animals

Manuscripts containing information related to human or animal use should clearly state that the research has complied with all relevant national regulations and institutional policies and has been approved by the authors' institutional review board or equivalent committee. These statements should appear in the Materials and methods section (or for contributions without this section, within the main text or in the captions of relevant figures or tables).

When reporting experiments on human subjects, authors should indicate whether the procedures followed were in accordance with the Helsinki Declaration. Patients have the right to privacy; therefore the identifying information (patient's names, hospital unit numbers) should not be published unless it is essential. In such cases the patient's informed consent for publication is needed, and should appear as an appropriate statement in the article.

The research using animal subjects should be conducted according to the EU Directive 2010/63/EU and following the Guidelines for the welfare and use of animals in cancer research (*Br J Cancer 2010;* **102:** 1555 – 77). Authors must identify the committee approving the experiments, and must confirm that all experiments were performed in accordance with relevant regulations.

Transfer of copyright agreement

For the publication of accepted articles, authors are required to send the Transfer of Copyright Agreement to the publisher on the address of the editorial office. A properly completed Transfer of Copyright Agreement, signed by the Corresponding Author on behalf of all the authors, must be provided for each submitted manuscript. The non-commercial use of each article will be governed by the Creative Commons Attribution-NonCommercial-NoDerivs license.

Conflict of interest

When the manuscript is submitted for publication, the authors are expected to disclose any relationship that might pose real, apparent or potential conflict of interest with respect to the results reported in that manuscript. Potential conflicts of interest include not only financial relationships but also other, non-financial relationships. In the Acknowledgement section the source of funding support should be mentioned. The Editors will make effort to ensure that conflicts of interest will not compromise the evaluation process of the submitted manuscripts; potential editors and reviewers will exempt themselves from review process when such conflict of interest exists. The statement of disclosure must be in the Cover letter accompanying the manuscript or submitted on the form available on www.icmje.org/coi_disclosure.pdf

Page proofs will be sent by E-mail or faxed to the corresponding author. It is their responsibility to check the proofs carefully and return a list of essential corrections to the editorial office within three days of receipt. Only grammatical corrections are acceptable at this time.

Reprints: The electronic version of the published papers will be available on www.versitaopen.com/ro free of charge.

AROMASIN®
eksemestan

Endokrino zdravljenje bolnic z rakom dojk po menopavzi

BISTVENI PODATKI IZ POVZETKA GLAVNIH ZNAČILNOSTI ZDRAVILA

AROMASIN 25 mg obložene tablete
Sestava in oblika zdravila: Ena obložena tableta vsebuje 25 mg eksemestana. **Indikacije:** Adjuvantno zdravljenje žensk po menopavzi, ki imajo invazivnega zgodnjega raka dojke s pozitivnimi estrogenskimi receptorji in so se uvodoma vsaj 2 do 3 leta zdravile s tamoksifenom. Zdravljenje napredovalega raka dojke pri ženskah z naravno ali umetno povzročeno menopavzo, pri katerih je bolezen napredovala po antiestrogenskem zdravljenju. Učinkovitost še ni bila dokazana pri bolnicah, pri katerih tumorske celice nimajo estrogenskih receptorjev. **Odmerjanje in način uporabe:** 25 mg enkrat na dan, najbolje po jedi. Pri bolnicah z zgodnjim rakom dojke je treba zdravljenje nadaljevati do dopolnjenega petega leta adjuvantnega hormonskega zdravljenja (tamoksifen, ki mu sledi eksemestan) oz. do recidiva tumorja. Pri bolnicah z napredovalim rakom dojke je treba zdravljenje nadaljevati, dokler ni razvidno napredovanje tumorja. **Kontraindikacije:** Preobčutljivost na zdravilno učinkovino ali na katerokoli pomožno snov, ženske pred menopavzo, nosečnice in doječe matere. **Posebna opozorila in previdnostni ukrepi:** Ne sme se predpisovati ženskam s predmenopavznim endokrinim statusom. Previdna uporaba pri jetrni ali ledvični okvari. Po uporabi so poročali o zmanjšanju mineralne gostote kosti ter večji pogostnosti zlomov. Ženskam z osteoporozo ali tveganjem zanjo je treba na začetku adjuvantnega zdravljenja izmeriti mineralno kostno gostoto s kostno denzitometrijo. Čeprav še ni dovolj podatkov, kako učinkujejo zdravila za zdravljenje zmanjšane mineralne kostne gostote, ki jo povzroča Aromasin, je treba pri bolnicah s tveganjem uvesti zdravljenje ali profilakso osteoporoze ter bolnice natančno spremljati. Zdravilo vsebuje saharozo, zato ga ne smejo jemati bolniki z redko dedno intoleranco za fruktozo, malabsorpcijo glukoze/galaktoze ali pomanjkanjem saharoza-izomaltaze. Vsebuje tudi metilparahidroksibenzoat, ki lahko povzroči alergijske reakcije (lahko zapoznele) in izjemoma bronhospazem. **Medsebojno delovanje z drugimi zdravili:** Sočasna uporaba zdravil – npr. rifampicina, antiepileptikov (npr. fenitoina ali karbamazepina) ali zdravil rastlinskega izvora s šentjaževko – ki inducirajo CYP3A4, lahko zmanjša učinkovitost zdravila Aromasin. Uporabljati ga je treba previdno z zdravili, ki se presnavljajo s pomočjo CYP3A4 in ki imajo ozek terapevtski interval. Kliničnih izkušenj s sočasno uporabo zdravila Aromasin in drugih zdravil proti raku ni. Ne sme se jemati sočasno z zdravili, ki vsebujejo estrogen, saj bi ta izničila njegovo farmakološko delovanje. **Vpliv na sposobnost vožnje in upravljanja s stroji:** Po uporabi zdravila je lahko psihofizična sposobnost za upravljanje s stroji ali vožnjo avtomobila zmanjšana. **Neželeni učinki:** Neželeni učinki so bili v študijah, v katerih so uporabljali standardni odmerek 25 mg na dan, ponavadi blagi do zmerni. ***Zelo pogosti (> 1/10):*** nespečnost, glavobol, vročinski oblivi, navzea, močnejše znojenje, bolečine v sklepih, mišicah in kosteh, utrujenost. **Način in režim izdajanja:** Predpisovanje in izdaja zdravila je le na recept zdravnika specialista ustreznega področja medicine ali od njega pooblaščenega zdravnika. **Imetnik dovoljenja za promet:** Pfizer Luksembourg SARL, 51, Avenue J. F. Kennedy, L-1855, Luksemburg. **Datum zadnje revizije besedila:** 31.8.2011
Pred predpisovanjem se seznanite s celotnim povzetkom glavnih značilnosti zdravila.

"SAMO ZA STROKOVNO JAVNOST"

ARO-01-12

Pfizer

Pfizer Luxembourg SARL, Grand Duchy of Luxembourg, 51, Avenue J.F. Kennedy, L-1855,
PFIZER, Podružnica za svetovanje s področja farmacevtske dejavnosti, Ljubljana, Letališka 3c, 1000 Ljubljana, SLOVENIJA

Radiology and Oncology | Ljubljana | Slovenia | www.versitaopen.com/ro

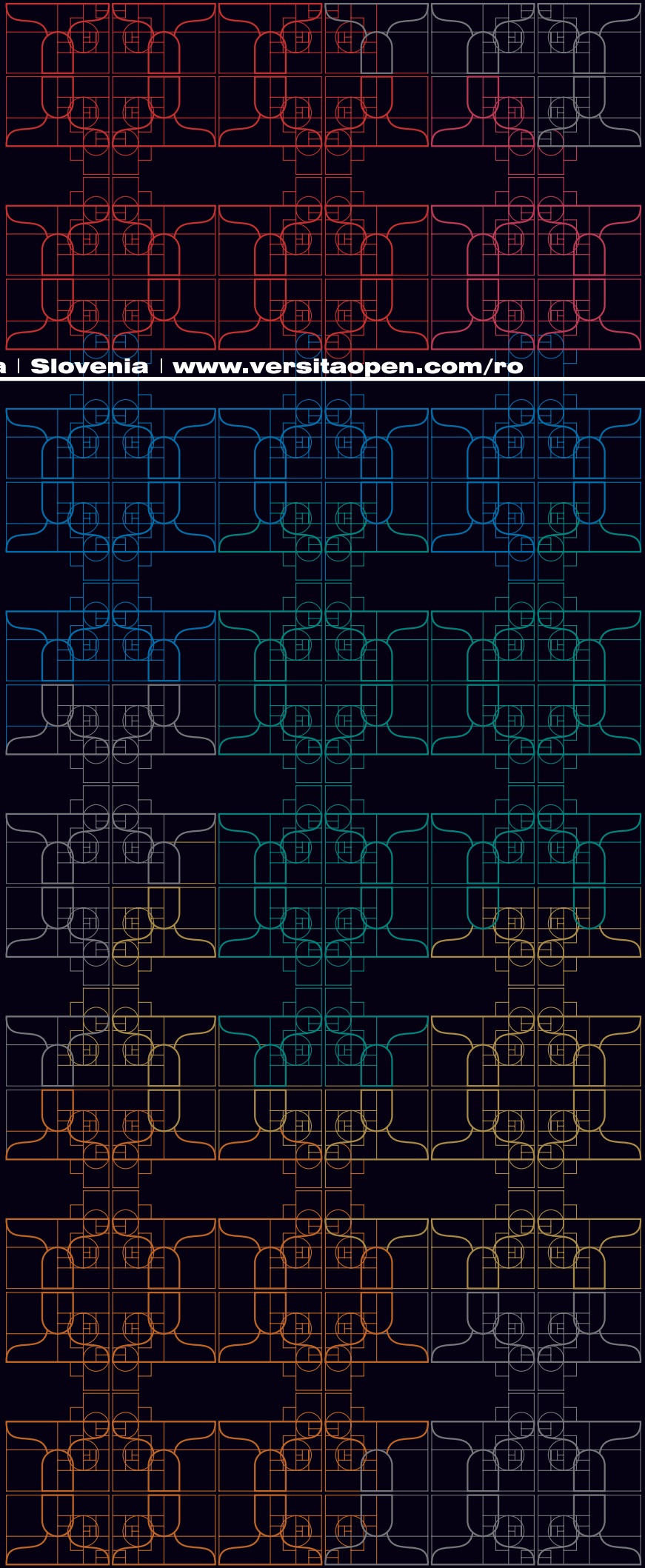

ISSN 1318 - 2099